AN ELECTROCHEMICAL STUDY OF THE SLAG-METAL SYSTEMS: SiO_2-CaO-MgO, Fe-Si AND SiO_2-CaO-MgO, Fe-C-Si

by

TERRENCE DOUGLAS AURINI, B. Eng., M.Eng.

A Thesis

Submitted to the Faculty of Graduate Studies

in Partial Fulfilment of the Requirements

for the Degree

Doctor of Philosophy

McMaster University

April 1968

DOCTOR OF PHILOSOPHY (1968)
(Metallurgy)

McMASTER UNIVERSITY
Hamilton, Ontario

TITLE : An Electrochemical Study of the Slag-Metal Systems: SiO_2-CaO-MgO, Fe-Si and SiO_2-CaO-MgO, Fe-C-Si.

AUTHOR: Terrence Douglas Aurini, B.Eng. (McMaster University)
M.Eng. (McMaster University)

SUPERVISORS: Professor R. G. Ward and W-K. Lu

NUMBER OF PAGES: (xiii); 246

SCOPE AND CONTENTS:

The reduction of silica saturated slags by carbon saturated iron in graphite crucibles has been studied in order to verify the existence of an electrochemical local cell reaction involving the slag/graphite crucible interface. This local cell reaction has been shown to exist and its contribution to the overall reduction kinetics was shown to be negligible. Based on the local cell reaction several successful reversible electromotive force cells were created to measure the standard free energy change for the oxidation of silicon by carbon monoxide, and to measure the activity of silicon in the Fe-Si binary and Fe-C-Si ternary.

ACKNOWLEDGEMENTS

The author wishes to express his sincere gratitude to his research supervisors, Dr. R. G. Ward and Dr. W-K. Lu, whose direction and encouragement throughout different stages of the work led to a successful completion of the project.

Thanks are also due the National Research Council of Canada for the award of a Student Fellowship, and to the American Iron and Steel Institute for their generous operating grant.

The author would like to thank members of the staff and graduate students of the McMaster Metallurgy Department, who through many discussions contributed to the solution of various problems. Special thanks go to Mr. M. Van Oosten and Mr. R. Adams for their assistance in providing the chemical analyses, and to Mrs. Marilyn Foster for her accurate typing of the thesis.

TABLE OF CONTENTS

LIST OF FIGURES

FIGURE	TITLE

The following illustrations are located at the end of the thesis.

LIST OF TABLES

CHAPTER 1

INTRODUCTION

The kinetics of many reactions involved in iron and steelmaking processes have been investigated by many authors, generally in an attempt to elucidate the rate controlling step, or steps, in the reaction mechanism. Because of the excessive temperatures utilized, and because of the relatively low diffusivities in metals and slags, it is widely accepted that the majority of these reactions are transport or diffusion controlled, and that chemical equilibrium is attained quickly at the interface in question. However, some reactions, notably the desulphurization of iron and the reduction of silica by carbon in iron, occur quite slowly and are conceded to be possibly controlled by a chemical mechanism.

Wagner[1] discussed chemical control mechanisms for reactions occurring at a slag/metal interface and noted that perhaps three types of chemical reactions could take place. First, the reacting molecules and atoms are in direct collision at the interface, resulting in a transfer of electrons from one species to another by traversing a few atomic distances, resulting in a change of chemical states. He then notes that because of the nature of the two phases involved, the slag phase being well established as ionic and the metal phase being essentially atomic, an electrochemical mechanism is quite probable and even necessary. In this type of reaction, the cathodic and anodic reactions are thought of as occurring simultaneously at different locations along the slag/metal interface, with the electrons

being transferred many atomic distances through the metal phase. Wagner considers the third type of reaction as an extension of the electrochemical reaction when slag-metal reactions are brought about in graphite crucibles. In this system an electrochemical local cell mechanism can operate with one electrode process occurring at the slag/metal interface and the other occurring at the slag/graphite crucible interface, with the consequent flow of electrons through the graphite crucible and the metal phase.

King and Ramachandran[2] have tentatively demonstrated the presence of an electrochemical reaction, as opposed to the direct chemical reaction, in their study of the desulphurization of iron. Baak and King[3], and Grimble et al.[4] have attempted to illustrate the electrochemical local cell reaction in their work on desulphurization of iron and the reduction of silica by carbon in iron in graphite crucibles, respectively.

This present study was initiated to conclusively measure the contribution of the local cell reaction in the reduction of silica by carbon in iron, using graphite crucibles. It is imperative to be aware of the contribution of the second interface (the slag/crucible interface) to the overall kinetics of silicon transfer in order to properly assess the kinetic data. The local cell reaction was effectively isolated from the slag-metal reaction, its contribution to the overall kinetics over a wide temperature range was measured, and the results thoroughly discussed.

Based on the presence of the local cell reaction in this system, several electrochemical cells were prepared and reversible electromotive force measurements were successfully made. The standard free energy of the reaction:

$$Si + 2CO = SiO_2 + 2C$$

was determined, and the activity of silicon in iron and in iron-carbon alloys was measured. All the results are presented along with current literature data and are thoroughly discussed.

CHAPTER 2

LITERATURE REVIEW

A. ELECTROCHEMISTRY

2.1 Electrolysis

2.1.1. Electrolytic Conduction

Solids and liquids which are able to conduct current are divided into two classes; metallic conductors, (first class conductors) and electrolytic conductors, (second class conductors). A metallic conductor consists of a rigid lattice of positive ions surrounded by relatively mobile electrons which will move in the opposite direction of an applied potential. An electrolytic conductor consists of positive and negative ions either fixed in a lattice or free in solution, and when an electric potential (sometimes referred to as electric tension) is imposed across the electrolyte, the positive ions migrate to the negative terminal and the negative ions migrate to the positive terminal. For the latter class, the conduction of current is brought about by a transfer of mass, which is referred to as electrolysis.

Since there is no lower limit to the magnitude of the electric potential required to pass a current, it is implied that the solution exists initially containing ions, and no initial work is required for the formation of ions from some uncharged species.

2.1.2. Laws of Electrolysis

The transfer of mass referred to in the above section is restricted by important relationships known as Faraday's Laws:

(a) The amount of any substance deposited or dissolved from an electrode is proportional to the quantity of electricty passed.

(b) The amounts of any substances deposited or dissolved by the same quantity of electricity are proportional to their chemical equivalent weights.

A common expression of the two laws is shown by the correlation:

$$W = \frac{Ite}{F} \qquad (2.1)$$

W ≡ weight of substance deposited or dissolved

I ≡ current passed (amps)

t ≡ time of current passage (sec)

e ≡ equivalent weight of the substance

F ≡ the Faraday; the quantity of electricity needed to deposit or dissolve 1 gm equivalent of any substance

2.1.3. Transference Numbers

The current carrying ability of an electrolyte is dependent upon the migration of cations and anions, and upon their ultimate equivalent discharge at their respective electrodes. Because of the variation in size and charge of ions, it is expected that the cations and anions will move at different speeds under the influence of the same applied potential. The total current passed through an electrolyte is proportional to the sum of the individual ionic velocities, and the amount of current carried by a single species is proportional to its own velocity. The fraction of the total current passed by any one ionic species is called its transference number, and is designated by:

$$t_+ = \frac{v_+}{v_+ + v_-} \qquad t_- = \frac{v_-}{v_+ + v_-} \qquad (2.2)$$

$t_+ \equiv$ fraction of the total current carried by the cation

$t_- \equiv$ fraction of the total current carried by the anion

$v_+ \equiv$ velocity of the cation

$v_- \equiv$ velocity of the anion

If the velocity of one ionic species is much greater than that of the other it is conceivable that all the current would be carried by that species alone. This condition is known to exist in certain solid and fused electrolytes, as will be shown later. In systems containing several cationic and anionic species the effect of the ion radius and ion charge becomes extremely important, and the magnitude of the radius to charge ratio determines the individual ion contributions to the overall current carried[5].

2.2 Electromotive Force

2.2.1. Galvanic Cells

The preceding sections dealt with chemical reactions which were forced to proceed by the passage of an electric current across ionic solution in the solid, molten or aqueous state. This electrolysis may be represented by:

$$A^+B^- \xrightarrow[\text{current}]{\text{electric}} A^\circ + B^\circ \qquad (2.3)$$

A^+ is reduced to A° and B^- is oxidized to B°.

The reaction represented by (2.3) is usually not spontaneous as written, and energy in the form of electrical energy is necessary for the reaction to proceed. When the reaction goes from right to left, that is when A°

and B° are brought together by some means, the reaction would proceed spontaneously releasing energy equivalent to the electrical energy needed previously. If A° and B° were brought into direct contact the energy would be liberated as heat. However, if they were connected through an appropriate electrolyte and connected externally by an electrical conductor, the liberated energy would be electrical in nature.

The energy required to remove an electron from a metal varies greatly from high energy for the noble metals to low energy for base metals. When copper and zinc are in contact, the copper tends to absorb electrons from the zinc until the potential difference set up by the transfer opposes any further transfer and no current flows, providing both contact points are at the same temperature. If the copper and zinc were joined through a solution of an electrolyte, current would flow due to the motion of the positive ions of the electrolyte to the copper and the negative ions to the zinc. A cell of this nature is called a galvanic cell.

2.2.2. The Standard Half-Cell

The total electromotive force of a reversible cell is determined by the algebraic sum of the electromotive forces at each of the electrodes. These single electromotive forces are a result of the tendency for a substance in contact with a solution of its own ions to give up or absorb electrons, and their absolute value can be calculated only if the absolute value of one electrode process be known. Attempts have been made to measure absolute values of electromotive force, but so far have been unsuccessful[6] and for that reason the hydrogen half cell was chosen as the arbitrary zero potential against which all other half cell potentials are measured[7].

The "electromotive force series of the elements" is obtained when these standard half cell voltages are listed in decreasing or increasing order of magnitude and is quite useful in determining the direction of a reaction involving two standard half cells. A similar series has been constructed by Delimarski[8] for the chlorides of twenty-one metals for temperatures 500°, 700°C and the fusion temperature, utilizing the sodium half cell as the arbitrary zero potential. The results of Hamer et al.[9] are essentially in accord with these findings.

2.3 Reversible Cells

In order to correlate the electrical energy produced by a galvanic cell to the thermodynamic properties of the reaction, it is necessary that the cell be reversible in the thermodynamic sense. If an electrochemical reaction proceeds between two electrodes in an electrolyte, and the potential between the electrodes is balanced by an external electromotive force (emf) no chemical or other change should occur if the cell is reversible[10]. Also, a slight decrease in the external emf should result in a small flow of current causing the electrochemical reaction to proceed, and an increase in this emf should cause the current to flow in the opposite direction causing the electrochemical reaction to be reversed.

A thermodynamically reversible system is one in which a change in the system is carried out infinitesimally slowly, so that the system is always in temperature and pressure equilibrium with its surroundings. Thus, in utilizing electromotive force measurements for reversible cells, the current flowing must be infinitesimally small so the system is always in virtual equilibrium, and all non-electrochemical and other electrochemical reactions must be suppressed.

A typical reversible cell is shown in Figure 1, depicting the Daniell Cell. The sliding contact S is moved along variable resistance PQ (with potential gradient C) until at X, the null galvanmeter G indicates no current, thus the reversible emf of the cell is equal to the potential difference between X and Q, and its magnitude is V.

2.4 Types of Reversible Electrodes

(a) A metal or non metal in contact with a solution of its own ions (zinc in a solution of zinc sulphate).

(b) A metal and a sparingly soluble salt of the metal in contact with a solution of a soluble salt of the same anion (mercury covered with slightly soluble mercurous sulphate immersed in potassium sulphate.)

(c) An unattackable electrode in a solution containing both the oxidized and the reduced states of the oxidation-reduction system (carbon or platinum in contact with a solution of Fe^{2+} and Fe^{3+} ions.)

2.5 Anomalies in EMF Measurements

2.5.1. Liquid Junction Potential

In many cases when measuring reversible cell emf's it is necessary that two electrolytic solutions be in contact -- as in the Daniell Cell -- in order to satisfy the individual electrode reactions. Such liquid to liquid contact introduces a potential in addition to the reversible potential, called the liquid junction potential. This potential occurs when the two electrolytic solutions are different, and also when the two solutions are qualitatively similar but of different concentration. If two solutions of HCl are in contact, the electrolyte tends to diffuse from the higher chemical potential solution to the lower one. Since H^+

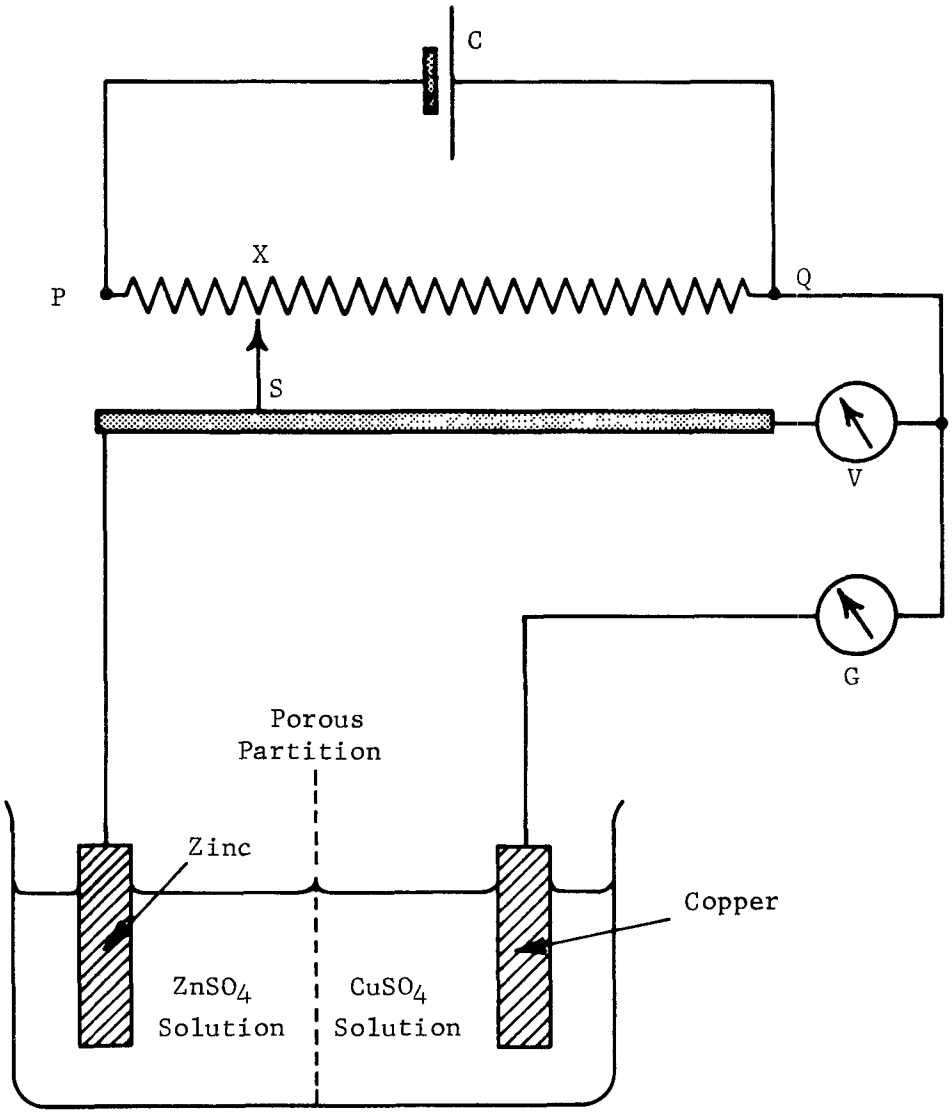

FIGURE 1 - DANIELL CELL AND SIMPLE POTENTIOMETER

has a much greater mobility than Cl^-, the dilute solution will have an excess of H^+ ions which causes it to be positive relative to the concentrated solution and creates an electric potential between the two liquids known as the liquid junction potential.

It can be shown[11] that the liquid junction potential E_ℓ is

$$E_\ell = (t_- - t_+) \frac{RT}{nF} \ln \frac{a_2}{a_1} \qquad (2.4)$$

$R \equiv$ gas constant

$T \equiv$ temperature

$a_1, a_2 \equiv$ activities of the ionic species at the two electrodes

In aqueous solutions this liquid junction potential can be virtually eliminated by the use of a salt bridge which is an inverted tube connecting the two solutions, filled with a saturated solution of potassium chloride. The ionic mobilities of K^+ and Cl^- are practically equal, so from (2.4) it is seen that $E_\ell \to 0$.

2.5.2 Overvoltage

In the electrolysis of many ionic solutions in which a gas is liberated at one or both electrodes, the decomposition potential is invariably higher than the theoretical reversible potential. This overvoltage is dependent upon the type of electrode and its physical state. The overvoltage for hydrogen evolution on platinum coated with platinum black is 0.00 volts, and on smooth platinum it is 0.09 volts. This phenomenon is attributed to a slow step in the ionic discharge process where the hydrated hydrogen ions migrate to the negative electrode, become absorbed, are discharged to form atomic hydrogen, and the atomic

hydrogen combines to form molecular hydrogen. The magnitude of the overvoltage generally decreases with increasing temperature. A more detailed interpretation of the hydrogen overvoltage is presented by Milazzo[12].

2.6 Thermodynamic Equivalence of the Reversible Cell

One of the fundamental relationships in the measurement of thermodynamic properties is derived from the concept of reversible electrode reactions. Combining the first and second laws of thermodynamics and applying the restriction of constant temperature and pressure, it can be shown:

$$\Delta G = - w' \tag{2.5}$$

$\Delta G \equiv$ free energy change of the reaction

$w' \equiv$ electrical work done by the system

The work required to transfer n gm electron through a field of strength ε is given by

$$w' = n F \varepsilon$$

$n \equiv$ number of gm electrons transferred

$F \equiv$ the Faraday, the charge of 1 gm electron

$\varepsilon \equiv$ reversible cell electromotive force

Therefore,

$$\Delta G = - n.F.\varepsilon \tag{2.6}$$

For a generalized reaction:

$$aA + bB + \ldots \rightleftharpoons \ell L + mM + \ldots \tag{2.7}$$

$$\Delta G = \Delta G^\circ + RT \ln \frac{a_L^{\ell} \cdot a_M^{m} \ldots}{a_A^{a} \cdot a_B^{b} \ldots} \tag{2.8}$$

a_A, a_B, ... a_L, a_M, ... are the activities of A,B,...L,M,... in the cell

Combining (2.8) and 2.6):

$$\varepsilon = \varepsilon^\circ - \frac{RT}{nF} \ln \frac{a_L^{\,l} \cdot a_M^{\,m} \cdots}{a_A^{\,a} \cdot a_B^{\,b} \cdots} \qquad (2.9)$$

$\varepsilon^\circ \equiv$ electromotive force when all substances are in their standard state (standard emf)

2.6.1. Temperature Coefficient of the Electromotive Force

The relationship expressed in (2.9) permits the ready evaluation of several other thermodynamic functions from the variation of the electromotive force with temperature.

$$\left(\frac{\partial(\Delta G)}{\partial T} \right)_p = - \Delta S \qquad (2.10)$$

$\Delta S \equiv$ entropy change of the reaction

Combining (2.10) with (2.6),

$$\Delta S = nF \left(\frac{\partial \varepsilon}{\partial T}\right)_p \qquad (2.11)$$

Also,

$$\Delta H = \Delta G + T \Delta S \qquad (2.12)$$

$\Delta H \equiv$ enthalpy change of the reaction

Combining (2.6), (2.11) and (2.12)

$$\Delta H = - nF \left[\varepsilon - T \left(\frac{\partial \varepsilon}{\partial T}\right)_p\right] \qquad (2.13)$$

A straight line dependence of ε on T indicates the constancy of the "entropy change" for the reaction. However, any departure from linearity represents the variation of "entropy change" with temperature:

$$\Delta S = \int \Delta C_p \, d \ln T \tag{2.14}$$

$\Delta C_p \equiv$ change in heat capacity of the system due to reaction at constant pressure

$$\left(\frac{\partial \Delta S}{\partial T}\right)_p = \frac{\Delta C_p}{T} \quad \text{therefore:} \quad n.F \left(\frac{\partial^2 \varepsilon}{\partial T^2}\right)_p = \frac{\Delta C_p}{T} \tag{2.15}$$

thus,

$$\Delta C_p = nFT\left(\frac{\partial^2 \varepsilon}{\partial T^2}\right)_p \tag{2.16}$$

2.6.2 Determination of Partial Entropy and Partial Enthalpy in Solution

If an electrochemical reaction proceeds according to the overall reaction:

$$A + B \rightarrow C \tag{2.17}$$

and if B and C are in their standard states, from (2.9),

$$\varepsilon = \varepsilon^\circ + \frac{RT}{nF} \ln a_A \tag{2.18}$$

$a_A \equiv$ activity of A in the solvent

For reaction of $A_{pure} \rightarrow A_{solution}$,

$$\Delta \bar{G}_A^M = RT \ln a_A = \Delta \bar{H}_A^M - T \, \Delta \bar{S}_A^M \tag{2.19}$$

$\Delta \bar{G}_A^M \equiv$ partial free energy of A in solution

$\Delta \bar{S}_A^M \equiv$ partial entropy of A in solution

$\Delta\bar{H}_A^M$ partial enthalpy of A in solution

Combining (2.18) and (2.19),

$$n.F\ (\varepsilon - \varepsilon^\circ) = \Delta\bar{H}_A^M - T\ \Delta\bar{S}_A^M$$

when $\Delta\bar{H}_A^M$ and $\Delta\bar{S}_A^M$ are temperature independent, thus,

$$\Delta\bar{H}_A^M = -\ nF\ \frac{d\left(\frac{\varepsilon^\circ - \varepsilon}{T}\right)}{d\ \frac{1}{T}} \qquad (2.20)$$

also,

$$\Delta\bar{S}_A^M = nF\ \frac{d(\varepsilon^\circ - \varepsilon)}{dT} \qquad (2.21)$$

B. THE NATURE OF SLAGS

2.7 Introduction

The understanding and interpretation of slag-metal reactions and equilibria has necessitated a more coherent and meaningful knowledge of the nature of slags. The evaluation and prediction of slag-metal phenomena are dependent solely on a workable model of the slag structure which permits an analysis of its behaviour. As more and more data have become available, suggested models of slag structure have evolved in order to adequately satisfy the increasingly demanding data.

2.7.1. The Early Theories of Slag Structure

Initially, liquid slags were envisioned as consisting of electroneutral oxides and their compounds[13], with the slag deriving its chemical activity from the "free oxide" which was that oxide in excess of the amount needed to form complex molecules[14]. Colclough[15] presented a more sophisticated concept when he postulated that the basic oxides present were not equivalent in reactivity. The fact that slags possessed a marked degree of reactivity even when there was no excess "free oxide" as defined by the molecular theory, resulted in the concept of partial dissociation of complex molecules, attributed to Schenck[16]. The molecular theory as originally formulated predicted no reactivity of iron oxide at the orthosilicate composition ($2FeO.SiO_2$) when it was known that the activity of FeO was near 0.7. According to Schenck, the orthosilicate partially decomposed into its constituent oxides:

$$2FeO.SiO_2 \rightleftharpoons 2\ FeO + SiO_2 \qquad (2.22)$$

so that,

$$D \equiv \frac{(\text{wt\% } FeO)^2(\text{wt\% } SiO_2)}{(\text{wt\% } 2FeO.SiO_2)} \qquad (2.23)$$

D ≡ dissociation constant

In steelmaking slags with at least eight major constituents capable of forming many complex molecules between themselves and silica, each requiring its individual dissociation constant, the use of the partial dissociation concept became far too cumbersome. The molecular theory was, however, valuable in that it recognized the predominant species in the slag as CaO, FeO and SiO_2, and led to the concept that is widely used to-day in works practise, the "V" ratio. The definition of the "V" ratio is quite varied[17-21] and is utilized successfully to interpret the data of particular practises.

2.7.2. The Ionic Nature of Slags

Despite the obvious advantage of the molecular theories, their inability to adequately account for sulphur and phosphorus transfer, and their resultant complexity, ultimately led to an ionic interpretation of slag structure. The ionic nature of slags was observed as early as 1906 by Aiken[22] who patented a process for the production of iron from the electrolytic decomposition of $FeO.SiO_2$ slags. However, the apparent success of the molecular theories precluded its use until the molecular theories had to be abandoned.

Doelter[23], in 1907, demonstrated that molten silicates could carry a current, and that the current increased with increasing temperature. Farup et al.[24] measured conductivities in the $CaO.SiO_2$ and $CaO.Al_2O_3.SiO_2$ systems which were higher than those for many fused salts, indicating good

ionic conduction. Sauerwald and Neuendorf[25], using iron anodes and iron or carbon cathodes, electrolyzed iron silicates, forming spongy iron at the cathode. Wejnarth[26] measured the conductivity of iron silicates and found an increase with increasing iron oxide content.

Martin and Derge[27] in 1943 presented the most comprehensive work to that time on the ionic structure of slags. Using carbon electrodes in synthetic slags (45% SiO_2. 10% Al_2O_3. 45% Ca O) they found a straight line relationship between the logarithm of the conductivity and the reciprocal of the temperature, obeying the Rasch-Hinrichsen law[28]. The positive temperature coefficient of conductivity is a strong indication of ionic conduction, since electronic conductors such as metals have a negative temperature coefficient of conductivity. Electrolysis of these slags resulted in a gas evolved at the anode along with a white deposit, and a slag analysis showed a slight SiO_2 increase at the anolyte and a slight CaO increase at the catholyte. These observations they concluded were due to a migration of silicon with negatively charged groups to the anode where they were discharged:

$$(SiO_4)^{4-} = (SiO_2)_{\text{white deposit}} + O_2 + 4e \qquad (2.24)$$

The evolution of O_2 at the anode is highly improbable since the anode is graphite and the formation of CO is more likely. The authors do not imply the cathodic reaction, but presumably in this system the Ca^{2+} cation carried all the current to the cathode, although it is not necessarily involved in the cathode reaction. A thermodynamically favourable reaction would be the deposition of silicon metal rather than calcium metal.

They state that since Si^{4+} and Al^{3+} ions are much smaller than Ca^{2+}, Mg^{2+} and Fe^{2+} ions, and since Si^{4+} and Al^{3+} ions also have larger charges, they exhibit a strong attraction for oxygen ions and in all probability exist in the form of silicate and aluminate ions rather than as free ions. The simplest silicate ion is said to be SiO_4^{4-} of tetrahedral structure with silicon at the center. As the silica content increases, the simple silicates polymerize into larger silicate groups made up of many tetrahedrals to form chains and rings:

$$2(SiO_4)^{4-} = (Si_2O_7)^{6-} + O^{2-} \qquad (2.25)$$

If an abundant supply of oxygen ions are present, the slag will consist of the simple tetrahedra resulting in a low viscosity, high conductivity slag. They also suggest that calcium and iron exist as ions, and, in opposition to the present attitude, that some neutral molecules such as Ca_2SiO_4, CaO and FeO might exist.

Bockris et al.[29] studied a similar system and proposed evidence for the existence of ionic slags:

(a) The conductivity was of the same order of magnitude as for molten salts.

(b) The positive temperature coefficient of conductance indicated ionic conduction and the energy of activation for conduction (10 to 35 Kcal/mole).

(c) The dependence of conductivity on the concentration of oxides of calcium and manganese is generally associated with ionic conductors, although at high MnO concentrations there was possibly a semi-conduction mechanism working.

(d) The rapid decrease of conduction at a temperature just above the melting point to a temperature just below the melting point was a sign of ionic

conduction. A typical value of this ratio for ionic conductors is 100 and for electronic conductors, 1.

(e) Passage of current produced electrolyses.

Bockris[30] performed Faradayan yield experiments on various silicate systems and observed 100% yields indicating solely ionic conduction. The results were compiled by analyzing the O_2 evolved, since it was difficult to isolate the deposited metal for it tends to (i) diffuse from the cathode, (ii) form a metal fog with the slag, (iii) volatilize, (iv) react with the material of the cell.

In a later paper, Bockris et al.[31] studied the electrical conductance of Li_2O, Na_2O, K_2O, MgO, CaO, SrO, BaO, MnO, Al_2O_3, and TiO_2 in solution with SiO_2 and found the Rasch-Hinrichsen law obeyed[28]:

$$\kappa = A \exp(-E_\kappa/RT) \qquad (2.26)$$

$\kappa \equiv$ specific conductance

$E_\kappa \equiv$ activation energy for conductance

Hofman and Marincek[32] measured electrical conductivities in the system $CaO.FeO.SiO_2.Al_2O_3$, using platinum crucibles and anodes. They determined the dependence of conductivity on the iron oxide content of acid, neutral and basic slags, and also the dependence of conductivity on the SiO_2 content when no FeO was present. The temperature range covered the liquid, liquid plus solid, and solid regions, obeying the Rasch-Hinrichsen law in all cases, as seen from Figure 2.

These results yielded an activation energy for conduction in the liquid phase only slightly lower than in the solid phase, illustrating

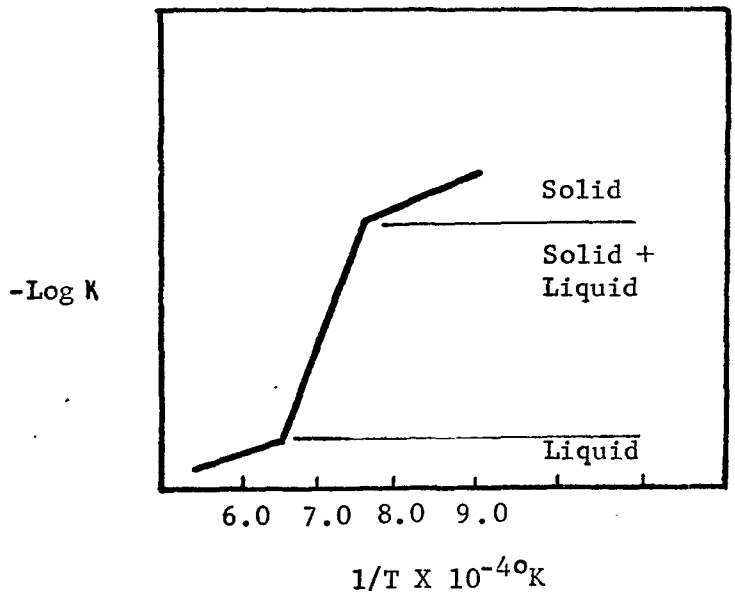

FIGURE 2 - SPECIFIC CONDUCTIVITY AS A FUNCTION OF TEMPERATURE[32]

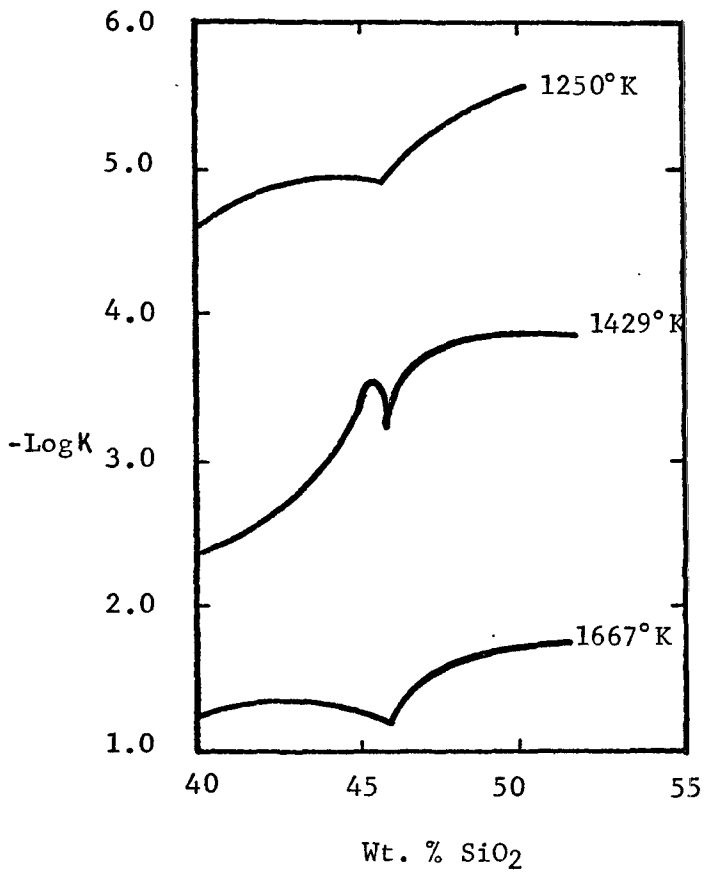

FIGURE 3 - SPECIFIC CONDUCTIVITY AS A FUNCTION OF SILICA CONTENT[32]

the structural similarity between the solid and the liquid. The activation energy for conduction in the solid plus liquid phase was considerably higher than in either the liquid or solid, and was tentatively attributed to bipolar conduction in this region (both cations and anions carry the current). However, the authors state that not enough is known of the melting process to accurately assess the data. They determined, in general, that the conduction increased with increasing FeO content but the increase was less pronounced as the basicity increased. The authors noted that at higher wustite concentrations the semi-conductance of the wustite became appreciable and an unusually high increase in conductivity was observed. The second series of tests showed that the conductivity decreased as the SiO_2 content increased as seen in Figure 3.

From Figure 3 it is noticed that the conductivity decreases with increasing SiO_2, but as the stoichiometric compound $CaO\text{-}SiO_2$ (46 wt.% SiO_2) is reached, the conductivity increases abruptly. The authors said the increase was associated with the dissociation of this compound into its ions, leading to the conclusion that in acid slags, dissociation into ions is not complete in the temperature range 1400-1500°C. If the ionization were complete as suggested by Herasymenko[33], they said that the conductivity would increase continuously as the CaO content increased. The validity of this statement is in doubt, as it is now accepted that ionization is indeed complete, and the conductivity is a function of the degree of polymerization of the silicate ions.

Simnad et al.[34] measured current efficiencies of iron silicate slags ranging from pure FeO to FeO saturated with SiO_2 using pure iron rods as anodes and an iron container as the cathode. The quantity of current

passed was measured along with the quantity of Fe^{2+} lost from the melt and the values were equated through Faraday's Law. In some cases, platinum was utilized as the anode and the O_2 evolved was monitored. The cell efficiency, i.e. the amount of Fe^{2+} deposited in relation to the theoretical prediction of Fe^{2+} deposited, is shown as a function of SiO_2 content in Figure 4.

From these results it is obvious that ionic conduction accounts for 10% of the current passed up to 10 wt.% SiO_2, the other 90% being electronic conduction. After 34 wt.% SiO_2 is reached, 90% of the current is passed ionically. Very little temperature effect was observed in these results between 1200° and 1400°C. They said that the electronic current was carried by a semi-conduction mechanism with electrons jumping from ferrous to ferric ions. The use of platinum as the anode resulted in the precipitation of silica and the evolution of oxygen, supporting the anodic reaction suggested earlier by Martin and Derge[27]. Transference numbers in silica saturated slags were measured by the Hittorf[35] method, and they found that the transference number for Fe^{2+} was unity in all cases.

Malkin[5], using radioactive tracer techniques, investigated the relative mobility of cations in the following three component systems: $Na_2O.K_2O.4SiO_2$, $Na_2O.CaO.4SiO_2$ and $K_2O.CaO.4SiO_2$. The results verified the ionic nature of the slags and also illustrated that the cations alone are carrying current since the vast size of the complex silicon anions renders them immobile (called unipolar conduction). He showed that the different cation mobilities were not independent of one another, and that the mobility increased as the cation field strength decreased. That is,

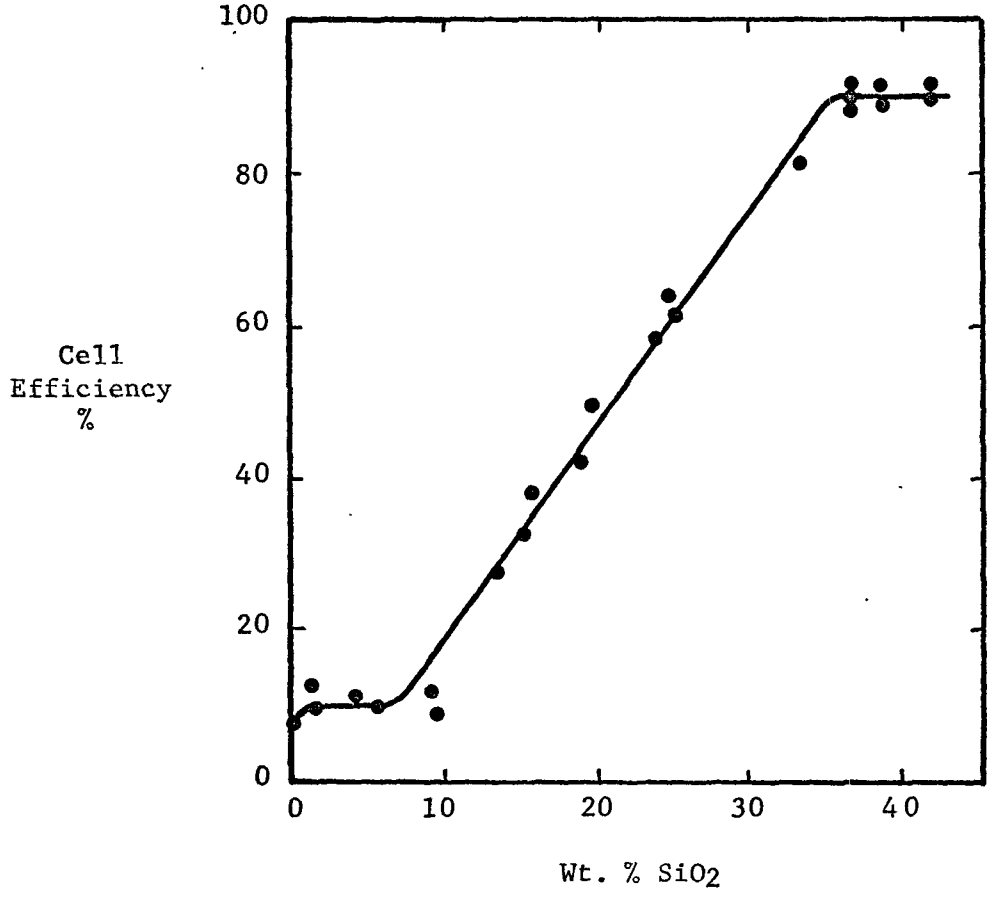

FIGURE 4 - CELL EFFICIENCY AS A FUNCTION OF SILICA CONTENT[34]

as the charge to radius ratio decreased, the mobility of the cation increased.

2.8 The Ionic Theory of Slag

2.8.1 Introduction

It is obvious from the preceding sections that the overwhelming evidence in favour of the ionic nature of slag was instrumental in re-shaping thought concerning the structure of slags. Regardless of the success of the molecular theory and any of its offspring, it was imperative to formulate a new theory or theories around the ionic species present in liquid slags. One of the major problems to be overcome was the designation of the actual form of each species in the slag.

2.8.2 The Ionic Theories

Ward[36] presents a thorough discussion of the ionic theory development commencing with the earliest attempt at a comprehensive ionic theory by Herasymenko[37], who attempted to interpret acid slag behaviour from the concept of a completely ionized slag. The dissociation of silica slags was postulated to occur according to:

$$2SiO_2 = Si^{4+} + (SiO_4)^{4-} \qquad (2.27)$$

This was perhaps the first and last attempt to rationalize the existence of free silicon ions in slag, and this assumption was instrumental in the non-acceptability of the theory. Temkin[38] introduced the first realistic approach to the consideration of slag-metal behaviour when he studied basic slags in which he said the highly charged and small ionic radius ions such as silicon, aluminum and phosphorus could only exist

as complexes, the simplest being SiO_4^{4-}, PO_4^{3-} and AlO_3^{3-} respectively. In basic slags, when the basic oxide content exceeds the orthosilicate composition, free oxygen ions, O^{2-}, are present along with the free metal ions of the basic oxides, Ca^{2+}, Mg^{2+}, Mn^{2+} and Fe^{2+}. Temkin treated the ionic solutions of slags as ideal, so that the activity of a basic oxide such as FeO was defined as:

$$a_{FeO} = N_{Fe^{2+}} \cdot N_{O^{2-}} \qquad (2.28)$$

where,

$$N_{Fe^{2+}} = \frac{M\ Fe^{2+}}{\Sigma\ M_{cations}} \quad \text{and} \quad N_{O^{2-}} = \frac{M_{O^{2-}}}{\Sigma\ M_{anions}}$$

$M_{Fe^{2+}}$ and $M_{O^{2-}}$ are the number of moles of free iron ions and free oxygen ions present, respectively. For a binary solution containing SiO_2, the mole fraction of the cation is always 1, thus the oxide activity is $N_{O^{2-}}$. This ideal approach was successful in explaining freezing point depression for dilute solutions of inorganic salts, but the concept of a highly concentrated ionic solution in which the ions are randomly oriented and in which no association occurs was sufficiently improbable to suggest a non-ideal treatment. Herasymenko and Speight[39] initiated the use of non-ideal behaviour in slag and represented the activity of an ion by:

$$a_{Fe^{2+}} = f_{Fe^{2+}} \cdot N_{Fe^{2+}} \qquad (2.29)$$

$f_{Fe^{2+}} \equiv$ activity coefficient for iron ion, dependent on overall slag composition

$a_{Fe^{2+}} \equiv$ activity of the iron ion in the slag

The Herasymenko and Speight formulation was successful in that it achieved a working empirical relationship between the equilibrium constant and the slag composition for phosphorus transfer. Flood et al.[40,41] went beyond this empirical relationship and obtained a truly constant "equilibrium constant" which did not vary with slag composition. This treatment involves the use of "electrically equivalent fractions":

$$N_M = \frac{v\, N_M^{v+}}{N_M^{+} + 2N_M^{2+} + 3N_M^{3+} + \ldots} \qquad (2.30)$$

$N_M \equiv$ electrically equivalent fraction for metal cation of charge v+

$N_M^{+}, N_M^{2+}, N_M^{3+} \ldots N_M^{v+} \equiv$ moles of metal cations with charges +, 2+, 3+, ... v+.

2.9 Physico-Chemical Properties from the Ionic Theory

Both the physical (density, surface tension, conductivity and viscosity) and chemical (reactivity) properties of slags have been interpreted from the concept of interionic forces attributed to Pauling[42]. Pauling introduced a scale representing the relative attraction of atoms for electrons in any chemical bond from which the degree of ionic or covalent bonding between two elements could be established. Slag systems are concerned with the cation-oxygen attraction which generally governs the polymerization of such melts. This ion-oxygen attraction has been estimated by the force of attraction between two point charges separated by distance r:

$$I = \frac{2Ze^2}{r^2} \qquad (2.31)$$

I ≡ ion-oxygen attraction

Z ≡ valence of cation

e ≡ charge on one electron

r ≡ internuclear distance between cation and oxygen ion

From these considerations, ions such as Si^{4+}, Al^{3+}, P^{5+} and Fe^{3+} which have high charges and low radii, form essentially covalent bonds with oxygen and are referred to as "network formers".

The physical properties of the slag depend to a large extent on the degree of polymerization of the simplest silicate anion, SiO_4^{4-} (29-31,43-46) which itself is dependent upon the attraction between oxygen ions and other cations in the melt. This interionic force treatment is useful in interpreting many physical and chemical properties in slag systems. However, it is based on coulombic attraction between two point charges, and is inadequate for more complex ions such as Fe^{2+} which are known to have directional charge shells(47).

C. ELECTROCHEMISTRY OF SOLID AND LIQUID SOLUTIONS

2.10 Introduction

The first section was concerned with the description and restrictions of electrolytic solutions, and the application of reversible electrochemical potential to the measurement of fundamental properties of the solution. Particular emphasis was on aqueous solutions at room temperature, principally because of the abundance of data available. However, the same principles apply unconditionally to salt and oxide systems[30], both fused and solid, at high temperatures. The use of high temperatures reduces the significance of gaseous overpotentials, but introduces difficulties not experienced at low temperatures[48]. The reversibility of high temperature electrochemical reactions cannot be as readily determined as it can be for systems carried out at room temperature but can only be inferred from the cell characteristics. Two of the main problems experienced at high temperatures are the designation of the proper electrochemical reaction occurring, and the occurrence of simultaneous side reactions.

The position of the electrode, the interchanging of electrodes and stirring conditions should not alter the emf of a truly reversible cell. The cell equilibrium should be reached in a short time and should be reproducible by reversing the direction of the temperature change. The choice of electrodes is limited generally to high melting point, unreactive metals, and non-metals such as platinum, molybdenum, tungsten, and silicon carbide and carbon. In certain instances it is necessary to utilize two electrodes of different material, constituting a thermocouple, which in some cases give rise to a considerable emf, large even in comparison to the

reversible emf[49,50]. Two electrodes of the same material, but at different temperatures, create a thermal emf which also must be accounted for[51]. Although not many high temperature reactions actually meet the requirements of a reversible electrochemical reaction, once the reversibility of a reaction has been established much useful thermodynamic information can be obtained.

2.11 Electrochemistry of Solid Electrolytes

2.11.1 Ionic Conductors

The mechanism of electrical conductivity in ionic crystals is closely related to the mechanism of diffusion[52] and is described as occurring by two alternate methods contributed by Frenkel[53] and Schottky[54].

Frenkel points out the necessity of stoichiometric composition in ionic compounds in order to satisfy electroneutrality, and that conduction takes place by one of two methods:

(a) The cations occupy interstitial spaces in the lattice and can move by means of their empty normal lattice sites, resulting in cationic conduction (examples are AgCl, AgBr, $AgNO_3$).

(b) The anions occupy the interstitial positions and conduction occurs by anion movement by means of their normal lattice sites (examples are PbF, BaF_2, $BaCl_2$).

Schottky suggests that equivalent numbers of cations and anions occupy interstitial positions leaving an equivalent number of vacant lattice sites which results in equal anion and cation conduction.

Frenkel and Schottky type oxides are: MgO, CaO, SrO_3, Sc_2O_3, Y_2O_3, La_2O_3, ThO_2, HgO, Al_2O_3, GaO_3, $CaSiO_3$, Al_2SiO_3, Al_2SiO_5, GeO_2, Sb_2O_3,

Zr_2O_3. These oxides are characterized by having anion or cation vacancies, or both.

2.11.2 Semi-Conductors

As seen above, ionic conductors transport current by means of ionic movement, but there is another class of non-metallic conductors, known as semi-conductors, in which electrons carry the majority of the current. Wagner[55] devised a model to explain the various diffusion mechanisms resulting in the electrical conductance of semi-conductors, based on a non-stoichiometric composition creating a metal excess or metal deficit. In metal deficit oxides, some metal ion lattice sites are vacant and electroneutrality is satisfied by an equivalent number of lattice metal ions existing in a higher oxidation state, which act as electron sites and are called positive holes. This type of oxide is known as a p-type semi-conductor and is an electron acceptor with conduction occurring by the migration of positive holes. The dependence of conductivity on oxygen pressure is given by:

$$\sigma_\theta = k_1 p_{O_2}^{1/m} \qquad (2.32)$$

$\sigma_\theta \equiv$ conductivity of semi-conductor

$k_1 \equiv$ constant

$m \equiv$ constant depending on the type of defect

The metal excess oxides exist either as a completely filled lattice with interstitial metal ions or as a lattice with vacant anion sites, with electroneutrality in both cases being maintained by electrons

in the lattice. This oxide is an n-type semi-conductor and is an electron donor with conduction occurring by electron migration. The dependence of conductivity on oxygen pressure is given by:

$$\sigma_e = k_2 pO_2^{-1/n} \qquad (2.33)$$

2.11.3 Auxiliary Electrolytes

For many important oxide systems it is impossible to establish a reversible electrochemical cell since the oxide electrolytes do not exhibit solely ionic transport, as indicated above. The total conductivity of an oxide can be made up of three components, one ionic and two electronic:

$$\sigma_t = \sigma_{ionic} + \sigma_e + \sigma_{\oplus} \qquad (2.34)$$

$\sigma_t \equiv$ total conductivity

$\sigma_{ionic} \equiv$ ionic contribution to conductivity

$\sigma_e, \sigma_{\oplus} \equiv$ electronic contribution to conductivity

In order to measure true reversible emf's of a cell, the total conductivity must be solely ionic, i.e. $\sigma_t = \sigma_{ionic}$. In order to measure the standard free energy change of the reaction

$$Fe + Cu_2O = 2Cu + FeO$$

using the reversible emf technique, it might first be thought that an electrochemical cell may be created, which is represented schematically by:

$$Fe \mid FeO \mid Cu_2O \mid Cu$$

where the bars are used to designate phase boundaries within the cell.

In fact the standard free energy change of this reaction is not measured by this type of cell since both Cu_2O and FeO are semi-conductors, and current is passed through the cell by a leakage path creating a non-reversible cell. Such systems are studied using auxiliary electrolytes which conduct current by ionic transport only: such an electrolyte is zirconium oxide doped with calcium oxide in which mobility of the cations is much less than the mobility of the anions, since essentially all the cation sites are filled and a substantial fraction of oxygen lattice sites are vacant[56]. Steele and Alcock[57] and Lasker and Rapp[58] determined the safe P_{O_2} operation zone for CaO doped ZrO_2 and Y_2O_5 doped ThO_2 respectively, when only oxygen ion transport is important.

For systems involving both ionic and electronic conduction, where the electronic conduction is not large, a correction can be made[59] to the experimental emf, ε such that the free energy of formation of compound AX is:

$$\Delta G_{AX} = -n_A F\varepsilon - \frac{n_A}{n_X} \int_{\bar{G}_{X_1}}^{\bar{G}_{X_2}} t_e \, d\,\bar{G}_X \qquad (2.35)$$

$t_e \equiv$ transference no. for electronic conduction

$n_A, n_X \equiv$ absolute value of the valence of metal A and non-metal X

$\bar{G}_{X_1}, \bar{G}_{X_2} \equiv$ partial molar free energies of non-metal X at the two electrodes

2.11.4 Use of Solid Electrolytes in Determination of Thermodynamic Properties

Roeder[60] verifed the anionic conduction of CaO stabilized ZrO_2 and used this electrolyte to determine the free energy of formation of

wustite with varying nickel content. Rapp and Maak[61] studied the thermodynamics of copper-nickel alloys using CaO doped ZrO_2 electrolyte. Muan[62-65] determined activities in Pt-Ni, Pt-Fe, Pt-Co, Pd-Ni, Pd-Fe and Pd-Co alloys by reversible emf and equilibrium measurements. They used an auxiliary electrolyte and equilibrated the alloys with pure NiO, FeO and CoO oxides at known oxygen pressures. The reversible cell is shown schematically:

$$(A - B) + BO \mid ZrO_2 + CaO \mid B + BO \qquad (2.36)$$

A is Pt or Pd and B is Ni or Co

Since oxygen ions carry all the current through the auxiliary electrolyte, cells of this type are oxygen concentration cells, whose individual electrode reactions are:

$$\tfrac{1}{2} O_{2_{alloy}} + 2e = O^{2-} \qquad \text{cathode}$$

$$O^{2-} = \tfrac{1}{2} O_2^{\circ} + 2e \qquad \text{anode}$$

$$\tfrac{1}{2} O_{2_{alloy}} = \tfrac{1}{2} O_2^{\circ}$$

$$\Delta G = RT \ln \left(\frac{P_{O_2}^{\circ}}{P_{O_{2_{alloy}}}} \right)^{1/2}$$

$P_{O_2}^{\circ} \equiv$ equilibrium pressure of B + BO

$P_{O_{2_{alloy}}} \equiv$ equilibrium pressure of (A - B) + BO

$$\therefore \varepsilon = - \frac{RT}{nF} \ln a_B$$

$a_B \equiv$ activity of the metal B in the A - B alloy

Fischer[50] worked with emf cells of the type:

$$Pt \mid Me_2O_3 + MeO \mid Me_2O_3 \mid Pt \qquad (2.37)$$

MeO is FeO or MgO and Me_2O_3 is Al_2O_3

The measured emf was plotted as a function of the FeO content of the $FeO.Al_2O_3$ phase, and the results were interpreted in terms of phases present in the FeO - Al_2O_3 system, and a new phase diagram was drawn. From the emf results the author determined the free energy of formation of the $FeO.Al_2O_3$ spinel by assuming that only cationic conduction was important, and that the transfer of aluminum ions results in spinel formation, therefore:

$$\Delta G = - (t_{Al} - t_{Fe}) \, n \, F\varepsilon \qquad (2.38)$$

t_{Al} and t_{Fe} are the transference numbers for Al and Fe respectively, and $(t_{Al} - t_{Fe})$ represents the fraction of current carried by the aluminum ions. The author estimated $(t_{Al} - t_{Fe})$ to be between 0.2 and 0.4, which indicates that the aluminum ions conduct more current than the ferrous ions, which is not consistent with earlier considerations based on ion size and charge.

2.12 Electrochemical Properties of Molten Electrolytes

One of the first systematic studies of the electrochemical properties of molten slags was undertaken by Chang and Derge[49], utilizing

the molten electrolyte systems $CaO.SiO_2$ and $CaO.Al_2O_3.SiO_2$. After considerable searching, a suitable electrode combination was found which yielded reproducible, reversible emf measurements. The slags were melted in graphite crucibles which also served as one electrode, and a silicon carbide rod immersed in the slag served as the second electrode. The graphite crucible electrode was found to be the cathode and the silicon carbide electrode the anode. They suggested that the only ions present were Ca^{2+}, Si^{4+}, and SiO_4^{4-}, and since the emf decreased with increasing CaO content, the Ca^{2+} ions did not participate in the reaction. They proposed several electrode reaction combinations, and by a process of elimination chose:

$$3Si^{4+} + 3Cgr + 12e = 3SiC \qquad \text{cathode}$$

$$3SiO_4^{4-} + 2SiC = 5SiO_2(\beta \text{ cristobalite}) + 2CO + 12e \qquad \text{anode}$$

$$6SiO_2(soln) + 3Cgr = SiC + 5SiO_2(\beta \text{ crist}) + 2CO \qquad (2.39)$$

The number of electrons involved in the reaction is 12, hence the experimental standard free energy for formation of reaction (2.39) was $\Delta G^\circ = -12F\varepsilon^\circ$, which agreed within 4.6% of the theoretical free energy of formation (determined from literature values for ΔG° for SiO_2, SiC and CO).

Sakagami and Matshushita[66] criticized the method of Chang and Derge since the thermal emf accounted for 80% of the total emf and since a cell reaction was devised to fit the emf results. These authors worked on the same system but were able to considerably reduce the thermal emf and showed the reaction to be more accurately represented by:

$$2SiO_2 + C = Si_{liquid} + SiO_2\ (\beta \text{ crist}) + CO + \frac{1}{2}O_2 \qquad (2.40)$$

Esin, Lepinskikh and Musikhan[64] determined the effect of hydrogen and nitrogen on the activity of silicon in carbon saturated iron by measuring reversible emf's of the cell:

$$Si_{solid} \mid (CaO.Ba_2O_3.SiO_2)_{liquid} \mid Fe, C, Si_{liquid} \qquad (2.41)$$

The cell represented by (39) is a silicon concentration cell, with the following electrode reactions:

$$2O^{2-}_{slag} + Si_{metal} = SiO_{2slag} + 4e \qquad \text{anode}$$

$$Si^{4+}_{slag} + 4e = Si_{alloy} \qquad \text{cathode}$$

$$Si_{metal} = Si_{alloy}$$

$$\therefore \ \ln a_{Si} = -\frac{4F\varepsilon}{RT}$$

For constant silicon compositions of 3.1 and 1.0 wt% in the Fe-C alloy the reversible emf was measured as a function of P_{H_2} and P_{N_2}. The temperature was 1250°C.

Schwerdtfeger and Engell[68,69] measured reversible emf's between electrodes of pure silicon, silicon alloyed in Fe, Co and Ni, and oxygen, which are represented by the sequence:

$$Pt, Si_{alloy} \mid CaO.SiO_2(liquid), SiO_2\ (solid) \mid O_2, Pt \qquad (2.42)$$

The overall reaction is the oxidation of silicon, thus,

$$\varepsilon = \varepsilon^\circ + RT \ln \frac{a_{Si}\ P_{O_2}}{a_{SiO_2}}$$

a_{Si} is the activity of silicon in the liquid alloy.

When pure silicon is the metal phase, $a_{Si} = 1$ and the measured reversible emf is then the standard reversible emf, ε°.

Schwerdtfeger[70] utilized a similar apparatus as above to measure the activity of lead in Pb-Pt and Pb-Pd alloys as well as the standard free energy of formation of PbO.

Feldman[71] attempted to determine silicon activities in carbon saturated iron at steelmaking temperatures by creating a silicon concentration cell utilizing mullite ($3Al_2O_3.2SiO_2$) as a solid electrolyte. The anode was silver saturated with silicon carbide, and the cathode was carbon saturated iron with varying amounts of silicon. Graphite rods made electrical contact to both electrodes, but the emf's obtained, although of the correct magnitude and sign, were non-reproducible due to the attack of the carbon saturated iron on the mullite electrolyte.

Sanbongi and Omori[72] measured activities of SiO_2 in the $CaO-SiO_2$ and $CaO-Al_2O_3-SiO_2$ systems by setting up concentration cells using a standard slag electrode and varying the SiO_2 content of the system investigated.

Sanbongi and Ohtani[73] initiated a series of electrochemical studies investigating the systems Fe-C, Fe-Si, Fe-Si-C, Fe-Mn and Fe-C-Mn, commencing with the determination of the activity of carbon in iron by using a concentration cell. The authors used a carbon saturated bath as the standard electrode, connected to an iron bath of varying carbon content by a carbide slag. The cell sequence is thus represented:

$$Fe\text{-}C_{alloy} \mid \text{Carbide Slag} \mid Fe\text{-}C_{sat'd} \qquad (2.43)$$

Thus the measured emf is related to the activity of carbon in the alloy phase by:

$$\varepsilon = - \frac{RT}{2F} \ln a_C$$

The ion valency, n, was determined by the authors to be 2.3 and they assumed that 2 was then the appropriate value to be utilized in subsequent activity calculations. From their results, the activity of carbon in iron was seen to be approximately equal to the mole fraction up to 0.04 N_C (1% C), but then a_C increased rapidly as N_C increased. Their results at 1550°C compared favourably with those of Chipman and Marshall[74] using P_{CO}/P_{CO_2} mixtures in equilibrium with carbon in iron.

Sanbongi and Ohtani[75] measured the activity of manganese in iron by using a concentration cell with pure manganese as the reference electrode, connected by a manganese slag to an Fe-Mn alloy, such that the cell sequence is:

$$\ominus \text{ Fe-Mn } | \text{ } SiO_2\text{-MnO-CaO.}M_gO \text{ } | \text{ Mn } \ominus \qquad (2.44)$$

As before, the measured emf is then:

$$\varepsilon = - \frac{RT}{2F} \ln a_{Mn}$$

$a_{Mn} \equiv$ activity of manganese in iron

From their results, the Fe-Mn binary was shown to be an ideal solution over the complete composition range.

Sanbongi and Ohtani[76] also measured the activity of silicon in iron by a similar method, using pure silicon as the reference electrode. In this case they determined the silicon valence to be 4.

Ohtani[77] measured the activity of silicon in molten Fe-Si-C alloys by a similar method. Their results are discussed in a later section, with reference to the present study.

Ohtani[78] also measured the activity of manganese in molten Fe-C-Mn alloys and his results were in disagreement with those of Schenck and Neumann[79] who used distribution equilibria data. It has been shown recently[80] that a preference is given to the results of Schenck and Neumann because of the possible interference of side reactions in the reversible emf experiments.

D. ELECTROCHEMISTRY OF SLAG-METAL REACTIONS

2.13 Introduction

Slag-metal systems consist of two immisible liquids with a reaction or transfer of matter occurring at the interface. This interchange of mass between an ionic liquid and a metallic liquid involves electron exchange, and to that extent an electrochemical treatment has been formulated for these interfacial reactions. Recently there has been a suggestion[81] that the solute can actually exist as ions in the metallic solvent, as in the case of carbon in iron.

This postulation is being tested by using the Hall Effect[82] and noting any concentration gradients occurring.

2.14 Displacement Reactions

Because of the ionic nature of the slag, the desulphurization of iron can be written:

$$[S] + (O^{2-}) = (S^{2-}) + [O] \qquad (2.45)$$

[ ] ≡ in liquid metal; ( ) ≡ in liquid slag; { } ≡ gas; < > ≡ solid

Equation (2.45) implies the direct collision between ions and atoms, but this is not necessarily so, for the overall reaction may be written in terms of its individual electrode reactions:

$$(O^{2-}) = [O] + 2e \qquad \text{anode}$$

$$[S] + 2e = (S^{2-}) \qquad \text{cathode}$$

The anodic and cathodic reactions occur simultaneously along the slag/metal interface to maintain electroneutrality. However, they are not

restricted to the same location at the interface. This is clear if the reaction:

$$2[Al] + 3(Fe^{2+}) = 3[Fe] + 2(Al^{3+}) \qquad (2.46)$$

is considered. A direct transfer of electrons between reacting species requires the simultaneous collision of five separate entities which is highly improbable, therefore an electrochemical reaction, occurring at different locations, is more likely.

Wagner[83] states that electrochemical reactions such as those above definitely occur at slag-metal interfaces, but whether their rate or the rate of direct exchange between atoms and ions controls the overall rate is questionable. He uses the expression for current density for the diffusion of ions under the influence of a concentration gradient and an electronic field, derived from the theory of absolute rates by Eyring[84], to describe the rate of the electrochemical reaction as:

$$n_i = k\, C_i^{(1-\alpha_i)} \qquad (2.47)$$

$n_i \equiv$ rate of the electrochemical transfer of component i

$k \equiv$ constant

$C_i \equiv$ concentration of i in the phase considered

$\alpha_i \equiv$ related to the symmetry of the energy barrier for diffusion (generally = 0.5)

The relationship of (2.47) may be applied to the deoxidation of iron by carbon[83]:

$$[C] + (FeO) = [Fe] + \{CO\} \qquad (2.48)$$

If (2.48) is chemically controlled, the rate of CO evolution (when the single step, direct exchange between species in the slag and metal phases predominates) ignoring the reverse reaction is written:

$$n_{CO} = k\, C_{Fe} \qquad (2.49)$$

$n_{CO} \equiv$ rate of CO evolution

C_{Fe} is concentration in the slag phase

If, however, an electrochemical mechanism is operable at the slag/metal interface, that is

$$[C] + (O^{2-}) = \{CO\} + 2e \qquad \text{anode}$$
$$(Fe^{2+}) + 2e = [Fe] \qquad \text{cathode}$$

then the rate of CO evolution is predicted by (2.47)

$$n_{CO} = k' C_{Fe}^{(1-\alpha)} \qquad (2.50)$$

Thus, if chemical control predominates, it is easy to determine whether an electrochemical or a chemical reaction is occurring simply by determining the power dependence of the rate of CO evolution on the concentration of iron in the slag. Wagner[83] says a fractional dependence of rate on concentration is an indication of electrochemical control.

2.15 Sulphur Transfer

Ramachandran, King and Grant[85] studied the desulphurization of iron and found the sulphur removed was equivalent to the CO evolved and the amount of iron, silicon and aluminum transferred from the metal to

the slag, i.e. :

$$2n_S = 2n_{Fe} + 4n_{Si} + 3n_{Al} + 2n_{CO} \qquad (2.51)$$

$n_i \equiv$ rate of transfer or evolution in mole/sec on component i

The mechanism is interpreted in terms of electrochemistry, with the electode reactions being,

$$[S] + 2e = (S^{2-}) \qquad \text{cathode} \qquad (2.52)$$

$$\begin{aligned} [Fe] &= (Fe^{2+}) + 2e \\ [Si] &= (Si^{4+}) + 4e \\ [Al] &= (Al^{3+}) + 3e \\ (O^{2-}) + [C] &= CO + 2e^* \end{aligned} \qquad \text{anode} \qquad (2.53)$$

Ramachandran and King[86] stated that in the later stages when [S] was essentially constant, the electrochemical reactions were:

$$C + (O^{2-}) = CO + 2e \qquad \text{anode} \qquad (2.54)$$

$$\begin{aligned} [S] + 2e &= (S^{2-}) \\ (Fe^{2+}) + 2e &= [Fe] \\ (Si^{4+}) + 4e &= [Si] \\ (Al^{3+}) + 3e &= [Al] \end{aligned} \qquad \text{cathode} \qquad (2.55)$$

---

* The authors said that this reaction was ill defined since the carbon source could be either carbon dissolved in the iron, or the graphite crucible itself with a local cell mechanism taking place

Assuming chemical reaction control after the failure of a transport control mechanism, the authors utilized (2.47) to determine the power dependence of the rate of CO evolution on the sulfur distribution:

$$\dot{n}_{CO} = k \left[\frac{[S]}{(S)}\right]^{(1-\alpha)} \qquad (2.56)$$

The value of $(1-\alpha)$ was found to vary between 0.4 and 0.55 and was said to be indicative of an electrochemical mechanism.

Baak and King[43] attempted to clarify the source of carbon in the electrochemical reaction (*) by studying desulphurization in alumina crucibles using a carbon free sulphur-silver alloy as the metal phase, and a sodium borate slag. A graphite rod was inserted into the slag, and a Ni rod was inserted into the metal and connected externally to the carbon rod. In this manner, only the local cell reaction could occur, and it could be measured by observing the current flow simultaneously with the sulphur transfer. Although the results have not been published, the authors said that the sulphur transferred according to the Faradayan relationship was close to the chemically determined sulphur transfer, indicating the presence of the local cell mechanism, according to:

$$\langle C_{gr} \rangle + (O^{2-}) = \{CO\} + 2e \qquad \text{anode} \qquad (2.57)$$

$$[S] + 2e = (S^{2-}) \qquad \text{cathode} \qquad (2.58)$$

The possibility exists in this study that the cell was actually an electrolytic cell, with the Thompson Effect[51] producing a thermal emf in nickel, creating an electron flow from the hot end to the cold end.

The direction of current flow in the carbon electrode is not known, but the combination of the two electrodes could produce a current and cause electrolytic transfer of sulphur.

Ward and Salmon[87] noted the similarity between the activation energies for sulphur and silicon transfer and interpreted this in terms of sulphur replacing the oxygen combined with silicon ions. In acid slags having little, if any, free O^{2-} ions present, the large S^{2-} ions (3.68Å) have difficulty replacing the O^{2-} (2.80Å), thus the transfer of sulphur would be enhanced by the transfer of silicon to the metal, leaving free O^{2-} ions having a "transient existence" at the slag/metal interface, providing an easier exchange with the sulphur in the iron.

In a later paper[88] the authors attempted to enhance the sulphur removal by applying a potential between a carbon anode in the slag and the metal cathode, causing electrolysis of the slag electrolyte. The electrochemical reactions which could occur were postulated to be:

$$2[S] + 4e = 2\,(S^{2-})$$
$$(SiO_4)^{4-} + 4e = [Si] + 4\,(O^{2-})$$
$$\tfrac{4}{3}\,(AlO_3)^{3-} + 4e = \tfrac{4}{3}\,[Al] + 4\,(O^{2-}) \qquad \text{cathode} \qquad (2.59)$$
$$2\,(Fe^{2+}) + 4e = 2\,[Fe]$$
$$2\,(Mg^{2+}) + 4e = 2\,\{Mg\}$$
$$2\,(Ca^{2+}) + 4e = 2\,\{Ca\}$$

$$2\,(O^{2-}) + 2C = 2\,\{CO\} + 4e$$
$$2\,(S^{2-}) = \{S_2\} + 4e \qquad \text{anode} \qquad (2.60)$$
$$4\,(SiO_4)^{4-} + 2C = 2\,\{CO\} + 2(Si_2O_7)^{6-} + 4e$$

They found that the sulphur removal could be increased and the low current efficiencies were obviously due to the many parallel reactions occurring.

2.16 Silica Reduction

2.16.1 Controlling Mechanism

Slag-metal reactions have long been the source of many studies to determine the controlling mechanism. The absolute reaction rate theory indicates that at high temperatures the approach to equilibrium at the reaction site is much faster than the transport rates to or from this site. This appears to be the case for most slag-metal reactions, but reactions such as the transfer of sulphur and silicon are so slow that a chemical control mechanism is not eliminated.

Fulton and Chipman[89] determined the activation energy for the reduction of silica by carbon in iron to be 130 Kcal/mole, and virtually independent of stirring. They concluded that the controlling mechanism was a step, or steps, in the chemical reaction, and a likely one was the breaking of the Si-O bonds or the slow removal of oxygen by carbon, either at the slag/metal interface or the metal/crucible interface. Ward[90] cites the Eyring approximation for the energy required for the breaking of four Si-O bonds of the tetrahedrally co-ordinated silicon ion to be 104 Kcal/mole and says, therefore, an activation energy in this vicinity would indicate chemical control. Schuhmann[91] in a discussion of the data of Fulton and Chipman, said that their results did not necessarily preclude the effect of transport control, since the slowness of the reaction could be due to the transport of oxygen across the liquid metal boundary layer at the slag/metal interface.

Turkdogan et al.[92] considered their results as indicative of chemical control when CO gas was impinged upon the slag/metal interface:

$$(SiO_2) + 2[C] = [Si] + 2\{CO\} \qquad (2.61)$$

Reaction (2.61) indicates a three phase reaction at an interface, which is impossible to realize, so they interpreted their results in terms of adsorption isotherms with the rate controlling step being the desorption of silica at the slag/metal interface to form a vacant site plus silicon and oxygen in the metal. They also determined that in the absence of CO impingment at the slag/metal interface, the rate of silicon transfer was greatly decreased, possibly because a transport mechanism such as the oxygen transfer from the slag/metal interface to the walls of the graphite container might be rate controlling.

Rawling and Elliot[93] investigated the kinetics of silica reduction by two experimental techniques. In the first case, the carbon was supplied by dissolved carbon in the iron, resulting in the formation of CO gas, according to (2.61). In the second case, a concentration cell was formed in which silicon transfer occurred but no CO gas was formed; here an electrochemical reduction was operative, with silicon being anodically consumed at the high silicon side of the cell and silicon being cathodically deposited at the low silicon side, according to:

$$Si_{Fe,Si,C} = (Si^{4+}) + 4e \qquad \text{anode}$$

$$(Si^{4+}) + 4e = Si_{Fe,\,C} \qquad \text{cathode}$$

The rate of silicon transfer in the second case was two to three times the rate in the first case, leading the authors to the conclusion that the slow step lie in the formation of CO gas. This slow step was said to be the diffusion of oxygen in the metal phase to the gas/metal interface and was strongly supported by the experimental rate curves, and an activation energy of 110 Kcal/gm mole (between 1525° and 1600°C). This high activation energy was shown to consist of several temperature dependent terms in the rate constant. At temperatures greater than 1600°C, the activation energy rose rapidly to 200 Kcal/gm mole, and the authors said that at higher temperatures the transport of oxygen might become so rapid that a chemical step, possibly the dissociation of the complex silicate ions, might control the rate.

Sharma[94] studied the reduction of solid silica by carbon in iron and concluded that the transport of oxygen in the liquid iron was the rate limiting step, yielding an activation energy of 75 to 90 Kcal/mole.

Grimble[95] found that the rate of reduction of silica from high silica slags was independent of the stirring rate and yielded an activation energy of 125 Kcal/mole, and concluded the reaction rate was chemically controlled. No evidence was given for the reaction mechanism, but the author stated that the theory that SiO is an intermediate reaction product was supported.

Wojcek[96] studied the kinetics of silica reduction using 3mm quartz and pyrex capillary tubing, which were inserted into baths of iron - carbon and held for various times. Concentration profiles of silicon were determined by microprobe analysis and were compared to calculated curves based on a diffusion mechanism. The results indicated chemical control for the

reduction of solid quartz and a diffusion control mechanism for the reduction of pyrex.

2.16.2 Local Cell Mechanism

Wagner[83] raised the question of the electrochemical contribution to chemical reaction at a slag/metal interface and also raised the point of electrochemical reduction occurring at a second interface, the slag/crucible interface, in a local cell mechanism. It was mentioned earlier that Baak and King[3] studied the local cell effect in sulphur removal. Grimble[4, 95] investigated the local cell effect in the reduction of silica by carbon in iron, using graphite crucibles. He performed kinetic experiments on two cells, one where the local cell reaction could not occur and another where the local cell reaction was said to occur by:

$$2(O^{2-}) + 2\langle C\rangle = 2\{CO\} + 4e \qquad \text{slag/crucible}$$

$$(Si^{4+}) + 4e = [Si] \qquad \text{slag/metal}$$

The local cell effect appeared to predominate at lower temperatures (1370°C) and became less, until at 1530°C there was no local cell contribution to the overall kinetics.

CHAPTER 3

EXPERIMENTAL APPARATUS

3.1 Introduction

The experimental portion of this project was performed in three primary stages. The first stage involved the creation of a Faradayan cell, which was used to illustrate the existence of a "local cell" reaction when the reduction of silica by carbon in iron occurred in graphite crucibles. The second stage involved two sets of kinetic experiments, one where the "local cell" reaction could occur and one where it could not occur, designed to illustrate the magnitude of the "local cell" reaction. The third stage involved the creation of various reversible electromotive force cells, based on the local cell effect, which were utilized to measure the standard free energy change of the reaction:

$$Si + 2CO = SiO_2 + 2C$$

and to measure thermodynamic properties in the iron-silicon and iron-carbon-silicon systems.

The equipment necessary for the experimental work is presented in the subsequent sections of this chapter.

3.2 Furnace Assembly

The majority of the experimental work for this project was performed on a vertically wound molybdenum resistance furnace. Several furnace designs were tried, but the one depicted in Figure 5 was chosen as the most satisfactory.

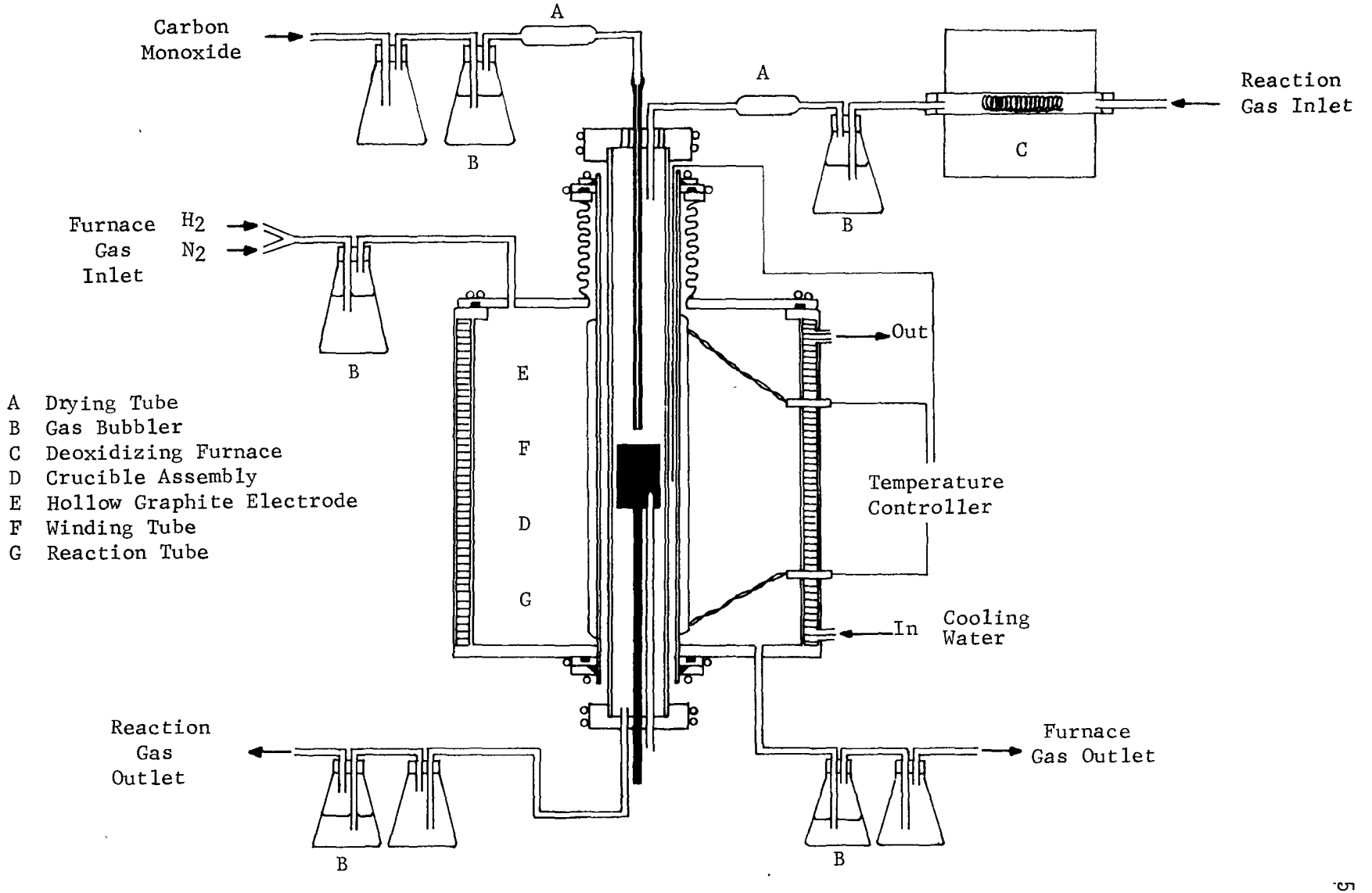

FIGURE 5- SCHEMATIC DIAGRAM OF THE FURNACE ASSEMBLY

The furnace had a double walled outer jacket which permitted water cooling so that the outer wall was kept essentially at room temperature. The removable furnace top plate was fitted with a water cooled "O" ring for gas tightness with the furnace body. The top plate was also fitted with a 6" long, single ply stainless steel bellows, in order to allow expansion and contraction of the refractory winding tube during the heating and cooling cycle. The top bellows had a water cooled "O" ring assembly to maintain gas tightness on the winding tube. A gas entrance was located on the top plate to allow the introduction of the protective furnace gas, which was a 50:50 mixture of dried nitrogen and hydrogen. The furnace bottom plate was welded to the furnace body and had a water cooled "O" ring assembly to maintain gas tightness on the winding tube. The furnace gas outlet was located on the bottom plate.

The furnace tube was MV30 mullite (McDanel Refractory Co.) with dimensions 25" long x 3 1/4" O.D. x 3" I.D. and was wound with approximately 110' of 0.050" molybdenum wire over a 13" length, symmetrically located along the length of the tube. The molybdenum resistance wire was wound on the tube by means of a lathe, using 10 turns per inch for 2 inches, 9 turns per inch for 2 1/2 inches, 8 turns per inch for 4 inches, 9 turns per inch for 2 1/2 inches and 10 turns per inch for 2 inches, over the 13" length. In this manner, a flat temperature profile was enhanced by adding more heat to the ends of the winding. The molybdenum winding was completely covered by a 1/8" thick layer of alumina cement. The electrical extension leads consisted of molybdenum wire wound in triplicate to reduce resistance and were connected to the power supply by electrical connectors passing through the double walled furnace body. The insulation

in the electrical connectors was provided by Sauerisen cement.

The furnace body was filled with two layers of high temperature insulating brick, to within 1" of the winding tube. The outside layer was capable of withstanding 1100°C (A.P. Green G20) and the inside layer could withstand 1760°C (A.P. Green G32). The space between the inside layer of insulating brick and the furnace tube was filled with alumina bubbles ranging in size from approximately 1/64" to 1/8".

The working tube was MV30 mullite with dimensions 30" x 2 3/4" O.D. x 2 1/2" I.D. and was fitted top and bottom with two gas tight water-cooled aluminum caps. The top cap was equipped with a sight hole (a quartz plate cemented onto a 3/4" hole, for continuous observation of the melt), a 5/8" diameter stoppered hole for taking samples of the melt and for making additions to the melt, a gas inlet for introduction of the reaction atmosphere (nitrogen or argon) and a central hole fitted to contain a 1/2" swagelock fitting which was electrically insulated from the aluminum cap by a teflon bushing. The swagelock fitting contained teflon ferrules, which maintained a gas tight seal on a 1/2" electrode or test piece and allowed random raising or lowering of the electrode or test piece. The internal diameter of the teflon ferrule could be varied from a maximum of 1/2" diameter to any lower diameter if it were desired to change the size of the electrode or test piece without any major modifications.

The bottom cap was similarly fitted with a centrally located 1/2" swagelock fitting containing teflon ferrules, and was electrically insulated from the cap by a teflon bushing. In this case, the swagelock was used to move the crucible assembly into or out of the furnace hot zone. The bottom cap also contained a reaction gas outlet and an eccentric 1/2"

swagelock with teflon ferrules. This eccentric swagelock was used to raise or lower a 3/8" diameter mullite thermocouple protection tube which contained a Pt-Pt/13% Rh thermocouple. The complete crucible assembly and bottom cap were supported by the tight "O" ring seal on the working tube. The working tube was held secure by a two pronged clamp which was attached to the furnace support, and by an aluminum rod which could be swung into place under the bottom cap to support the complete assembly.

A Pt-Pt/13% Rh thermocouple in a 1/8" diameter 2 hole alumina insulator was placed between the working tube and the furnace tube so that the thermocouple tip reached to the center of the 13" long resistance winding. This thermocouple was used to control the temperature.

With this furnace design the furnace could be operated safely at temperatures approaching 1600°C for considerable periods of time.

3.3 Temperature Control

Initially the temperature was controlled by a transistorized, proportional on-off control unit which was found to be inadequate for good temperature control. As an alternate method, a saturable core reactor unit designed by Honeywell Corporation was utilized. In this control system a signal from the control thermocouple was fed to a Honeywell current proportioning controller, (model 105R212), which sent out a low level signal to a Brown magnetic amplifier. The amplifier boosted the signal from the primary controller to a high level output to supply continuous electrical control of a saturable core reactor, (Hammond Reactor #64576, rated at 3KVA, 240 volts and 60 cycles), which supplied proportioning current to the furnace load. The temperature was raised slowly by means of a 240 volt

A.C., 30 amp powerstat, until the power input was 100%.

3.4 Induction Furnace

In order to facilitate the experimental procedure a furnace was constructed using a high frequency induction unit, (300 KC), as the power supply. This unit, shown in Figure 6, was used to prefuse the metal starting material in kinetic and equilibrium studies. This type of heating assembly is characterized by short heating and cooling periods. The heating assembly consisted of a 1/4" copper tubing wound for a length of 4" with 11 turns around a 25" x 3" O.D. x 2 3/4" I.D. vycor tube, open both ends. The heating length was insulated by a 10" x 8" O.D. x 7" I.D. transite tube filled with alumina bubbles. Gas tightness was maintained by two rubber stoppers, top and bottom. The top stopper was fitted with a sample hole, a pyrometer sight hole,a cooling coil, a gas entrance tube and a centrally located 1/2" swagelock fitting to allow raising or lowering of an electrode or test piece. The bottom stopper was fitted with a gas exit tube, an eccentric swagelock fitting to fit a thermocouple protection tube and a central 1/2" swagelock fitting to raise or lower the crucible assembly. The temperature was controlled by manual adjustment of the high frequency power supply.

3.5 The Carbon Monoxide Measuring Furnace

A method of measuring the volume of carbon monoxide gas evolved in a chemical reaction has been developed[94], utilizing a high frequency induction unit. A similar apparatus was used in this investigation, and is shown in Figure 7. The silica reaction vessel was connected to the capillary section by a gas tight teflon reducer. When the reaction proceeded

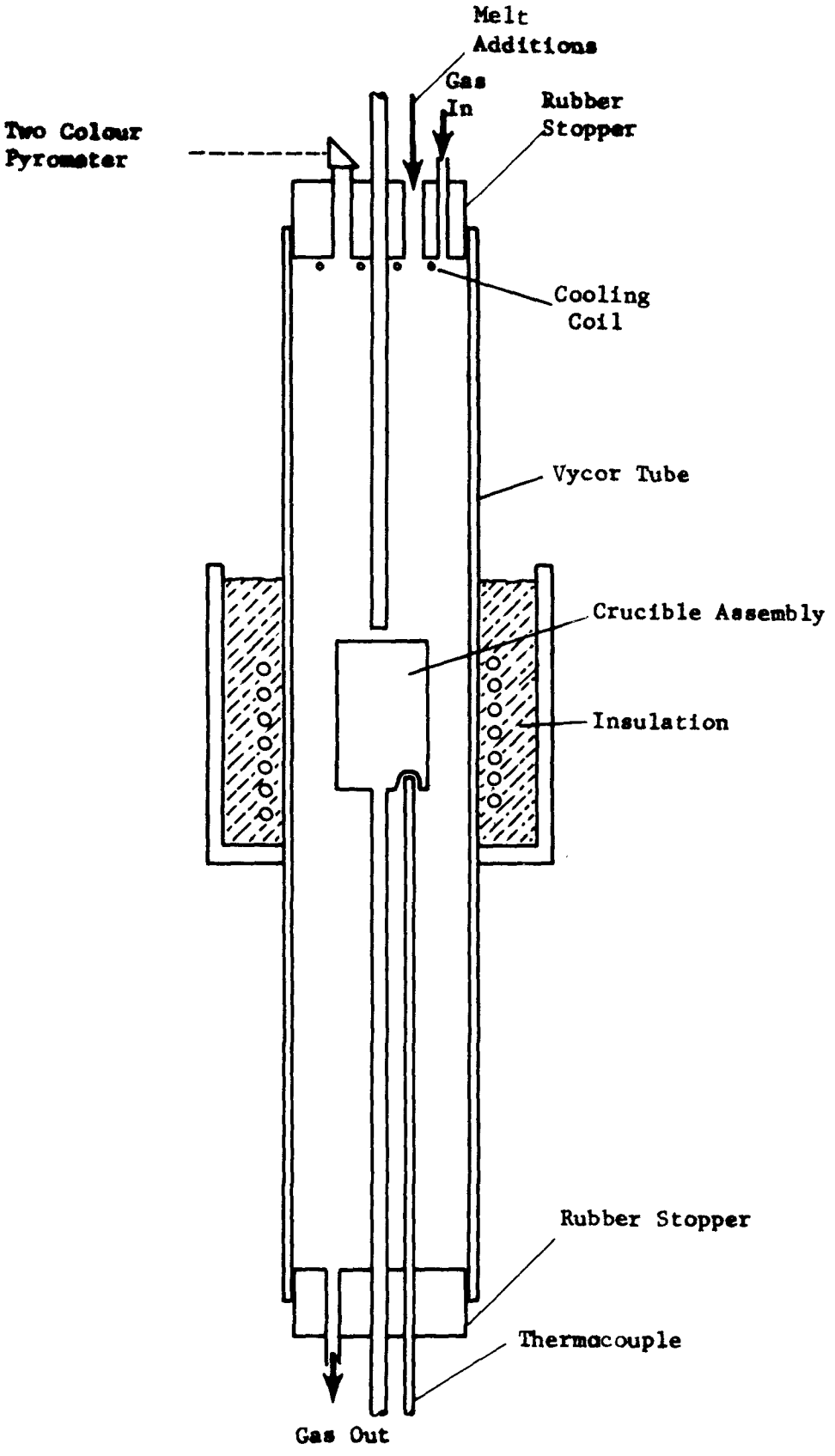

FIGURE 6 - SCHEMATIC DIAGRAM OF THE INDUCTION FURNACE

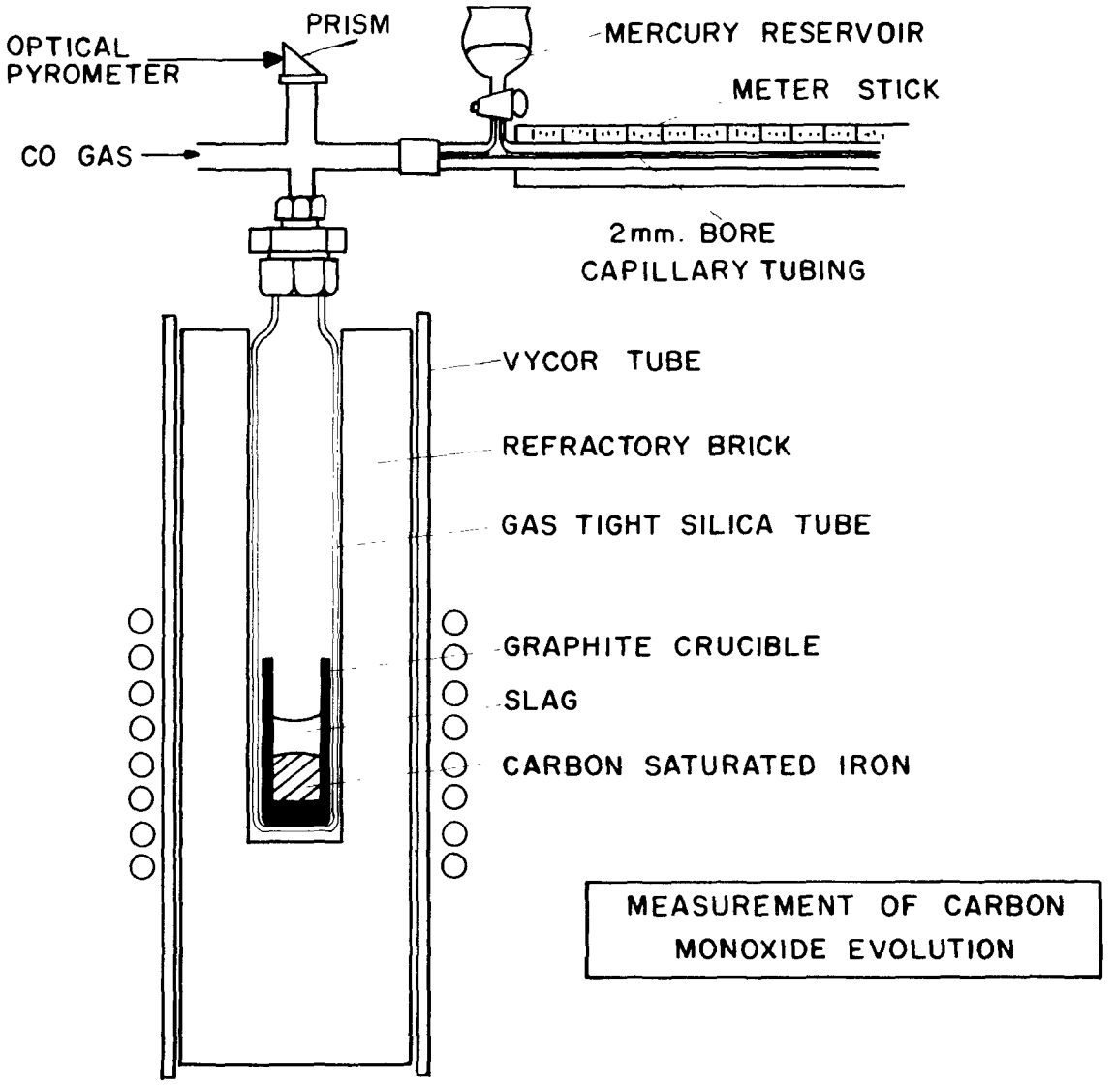

FIGURE 7 - SCHEMATIC DIAGRAM OF THE CARBON MONOXIDE MEASURING FURNACE

CO was evolved, and a pellet of mercury was introduced into the capillary of known diameter from the mercury reservoir. The volume of CO produced was measured by the volume displaced by the mercury droplet. The temperature was measured by a two-colour optical pyrometer sighting through the top prism or by a Pt-Pt/13% Rh thermocouple located at the side of the crucible.

3.6 Carbon Resistance Furnace

Several kinetic experiments were performed in a carbon resistance furnace which is described elsewhere[97].

3.7 Gas Deoxidizing Furnace

The reaction gas for the emf experiments was deoxidized in a small tubular furnace wound with nichrome resistance wire, capable of reaching 600°C. The tube was filled with copper turnings so the oxygen potential of the gas passing through could be maintained between 10^{-13} and 10^{-19} atmospheres, at 400° and 600°C respectively.

3.8 Electromotive Force Measurement

The electric potentials were initially measured with a Croydon P3 null type potentiometer. However, this instrument proved too sensitive to voltage changes and had the added disadvantage that the voltage fluctuations could not be determined. More success was attained with a Hewlett Packard 427A voltmeter, which is a vacuum tube voltmeter with an input impedance of 10×10^6 ohms and 2% error full scale. Some measurements were made with a Keithley 610A Electrometer with an input impedance greater than 10^{14} ohms and 2% error full scale. The VTVM and Electrometer had sufficiently high input impedances so no cell polarization could occur, and the voltage fluctuations could easily be measured.

3.9 Gas Analysis

Gas analyses were done on a Fisher Gas Partitioner with thermal stabilizer, connected to a Honeywell Electronik 18 recorder. The column used detected the following gases in order, CO_2, H_2, O_2, N_2, CH_4, CO.

3.10 Crucible Construction

3.10.1 Faradayan Yield Experiments

Initially a Faradayan yield experiment was performed in a crucible shown in Figure 8, but the results were unsatisfactory, (as shown later), and the crucibles shown in Figures 9 and 10 were used. In this set-up a silica crucible rested in a graphite crucible, with electrical contact being made between the graphite and the metal in the silica crucible by a small length of 0.010" tungsten wire through a pinhole in the silica crucible. The top electrode was 3/8" A.U.C. electrode graphite, and in Figure 10 the top and bottom electrodes were drilled out and filled with 1/4" copper rod to reduce the electrical resistance of the external circuit.

3.10.2 Kinetic Experiments

The kinetic experiments were carried out in plain graphite crucibles and in silica lined graphite crucibles, as shown in Figure 11. A. U. C. electrode graphite was used to make the crucibles of dimensions 5" x 2" O.D. x 1 1/4" I.D. The total depth of the crucible was 4" and the slag plus metal depth was maintained at approximately 2". The inside diameter of the translucent silica sleeve corresponded to the inside diameter of the plain graphite crucibles. The silica sleeve height was adjusted to be slightly below the slag/metal interface,so the interface was insulated from the graphite crucible and was held in place by two graphite plugs, in holes drilled with a diamond

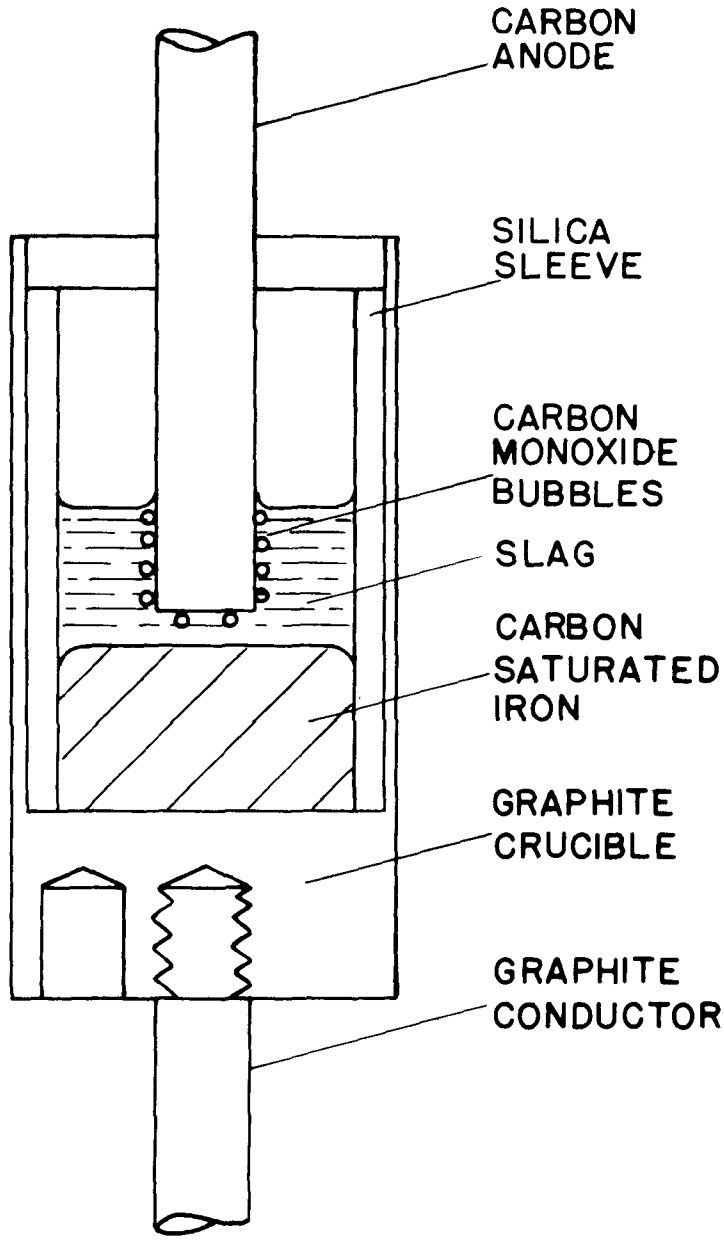

FIGURE 8 - THE ORIGINAL FARADAYAN CELL (CARBON-SATURATED IRON AS THE METAL PHASE)

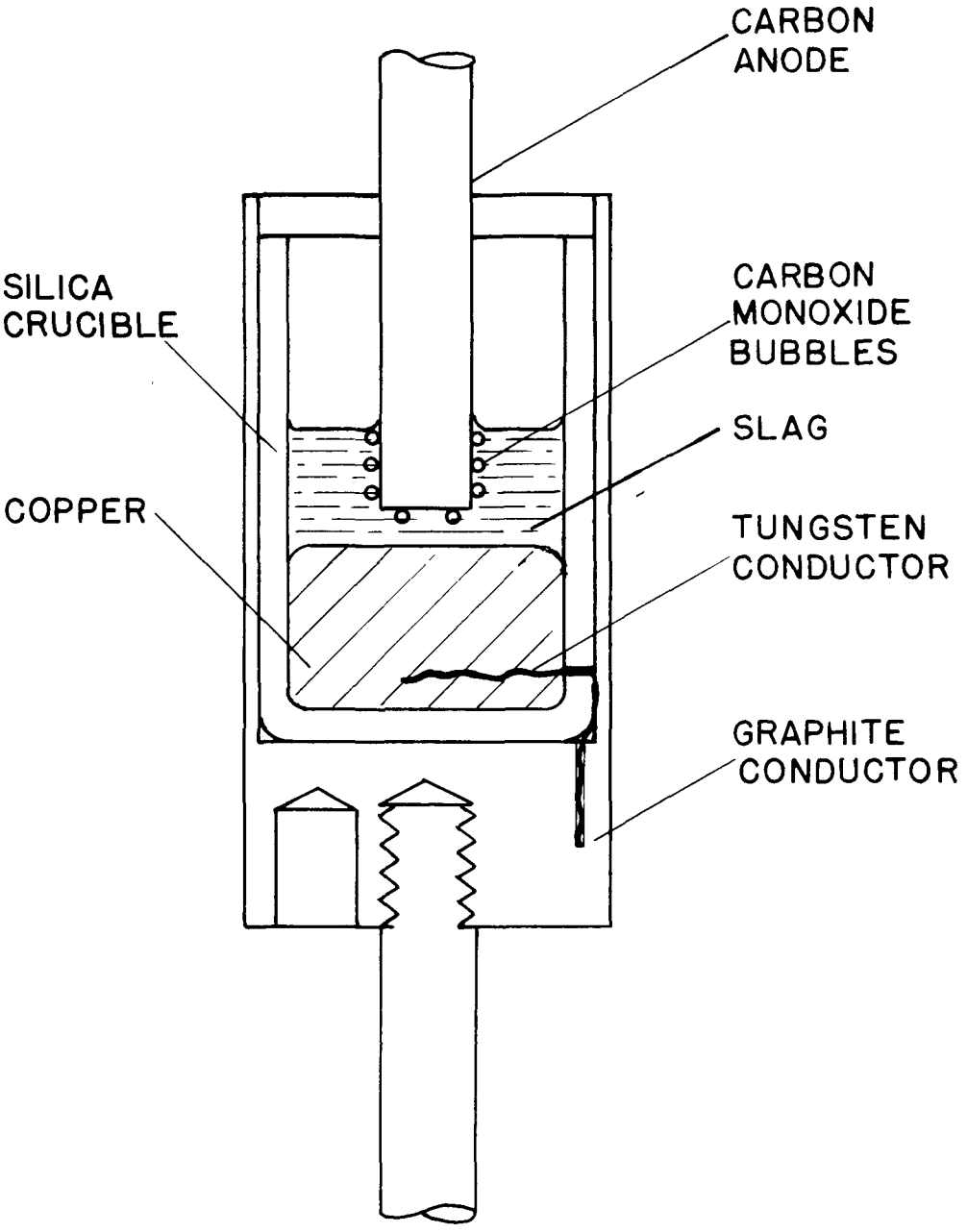

FIGURE 9 - FARADAYAN CELL WITH COPPER AS THE METAL PHASE
(LARGE SiO_2 CRUCIBLE)

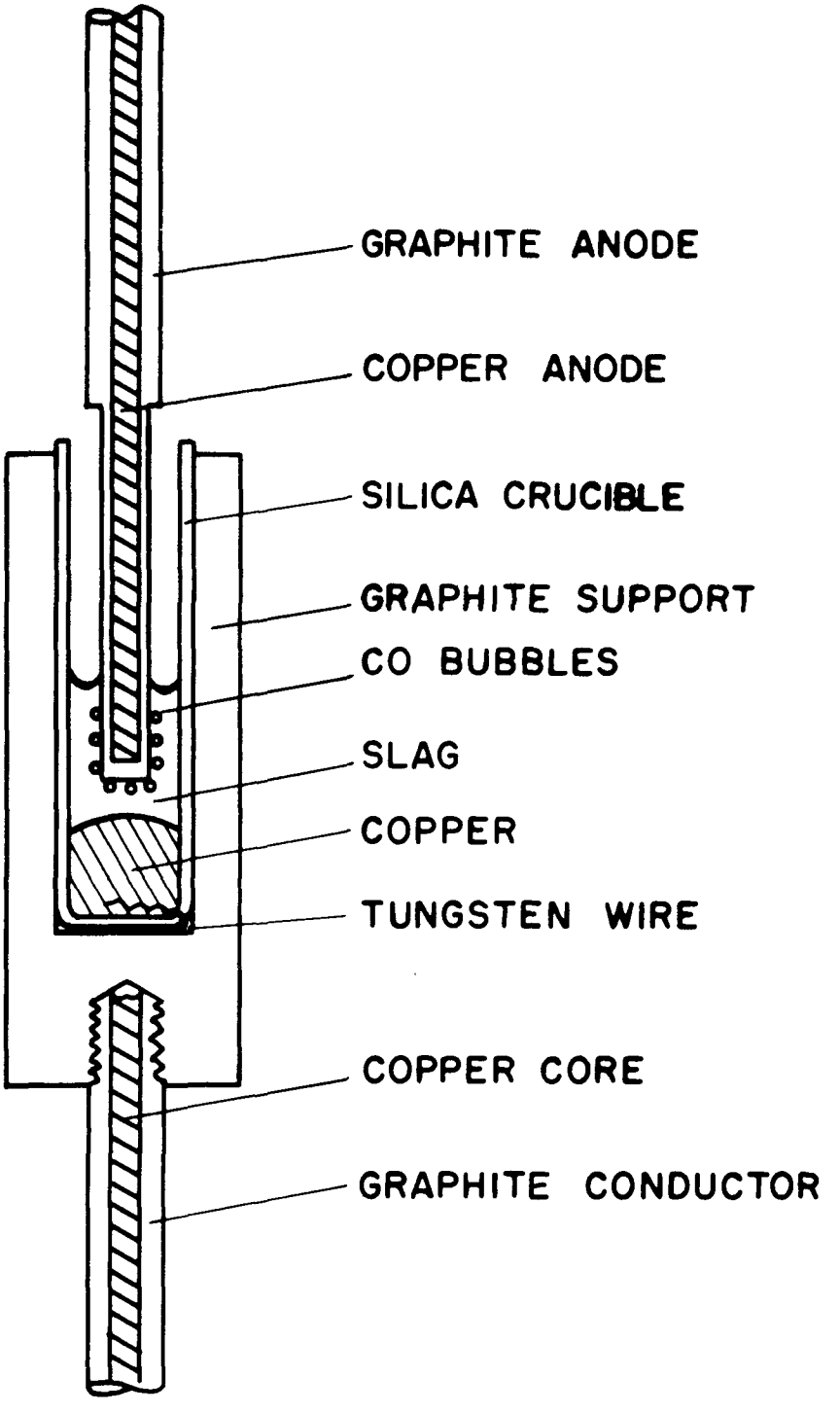

FIGURE 10 - FARADAYAN CELL WITH COPPER AS THE METAL PHASE (SMALL SiO_2 CRUCIBLE)

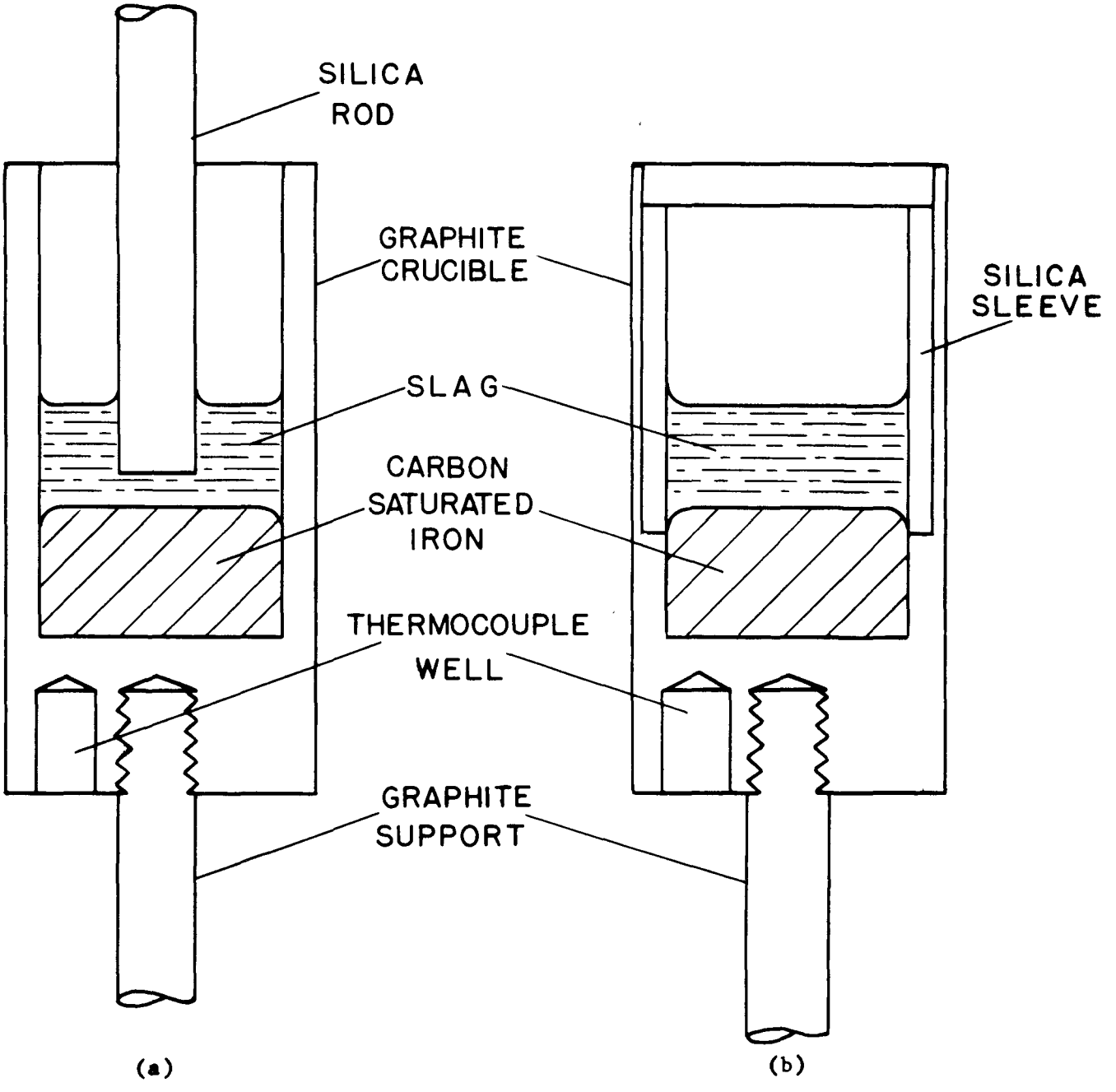

FIGURE 11 - GRAPHITE CRUCIBLES FOR KINETIC EXPERIMENTS
(a) Unsleeved
(b) Sleeved

drill 1/8" below the top of the crucible. In some cases a zirconium oxide (ZrO_2) sleeve was used, and a SiO_2 rod inserted into the slag.

The crucible bottoms were drilled and tapped centrally to allow the connection of a 1/2" graphite rod which acted both as a crucible assembly support and as an electrical connection for emf measurements. An eccentric 3/8" hole was also drilled in the bottom to provide a thermocouple well for temperature measurement.

The kinetic experiments done on the carbon monoxide measuring furnace utilized smaller A.U.C. graphite crucibles, with dimensions 2" x 3/4" O.D. x 5/8" I.D. No sleeved experiments were carried out on this furnace.

3.10.3 Electromotive Force Crucibles

The crucibles used in these experiments were the same as those described for the sleeved kinetic experiments, with the exception that the sleeve (SiO_2, or ZrO_2) extended to the bottom of the crucible.

Initially, emf experiments were carried out in crucibles which were suspended from the top plate. Both electrodes protruded through the top cap, with one being used to lower the crucible assembly into the hot zone. This arrangement was unsatisfactory because of the excessive load on the lowering electrode, and because the extra space required for the lowering electrode reduced the slag/metal interfacial area.

In a few of the emf experiments, instead of a silica sleeve being used, a silica crucible was used which was centrally drilled on the bottom to produce a 1/2" diameter hole, through which electrical contact could be maintained to the graphite crucible. This crucible is shown in Figure 12.

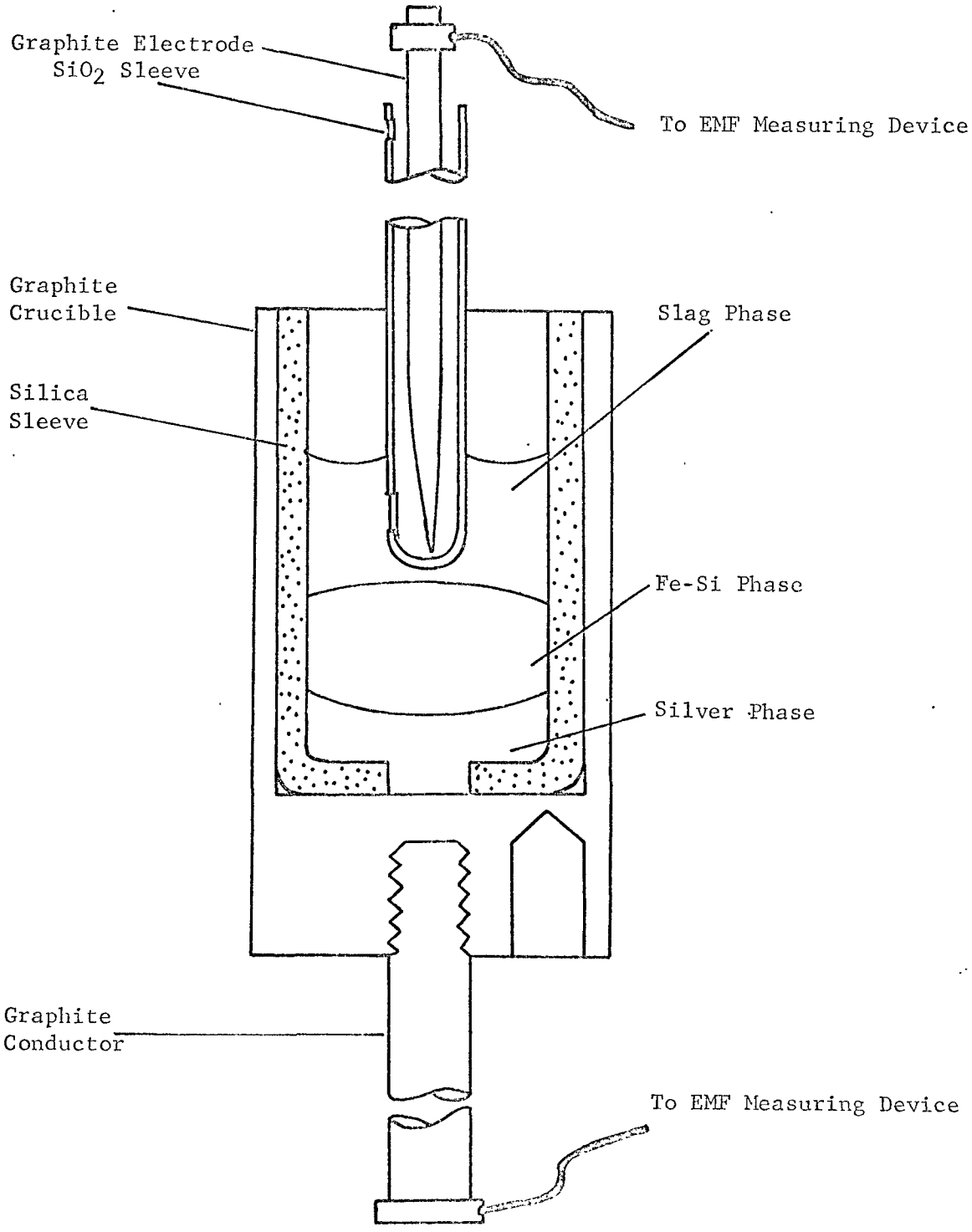

FIGURE 12 - ELECTROMOTIVE FORCE CRUCIBLE WITH SILICA SLEEVE CONTAINING 1/2" HOLE IN THE BOTTOM.

3.11 Electromotive Force Electrodes

Initially the graphite electrodes used were simple 25" x 1/2" diameter AUC graphite. The final graphite electrode chosen consisted of a 25" x 1/4" diameter AUC graphite electrode ground to a point at one end and shielded by a 24" x 1/2" diameter silica tube. The silica tube was closed at one end and had a 1/4" diameter hole approximately 1/4" from the closed end to allow slag to contact the graphite electrode. The graphite electrode was sealed to the silica at the other end and a small pin hole was introduced so the pressure in the electrode would not exceed one atmosphere (Figure 12).

The silicon carbide electrode consisted of a 3" x 3/8" diameter piece of silicon carbide, with a "U" notch close to one end. This end was inserted into a 20" x 1/2" diameter AUC electrode, which was drilled at one end to fit the silicon carbide piece. A graphite set screw was fitted to secure the silicon carbide by the "U" notch (Figure 13(a))

The silicon electrode was prepared in a similar way, with a 2" x 1/2" diameter silicon piece being secured by a graphite sleeve to a 20" x 1/2" diameter AUC graphite electrode (Figure 13(b)). The graphite electrodes used in the emf experiments using pure silicon as the metal phase, were hollow, 25" long x 1/2" diameter AUC graphite electrodes.

3.12 Sampling Apparatus

Samples were taken from the melt with graphite spoons and by suction up a 2 or 3 mm I.D. silica tube. The suction samples were preferred because they were easier to take and easier to prepare for analysis.

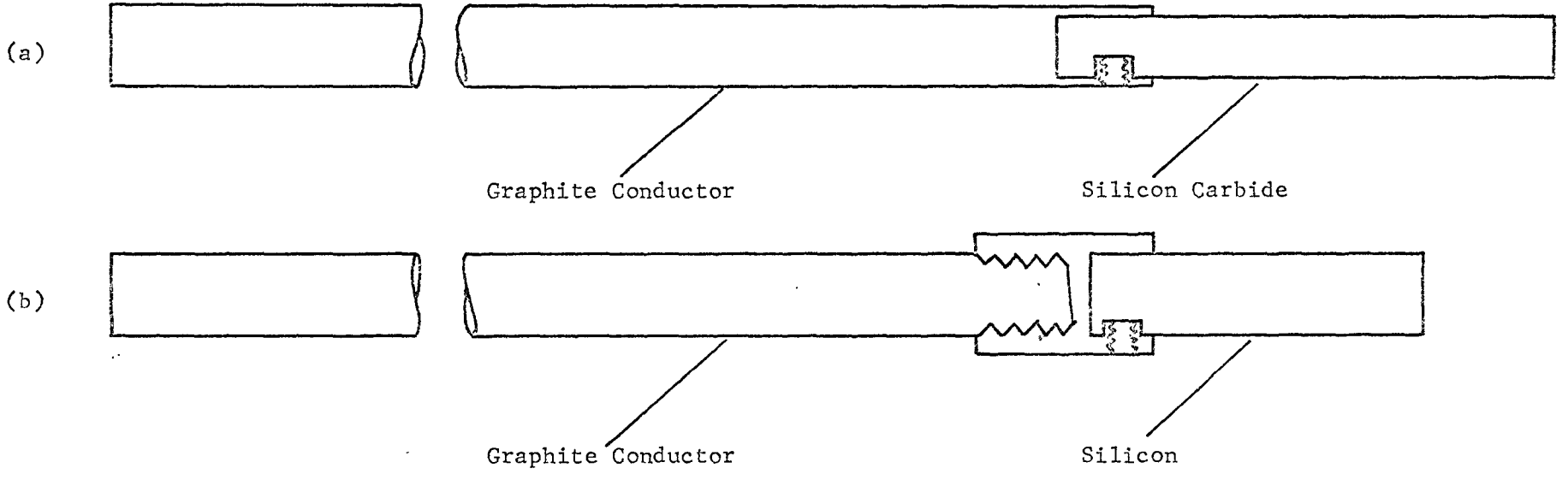

FIGURE 13(a) - SILICON CARBIDE ELECTRODE
(b) - SILICON ELECTRODE

3.13 Melt Additions

When the system was at temperature it was sometimes necessary to make additions of either slag or metal to the melt. The method devised was a hollow graphite tube 5" x 7/8" O.D. x 3/4" I.D. which was open at one end and drilled and tapped at the other end to screw onto a carbon connective rod, as seen in Figure 14 (a),(b).

The material to be added was inserted into the graphite cylinder followed by approximately one square inch of filter paper which was folded up non uniformly and pushed into the end of the tube. The material in the tube was thus held in securely and as soon as the tube was lowered into the vicinity of the hot zone, the filter paper burned away and the charge was deposited into the crucible. A method was tried where the end of the tube was drilled (1/16") around the diameter and a fine iron grid was woven which burned away in the hot zone. This method was too time consuming and the iron grid inadequately held the finely ground slag charge.

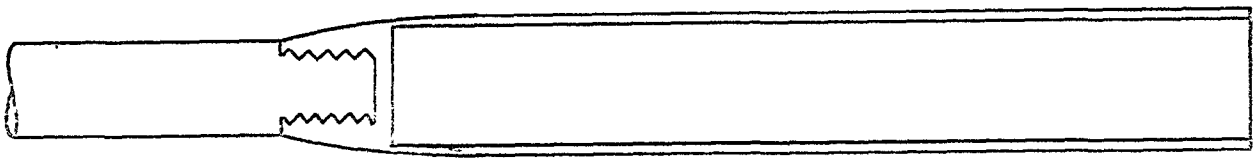

(a)

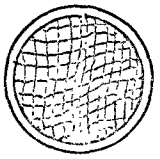

Wire Mesh

(b)

Filter Paper

FIGURE 14 - GRAPHITE ADDITIONER
(a) Wire Mesh
(b) Filter Paper

CHAPTER 4

EXPERIMENTAL PROCEDURE

4.1 Material Preparation

4.1.1 Slags

The slags used in this investigation were mainly from the SiO_2-CaO-MgO system with 61.5% SiO_2, 30.5%CaO, 8% MgO by weight, having a melting point of 1320°C[98](Figure 15). In some cases, BaO was added to SiO_2 to form a high density slag with a melting point at high BaO concentrations of 1450°C[98](Figure 16). To create low melting point slags, SiO_2-CaO-BaO slags were also used (Figure 17). All the slags were synthetically made in powder form and then fused.

The SiO_2 was prepared by dehydrating precipitated silicic acid ($H_2SiO_3.nH_2O$) at 600°C for 48 hours. The CaO, MgO and BaO were reagent grade and were dried at 600°C for several hours.

Oxide components were weighed to within 5 gm. to a toal of 2000 gm, added to a 5 litre jar and mixed for 24 hours by mechanical rotation. One of four methods was then used to prefuse the slag:

(a) The oxide mixture was set in a steel dish of dimensions 6" x 4" x 1" to a depth of 1" and a carbon arc was struck above the slag surface forming a pool of molten slag. Fresh material was added so the molten pool contacted only oxide mixture and was not contaminated.

(b) The oxide mixture was pelletized in a compression mold, removed and fused with an oxygen-natural gas torch.

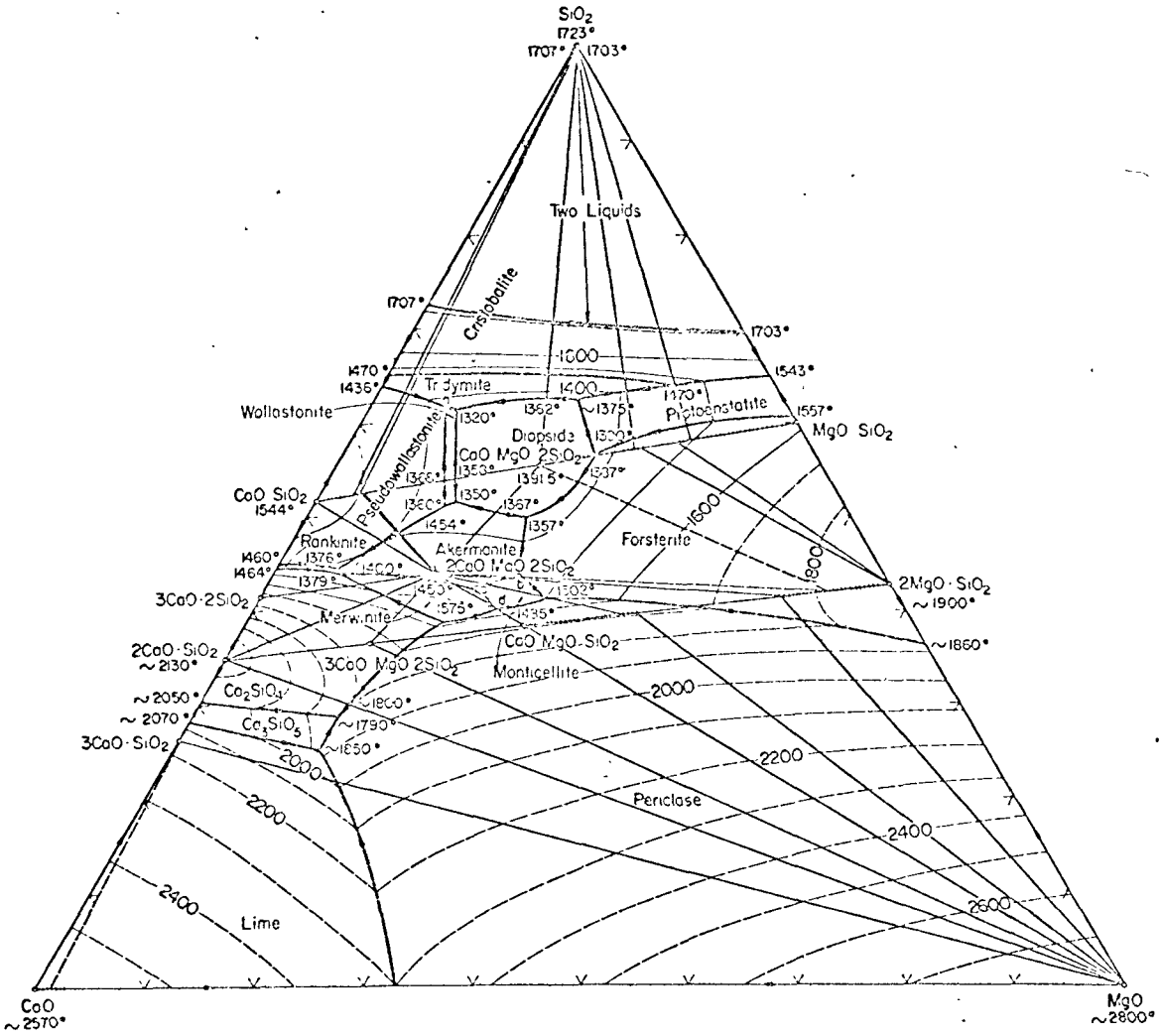

-System CaO–MgO–SiO_2; composite.

FIGURE 15 - SiO_2-CaO-MgO PHASE DIAGRAM

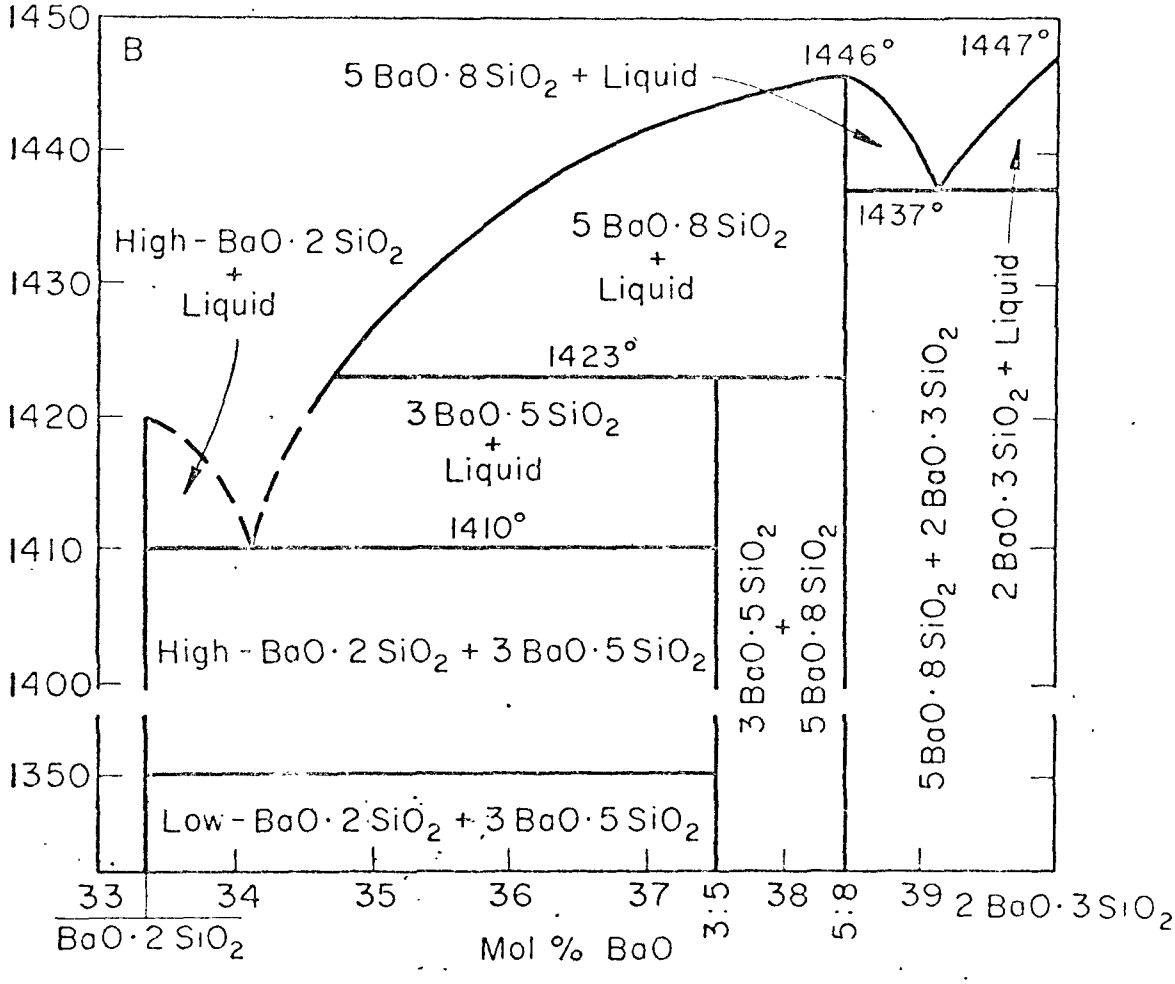

FIGURE 16 - SiO_2 - BaO PHASE DIAGRAM

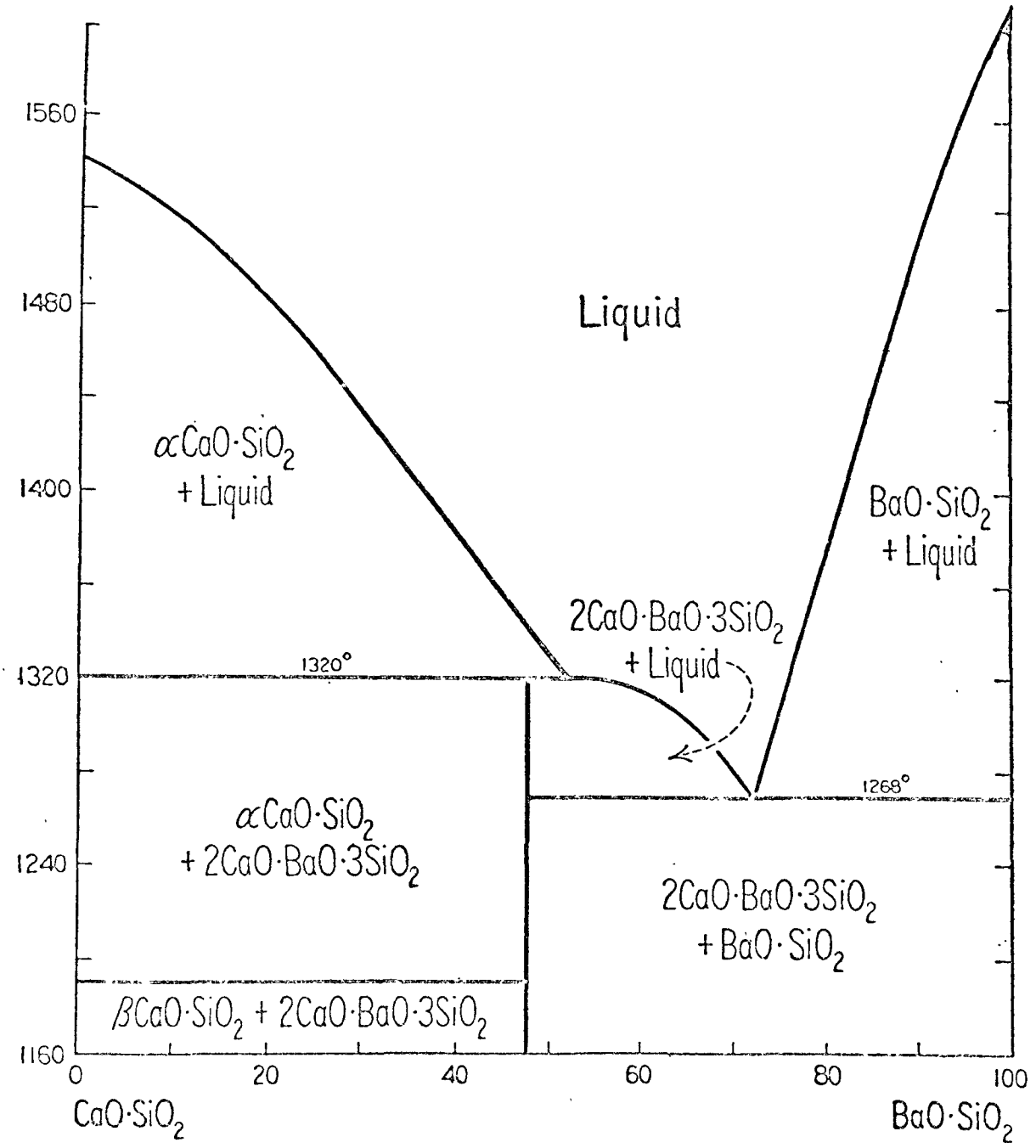

–System $BaO \cdot SiO_2$–$CaO \cdot SiO_2$.

FIGURE 17 - SiO_2-CaO-BaO PHASE DIAGRAM

(c) The oxide mixture was added to a graphite crucible of dimensions 7" x 5" O.D. x 4" I.D. and melted in a 3 KC open air induction unit. The molten slag was then poured from the crucible onto a tilted 1/4" steel plate for rapid cooling.

(d) The oxide mixture was added to a SiO_2 crucible which was inserted into the graphite crucible described in (c), was fused and poured as in (c).

Methods (a) and (b) were unsatisfactory because very little slag could be obtained in a long period of time, and in (a) the oxide mixture was blown out of the crucible by the arc, and graphite from the electrodes contaminated the fused slag. Method (c) was abandoned because the carbon in the crucible contaminated the slag which was found to contain up to 0.04% carbon, and it was felt that the kinetic and emf results might be affected. Method (d) was chosen as the best means of producing large quantities of uniform starting material. Typical analyses of this synthetic slag are shown in Table 1, for three different preparations.

TABLE 1

Analyses of Fused, Synthetic Slag

Slag No.	SiO_2 (wt.%)	CaO (wt.%)	MgO (wt.%)
A_{18}	61.5	26.9	8.9
A_{27}	60.7	29.8	8.1
A_{27}	60.8	28.5	6.9
A_{30}	60.5	30.2	7.7

The fused slag was crushed in an iron mortar and pestal, mechanically mixed for 24 hours and set aside for future use.

4.1.2 Metals

Carbon saturated iron for the kinetic and emf work was prepared from armco iron melted in a graphite crucible (dimensions 7" x 5" O.D. x 3" I.D.) by a 3 KC induction unit. The melt was allowed to saturate with carbon at approximately 1500°C (the temperature was measured by a disappearing filament optical pyrometer) and was poured at approximately 50° above the eutectic temperature. The total charge of 10 lb. was poured intermittently into a preheated, mild steel pencil mold containing four hollow pencils of dimensions 7" long x 5/16" diameter.

The other metals used were obtained commercially and are listed in Table 2, along with the purity.

Union Carbide AUC high purity graphite was used for the graphite crucible and electrode construction. Average analyses are shown in Table 3.

4.2 Quartz

The silica sleeves and silica rods used for sleeved and unsleeved experiments respectively were high purity, translucent quartz obtained from the General Electric Company.

4.3 Chemical Analyses

4.3.1 Silicon in Iron

The samples taken from the melt were surface ground, cleaned with acetone, crushed and analysed for silicon by the standard perchlorate technique.

4.3.2 Carbon in Iron

A standard combustion technique was used to determine carbon in iron. The sample was melted in a small induction unit, the carbon was

TABLE 2

METAL PURITY

Metal	Type	Purity (wt%)
Si	-	99.9
Cu	O.F. H. C.	99.99
Ag	electrolytic	99.999

TABLE 3

AUC GRAPHITE SPEC IFICATIONS

	S	Cu	Fe	Si	Total Ash as Oxide
Amount (wt%)	.004	.0043	.005	.0014	.03

oxidized to CO_2, and the CO_2 was absorbed in a potassium hydroxide solution.

4.3.3 Carbon in Silicon

A similar technique as in 4.3.2 was used to determine carbon in silicon. The method was checked by determining the carbon content in stoichiometric silicon carbide.

4.3.4 Carbon in Slag

The same combustion technique was used for carbon in slag, but in this case, iron chips were added as a susceptor in order to melt the slag in the induction unit.

4.3.5 Silicon in Copper

The silicon in copper was analysed spectrographically by a technique developed by the Steel Company of Canada Ltd.[99].

4.3.6 Slag Analyses

The SiO_2-CaO-MgO slags were crushed , dissolved partially in HCl and the solution was filtered. The residue was fired at high temperature and then fused with a mixture of Na_2CO_3 and Na HCO_3. This fused mixture was then filtered, the residue was fired at high temperature and weighed as per cent SiO_2. The second filtrate was diluted and separated aliquots were taken to analyze for CaO and MgO, using the appropriate indicator and EDTA (ethane-diamino-tetra-acetic acid) as the titrant.

The slags which were used in zircoa (ZrO_2) lined crucibles were analyzed spectrographically[99] for ZrO_2 and although the results were scattered, the ZrO_2 content appeared to vary between 2 and 5% by weight.

4.4 Temperature Profile

The temperature profile of the furnace was determined by a travelling Pt/Pt-13%-Rh thermocouple inserted from the top cap of the reaction tube into a graphite sheath located at the hot zone. Two typical profiles at two temperature levels are in Figure 18, in which the temperature did not vary more than $\pm 10^{o}C$ over a length of 2 1/2 inches.

4.5 Kinetic Experiments

4.5.1 Unsleeved Graphite Crucible

The pencils of carbon saturated iron were fractured into 1" to 1 1/4" lengths, and between 175 and 200 gm was placed in the unsleeved crucibles and premelted in the induction unit described previously (3.4). Next, 62.5 gm of the prefused slag was added, and the crucible was screwed onto a 1/2" carbon rod and inserted along with a thermocouple sheath in the aluminum bottom cap which was fitted on the bottom of the reaction tube. The reaction gas deoxidized by the copper turnings and dried by a potassium perchlorate solution was passed.

The cold crucible and charge were held at the bottom of the reaction tube and slowly raised into the hot zone. Once the crucible was in place in the hot zone the power input was cautiously raised to 90% from 40% of total power in steps of 10% every 1 hour. Melt additions, if required, were then made. The power input of the furnace was kept continuously at 40% (approximately 800°C) to negate thermal shock effects on the refractory tubes.

Simultaneous with the above operation, a 1/2" pure SiO_2 rod was lowered carefully into the hot zone and inserted into the slag to a depth of 3/4". This rod was used to maintain silica saturation throughout the

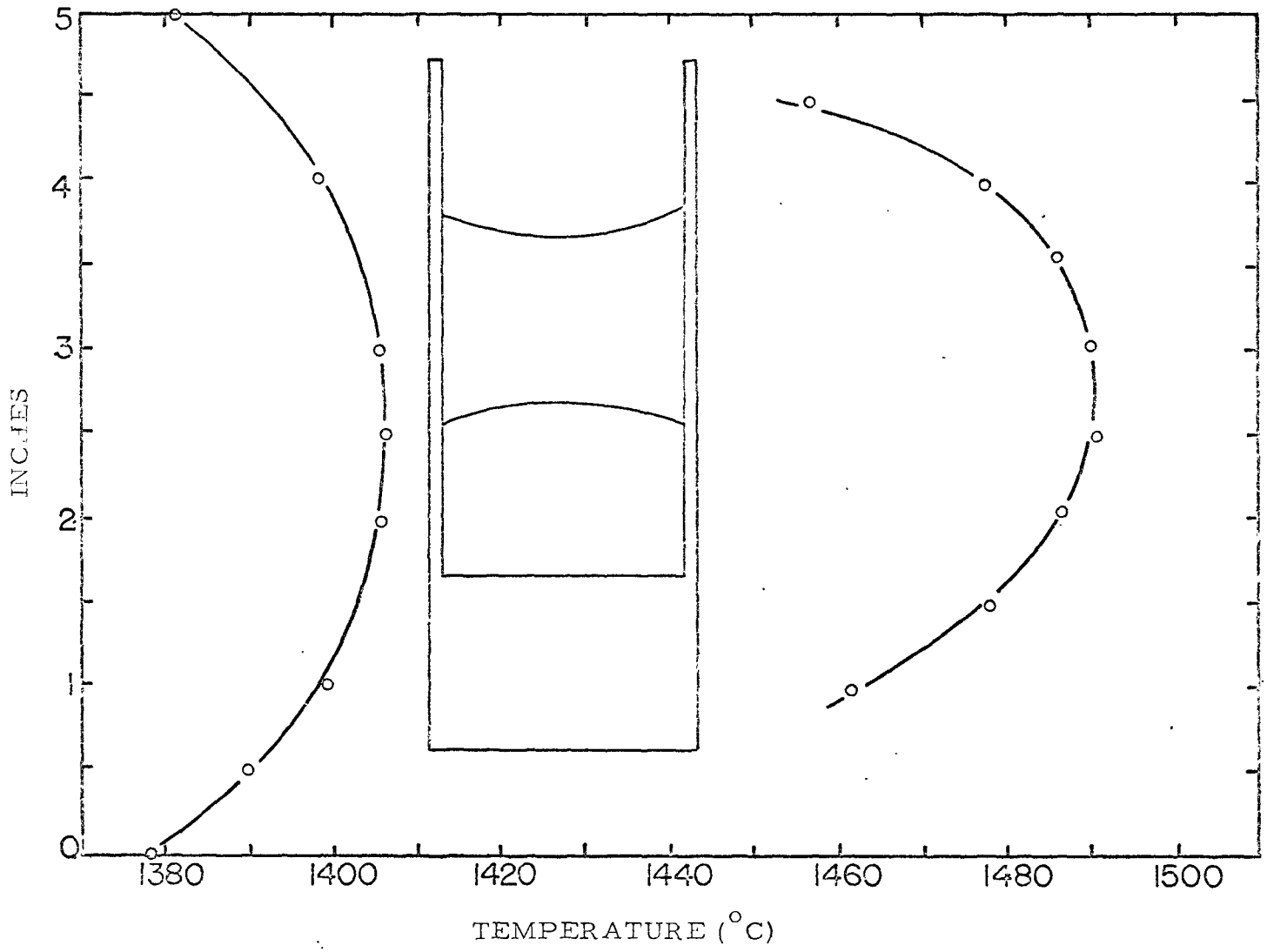

FIGURE 18 - FURNACE TEMPERATURE PROFILES

the experimental period. After allowing several minutes for the melt to homogenize at the chosen experimental temperature, samples of metal phase were taken every one to two hours. No external stirring was provided, but before each sample was taken the melt was stirred vigorously by bubbling the reaction atmosphere through the metal, using the rubber bulb on the sampling tube. The hot samples were quenched immediately in a cold water bath and set aside for silicon, and, in some cases, carbon analyses.

In the early experiments, after a reaction time of 12 hours, the temperature was lowered, and the crucible withdrawn. However, in later experiments, several kinetic runs were performed one after another at different temperatures on the same crucible. At the end of one experimental period, the amount of sample taken was weighed and an equivalent amount of carbon-saturated iron was added to return the metal phase to the original level. The temperature was raised, and another run was commenced for a maximum of five runs per crucible. This sequence of experiments on one crucible was started at a low temperature continuing to higher temperature to prevent graphite precipitation at the slag/metal interface which could conceivably interfere with the reaction kinetics.

The cooling sequence of the furnace was similar to the heating sequence, the power being dropped in 10% steps every hour , and once 40% power input was reached the crucible assembly was quickly removed and allowed to cool slowly. In several cases the crucibles were split open to examine the various interfaces.

4.5.2 Carbon Monoxide Measuring Furnace Experiments

The system was continuously flushed with carbon monoxide gas until

the reaction temperature was reached, the gas flow was stopped, a pellet of mercury was introduced into the capillary tube, and then the kinetic measurement commenced. The rate of the pellet movement in the capillary of known and uniform diameter was related directly to the volumetric rate of CO formation. When a pellet was near the end of the measured length of capillary a new pellet was inserted, and its movement was followed, giving a continuous measurement of the rate of CO evolved.

4.5.3 Sleeved Graphite Crucible

A similar procedure was followed for sleeved runs as for unsleeved runs, the only difference being that the slag for sleeved runs was maintained at silica saturation by the silica sleeve.

In several sleeved experiments the reaction kinetics were observed by two methods, one in which the melt was sampled intermittently and analysed for silicon as usual, and one in which the carbon monoxide content of the exit gas was measured. Exit reaction gas flow rates were measured by a simple flowmeter device described elsewhere[100], and the per cent carbon monoxide was determined by a gas analyser (3.9). The reaction gas used in these experiments was nitrogen, and the analyser was standardized with three known nitrogen mixtures shown in Table 4.

TABLE 4

Calibration Gases for Gas Analyzer

Gas	Per Cent Nitrogen (vol.)
technical grade nitrogen	99.9
technical grade nitrogen + hydrogen	95.0
air	79.0

The nitrogen content of the reaction gas was determined, and the carbon monoxide content was calculated by difference, since only nitrogen and carbon monoxide were present. In this manner the silicon transfer rate could be calculated from the stoichiometry of reaction (2.61)

It was imperative that the gas analysis should be taken several minutes after a sample had been taken, to allow the system to be thoroughly flushed. Gas samples taken prematurely exhibited an unusually high CO content, due to reaction of the graphite with the oxygen introduced when a sample was taken.

4.6 Faradayan Yield Experiments

4.6.1 Carbon Saturated Iron as the Metal Phase

The starting procedure for the Faradayan yield experiments was the same as that for the sleeved kinetic runs. A 1/2" graphite rod was inserted into the slag to act as an anode. This graphite rod, and the 1/2" graphite rod used to support the crucible assembly, were connected by a coaxial cable (the outer shield was grounded to avoid electrical noise pick-up) through a d.c. milliammeter. The melt was sampled periodically and the number of coulombs passed were measured. Great care was taken to avoid touching the crucible to the inner wall of the reaction tube in order to minimize electrical pick-up from the refractories.

4.6.2 Copper as the Metal Phase

Two experiments were performed using copper as the metal phase. In the first experiment 200 gm of copper in a 30 mm diam. SiO_2 crucible was used and the second experiment 60 gm of copper in a 20 mm diameter SiO_2 crucible was used. The copper was obtained from 1/8" diam. copper

wire which was thoroughly cleaned in a solvent, cut into 2" lengths, weighed and inserted into the SiO_2 crucible located inside a graphite crucible. The temperature was raised until the copper was molten, and then 30 gm of slag were added by the graphite charge additioner. The silica crucibles had small pinholes near the bottom through which a 0.015" tungsten wire electrically connected the copper melt to the graphite crucible.

In the case of the large SiO_2 crucible, a 1/4" graphite rod was inserted into the slag and was connected to the bottom graphite rod through a milliameter, which measured the current passed. Copper samples were taken over a period of 28 hours and analyzed for silicon. When the smaller SiO_2 crucible was used, both the top and bottom electrodes were drilled out and filled with a 1/4" copper rod to minimize the resistance of the external circuit. This experiment was carried out over a period of 106 hours.

A blank experiment was conducted with copper and slag in a SiO_2 crucible without maintaining electrical contact to the graphite crucible. The copper was sampled over a period of 48 hours and analyzed spectrographically for silicon.

4.7 Electromotive Force Experiments

4.7.1 Silicon as the Metal Phase

The experimental set-up for emf experiments using pure silicon as the metal phase is shown in Figure 19. In the initial experiments, silicon was added to the crucible in lumps totalling 60 gm. The slag, also totalling 60 gm. was then added and the crucible was brought to temperature in the normal manner. No results were obtainable, and when the

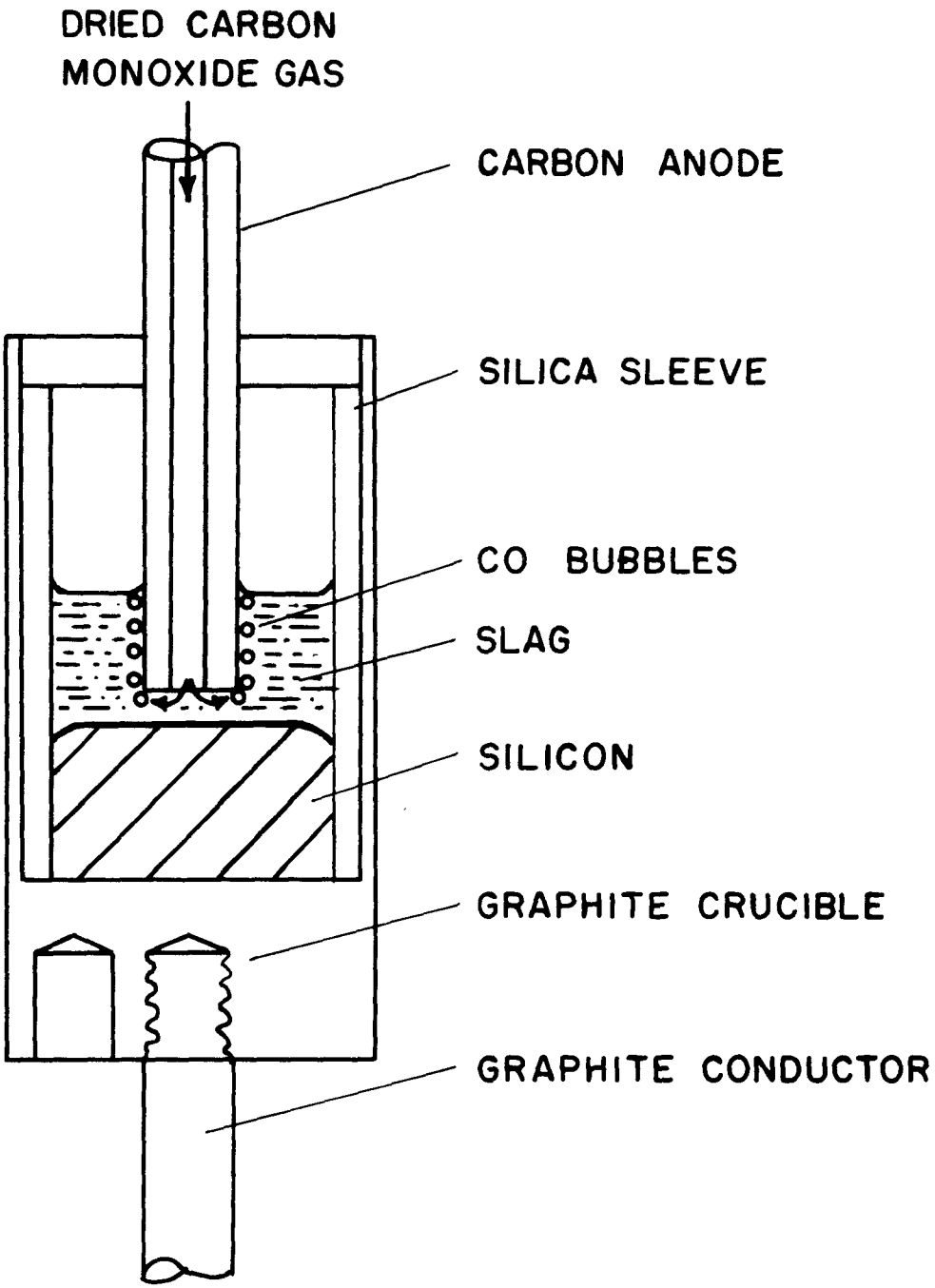

FIGURE 19 - ELECTROMOTIVE FORCE CRUCIBLES
(SILICON AS THE METAL PHASE)

crucible was split open for examination it was seen that the silicon and slag had not separated into two distinct layers, in all probability due to the similarity in densities. A $BaO-SiO_2$ slag was then used to create a denser slag phase to enhance slag-metal separation, but again no separation occurred. Finally, the silicon was prefused (without the slag) in the crucible using the auxiliary induction furnace, and the slag was added when the crucible was in the hot zone, effecting a good slag-metal separation. Dried carbon monoxide gas was blown down the hollow graphite anode into the slag, so that a CO bubble reached the slag-atmosphere surface every 1 or 2 seconds. The graphite anode and the graphite support were connected through a grounded coaxial cable to an electronic voltmeter. Great care was taken so the crucible did not touch the sides of the reaction tube. The temperature was held constant until the emf was constant, then the temperature was raised in steps and the constant emf for each temperature was noted. In one run, the temperature was lowered in steps and the corresponding emf's were determined. A "short" voltage was obtained by inserting the graphite anode into the silicon phase and noting the electrometer reading. Silicon samples were taken and analyzed for carbon.

The furnace gas in all the electromotive force experiments was argon, since there was some possibility that nitrogen would react with silicon, either pure or in solution with iron, to form a nitride which might interfere with the reversibility of the studied reaction.

4.7.2 Iron-Silicon as the Metal Phase

Reversible electromotive force experiments were tried on electro-

chemical cells using iron-silicon alloys as the metal phase or cathode, and a pure silicon or graphite electrode as the anode or top electrode. When pure silicon was used as the top electrode (anode), the cell constituted a concentration cell and when graphite was used, a chemical reaction cell resulted. The use of pure silicon severely limits the temperature range to below that for the melting point of silicon (1413°C). In order to extend the range of the experiments to lower temperatures, a low melting point slag was tried (SiO_2-CaO-BaO). The metal phase initially contained a Fe-15 wt.% Si alloy with a melting point of approximately 1180°C[101], and the silicon concentration could be reduced by making additions of armco iron to the melt.

Emf measurements utilizing Fe-Si alloys, regardless of the nature of the anode (silicon or graphite) were done in crucibles shown in Figure 12. In this arrangement the Fe-Si alloy was isolated from the graphite crucible but maintained in electrical contact with it by the denser silver phase. The crucible containing 100 gm. of silver was brought to temperature, the iron-silicon alloy was added, and then the slag was added. When the entire slag-metal system was molten, the top electrode was inserted into the slag phase to a depth of approximately 1/2" and the temperature was held constant until the emf was relatively constant. The temperature or the concentration could then be changed, and thus the emf was recorded for a series of experiments as a function of both temperature and silicon concentration.

4.7.3 Iron-Carbon-Silicon as the Metal Phase

Reversible electromotive force measurements were attempted using

the iron-carbon-silicon system as the metal phase or cathode, and a graphite, silicon carbide or silicon electrode as the anode. Utilizing the graphite electrode, the cell was sleeved completely with a silica sleeve, forcing the anodic reaction (discussed in section 2.16.2) to occur at the graphite electrode. The graphite electrode chosen as the most satisfactory for reversible emf measurements in the Fe-Si and Fe-C-Si systems was the one sleeved with silica (Figure 12).

Initially, carbon saturated iron alloys of very low silicon content were used, and the emf was measured as a function of both the silicon concentration and temperature. In this system, the silicon concentration increases constantly because of the continuous slag-metal and metal-sleeve reactions producing silicon dissolved in the Fe-C-Si phase. After the emf was followed for some time, with the melt being sampled periodically to determine the silicon content, the temperature was varied (in some cases) to determine the emf-temperature relationship at a particular silicon level.

In later experiments, carbon saturated iron with high silicon contents, approaching the saturation limit for silicon carbide formation, was used. Emf-temperature relations were determined for a specific silicon level, and more Fe-C alloy was added to lower the silicon level. Thus emf-temperature relationships were determined for various silicon concentrations.

A similar series of experiments was attempted using silicon carbide and pure silicon as the top electrode. The use of silicon as an electrode in this manner severely limits the temperature range, permitting temperatures no higher than 1400°C. For most emf experiments in the Si, Fe-Si and Fe-C-Si systems, the bottom crucible support was grounded and the

effect of induced voltages was eliminated by measuring the emf when the power input to the furnace was shut off. The change in the emf when the power was turned off was so small that in many cases measurements were made with the power on.

4.8 Electrolysis of the Slag

The possibility that hydrogen was dissolved in the slags in the form of hydroxyl ions which could then discharge and perhaps interfere with the observed electrochemical reaction, led to the cells being electrolyzed for a few moments in the early experiments. An external emf, supplied by either a 0 to 100 volt A.C. source or a 4.5 volt D.C. battery, was applied between the top electrode and the bottom graphite conductor. This external emf was applied in several experiments when the measured emf was particularly erratic, to see if the emf fluctuations could be eliminated.

4.9 Resistance of Silica Sleeve at High Temperature

The resistance across the 1/4" translucent silica sleeve was measured as a function of temperature to determine whether the sleeves were conducting at high temperature. Platinum leads were fused to the silica across the 1/4" wall thickness and the sleeve was inserted into a graphite core which then could be inductively heated. The resistance was then measured as a function of temperature by an electronic testmeter. The temperature was measured by a Pt-Pt/13% Rh thermocouple inserted from the top into the graphite core.

CHAPTER 5

RESULTS

5.1 Faradayan Yield Experiments

5.1.1 Carbon Saturated Iron as the Metal Phase

A Faradayan cell was constructed, as shown in Figure 8, with carbon saturated iron as the metal phase. The top graphite electrode was noted to be negatively charged, and when it was externally connected to the bottom graphite conductor through a milliammeter, a constant current of the order 6 - 8 milliamps was observed. Using expression (2.1) this current was calculated to be equivalent to a silicon transfer rate of 0.002 gm/hr., if all the current resulted from an electrochemical transfer of silicon. The metal phase was sampled periodically and analyzed for silicon. From the straight line kinetics the silicon transfer rate was determined to be 0.80 gm/hr.

5.1.2 Copper as the Metal Phase

Two Faradayan cells were constructed using carbon-free O.F.H.C. copper as the metal phase; one cell had a relatively large volume of copper and the other a small volume. In both cases, the top graphite electrode was observed to be negatively charged, and when it was externally connected to the bottom graphite conductor through a milliammeter, a constant current of the order 2 - 7 milliamps was observed after a few minutes.

The total current passed over a period of time was measured and related to silicon transfer by expression (2.1), again assuming that all the current resulted from an electrochemical transfer of silicon. The copper melt was sampled periodically by suction up a quartz tube and analyzed spectrographically for silicon. The analyzed silicon contents are shown as a function of the predicted silicon (from the number of coulombs passed) in Tables V and VI and in Figures 22 and 23. Both experiments were conducted at 1450°C.

The current passed increased as the graphite electrode was inserted further into the slag, and was a maximum when the electrode was first inserted into the slag, gradually decreasing in a few minutes from a value near 18 ma. to a constant value between 2 and 7 ma. This latter observation was made after each sample was taken since the top electrode was removed from the slag in order to take a sample and then re-inserted.

A blank experiment was run on a similar cell with no provision made for any electrochemical transfer of silicon resulting in a pick-up of silicon which reached a constant value of 0.015 wt.% within 4 hours. This value would have been reached in the Faradayan experiments before the electrochemical measurements were commenced, hence this amount was not attributed to electrochemical transfer and was subtracted from the analyzed values.

5.2 Kinetic Experiments

5.2.1 Unsleeved System

The kinetic data from the unsleeved experiments are listed in Table VII and are plotted in Figures 24 to 31. The results illustrate that the amount of silicon transferred to the metal phase is a linear

TABLE V

Faradayan Yield Experiment
(Large Silica Crucible)

Sample No.	Time Until Sample(min.)	Average Current Between Samples (ma)	Silicon Content Calculated from No. of Coulombs Passed (wt. %)	Silicon Content Analyzed (wt. %)
1	190	4.6	.002	.009
2	784	5.0	.010	.012
3	1,103	14.0	.021	.024
4	1,260	7.0	.024	.015
5	1,455	6.0	.028	.041
6	1,715	5.0	.031	.020

TABLE VI

Faradayan Yield Experiment
(Small Silica Crucible)

Sample No.	Time Until Sample(min.)	Average Current Between Samples (ma)	Silicon Content Calculated from No. of Coulombs Passed (wt. %)	Silicon Content Analyzed (wt.%)
1	0	0	0	.001
2	757	2.2	.012	.015
3	2,317	1.1	.024	.022
4	3,649	0.6	.030	.022
5	5,182	1.0	.041	.037
6	5,717	1.3	.046	.038
7	6,370	1.2	.051	.044
8	6,370	0	.051	.045

function of the time of reaction. Every experiment in this group was performed in the molybdenum resistance furnace with the exception of number 25, which was done in the carbon resistance furnace. Silica saturation in the slag was not maintained in experiment 25. The slopes of the kinetic curves were determined to a 95% confidence level by the least squares method illustrated in Appendix A. The slopes are listed along with the height of the metal phase, the temperature at which the experiment was conducted and the density of a carbon saturated iron melt at that temperature, in Table XI. A photograph of a split crucible is shown in Figure 20 (b).

5.2.2 Unsleeved System by Carbon Monoxide Evolution Technique

The kinetic data from the unsleeved system utilizing the high frequency furnace, and the carbon monoxide measuring unit are listed in Table VIII and are plotted in Figures 32 and 33. The results illustrate a linear relationship between the carbon monoxide evolved and the time of reaction. The slopes of the kinetic curves were determined to a 95% confidence level by the least squares method described in Appendix A. The slopes determined were equivalent to the carbon monoxide evolution rate (cc/min.) and were used to calculate the silicon transfer rate (wt.% Si/min) from the stoichiometry of reaction (2.61). The slopes are listed along with the height of the metal bath, the temperature at which the experiment was conducted, and the density of a carbon saturated iron melt at that temperature, in Table XII.

(a) (b) (c)

FIGURE 20 - CROSS SECTIONS OF KINETIC CRUCIBLES
(a) Sleeved Crucible (SiO_2)
(b) Unsleeved Crucible
(c) Sleeved Crucible (ZrO_2)

5.2.3 Sleeved System

The kinetic data from the sleeved experiments are listed in Table IX and are plotted in Figures 34 to 41. The results illustrate a linear relationship between the amount of silicon transferred and the time of reaction. All the experiments were done in the molybdenum resistance furnace with the exception of experiment 22 which was done in the carbon resistance furnace. In experiments 18, 19 and 20 the silica sleeve extended directly to the bottom of the crucible rather than terminating just below the slag/metal interface, as in the other experiments. Experiments 13, 14 and 21 were done using a zirconium oxide sleeve (ZrO_2) extending to the bottom of the crucible, and in experiments 13 and 14 silica saturation in the slag was maintained by the insertion of a 1/2" silica rod. The slag used in experiment 21 was not maintained at silica saturation.

The slopes of the kinetic curves were determined to a 95% confidence limit utilizing the least square technique illustrated in Appendix A. The slopes are listed along with the height of the metal phase, the temperature of the experiment and the density of a carbon saturated iron melt at that temperature in Table XIII. A photograph of a split crucible is shown in Figure 20(a) for the silica sleeved system and Figure 20(c) for the ZrO_2 sleeved system.

In addition to the normal method of determining the silicon transfer rate - by sampling and analyzing for silicon in the metal phase - the kinetics of experiments 18, 19 and 20 were followed by another method. The reaction gas (argon) flow rate was determined and from the carbon monoxide content (using gas chromatography), the carbon monoxide evolution

rates were calculated and are listed in Table X. Two reaction gas flow-rates were used for experiments 18 and 20 to test the effect of flow rate upon the kinetics. From the stoichiometry of reaction (2.61), the silicon transfer rate was determined from the measured carbon monoxide evolution rate, assuming all the carbon monoxide was produced by reaction (2.61) at the slag/metal interface. This transfer rate (gm. Si/min.) was converted to an "equivalent slope" to match the units of the slopes determined from the kinetic data (wt.% Si/min.), and these "equivalent slopes" are listed along with the bath height, the temperature at which the experiment was carried out and the density of a carbon saturated iron melt at that temperature, in Table XIV.

5.3 Effect of Silicon on the Solubility of Graphite in Liquid Iron

Each metal sample taken in the kinetic experiments was analyzed for silicon and when there was sufficient sample left, carbon analyses were done. The results are listed with the silicon results, in Tables VII and IX. The relationship between the silicon content and the saturation carbon content is approximately linear[102] up to moderate silicon contents, with the graphite solubility decreasing with increasing silicon content. The amount the solubility is depressed by the silicon is determined from the differential equation[103]:

$$\frac{d\Delta C_c}{d\, C_{Si}} = - k \qquad (4.1)$$

which upon integration gives:

$$\Delta C_C = - k\, C_{Si} \qquad (4.2)$$

$\Delta C_C \equiv$ saturation carbon content in the Fe-C-Si ternary - saturation carbon content in the Fe-C binary

$C_{Si} \equiv$ silicon content of the Fe-C-Si ternary

$k \equiv$ proportionality constant

Values of k were determined by the least square method described in Appendix A, for a 90% confidence interval, and are listed in Table XV. The average slope is: -0.37 ± 0.56.

5.4 Effect of Stirring

Although no provision was made for continuous stirring of the slag or metal phases, before each metal sample was taken, the complete system was stirred by depressing the aspirator bulb and bubbling the reaction gas through the melt. In this manner, the melt was stirred mechanically every one to two hours, depending on when the samples were taken. In order to test the effectiveness of this type of stirring, unsleeved experiment 20 was sampled only three times, with one sample being taken at the beginning of the experiment and two samples being taken sixty-nine hours later at the end.

5.5 Effect of Sleeve Material

The majority of the sleeved experiments were carried out using translucent silica sleeves, and to test whether the sleeve composition had any effect on the kinetics of the reaction, zirconia sleeves were used in some cases. Experiments 13, 14 and 21 were done utilizing zirconium

oxide sleeves which extended to the bottom of the crucibles. The effect of the slag and metal phases on the zirconium oxide sleeve is shown in the photograph of a spent crucible in Figure 20(c).

The slag from experiments 13 and 14 was analyzed spectrographically for zirconium oxide and the results indicated that between 2 and 5% by weight of the slag was ZrO_2, as shown in Table XVI.

From Figure 20(a), (b) and (c) it is seen that the greatest dissolution of material, either from the sleeve or graphite seems to occur at the slag-metal interface.

5.6 Effect of Surface Area and Bath Height

The effect of the height of the metal bath on the kinetics of the unsleeved system was determined by experiments 25 and 26 which were done on a bath height approximately one half the normal bath height. Also, the slag/metal cross-sectional area was increased in experiment 26 by one third over the normal area which was dictated by the internal diameter of the silica sleeve used in the sleeved experiments. The kinetic experiments performed on the high frequency carbon monoxide measuring unit had an interfacial area less than one half that in the experiments done in the resistance furnace. The bath height was also somewhat less than the normal height.

In the sleeved system the zirconium oxide sleeves had an internal diameter of 1.5" compared to 1.25" for the silica sleeves, resulting in a larger cross-sectional slag/metal contact area.

5.7 Effect of Sampling Technique

Metal samples were initially taken with graphite spoons, but at times it was impossible to obtain any metal sample. Eventually all metal samples were taken by suction up a 2 or 3 mm. I.D. silica tube which permitted very good samples to be obtained. The best slag samples were taken with the graphite spoons.

Experiments 1, 25 and 26 of the unsleeved system and experiment 22 of the sleeved system were taken with the graphite spoons. During experiment 16 of the unsleeved system both graphite spoon and silica sampling were used. The results are shown in the kinetic curve in Figure 26.

5.8 Slag Composition

Some slag samples were taken at random from the sleeved and unsleeved kinetic experiments and analyzed for SiO_2, CaO and MgO mainly to determine if the slags were being maintained at silica saturation. Table XVII shows the results obtained. The silica content rises from 64.9% at 1395°C to 68.2% at 1534°C.

5.9 Silica Sleeve Resistance

The resistance of the silica sleeve at room temperature was determined to be greater than 10^{12} ohms gradually decreasing to 1.2×10^6 ohms at 1500°C.

5.10 Electromotive Force Experiments

5.10.1 Silicon as the Metal Phase

The electromotive force was measured between a hollow graphite electrode inserted into the slag, and a graphite conductor which was

electrically connected to a pure silicon melt by the graphite crucible. The emf is shown in Figure 42 and Table XVIII as a linear function of temperature. The top electrode was positively charged, and at 1384°C the emf was observed to increase from an initial value of 93 mV to a constant value of 190 mV with very little fluctuation. The temperature was increased in steps and constant values of the emf were recorded until a value of 57 mV was observed at 1534°C. At temperature in excess of 1534°C the emf readings became unstable and difficult to measure. One experiment (no. 3) was commenced at a high temperature and the emf was seen to increase as the temperature was lowered. During experiment number 1, four silicon samples were taken and analyzed for carbon, the results are shown in Table XIX.

TABLE XIX

Carbon in Silicon

Sample No.	% C (wt.%)
1	0.019
2	0.017
3	0.008
4	0.007

The silicon/graphite crucible interface was examined under microscope to see if a third phase (silicon carbide) was present - none was observed.

However, in an experiment where silicon was allowed to sit in a graphite crucible for 20 hrs. at 1450°C, a minute trace of a third phase

was observed. This third phase was tentatively identified as silicon carbide by microprobe analysis.

The emf appeared to be independent of the rate at which CO was passed down the cathode and was unaffected when the CO flow was stopped entirely, although the flow was stopped for only a few minutes. In several experiments it was impossible to obtain any meaningful results since the emf fluctuations were too great. All readings were taken at zero power input to ensure that no induced voltage from the inductively wound furnace tube would affect the results. A non-inductively wound furnace tube was prepared for one set of experiments but failed because of a short, and no further attempts were made to wind a furnace non-inductively.

5.10.2 Iron-Silicon Alloys as the Metal Phase

An electrochemical cell was constructed as shown in Figure 12. The metal phase was an iron-silicon alloy, separated from the graphite crucible by a layer of pure silver which served to keep graphite from solubilizing in the iron-silicon phase and also to maintain electrical contact to the iron-silicon phase. A split crucible is shown in Figure 21. The variation of the electromotive force between an electrode (graphite or silicon) inserted in the slag phase, and the bottom graphite conductor was measured as a function of both the temperature and the silicon content of the Fe-Si binary. Depending on the silicon content of the melt, and the temperature , the top electrode was either positive or negative. The emf measured was independent of the depth of the electrode and its eccentricity in the slag. When the graphite electrode was inserted into the metal phase (at the end of an experiment) the emf dropped immediately

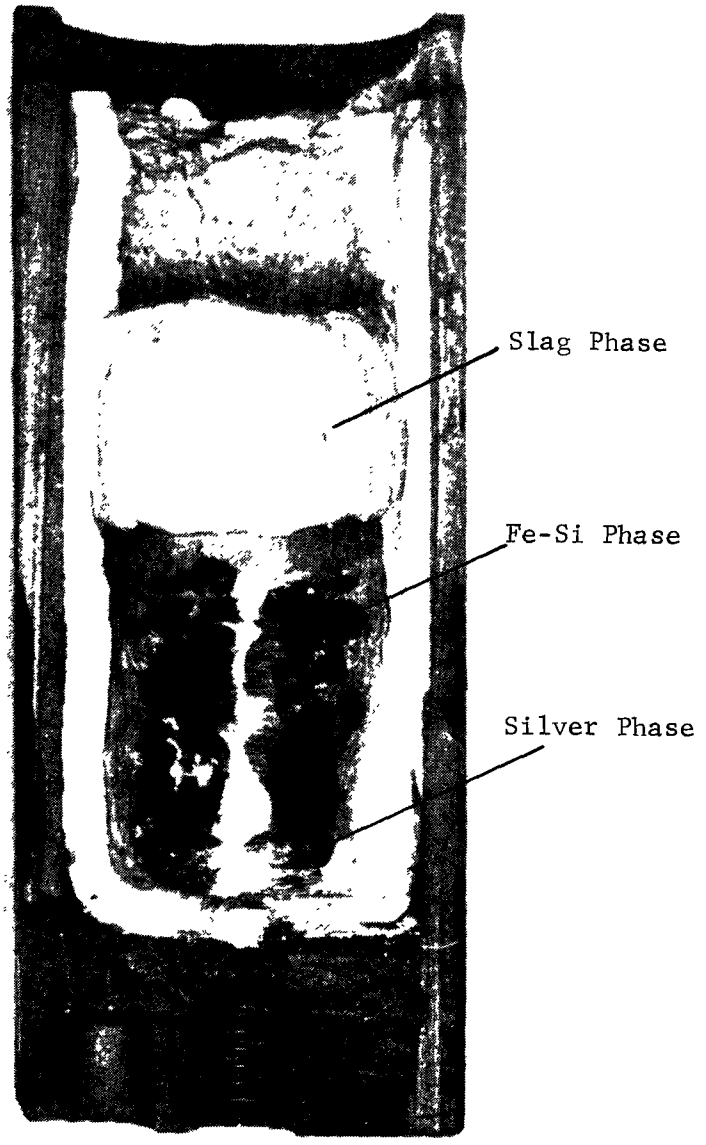

FIGURE 21 - CROSS SECTION OF ELECTROMOTIVE CRUCIBLE
(Fe-Si as the Metal Phase)

to zero. In most cases the emf measurement was made with the bottom electrode grounded, and the furnace power at zero.

Experiments were started using a silicon electrode (section 3.11) as the top electrode, severely limiting the high temperature range to somewhat below the melting point of silicon (1413°C). In order to increase the overall temperature range a low melting point slag, SiO_2-CaO-BaO was tried, however,the slag foamed out of the crucible and this system of runs was terminated. The normal SiO_2-CaO-MgO slag system was then used for the succeeding experiments.

In experiment 1, 17.8 wt.% Si alloy was brought to temperature at 1350°C and held until the emf reached a constant value of 126 mV, with the top electrode negatively charged. The temperature was raised to 1380°C and the emf rose to 141 mV. In order to change the silicon concentration of the alloy, some cold armco iron was added - the emf was observed to rise very high to 260 mV and then decrease to 150 mV in several minutes. The temperature was lowered and the emf decreased to a constant value of 126 mV. The results are shown in Table XX and Figure 43.

Experiment 2 was done with a graphite electrode as the top electrode, at a temperature of 1390°C. The silicon content of the melt was varied twice by adding cold armco iron, and the corresponding emf was observed. The results are shown in Table XX and in Figure 44.

Experiment 3 was done using graphite as the top electrode, and starting with a high silicon alloy. Initially, the top electrode was positively charged, but as the temperature was increased the emf became more positive, that is the top electrode became progressively less

positive and eventually turned negative. The silicon content was varied twice by adding cold armco iron, and various temperature changes were made. The results are shown in Table XX and Figure 45.

Experiment 4 was also done using a graphite top electrode and a high silicon alloy. The top electrode was positive for all measurements and hence the emf was negative. The results are shown in Table XX and Figure 46.

The effectiveness of the silver layer in preventing any graphite from solubilizing in the iron-silicon phase was checked by analyzing the iron-silicon melt for carbon. In none of the experiments was there any detectable amount of carbon in the iron-silicon phase.

5.10.3 Iron-Carbon-Silicon Alloys as the Metal Phase

The electromotive force was measured between a graphite electrode inserted into the slag phase, and a graphite conductor which was in electrical contact with an iron-carbon alloy of varying silicon content. The emf's of such electrochemicl cells are listed in Table XXI and are plotted in Figures 47 to 53. In some systems the silicon content was altered and the variation of the cell emf was observed; in others the silicon content was constant and the cell emf was observed as a function of temperature.

In most cases (silicon content < 0.2 mole fr.) the top graphite electrode was negatively charged, acting as the anodic electrode. In two cases (experiment 15) where $N_{Si} > 0.2$, the graphite electrode was positive, acting as a cathode surface. For the majority of experiments the instantaneous emf fluctuations were very small varying between $\pm$ 2 mV, however, in other cases the instantaneous voltage was fluctuating wildy,

varying up to 50 mV, making any readings impossible. When a steady emf was observed it was found that the emf was independent of the height of the graphite electrode above the metal phase. The emf immediately went to zero in all experiments when the graphite electrode was inserted into the metal phase and appeared to be unaffected by the furnace power when the bottom electrode was grounded. The majority of the measurements were made at full power input with the bottom graphite conductor grounded.

Experiment 5 was done on an alloy of 1.91 wt.% Si and 4.97 wt.%C at 1480°C. A constant emf was obtained but when the temperature was raised to determine the emf-temperature relationship, the emf became very unsteady. The top graphite electrode was connected to the bottom graphite conductor, through a milliammeter, and a constant current of 13 ma was passed.

Experiment 6 was done on a 0.20 wt.% Si alloy (graphite saturation) at 1450°C. The emf was constant at 180 mV but as the temperature was raised, it became unstable, and the test was terminated.

Experiment 7 was done on a 2.94 wt.% Si alloy (graphite saturation) at 1450°C, and the emf was fluctuating at approximately 100 mV. It was thought that the fluctuations were perhaps due to the discharge of hydroxyl ions, since the fluctuations did not appear to originate from the power input. The 4.5 D.C. battery was inserted between the top graphite electrode (making it negative) and the bottom graphite conductor for a period of 60 seconds. When the imposed emf was removed, the emf between the electrodes was 60 mV (the top electrode was negative) and rose steadily to a relatively steady value of 115 mV in 10 minutes. The D.C. source was again inserted, making the top graphite electrode positive for 60 seconds, and when it was removed the cell emf was seen to decrease from a maximum 180 mV to

115 mV in 3 minutes. In both cases the emf fluctuations returned, and did not appear to be noticeably reduced by the imposed D.C. emf.

The emf of experiment 8 was observed to fluctuate between 110 and 120 mV at 1350°C. Twenty volts A.C. were applied across the top graphite electrode and the bottom graphite conductor for 60 seconds, after which the emf was steady at 120 mV. The fluctuations returned after a few minutes.

Experiments 5 to 8 were performed in emf cells discussed in section 3.10.3. However, the size of the crucible made it very difficult to prevent the cell assembly from touching the reaction tube walls and picking up stray emf's. The fluctuations still occurred even when the furnace power was turned off. The type of cell shown in Figure 8 was used in the remaining emf experiments with silica sleeved graphite serving as the top electrode.

Experiment 9 was done on 0.03 wt.% Si alloy (carbon saturated) at 1370°C. The graphite electrode was shorted to the metal phase, and when it was raised into the slag phase the emf jumped from 0 mV to 185 mV and rose steadily to a constant value of 223 mV in a few minutes. The temperature was raised butthe emf began to fluctuate, and it was noticed that the cell was touching the refractory tube, so the experiment was terminated.

Experiment 10 was done at 1425°C starting with a 0.56 wt.% Si alloy (carbon saturated) and it represented the first attempt to measure the emf as a function of changing silicon content. The silicon content changed due to the slag/metal and metal-sleeve reactions which provided a constant silicon transfer to the melt. Both the emf and silicon content

are plotted as a function of time in Figure 47. The best straight line for emf-time data was determined by the least square method of Appendix A. From Figure 47 the emf is seen to decrease as the silicon content increases, and the variation of the emf values on the average is less than 10%. The emf reading appeared steadiest immediately after a sample was taken and the melt stirred by bubbling the furnace gas through it.

Experiment 11 was done using a hollow graphite electrode in the slag phase so a carbon monoxide atmosphere could be blown across the slag/electrode surface. The experiment was started at 1400°C, and the emf was observed as a function of the silicon content of the metal phase (sampled periodically) which was increasing with time because of the slag-metal and sleeve-metal reactions. After several hours the temperature was raised to 1440°C and the emf was seen to increase from 74 mV to a relatively constant value of 98 mV. A further increase of temperature to 1480°C resulted in a drop of emf for several minutes, but then it increased to a relatively constant value of 102 mV. The results are plotted as emf and wt.% Si as a function of time in Figure 48, and are listed in Table XXI. No affect of CO flowrate could be determined on the emf.

Experiment 12 was done using a zirconium oxide (ZrO_2) sleeve, with the silica saturation in the slag being maintained by an excess of silica floating on the surface. Carbon monoxide gas was blown down a hollow graphite electrode. The temperature was kept constant at 1400°C and the emf-wt.% Si relationship was determined as a function of time. The results are listed in Table XXI and are plotted in Figure 49. Again the carbon monoxide flow rate did not affect the emf results.

Experiment 13 was done at 1400°C, and the emf wt.% Si relationship was determined as a function of time. The results are listed in Table XXI and are plotted in Figure 50. The line in Figure 50 was calculated by the least mean method described in Appendix A. The emf is seen to increase slightly, as the silicon content increases, also slightly. The scatter of the emf readings was the highest for this experiment, being near 20%. An addition of 15 gm. of cold slag was made at 126 minutes and the emf jumped to a high value and decreased again in a few minutes.

Experiment 14 was done at 1444°C, over a short period of 129 minutes during which time the silicon content was approximately 0.71 wt.%. The results are shown in Table XXI and in Figure 51. The slope of the line in Figure 5 was determined by the least square method of Appendix A.

Experiment 15 was done at 1420°C, commencing with a high silicon alloy (0.311 mole fr. Si in carbon saturated iron). When a constant emf was observed, more iron-carbon alloy was added to reduce the silicon content, and the emf was measured as a constant for two such additions. The results are listed in Table XXI and in Figure 52. For the 0.311 mole fr. alloy and the 0.214 alloy the top graphite electrode was observed to be positive, and hence the emf is recorded as negative. During the first two measurements, no carbon monoxide bubbles were observed breaking at the slag/furnace atmosphere surface.

Experiment 16 was done at 1450°C and the emf was observed as a function of the silicon content of the melt as it increased because of the slag-metal and metal-sleeve reactions. The silicon content was then increased more rapidly by adding cold charges of a 30 wt.% Si in Fe alloy.

The emf was observed to decrease, in general, as the Si content increased. The carbon content was also determined. The results are shown in Figure 53 and Table XXI.

Two experiments were done using silicon carbide as the top electrode; in one case the entire electrode was made of silicon carbide and in the other, a 2" silicon carbide electrode was connected to a graphite conductor, which led out of the furnace. Starting with a 1.2 wt.% silicon alloy as the metal phase, the long SiC electrode was negatively charged, and the emf measured between the SiC electrode and the bottom graphite conductor was seen to fluctuate between 300 and 410 mV. When the SiC electrode was inserted into the metal phase, the "short" voltage was fluctuating between 270 and 345 mV. The emf measured between the short SiC electrode with the graphite conductor and the bottom graphite conductor was approximately -180 mV (the SiC electrode being positive), and the "short" voltage fluctuated between +20 and +40. No results were obtained with a top silicon electrode because in the two attempts that were made, the electrode melted.

Several electrochemical cell experiments similar to the above were attempted on the high frequency unit described earlier. In these experiments there was a considerable pick-up of induced A.C. and D.C. voltages by the graphite conductors, from the high frequency furnace. An attempt was made to filter the A.C. voltages to ground through 0.01μf capacitors. However, the emf's measured were very erratic and no results are reported.

TABLE VII

Concentration - Time Measurements (Unsleeved Runs)

Run No.	Time (min)	Silicon Concentration (wt.%)	Carbon Concentration (wt.%)	Run No.	Time (min.)	Silicon Concentration (wt.%)	Carbon Concentration (wt.%)
1	0.0	0.002		2	0.0	0.03	4.82
	101.0	0.12			62.0	0.05	4.94
	163.0	0.15			117.0	0.07	4.90
	223.0	0.15			180.0	0.11	4.77
	283.0	0.18			244.0	0.13	4.84
	343.0	0.15			306.0	0.14	4.91
	508.0	0.23			518.0	0.16	4.92
	528.0	0.26			533.0	0.20	4.78

continued on Page 111 . . .

TABLE VII (continued)

Concentration - Time Measurements (Unsleeved Runs)

Run No.	Time (min)	Silicon Concentration (wt.%)	Carbon Concentration (wt.%)	Run No.	Time (min)	Silicon Concentration (wt.%)	Carbon Concentration (wt.%)
3	657.0	0.18	4.93	4	1,464.0	0.69	4.75
	1,269.0	0.49	4.70		1,524.0	0.74	4.85
	1,329.0	0.57	4.72		1,584.0	0.70	4.85
	1,389.0	0.57	4.72		1,639.0	0.81	4.62
					1,759.0	0.86	4.67
					1,856.0	0.90	4.72
5	1,856.0	0.90	4.72	6	2,712.0	1.84	4.48
	1,879.0	0.86	4.65		2,757.0	1.92	4.46
	2,064.0	1.17	4.57		2,807.0	1.97	-
	2,700.0	1.84	4.35		2,871.0	2.09	4.52
	2,712.0	1.84	4.48		2,914.0	2.15	4.48
					2,989.0	2.28	4.28

continued . . .

TABLE VII (continued)

Concentration - Time Measurements (Unsleeved Runs)

Run No.	Time (min)	Silicon Concentration (wt.%)	Carbon Concentration (wt.%)	Run No.	Time (min)	Silicon Concentration (wt.%)	Carbon Concentration (wt.%)
7	0.0	0.009	-	8	699.0	0.28	4.93
	182.0	0.13	5.06		1,316.0	0.43	5.02
	302.0	0.15	4.97		1,380.0	0.47	
	362.0	0.22	5.08		1,442.0	0.47	5.10
	699.0	0.28	4.93		1,482.0	0.52	5.12
9	1,482.0	0.52	5.12	10	2,069.0	0.79	4.66
	1,542.0	0.53			2,162.0	0.79	
	1,602.0	0.55			2,770.0	1.22	
	1,662.0	0.59	4.34		2,827.0	1.20	
	1,722.0	0.66	5.06				
	1,783.0	0.68	4.69				
	2,027.0	0.70	-				

continued . . .

TABLE VII (continued)

Concentration - Time Measurements (Unsleeved Runs)

Run No.	Time (min)	Silicon Concentration (wt.%)	Carbon Concentration (wt.%)	Run No.	Time (min)	Silicon Concentration (wt.%)	Carbon Concentration (wt.%)
11	2,887.0	1.22	4.82	12	0.0	0.01	
	2,932.0	1.29			120.0	0.04	
	2,977.0	1.30			240.0	0.07	
	3,022.0	1.36			310.0	0.07	
	3,067.0	1.65	4.89		465.0	0.12	
	3,197.0	2.01					

continued . . .

TABLE VII (continued)

Concentration - Time Measurements (Unsleeved Runs)

Run No.	Time (min)	Silicon Concentration (wt.%)	Carbon Concentration (wt.%)	Run No.	Time (min)	Silicon Concentration (wt.%)	Carbon Concentration (wt.%)
13	675.0	0.17		14	1,310.0	0.41	
	680.0	0.17			1,435.0	0.48	
	1,263.0	0.38			1,575.0	0.56	
	1,266.0	0.38			1,633.0	0.60	
					1,718.0	0.65	
					1,765.0	0.67	
					1,847.0	0.72	
					1,950.0	0.78	
					2,085.0	0.85	
					2,699.0	1.17	
					2,711.0	1.23	

continued . . .

TABLE VII (continued)

Concentration - Time Measurements (Unsleeved Runs)

Run No.	Time (min)	Silicon Concentration (wt.%)	Carbon Concentration (wt.%)	Run No.	Time (min)	Silicon Concentration (wt.%)	Carbon Concentration (wt.%)
15	2,911.0	1.30		16 i)	3,370.0	1.64	
	3,024.0	1.38		(ii)	3,370.0	1.66	
	3,145.0	1.47		(i)	4,152.0	2.54	
	3,192.0	1.54		(ii)	4,152.0	2.48	
	3,281.0	1.60		(i)	4,233.0	2.64	
	3,342.0	1.65		(ii)	4,233.0	2.62	
(i)	3,370.0	1.64			4,300.0	2.78	
(ii)	3,370.0	1.66		(i)	4,500.0	3.03	
				(ii)	4,500.0	3.00	

(i) - quartz sampler

(ii) - graphite sampler

continued . . .

TABLE VII (continued)

Concentration - Time Measurements (Unsleeved Runs)

Run No.	Time (min)	Silicon Concentration (wt.%)	Carbon Concentration (wt.%)	Run No.	Time (min)	Silicon Concentration (wt.%)	Carbon Concentration (wt.%)
17	0.0	0.03		18	891.0	0.38	5.12
	60.0	0.04			959.0	0.45	4.92
	122.0	0.05			1,036.0	0.56	4.91
	809.0	0.32			1,101.0	0.63	4.87
	832.0	0.33			1,283.0	0.73	4.82
	842.0	0.35					
19	1,309.0	0.76	4.65	20	0.0	0.0	
	1,401.0	0.93	-		4,125.0	2.90	
	1,443.0	1.17	4.75		4,126.0	2.90	
	1,711.0	1.77	4.56				
	1,714.0	1.83	4.24				

continued . . .

TABLE VII (continued)

Concentration - Time Measurements (Unsleeved Runs)

Run No.	Time (min)	Silicon Concentration (wt.%)	Carbon Concentration (wt.%)	Run No.	Time (min)	Silicon Concentration (wt.%)	Carbon Concentration (wt.%)
21	0.0	0.37		22	575.0	1.43	
	60.0	0.49			604.0	1.52	
	120.0	0.63			634.0	1.60	
	180.0	0.75			649.0	1.66	
	240.0	0.86					
	268.0	0.99					
	383.0	1.18					
	528.0	1.45					

continued . . .

TABLE VII (continued)

Concentration - Time Measurements (Unsleeved Runs)

Run No.	Time (min)	Silicon Concentration (wt.%)	Carbon Concentration (wt.%)	Run No.	Time (min)	Silicon Concentration (wt.%)	Carbon Concentration (wt.%)
23	0.0	0.03		24	1,432.0	0.35	
	105.0	0.04			1,515.0	0.38	
	230.0	0.05			1,627.0	0.41	
	349.0	0.09			1,779.0	0.45	
	475.0	0.11			2,069.0	0.55	
	573.0	0.14			2,790.0	0.81	
	764.0	0.16					
	1,397.0	0.32					
	1,410.0	0.34					

continued . . .

TABLE VII (continued)

Concentration - Time Measurements (Unsleeved Runs)

Run No.	Time (min)	Silicon Concentration (wt.%)	Carbon Concentration (wt.%)	Run No.	Time (min)	Silicon Concentration (wt.%)	Carbon Concentration (wt.%)
25	0.0	0.13		26	0.0	0.36	
	115.0	0.27			115.0	0.38	
	135.0	0.30			310.0	0.83	
	307.0	0.39			462.0	1.26	
	433.0	0.55			553.0	1.43	
	658.0	0.77					

TABLE VIII

CARBON MONOXIDE VOLUME - TIME MEASUREMENTS

Run No.	Time (min)	Pellet Distance (cm)	Run No.	Time (min)	Pellet Distance (cm)
1	0.0	12.0	1	10.50	262.5
	1.00	14.5		11.25	280.9
	1.50	24.6		12.00	288.8
	1.75	33.0		13.00	306.9
	2.00	40.9		13.50	324.9
	2.25	48.5		14.00	340.7
	2.50	57.7		14.50	354.6
	2.75	65.5		15.00	365.7
	3.00	73.5		15.50	370.6
	3.75	80.3		16.00	383.2
	4.10	96.2		16.50	402.0
	5.00	105.2		17.50	435.5
	6.00	138.2		18.00	450.2
	6.50	155.7		19.00	473.7
	7.00	171.2		19.50	491.9
	7.75	187.0		20.00	497.0
	8.00	189.4		20.75	510.7
	9.00	209.4		21.00	513.4
	10.00	247.1		21.50	519.8

continued . . .

TABLE VIII
(continued)

CARBON MONOXIDE VOLUME - TIME MEASUREMENTS

Run No.	Time (min)	Pellet Distance (cm)	Run No.	Time (min)	Pellet Distance (cm)
1	22.00	524.7	3	4.00	44.2
	23.00	528.9		5.00	54.3
	24.00	531.7		6.00	60.3
	25.00	533.1		7.00	65.6
	26.00	534.1			
	27.00	535.6	4	0.0	0.2
	28.00	539.3		0.25	5.4
	29.00	546.4		1.25	22.3
				2.00	36.5
2	30.00	554.0		3.00	53.9
	32.00	567.7		4.00	71.8
	33.00	581.5		5.00	86.0
	34.00	594.5		6.00	102.3
	35.00	607.3			
	36.00	617.8			
	37.00	624.6			
3	0.0	6.3			
	1.00	15.6			
	2.00	24.6			
	3.00	35.8			

TABLE IX

CONCENTRATION - TIME MEASUREMENTS (SLEEVED RUNS)

Run No.	Time (min)	Silicon Concentration (wt.%)	Carbon Concentration (wt.%)	Run No.	Time (min)	Silicon Concentration (wt.%)	Carbon Concentration (wt.%)
1	0.0	0.27	-	2	1,385.0	1.42	4.59
	67.0	0.31	4.54		1,482.0	1.45	4.50
	173.0	0.44	4.77		1,572.0	1.59	4.42
	237.0	0.47	4.16		1,634.0	1.69	4.52
	367.0	0.57	4.60		1,692.0	1.77	4.33
	467.0	0.70			1,814.0	1.92	4.44
	1,212.0	1.37	4.29				
	1,272.0	1.43	3.88				
	1,337.0	1.54	4.04				

continued . . .

TABLE IX

(continued)

CONCENTRATION - TIME MEASUREMENTS (SLEEVED RUNS)

Run No.	Time (min)	Silicon Concentration (wt.%)	Carbon Concentration (wt.%)	Run No.	Time (min)	Silicon Concentration (wt.%)	Carbon Concentration (wt.%)
3	2,057.0	1.64		4	0.0	0.03	
	2,757.0	2.46	4.45		92.0	0.06	
	2,972.0	2.94			298.0	0.11	
	3,271.0	3.06	4.32		966.0	0.33	
					1,039.0	0.36	
					1,109.0	0.38	
5	1,166.0	0.38		6	1,759.0	0.82	
	1,290.0	0.52			2,426.0	1.23	
	1,349.0	0.59			2,496.0	1.40	
	1,431.0	0.64			2,527.0	1.45	
	1,581.0	0.78			2,733.0	1.55	
	1,727.0	0.95			2,839.0	1.72	

continued . . .

TABLE IX

CONCENTRATION - TIME MEASUREMENTS (SLEEVED RUNS)

Run No.	Time (min)	Silicon Concentration (wt.%)	Carbon Concentration (wt.%)	Run No.	Time (min)	Silicon Concentration (wt.%)	Carbon Concentration (wt.%)
7	0.0	0.04		8	1,044.0	0.77	
	93.0	0.13			1,046.0	0.76	
	167.0	0.31			1,103.0	0.87	
	210.0	0.26			1,183.0	1.00	
	261.0	0.27			1,193.0	0.98	
	965.0	0.82			1,253.0	1.03	
	990.0	0.83					

continued . . .

TABLE IX

CONCENTRATION - TIME MEASUREMENTS (SLEEVED RUNS)

Run No.	Time (min)	Silicon Concentration (wt.%)	Carbon Concentration (wt.%)	Run No.	Time (min)	Silicon Concentration (wt.%)	Carbon Concentration (wt.%)
9	1,253.0	1.03		10	0.0	0.15	
	1,305.0	1.15			61.0	0.33	
	1,343.0	1.30			119.0	0.35	
	1,415.0	1.44			179.0	0.51	
					239.0	0.67	
					303.0	0.80	
					359.0	0.87	
					408.0	0.95	

continued . . .

TABLE IX

CONCENTRATION - TIME MEASUREMENTS (SLEEVED RUNS)

Run No.	Time (min)	Silicon Concentration (wt.%)	Carbon Concentration (wt.%)	Run No.	Time (min)	Silicon Concentration (wt.%)	Carbon Concentration (wt.%)
11	0.0	0.08		12	482.0	0.50	
	60.0	0.11			485.0	0.50	
	120.0	0.19			546.0	0.59	
	180.0	0.27			1,207.0	1.09	
	240.0	0.29			1,267.0	1.23	
	280.0	0.34			1,342.0	1.28	
	389.0	0.49					
	450.0	0.56					

continued . . .

TABLE IX

CONCENTRATION - TIME MEASUREMENTS (SLEEVED RUNS)

Run No.	Time (min)	Silicon Concentration (wt.%)	Carbon Concentration (wt.%)	Run No.	Time (min)	Silicon Concentration (wt.%)	Carbon Concentration (wt.%)
13	0.0	0.13		14	586.0	0.32	
	104.0	0.18			602.0	0.35	
	165.0	0.19			1,260.0	0.86	
	225.0	0.26			1,580.0	0.98	
	295.0	0.29					
	345.0	0.32		15	0.0	0.06	4.89
	530.0	0.41			138.0	0.10	4.06
	535.0	0.38			241.0	0.14	5.17
					359.0	0.21	4.45
					574.0	0.30	4.83
					583.0	0.33	4.42

continued . . .

TABLE IX

CONCENTRATION - TIME MEASUREMENTS (SLEEVED RUNS)

Run No.	Time (min)	Silicon Concentration (wt.%)	Carbon Concentration (wt.%)	Run No.	Time (min)	Silicon Concentration (wt.%)	Carbon Concentration (wt.%)
16	620.0	0.35	4.75	17	1,471.0	1.06	5.05
	714.0	0.38	4.89		1,628.0	1.18	4.60
	1,364.0	0.88	4.77		1,696.0	1.25	4.97
	1,388.0	0.89	4.69		1,748.0	1.37	4.60
					1,812.0	1.51	4.36
					1,952.0	1.71	4.65
					1,964.0	1.72	4.76

continued . . .

TABLE IX

CONCENTRATION - TIME MEASUREMENTS (SLEEVED RUNS)

Run No.	Time (min)	Silicon Concentration (wt.%)	Carbon Concentration (wt.%)	Run No.	Time (min)	Silicon Concentration (wt.%)	Carbon Concentration (wt.%)
18	0.0	0.08	0.08	19	933.0	0.94	4.56
	60.0	0.16	4.88		933.0	1.07	-
	121.0	0.19	4.75		995.0	1.07	4.71
	147.0	0.26	4.80		1,065.0	1.24	4.67
	900.0	0.89	-		1,113.0	1.37	4.74
	904.0	0.89	4.48		1,200.0	1.60	-
					1,264.0	1.72	4.25

continued . . .

TABLE IX

CONCENTRATION - TIME MEASUREMENTS (SLEEVED RUNS)

Run No.	Time (min)	Silicon Concentration (wt.%)	Carbon Concentration (wt.%)	Run No.	Time (min)	Silicon Concentration (wt.%)	Carbon Concentration (wt.%)
20	1,284.0	1.75	4.37	22	0.0	0.10	
	1,409.0	2.25	4.15		147.0	0.42	
	1,474.0	2.68	4.22		320.0	0.63	
	1,534.0	2.92	-		410.0	0.85	
	1,544.0	2.98	-		622.0	1.06	
	1,561.0	2.98	4.33				
21	0.0	0.71					
	60.0	0.75					
	230.0	0.77					
	367.0	0.90					
	581.0	1.00					

TABLE X

CARBON MONOXIDE FLOW RATES

(Sleeved Kinetic Experiments)

Run No.	Per Cent CO (vol.%)	Total Flowrate (ml/min)	CO Flowrate at S.T.P. (ml/min)
18	1.1	222	2.25
	1.3	250	3.00
19	2.4	258	5.71
20	2.1	500	10.13
	3.6	386	12.82

TABLE XI

SPECIFIC REACTION RATE CONSTANT

(Unsleeved System)

Run No.	Slope x 10^4 (gm/min)	Error in Slope x 10^4	Bath Height (cm)	Temperature (°C)	$1/T$ ($°K^{-1}$ x 10^4)	Denisty (gm/cm^3)	Apparent Rate Constant x 10^5 ($moles/cm^2/min$)
1	2.84	1.32	3.20	1412	5.93	6.87	2.23
2	2.80	0.83	3.50	1419	5.91	6.86	2.40
3	4.79	1.00	3.54	1453	5.79	6.84	4.14
4	5.58	2.69	3.75	1465	5.75	6.82	5.10
5	11.22	1.58	3.01	1496	5.65	6.80	8.20
6	15.72	1.40	3.34	1516	5.59	6.78	12.71
7	2.83	1.40	3.00	1394	6.00	6.89	2.09
8	2.80	0.93	3.50	1419	5.91	6.86	2.40
9	5.13	0.94	3.06	1441	5.83	6.84	3.83
10	6.06	2.50	3.02	1458	5.78	6.83	4.46
11	26.46	10.70	3.02	1534	5.53	6.77	19.32

continued . . .

TABLE XI

SPECIFIC REACTION RATE CONSTANT

(Unsleeved System)

Run No.	Slope x 10^4 (gm/min)	Error in Slope x 10^4	Bath Height (cm)	Temperature (°C)	$1/T$ ($°K^{-1}$ x 10^4)	Density (gm/cm^3)	Apparent Rate Constant x 10^5 ($moles/cm^2/min$)
12	2.27	0.66	3.41	1395	6.00	6.89	1.90
13	3.32	1.14	3.01	1410	5.94	6.87	2.45
14	5.65	0.20	2.93	1434	5.86	6.85	4.05
15	7.90	0.78	2.96	1460	5.77	6.83	5.10
16	11.99	0.67	2.98	1492	5.67	6.81	8.69
17	3.81	0.34	3.20	1404	5.98	6.88	3.00
18	10.83	1.72	3.20	1473	5.73	6.82	8.44
19	26.00	4.92	3.00	1409	5.61	6.79	18.92
20	7.03	-	3.29	1460	5.77	6.83	5.64
21	20.74	1.42	2.97	1510	4.61	6.79	14.94
22	30.32	6.11	2.99	1528	5.55	6.78	21.95

continued . . .

TABLE XI

SPECIFIC REACTION RATE CONSTANT

(Unsleeved System)

Run No.	Slope x 10^4 (gm/min)	Error in Slope x 10^4	Bath Height (cm)	Temperature (°C)	1/T ($°K^{-1}$ x 10^4)	Density (gm/cm^3)	Apparent Rate Constant x 10^5 ($moles/cm^2/min$)
23	2.22	0.22	3.01	1380	6.05	6.89	1.64
24	3.38	0.23	2.67	1396	5.99	6.88	2.22
25	9.34	1.46	1.52	1450	5.50	6.84	3.47
26	20.90	7.04	1.42	1460	5.77	6.83	7.24

TABLE XII

SPECIFIC REACTION RATE CONSTANT FROM CARBON

MONOXIDE VOLUME EXPERIMENTS (UNSLEEVED)

Run No.	Slope x 10^4 (gm Si / min)	Bath Height (cm)	Temperature (°C)	1/T °K x 10^9	Density (gm/cm^3)	Apparaent Rate Constant x 10^5 ($moles/cm^2/min.$)
1	17.90	2.30	1505	5.62	6.80	10.00
2	5.73	2.30	1445	5.82	6.84	3.22
3	5.47	2.30	1430	5.87	6.87	3.08
4	12.10	2.30	1485	5.69	6.82	6.78

TABLE XIII

SPECIFIC REACTION RATE CONSTANT

(Sleeved System)

Run No.	Slope x 10^4 (gm/min)	Error in Slope x 10^4	Bath Height (cm)	Temperature (°C)	$1/T$ ($°K^{-1}$ x 10^4)	Density (gm/cm^3)	Rate Constant x 10^5 ($moles/cm^2/min$)
1	9.34	0.34	1.78	1425	5.89	6.86	4.07
2	12.44	2.80	1.81	1468	5.74	6.82	5.48
3	12.29	0.65	3.06	1496	5.65	6.80	9.13
4	3.10	0.16	2.98	1398	5.98	6.88	2.33
5	9.82	1.00	1.98	1430	5.87	6.85	4.78
6	8.11	2.17	2.76	1454	5.79	6.83	5.46
7	7.80	0.50	2.98	1459	5.77	6.82	5.66
8	13.59	3.77	2.96	1490	5.67	6.81	9.78
9	25.93	10.32	2.89	1512	5.60	6.78	18.18
10	19.82	2.28	3.20	1506	5.62	6.79	15.38
11	10.80	1.21	2.82	1466	5.75	6.83	7.43

continued . . .

TABLE XIII

SPECIFIC REACTION RATE CONSTANT

(Sleeved System)

Run No.	Slope x 10^4 (gm/min)	Error in Slope x 10^4	Bath Height (cm)	Temperature (°C)	$1/T$ ($°K^{-1}$ x 10^4)	Density (gm/cm^3)	Rate Constant x 10^5 ($moles/cm^2/min$)
12	8.80	1.06	3.43	1472	5.73	6.82	7.35
13	5.10	0.85	2.06	1415	5.92	6.87	2.58
14	6.85	2.63	2.60	1454	5.79	6.84	4.34
15	4.60	0.80	3.00	1410	5.94	6.87	3.39
16	7.30	1.19	3.30	1450	5.80	6.84	5.88
17	16.89	1.56	3.60	1515	5.59	6.78	14.72
18*	8.78	0.60	3.00	1425	5.89	6.86	6.45
19*	24.31	1.22	3.00	1475	5.72	6.82	17.76
20*	46.81	6.39	3.00	1515	5.59	6.78	34.00
21	5.99	2.08	2.22	1408	5.95	6.87	2.71
22	15.41	4.12	1.77	1453	5.79	6.84	6.66

* Full Sleeve

TABLE XIV

SPECIFIC REACTION RATE CONSTANT

(Sleeved System by Carbon Monoxide Analyses)

Run No.	Silicon Transfer Rate (gm/min x 10^4)	Equivalent Slope (wt.% Si/ min x 10^4)	Bath Height (cm)	Density gm/cm^3	Temperature °C	$1/T$ $°K^{-1}$ x 10^4	Rate Constant x 10^5 (moles/cm^2/min.)
18	14.1	7.05	3.00	6.86	1425	5.89	5.18
	18.7	9.40	3.00	6.86	1425	5.89	6.82
19	35.7	17.90	3.00	6.82	1475	5.72	13.10
20	63.2	31.60	3.00	6.78	1515	5.59	23.00
	80.1	40.05	3.00	6.78	1515	5.59	29.18

TABLE XV

VARIATION IN CARBON SATURATION WITH SILICON CONCENTRATION

Experiment No.	Slope -k(%C change/% Si)
Unsleeved	
2	.27 ± .88
3	.56 ± .35
4	.51 ± 1.19
5	.27 ± .16
6	.33 ± .57
18	.72 ± .53
19	.31 ± .63
Sleeved	
1	.45 ± .36
2	.29 ± .39
16	.17 ± .46
17	.42 ± .74
18	.37 ± .50
19	.43 ± .69
20	.03 ± .38
Average	.37 ± .56

TABLE XVI

SLAG ANALYSES

(Zirconium Oxide Sleeves)

Slag No.	% SiO_2 (wt.%)	% CaO (wt.%)	% MgO (wt.%)	% ZrO_2 (wt. %)	Total
1	56.0	29.4	8.1	3.0	96.4
2	55.2	30.0	6.9	2.0	94.1
3	60.3	27.3	8.1	2.0	97.7
4	51.8	26.2	5.3	5.0	88.3

TABLE XVII

SLAG ANALYSES

Experiment No.	SiO_2 (wt.%)	CaO (wt.%)	MgO (wt.%)	Total	Temperature °C
Unsleeved					
1	65.2	29.3	4.0	98.5	1412
2	65.7	26.7	5.3	98.7	1419
5	67.0	28.4	5.5	100.9	1496
8	64.2	28.1	7.6	99.9	1419
11	68.2	24.0	6.2	98.4	1534
12	64.9	26.9	8.2	100.0	1395
16	66.3	26.1	8.2	99.6	1492
17	65.1	27.3	7.4	99.8	1404
Sleeved					
8	64.9	26.4	8.1	99.4	1490
	64.3	26.4	7.7	98.4	1490

TABLE XVIII

ELECTROMOTIVE FORCE MEASUREMENTS

(Silicon as the Metal Phase)

Run No.	EMF (mv)	Temperature °C	Temperature °K	Standard Free Energy Change (cal/gm mole)
1	189	1379	1652	- 17,435
	181	1386	1659	- 16,697
	167	1407	1680	- 15,405
	153	1422	1695	- 14,114
	142	1437	1710	- 13,099
	128	1452	1725	- 11,808
	108	1466	1739	- 9,963
	91	1486	1759	- 8,395
	70	1516	1789	- 6,467
	52	1533	1806	- 4,797
2	135	1441	1709	- 12,454
	120	1454	1727	- 11,070
	104	1463	1736	- 9,594
3	74	1507	1780	- 6,826
	165	1400	1673	- 15,221
	175	1397	1670	- 16,143

TABLE XX

ELECTROMOTIVE FORCE MEASUREMENTS

(Fe-Si as the Metal Phase)

Experiment No.	Time (min)	Experimental EMF (mv)	Silicon Content (wt.%)	Temperature °C
1	0	123	17.8	1350
	16	120		
	19	128		
	20	125		
	32	130		
	67	147		1370
	74	140		
	75	147		
	92	148		1385
	107	132		
	134	140		
	152	265	14.4	1380
	155	256		
	160	203		
	284	150		1350
	289	151		
	236	126		1350
	335	121		

continued . . .

TABLE XX

ELECTROMOTIVE FORCE MEASUREMENTS

(Fe-Si as the Metal Phase)

Experiment No.	Time (min)	Experimental EMF (mv)	Silicon Content (wt.%)	Temperature °C
2	0	46	7.55	1390
	45	52		
	47	52		
	56	53		
	58	53		
	60	53		
	82	54		
	87	55		
	166	61		
	201	63		
	212	63		
	219	63		
	240	63		
	252	63		
	309	64		1400
	320	65		
	332	66		
	368	65		
	382	64		

continued . . .

TABLE XX

ELECTROMOTIVE FORCE MEASUREMENTS

(Fe-Si as the Metal Phase)

Experiment No.	Time (min)	Experimental EMF (mv)	Silicon Content (wt.%)	Temperature °C
2	1,384	58		
	1,387	59		
	1,431	59		
	1,446	58		
	1,460	58		
	1,490	58		
	1,661	58		1390
	1,782	73	6.10	
	1,787	76		
	1,801	79		
	1,811	81		
	1,826	82		
	2,088	88		
	2,779	90		
	2,829	88		
	2,852	88		
	2,865	88		1395
	2,912	88		
	2,933	85		
	2,960	85		

continued . . .

TABLE XX

ELECTROMOTIVE FORCE MEASUREMENTS

(Fe-Si as the Metal Phase)

Experiment No.	Time (min)	Experimental EMF (mv)	Silicon Content (wt.%)	Temperature °C
2	2,962	85		
	2,982	75		
	2,994	75		
	3,096	78		
	3,101	78		
	3,105	77		
	3,119	78		
	3,137	75		
	4,295	77		
	5,870	87	5.12	1390
	5,872	89		
	5,875	90		
	5,878	89		
3	0	- 16.0		1440
	13	- 15.0	19.91	
	21	- 13.5		
	25	- 14.5		
	31	- 15.2		
	40	- 14.5		
	48	- 13.8		1469

continued . . .

TABLE XX

ELECTROMOTIVE FORCE MEASUREMENTS

(Fe-Si as the Metal Phase)

Experiment No.	Time (min)	Experimental EMF (mv)	Silicon Content (wt.%)	Temperature °C
3	51	- 13.5		
	56	- 13.3		
	63	- 11.4		
	70	- 9.2		1475
	75	- 8.4		
	90	- 7.0		
	96	- 5.2		
	125	- 1.9		
	132	- 2.0		
	150	- 1.0		
	840	- 3.3		1476
	873	- 3.2		1475
	885	- 4.4		
	895	- 5.5		
	908	- 5.5		
	950	- 1.3		
	983	- 0.3		
	1,032	+ 5.3		1510
	1,060	+ 6.5		

continued . . .

TABLE XX

ELECTROMOTIVE FORCE MEASUREMENTS

(Fe-Si as the Metal Phase)

Experiment No.	Time (min)	Experimental EMF (mv)	Silicon Content (wt.%)	Temperature °C
3	1,074	+ 6.0		1510
	1,083	+ 18.5	15.42	
	1,086	+ 21.0		
	1,105	+ 37.0		
	1,113	+ 37.5		
	1,130	+ 40.5		
	1,133	+ 40.5		1512
	1,160	+ 40.6		1475
	1,172	+ 42.5		1475
	1,186	+ 43.5		
	1,234	+ 51.8		
	1,277	+ 52.5		
	1,278	+ 54.5		
	1,315	+ 54.8		
	1,446	+ 53.8		
	1,459	+ 54.8		1487
	1,463	+ 55.5		
	1,472	+ 54.5		
	1,480	+ 54.5		
	1,482	+ 51.0	11.61	1490

continued . . .

TABLE XX

ELECTROMOTIVE FORCE MEASUREMENTS

(Fe-Si as the Metal Phase)

Experiment No.	Time (min)	Experimental EMF ($_{mv}$)	Silicon Content (wt.%)	Temperature °C
3	1,487	+ 56.0		
	1,497	+ 59.5		
	1,507	+ 60.0		
	1,555	+ 61.8		
	1,562	+ 62.0		1490
	1,567	+ 62.0		1490
	2,280	+ 39.2		1425
	2,322	+ 37.5		
	2,326	+ 39.2		1425
	2,529	+ 46.2		1505
	2,560	+ 48.5		1505
	2,628	+ 49.2		1505
4	0	- 23	29.0	
	4	- 30		1530
	16	- 35		
	21	- 36		
	43	- 30		
	166	- 46		1475
	196	- 48		

continued . . .

TABLE XX

ELECTROMOTIVE FORCE MEASUREMENTS

(Fe-Si as the Metal Phase)

Experiment No.	Time (min)	Experimental EMF (mv)	Silicon Content (wt.%)	Temperature °C
4	216	- 49		
	226	- 46		
	256	- 48		
	276	- 49		
	296	- 33	22.5	1480
	981	- 30		
	1,006	- 26		
	1,031	- 20		
	1,061	- 19		1480
	1,081	- 18		
	1,107	- 19		
	1,136	- 18		1483
	1,400	- 19		

TABLE XXI

ELECTROMOTIVE FORCE MEASUREMENTS

(Fe-C-Si as the Metal Phase)

Run No.	Time (min)	EMF Experimental (mv)	Silicon Content (wt.%)	Carbon Content (wt.%)	Temperature °C
5		137	1.91		1480
6		180	0.20		1450
7		115	2.94		1450
8		120	0.10		1350
9		223	0.03		1370
10	0	152	0.56		
	242	150			
	790	171			
	792	154	0.72	4.88	
	801	166			
	828	146			
	838	152			
	843	165			
	1,075	163 $\pm$ 5			
	1,078		0.84	4.90	
	1,080	161			
	1,081	161			
	1,095	160			

continued . . .

TABLE XXI

ELECTROMOTIVE FORCE MEASUREMENTS

(Fe-C-Si as the Metal Phase)

Run No.	Time (min)	EMF Experimental (mv)	Silicon Content (wt.%)	Carbon Content (wt.%)	Temperature °C
10	1,100	161			
	1,101	163			
	1,102	164			
	1,103	161			
	1,104	150			
	1,104	152			
	1,105	153			
	1,106	155			1428
	1,107	158			
	1,108	163			
	1,109	159			
	1,110	158			
	1,111	160			
	1,112	159			
	1,113	161			
	1,341	158			
	1,342	151	0.94	4.58	
	1,344	150			
	1,346	134			

continued . . .

TABLE XXI

ELECTROMOTIVE FORCE MEASUREMENTS

(Fe-C-Si as the Metal Phase)

Run No.	Time (min)	EMF Experimental (mv)	Silicon Content (wt.%)	Carbon Content (wt.%)	Temperature °C
10	1,352	142			
	1,818	147			
	1,821		1.09		
	1,823	134			
	2,520	130			
	2,521	150			
	2,525	149	1.35	4.66	
	2,527	146			
	2,530	144			
	2,531	147			1425
	2,532	144			
11	0	190			1400
	2	193			
	4	192			
	5	192			
	8		0.16	-	
	12	190			
	18	188			
	20	182			

continued . . .

TABLE XXI

ELECTROMOTIVE FORCE MEASUREMENTS

(Fe-C-Si as the Metal Phase)

Run No.	Time (min)	EMF Experimental (mv)	Silicon Content (wt.%)	Carbon Content (wt.%)	Temperature
11	30	178			
	35	170			
	40	170			
	65	160			
	71	157			
	77	154			
	80	150	0.21	4.90	1398
	83	150			
	95	144			
	105	142			
	122	140			
	211	120			
	220	123	0.35	4.72	
	480	93			
	1,082		0.74	4.60	
	1,121	77			
	1,122		0.74	4.63	
	1,127	73			
	1,128	75			

continued . . .

TABLE XXI

ELECTROMOTIVE FORCE MEASUREMENTS

(Fe-C-Si as the Metal Phase)

Run No.	Time (min)	EMF Experimental (mv)	Silicon Content (wt.%)	Carbon Content (wt.%)	Temperature
11	1,129	74			
	1,130	71			
	1,133	72			
	1,140	71			
	1,146	72			
	1,195	72			
	1,196				
	1,199	75			1410
	1,212	96			1440
	1,213	99			
	1,216	99			
	1,224		0.82	4.59	
	1,244	99			
	1,250	100			
	1,264	99			
	1,297	94			
	1,318	91			
	1,323	90			
	1,355	88			
	1,357		1.01		

continued . . .

TABLE XXI

ELECTROMOTIVE FORCE MEASUREMENTS

(Fe-C-Si as the Metal Phase)

Run No.	Time (min)	EMF Experimental (mv)	Silicon Content (wt.%)	Carbon Content (wt.%)	Temperature °C
11	1,359	84			
	1,381	91			1440
	1,386	93			1455
	1,394	91			1461
	1,398	96			1480
	1,401	103			
	1,408	104			
	1,425	101			
	1,430	98	1.20		
	1,434	101			1481
	fluctuating				

TABLE XXI

ELECTROMOTIVE FORCE MEASUREMENTS

Experiment No. 12

(ZrO_2 sleeve)

Time (min)	EMF (mv)	% Si	Temperature °C	Time (min)	EMF (mv)	% Si	Temperature
0	107	.12	1400	86	103		1401
6	118			186	128		1408
7	123			188	122	.18	
12	130			191	128		
17	132			197	128		
21	135			201	126		
25	136			217	124		
30	139			224	121		
32	141			243	108		
37	140			251	105		
47	144			278	102		
54	145			309	82	.24	
61	143		1402	326	92		
63	131			337	91		
75	127		1400	1,013	57	.71	
67	125			1,016	54		
69	117			1,021	57		
71	111			1,042	53		1402
73	115			1,085	59		
82	103		1400				

TABLE XXI

ELECTROMOTIVE FORCE MEASUREMENTS

Experiment No. 13

Time (min)	EMF (mv)	% Si	Temperature °C	Time (min)	EMF (mv)	% Si	Temperature
0	106		1390	140	79		
6	106	.61		150	91		
8	95			154	95		
22	89		1401	211	101		
32	80			218	113		
111	78			226	107	.73	
112	98			228	107		
117	94			233	115		1403
120	105	.67		234	120		
121	97			235	123		
127	108			253	110		
128	95			257	111		
				403	85		
			Experiment No. 14				
0	160		1439	27	159	.71	
12	165		1444	35	158		
24	165			56	154		
				124	159		1444

TABLE XXI

ELECTROMOTIVE FORCE MEASUREMENTS

Experiment No. 15

Time (min)	EMF (mv)	% Si	Temperature °C	Time (min)	EMF (mv)	% Si	Temperature °C
0	- 95	18.97	1420	173	- 10		
148	- 107			174	- 17		
153	- 92			178	- 16		
155	- 96			180	- 15		
156	- 107			186	- 14		
160	- 110			197	- 13		
167	- 107			212	+ 14		
168	- 25	12.55		219		11.18	
171	- 30			222	+ 3		
172	- 20			229	+ 4		1418
				236	+ 5		

TABLE XXI

Experiment 16

Time (min)	EMF (mv)	% Si	% C	Temperature °C
0	176	.28		1450
8	176			
41	168			
48	153			
61	152			
66	147			
71	152			
72	149			
74	151			
116	132	.70	4.82	
123	134			
126	132			
246	110			
252	78			
257	76			
260	77			
263	84			
267	91			1445
269	94			
272	97			
300	91			

continued . . .

TABLE XXI

Experiment 16

Time (min)	EMF (mv)	% Si	% C	Temperature °C
303	89			
324	84			
326	84			
362	79			
402	73	1.26	4.25	
409	84			
411	80			
414	75			
1,031	40			
1,033	43			
1,036	47	2.49	4.14	
1,042	54			
1,044	50			
1,081	48			1452
1,119	53			
1,153	41			
1,156	41			
1,164	44			
1,195	42			1458
1,198	43			
1,289	56			

continued . . .

TABLE XXI

Experiment 16

Time (min)	EMF (mv)	% Si	% C	Temperature °C
1,291	42			
1,385	42			
1,639	61	3.21	4.07	
1,677	60			
1,716	66			
1,720		4.46	3.44	
1,748	47			
1,753	52			
1,754	49			1450
1,791	55			
1,795	60	11.27	2.57	
1,798	63			
2,424	30			
2,426	31			
2,456	32			
2,521	33			
2,532	33			
2,540	33			
2,596	34	11.35	1.44	
2,501	34			1493
2,634	33			

continued . . .

TABLE XXI

Experiment 16

Time (min)	EMF (mv)	% Si	% C	Temperature °C
2,651	33			
2,679	- 9			
2,713	- 3.3			
2,750	- 0.6			
2,721	- 0.4			1451
2,853	- 0.3	13.68		
3,774	- 2.5			
3,783	- 2.5			
3,881	- 2.5			

TABLE XXII

ACTIVITY COEFFICIENT OF SILICON IN IRON-SILICON ALLOYS

Experiment Number	EMF (mv)	Temperature °C	N_{Si}	$a_{Si} \times 10^3$	γ_{Si}	$-\log\gamma_{Si}^{T}$	$-\log\gamma_{Si}^{1420}$
1*	126	1350	0.30	27.90	0.093	1.03	0.98
	141	1380	0.30	19.50	0.059	1.23	1.19
	150	1380	0.25	15.10	0.060	1.22	1.18
	126	1350	0.25	27.90	0.112	0.95	0.91
2	59	1390	0.140	0.1325	0.000946	3.02	2.96
	81	1390	0.115	0.0717	0.000623	3.21	3.15
	91	1390	0.101	0.0542	0.000537	3.27	3.21
3	- 14	1440	0.390	4.369	0.0112	1.95	1.97
	- 4	1475	0.390	9.078	0.0233	1.63	1.69
	5	1510	0.390	18.800	0.0482	1.32	1.41
	41	1510	0.266	7.365	0.0277	1.56	1.70
	55	1475	0.266	1.880	0.00707	2.15	2.24
	62	1490	0.207	2.422	0.0117	1.93	2.06
	41	1425	0.207	0.607	0.00293	2.53	2.53
	51	1506	0.207	5.079	0.0245	1.61	1.75
4	- 30	1528	0.448	75.106	0.168	0.77	0.86
	- 58	1476	0.448	29.209	0.0650	1.19	1.23
	- 19	1480	0.366	15.532	0.0424	1.37	1.41

* silicon electrode

TABLE XXIII

ACTIVITY COEFFICIENT OF SILICON IN IRON-CARBON-SILICON ALLOYS

Experiment Number	EMF (mv)	Temperature °C	N_C	N_{Si}	$a_{Si} \times 10^3$	γ'_{Si}	$-\log\gamma'_{Si}$	$-\log\gamma_{Si}$	$\log\gamma^C_{Si}$
5	137	1480	0.193	0.032	0.264	0.00825	2.08	3.12	1.04
6	180	1450	0.197	0.00336	0.0334	0.00994	2.00	3.35	1.35
7	175	1450	0.188	0.0353	0.180	0.00510	2.19	3.20	1.01
8	120	1350	0.186	0.00170	0.0068	0.0040	2.40	3.53	1.13
9	223	1370	0.186	0.000509	0.0007	0.00138	2.86	3.51	0.65
10	165	1425	0.192	0.00857	0.0218	0.00254	2.60	3.40	0.80
	160	1425	0.192	0.0117	0.0250	0.00214	2.67	3.36	0.69
	154	1425	0.185	0.0152	0.0294	0.00193	2.71	3.35	0.64
	149	1425	0.185	0.0185	0.0338	0.00183	2.74	3.31	0.57
	144	1425	0.185	0.0218	0.0387	0.00177	2.75	3.31	0.56
11	194	1400	0.193	0.00269	0.0042	0.00156	2.81	3.46	0.65
	166	1400	0.193	0.00337	0.0091	0.00270	2.57	3.46	0.89

continued . . .

TABLE XXII

ACTIVITY COEFFICIENT OF SILICON IN IRON-CARBON-SILICON ALLOYS

Experiment Number	EMF (mv)	Temperature °C	N_C	N_{Si}	$a_{Si} \times 10^3$	γ'_{Si}	$-\log\gamma'_{Si}$	$-\log\gamma_{Si}$	$\log\gamma^C_{Si}$
11	129	1400	0.190	0.00509	0.0255	0.00501	2.30	3.46	1.16
	109	1400	0.186	0.00676	0.0445	0.00658	2.19	3.45	1.76
	94	1400	0.184	0.00846	0.0675	0.00798	2.10	3.45	1.35
	82	1400	0.182	0.0102	0.0941	0.00923	2.04	3.44	1.40
	76	1400	0.182	0.0118	0.1112	0.00949	2.02	3.43	1.41
	98	1440	0.182	0.0135	0.2099	0.0155	1.81	3.28	1.47
	102	1480	0.181	0.0186	0.5436	0.0292	1.54	3.20	1.66
12	150	1400	0.192	0.00202	0.0143	0.00708	2.15	3.45	1.30
	112	1400	0.191	0.00304	0.0409	0.0135	1.87	3.45	1.58
	88	1400	0.190	0.00456	0.0797	0.0175	1.76	3.44	1.68
	74	1400	0.189	0.00599	0.1175	0.0196	1.71	3.43	1.72
	66	1400	0.188	0.00751	0.1467	0.0195	1.71	3.42	1.71

continued . . .

TABLE XXIII

ACTIVITY COEFFICIENT OF SILICON IN IRON-CARBON-SILICON ALLOYS

Experiment Number	EMF (mv)	Temperature °C	N_C	N_{Si}	$a_{Si} \times 10^3$	γ'_{Si}	$-\log\gamma'_{Si}$	$-\log\gamma_{Si}$	$\log\gamma^C_{Si}$
12	60	1400	0.186	0.00928	0.1733	0.0187	1.73	3.42	1.69
	47	1400	0.185	0.0114	0.1882	0.0165	1.78	3.41	1.63
	54	1400	0.185	0.0127	0.2047	0.0161	1.79	3.41	1.62
13	92	1400	0.185	0.0103	0.0713	0.00692	2.16	3.42	1.26
	98	1400	0.185	0.0118	0.0604	0.00512	2.29	3.41	1.12
	109	1400	0.185	0.0137	0.0944	0.00324	2.49	3.41	0.92
14	162	1444	0.188	0.0119	0.0421	0.00359	2.45	3.34	0.89
15	-102	1420	0.027	0.3-1	27.105	0.0872	1.06	1.48	0.42
	- 15	1420	0.046	0.214	2.497	0.0117	1.93	21.0	0.17
	5	1420	0.052	0.192	1.442	0.00151	2.12	2.25	0.13
16	180	1450	0.184	0.0051	0.0313	0.00614	2.21	3.32	1.11
	160	1450	0.183	0.0076	0.0537	0.00707	2.15	3.30	1.15

continued

TABLE XXIII

ACTIVITY COEFFICIENT OF SILICON IN IRON-CARBON-SILICON ALLOYS

Experiment Number	EMF (mv)	Temperature °C	N_C	N_{Si}	$a_{Si} \times 10^3$	γ'_{Si}	$-\log\gamma'_{Si}$	$-\log\gamma_{Si}$	$\log\gamma^C_{Si}$
16	140	1450	0.181	0.0107	0.0920	0.00860	2.07	3.30	1.23
	120	1450	0.178	0.0124	0.1517	0.0127	1.90	3.28	1.38
	100	1450	0.174	0.0153	0.2703	0.0177	1.75	3.25	1.50
	80	1450	0.168	0.0178	0.4633	0.0260	1.59	3.23	1.64
	60	1450	0.166	0.0272	0.7941	0.0292	1.54	3.18	1.64
	50	1450	0.162	0.0358	1.0397	0.0290	1.54	3.14	1.60
	44	1450	0.160	0.0473	1.2221	0.0258	1.59	3.03	1.44
	58	1450	0.139	0.076	0.8381	0.0110	1.91	2.88	0.88
	32	1450	0.058	0.193	1.6887	0.00875	2.06	2.22	0.16
	- 3	1450	0.026	0.257	4.338	0.0109	1.72	1.78	0.06

TABLE XXIV

ACTIVATION ENERGIES

Experimental Set-Up	Slope x 10^{-4}	Activation Energy kcal/gm mole	Error in Activation Energy kcal/gm mole	A
Sleeved	-47.25 ± 6.767	93.9	13.4	29.12 ± 0.31
Unsleeved	-50.20 ± 5.304	99.7	10.5	30.72 ± .37
Sleeved (full)	-56.28 ± 3.585	111.8	7.1	35.03 ± .07
Unsleeved (CO)	-49.70 ± 2.429	98.8	4.8	30.21 ± .16
Composite (sleeved and unsleeved)	-49.05 ± 4.166	97.5	8.3	-

CHAPTER 6

DISCUSSION OF RESULTS

FARADAYAN YIELD AND KINETIC EXPERIMENTS

A. Faradayan Yield Experiments

6.1 The Local Cell Reaction

It was mentioned in section (2.14) that Wagner[83] suggested that slag-metal reactions necessarily involved electrochemical processes en route to the ultimate reaction. When considering slag-metal reactions occurring in graphite crucibles he posed the possibility of three types of reactions taking place. First he considered the conventional type where molecules or atoms involved in the reaction collided at the slag/metal interface and electrons transferred directly between the colliding species, forming the products. This type of reaction was referred to as a direct chemical reaction. Secondly, he considered the reaction to occur by a series of electrochemical reactions in which anodic and cathodic reactions took place simultaneously at different locations along the slag/metal interface, with electrons transferring many atomic distances through the metal phase adjacent to the interface. Thirdly, he considered that a local cell reaction could occur. This local cell reaction was said to be electrochemical in nature, but was distinguished from the electrochemical reaction occurring at the slag/metal interface, (referred to as the first interface) since it involved a second interface - the slag / crucible interface. Wagner said that an anodic reaction could

occur at the slag/crucible interface, and a corresponding cathodic reaction could occur at the slag/metal interface. The electrons were transferred in the graphite and metal phase and the metal ions migrated in the slag phase. The relative contribution of this local cell reaction involving the second interface, in comparison to the direct chemical and electrochemical reaction at the slag/metal interface, must be known before an attempt is made to interpret the kinetics of any slag-metal system.

6.2 The Local Cell Reaction in Steelmaking Systems

Baak and King[3] investigated the desulphurization of iron in graphite crucibles in terms of the local cell concept of Wagner. They proposed the anodic reaction at the slag/graphite interface to be:

$$O^{2-}_{slag} + C_{graphite} = CO_{gas} + 2e \qquad (6.1)$$

The corresponding cathodic reaction was proposed to be:

$$S_{metal} + 2e = S^{2-}_{slag} \qquad (6.2)$$

In order to test the occurrence of the local cell reaction in this system, they created a model system using a carbon free silver-sulphur alloy as the metal phase and a low melting point sodium borate slag. The experiments were carried out in alumina crucibles with a graphite rod inserted into the slag to act as the anode and a nickel rod was inserted through the slag into the metal to act as the cathode. With this experimental set-up, desulphurization of the metal could only occur by a local cell reaction, and only when the graphite electrode was connected externally to the nickel electrode to provide a path for the electrons. They

attempted to measure the current passed between the electrodes and to correlate it through expression (2.1) to the amount of desulphurization occurring. However, contrary to present belief their results were spurious, and they were unable to make any definite conclusions concerning the occurrence of the local cell reaction in this system[104].

Grimble[95] and Grimble and Ward[4] investigated the presence of the local cell effect in the system involving the reduction of silica from high silica slags by carbon saturated iron, in graphite crucibles. They proposed the anodic reaction at the slag/graphite interface to be:

$$2\,O^{2-}_{slag} + 2\,C_{graphite} = 2\,CO_{gas} + 4e \qquad (6.3)$$

The cathodic reaction at the slag/metal interface was proposed to be:

$$Si^{4+}_{slag} + 4e = Si_{metal}$$

They suggested that if the local cell reaction were present in the silica reduction system, then it would be possible to assume that the reduction of other oxides in the slag could also occur in part by a local cell reaction. These oxides were said to be: MnO, FeO, CrO, P_2O_5, etc., and the common anodic reaction would be:

$$O^{2-}_{slag} + C_{graphite} = CO_{gas} + 2e$$

The individual cathode reactions would be:

$$\begin{aligned} Mn^{2+}_{slag} + 2e &= Mn_{metal} \\ Fe^{2+}_{slag} + 2e &= Fe_{metal} \\ Cr^{2+}_{slag} + 2e &= Cr_{metal} \\ \tfrac{2}{5}\,P^{5+}_{slag} + 2e &= \tfrac{2}{5}\,P_{metal} \end{aligned} \qquad (6.4)$$

6.3 The Local Cell Reaction in the Silica Reduction System

In order to test the existence of this local cell reaction in graphite crucibles, a Faradayan cell was created by eliminating the anodic slag/crucible interface with a silica sleeve and by inserting a graphite rod into the slag phase to act as the anode. In this manner the current passing between the graphite anode and a graphite conductor connected to the metal phase which acts as cathode, could be related through expression (2.1) to the amount of silicon transferred by the local cell reaction.

When carbon saturated iron was used as the metal phase, the current passed between the graphite anode and the metal phase was equivalent to a silicon transfer rate of only 0.002 gm/hr. and was insignificant when compared to the overall silicon transfer rate of 0.80 gm/hr. In a similar experiment Grimble and Ward[4] observed a maximum current of 18 ma, larger than that observed here because of the larger crucible design and greater anode area. In the present work, the current was found to increase as the graphite anode/slag area increased by inserting the anode further into the slag. When the anode was inserted into the metal phase, the current immediately dropped to zero, indicating there were no thermal effects or electrical pick-up from the winding. When the cell was operating, however, current fluctuations did occur and are possibly related to cell polarization, for as the reaction proceeds, carbon monoxide is formed at the anode where it adheres and is evolved intermittently. The carbon monoxide evolved at the slag/metal interface could also create fluctuations in current.

The existence of the local cell reaction could not be tested conclusively with iron-carbon melt as cathode, because the electrochemical

current could not be related to the amount of silicon transferred to the metal phase since the slag/metal reaction was far too great in comparison. The use of carbon free iron was ruled out because the excessive temperatures required would preclude the use of a silica crucible.

A system was chosen using a carbon-free copper metal phase in a silica lined graphite crucible with a tungsten wire maintaining electrical contact between the copper and the graphite crucible through a pinhole in the silicon liner. The anode was a graphite rod inserted with the slag. Any silica transferred electrochemically to the copper phase could be measured by the current passed between the graphite anode and the copper cathode. The first experiment involved a relatively large mass of copper and the low silicon concentration in the copper had to be determined spectrographically, resulting in a large analytical error. In the second experiment a smaller volume of copper was used. However, the silicon transferred was correspondingly less because of the reduced electrode area. The graphite anode and the bottom graphite conducter were hollowed out and filled with copper to reduce the resistance of the external circuit. For this second experiment, the spectrographic technique was improved considerably and more accurate results were obtained. Grimble and Ward[4] obtained similar results and also experienced a low rate of silicon transferred electrochemically, resulting in a large error in the analytical results.

The results obtained (Figures 22 and 23) along with those of Grimble and Ward, are conclusive proof that the local cell effect is present in this reduction system. The very small rates of silicon transferred could be interpreted as indicating that even though the local cell

effect does exist, its contribution to the overall transfer of silicon is negligible. If this were true, there would be no need to be concerned about the second interface when considering slag-metal reactions in graphite crucibles. However, it could be argued that in this experimental system, the resistance of the external circuit, which is the path for electron flow (graphite anode, copper leads, graphite conductor, graphite crucible) is considerably greater than the essentially short circuit path existing in a bare graphite crucible. Grimble and Ward[4] measured the internal resistance of the cell to be approximately 2.0 ohms at 1500°C, and they estimate the external resistance to be 16 ohms. The present author, assigning the majority of the external resistance to the 1/2" graphite anode and graphite conductor (36" length total) and assuming a temperature of 1500°C, calculated the resistance as 0.12 ohm. The use of copper filled electrodes would reduce this resistance by a factor of at least 20, but did not appear to influence the transfer rates. No direct conclusions can be made from these results concerning the contribution of the local cell reaction to the overall reduction kinetics in bare graphite crucibles. In the case considered, silicon is transferring to a copper phase and in the system in question, it is transferring to an iron-carbon-silicon phase. It is felt that the very small values of silicon transferred cannot be entirely attributed to differences in resistance paths between the two systems. In order to clarify the magnitude of the local cell contribution, a series of kinetic experiments were designed.

B. Kinetic Experiments

6.4 Design of the Experiments

Having established the existence of the local cell effect in the silica reduction system, the contribution of the local cell reaction to the overall rate of silicon transfer had to be determined. This was achieved by a series of kinetic experiments utilizing graphite crucibles as described earlier . In the first case, the second interface (slag/graphite) was allowed to contribute to the overall kinetics of the silicon transfer and in the second case this interface was isolated by a silica sleeve. The slag was maintained at silica saturation, and the iron at carbon saturation in both cases. In this manner, both the slag-metal reaction and the electrochemical local cell reaction involving the slag/crucible interface were operative in the bare graphite (unsleeved) crucible, and only the slag-metal reaction was operative in the sleeved crucible system. Both sets of experiments were performed over a wide temperature range (1380° to 1535°C). Any increase in the kinetics of silicon transfer in the unsleeved system over that in the sleeved system would be due to the local cell contribution of the second interface, if other possible rate varying steps associated with the changing cell conditions are eliminated.

At first, a slag-crucible reaction might be considered in which pure liquid silicon is produced and transferred to the metal phase, thus increasing the rate of silicon pick-up. However, this reaction is thermodynamically impossible at the temperatures studies. Grimble[95] investigated how the rate was affected by changing the nucleating conditions for carbon monoxide bubbles (assuming the nucleation occurs at the crucible

wall) when the nucleation surface varies from a porous one (graphite) to a smooth one (silica sleeve). Using three types of graphite crucibles with a wide difference in porosity he was able to detect no effect of different nucleating conditions for CO bubbles on the rate of silicon transfer.

6.5 The Reaction Mechanism

6.5.1 Introduction

The kinetic data had to be examined on a basis independent of the geometry of the crucible design and dependent only on temperature. Experimentally, a linear relationship existed between the amount of silicon transferred and the time of the reaction, and in an attempt to elucidate this behaviour, the reaction system was analysed in terms of possible rate limiting steps.

The stoichiometric equation of the overall reaction is:

$$SiO_{2_{slag}} + 2C^{*} = Si_{metal} + 2\ CO_{gas} \qquad (6.5)$$

It is highly unlikely that this trimolecular reaction is representative of the mechanism of the reaction since it suggests a three-phase reaction (slag, metal, gas), which can only occur at a three-phase interface.

In principle, the overall reaction can be considered to consist

---

* In the sleeved experiments the carbon in the reaction is supplied by the metal phase, but in the unsleeved expeirments, the carbon source is either the metal and/or the graphite crucible.

mainly of two interfacial reactions and four transport processes:

1) Diffusion of silica from the bulk slag to the slag/metal interface.

2) Decomposition reaction of silica at the slag/metal interface to form dissolved silicon and oxygen in the metal side of the interface, that is:

$$SiO_{2_{slag}} = \underline{Si} + 2\,\underline{O} \qquad (6.6)$$

3) Diffusion of silicon from the slag/metal interface to the bulk metal.

4) Diffusion of oxygen from the slag/metal interface to a gas/metal interface.

5) Diffusion of carbon in the bulk metal to a gas/metal interface.

6) Reaction of carbon and oxygen at a gas/metal interface to form carbon monoxide:

$$\underline{C} + \underline{O} = CO_{gas} \qquad (6.7)$$

In considering the individual rate limiting steps, step (1) is eliminated because of the high concentration of silica in the slag, because the carbon monoxide evolution stirs the slag, and also because silica is surface active and would tend to accumulate at the interface[105]. Step (3) is discarded as a possible rate controlling step since Rawling[106] showed that if the silicon diffusion were rate controlling, the rate of silicon transfer would be considerably higher than he determined experimentally. The independence of the rate on silicon concentration would also appear to negate the diffusion of silicon as a rate limiting step. Step (5) is not regarded as a rate limiting step because of the high concentration of carbon and because the stirring in the metal layer adjacent to the slag/metal interface due to the evolution of CO bubbles would tend to eliminate concentration gradients. Rawling[106] also showed

that if diffusion of carbon were the rate limiting step, the rate of silicon transfer would be considerably higher than that found experimentally. It has been determined[107] that during the reduction of solid silica by high carbon melts, the rate of silicon transfer was independent of stirring rates up to 600 r.p.m., and that above 0.1 mole fr. of carbon the rate was independent of carbon concentration. Step (6) is not considered to be rate controlling because it is generally accepted[108] that equilibrium is attained quite rapidly after the gas/metal interface has been established.

Steps (2) and (4) are left as possible rate limiting steps, the former indicating chemical reaction control, and the latter indicating diffusion control. The opinions expressed in the literature by previous authors are by no means unanimous and those favoring chemical control mechanism are as numerous as those espousing a diffusion control mechanism.

6.5.2 Previous Investigations Concerning the Reaction Mechanism

Fulton and Chipman[89] studied the reduction of high silica slags by carbon saturated iron, and their results indicated that the reaction was controlled by a slow step or steps in the chemical reactions. They determined that stirring of both the metal and slag phases had no effect on the kinetics, and when CO was bubbled into the metal phase the kinetics were unaltered. They stated that the slow rate and high activation energy (110 kcal/gm mole) suggested the slow step could involve the breaking of Si-O bonds. In a discussion of this paper, Schuhmann[91] said that the rate controlling step could also be the diffusion of oxygen across a stagnant boundary layer in the metal phase. This conclusion was based

on many assumptions made concerning the following possible reaction steps:

1) $SiO_2 = \underline{Si} + 2\,\underline{O}$.

2) Diffusion of oxygen across the liquid metal boundary layer at the slag/metal interface.

3) Convection within the bulk liquid metal, transporting oxygen.

4) Diffusion of oxygen across the boundary layer at the metal/gas interface.

5) Reaction of carbon and oxygen at the metal/gas interface:

$$\underline{C} + \underline{O} = CO$$

6) Solution of graphite into liquid iron:

$$C_{graphite} = \underline{C} \qquad (6.8)$$

Schuhmann assumed that equilibrium was complete in (1), (5) and (6), convection was quick, and that Si and C diffusion were easier than O diffusion. He also said since Fulton and Chipman showed that bubbling of CO did not affect the rate step (4) was unimportant and thus (2) must be the rate limiting step. With step (2) as the limiting step, he calculated the maximum silicon transfer rate under the experimental conditions used by Fulton and Chipman to be between 0.002 and 0.2 wt.% Si/hr., which compared with Fulton and Chipman's experimental rate of 0.03 wt.%Si/hr. Many assumptions were made before Schuhmann arrived at this conclusion, not all of which are completely reasonable (for example, that equilibrium in (1) is established). The zero effect of stirring of the metal phase was ignored. However, it would be expected that a diffusion controlled process (in the metal boundary layer) would indeed be affected by stirring.

Wojcek[96] examined the reduction of solid silica in the form of quartz capillaries by carbon saturated iron. In his system the capillaries were dipped into a carbon saturated bath, and the convection-free liquid filled the capillaries and was allowed to react for a specific time after which the capillaries were removed and quenched. The cross-sections of the quenched specimens were then studied by microprobe analysis to determine the silicon distribution as a function of time and distance from the reaction surface. Utilizing a solution of Fick's second law applying to a system with a constant concentration at a plane interface with a parallel diffusion flux within a semi-infinite solid, Wojcek calculated theoretical silicon distribution curves based on a range of silicon diffusivities from the literature (D varies from 1×10^{-5} to 6×10^{-5} cm^2/sec). The solution of the diffusion equations indicated a much greater penetration of silicon into the specimen than was observed experimentally, which Wojcek said suggested that the reaction was not diffusion controlled (at least not silicon diffusion) but that the slow, limiting step occurred in the reaction proper. The observation was in agreement with the calculation of Rawling that the diffusion of silicon could not account for the reaction kinetics, but it did not necessarily preclude other diffusion steps which the author ignored.

Sharma[94] studied the same reaction (solid silica reduction by carbon in iron) utilizing an induction stirred melt. He rejected chemical reaction control on ambiguous grounds, stating that the stoichiometric reaction as written in equation 2.61 was unlikely to represent the real reaction path because of the requirement of a three-phase

interface (as discussed earlier). He continued to say that if chemistry did indeed control the reaction rate, the silicon flux would be represented in terms of the equation he already stated could not possibly represent the mechanism. The rate equation was said to be:

$$\frac{dn_{Si}}{dt} = A\,[k_1\, a_{SiO_2}\, a_c^{\,2} - k_2 a_{Si} P_{co}^{\,2}] \qquad (6.9)$$

$k_1 \equiv$ forward reaction rate constant

$k_2 \equiv$ reverse reaction rate constant

From the experimental results, the author calculated the ratio k_1/k_2 which is the equilibrium constant for reaction (2.61). Since there was a considerable variance between the accepted equilibrium constant and the observed k_1/k_2 ratio, the chemical control model was abandoned. The author resorted to a diffusion or transport control model based on the diffusion of oxygen in the metal phase, which was essentially the same mechanism formulated by Rawling and Elliot[93]. The author determined activation energies for the reaction to be in the range 75 - 90 kcal/g.mole.

The transport mechanism proposed by Rawling and Elliot[93] is internally consistent, but the criterion for choosing this mechanism is somewhat doubtful. The authors created an electrochemical graphite cell which consisted of two compartments, one containing a high silicon Fe-C-Si (18.5% Si) ternary alloy, and the other containing a low silicon carbon saturated iron alloy so that silicon was transferred electrochemically from the high silicon side (anodic surface) to the low silicon side (cathodic surface). No gas evolution was observed from either side of

the cell. The rate of silicon pick-up in the low silicon side was two to three times the rate of silicon pick-up in a normal slag-metal reaction when carbon monoxide was evolved. From these observations, the authors concluded that the rate limiting step in the ordinary slag-metal reaction must be in the formation of CO bubbles. They said that the driving force for the transfer of silicon was similar in both systems (the electrochemical system and the slag-metal system) because the composition of the slag and the metal phases was the same, the only difference being that CO gas was evolved in the slag-metal system. However, the driving forces are not identical, for in the electrochemical cell system, the driving force is a function of the difference in silicon concentration between the high silicon and the low silicon compartments and in the normal system the driving force is the free energy charge of the chemical reaction. These two driving forces are not comparable and no conclusions can be drawn concerning possible rate limiting steps from the variation in transfer rates between the two systems. Based on their diffusion model, the authors determined an activation energy of 110 Kcal/g.mole at 1600°C and 200Kcal/g.mole at 1700°C. From these results they concluded that at temperatures up to 1600°C the transport of oxygen in the metal was rate limiting, but at higher temperatures another step in the reaction, which may be chemical in nature, became rate limiting.

Turkdogan et al.[92] experimented on the same reaction using an apparatus where a stream of CO gas impinged upon the slag/metal interface. Because of the presence of the gas impingment at the slag/metal interface, and because of the linear relationship between silicon concentration and

time, they suggested a chemical control mechanism rather than a transport one. The authors adopted a chemical control mechanism in which an adsorption isotherm was used to describe the adsorption of silica at the slag/metal interface. When CO was not impinged upon the interface (accidentally) the authors observed a noticeable decrease in the silicon transfer rate, and concluded that in the absence of CO bubbles the diffusion of oxygen from the slag/metal interface to the crucible walls was rate limiting. The formulation was similar to that used by Rawling and Elliot. The effect of CO impingment on the slag/metal interface, observed by these authors, did not agree with the effect of CO determined by Fulton and Chipman[89]. Fulton and Chipman did not impinge CO on the slag/metal interface, but they did bubble CO into the metal phase, which would present CO bubbles at the slag/metal interface, negating any necessity for CO nucleation. They found no effect of bubbling CO into the metal on the kinetics of silicon transfer.

Grimble[95] studied this reaction and found that the transfer kinetics involving slags of high silica contents (activity > 0.9) and low viscosity were unaffected by stirring and yielded an activation energy for the reaction of 127 Kcal/g.mole. He suggested that these observations indicated a chemical control mechanism, but he did not present any data to support which step in the reaction was rate controlling. He said it was likely that silicon monoxide formation was an intermediate step, and that Fulton and Chipman were correct to choose the slow step as being the breaking of silicon-oxygen bonds. He also observed that as the silica content decreased, the kinetics were more affected by stirring, indicating a progressive shift to a diffusion mechanism at low silica activities.

Activation energies evaluated for this case were in the order of 40 Kcal/g.mole. The rate of transfer for high SiO_2 slags was said to be diffusion controlled at low temperature, with a change to chemical control at higher temperature as the slag viscosity is decreased, the diffusivity is increased and also as CO evolution is increased, causing greater stirring effects.

Several diffusion steps were considered as being possibly rate limiting:

1) Diffusion of (a) silicon and (b) oxygen ions across the slag side of the slag/metalinterface.

2) Diffusion of (a) silicon and (b) oxygen across the metal side of the slag/metal interface.

3) Diffusion of silicon into the bulk.

4) Diffusion of oxygen through the bulk to the metal/gas interface.

5) Diffusion of oxygen across the boundary layer at the metal/gas interface.

6) Diffusion of carbon from the walls to the bulk metal.

1(a), 2(a) and 3 were eliminated since the experimental observations indicated that the silicon transfer was independent of the silicon content in the metal, which would not be the case if silicon diffusion were the rate limiting step. Grimble said that step 2(b), oxygen diffusion across the boundary layer on the metal side, would result in an activation energy for the reaction of approximately 10 Kcal/g.mole. Since it was determined experimentally that the activation energy was an order of magnitude higher, this step was precluded as a rate limiting step. Step (4) was eliminated because if this step were controlling, the rate should remain constant or vary inversely with the crucible cross-sectional area, which was not the

case. He also said that stirring the melt just before a sample was taken should have an effect on the rate, but did not. He argued that if step (5) or (6) were rate limiting, the transfer rate would be independent of the slag-metal interfacial area, which was not the case, experimentally.

The basis upon which the author rejected steps 2(b), 4 and 5 as being rate limiting steps appears to be ill founded. Rawling and Elliot[93] showed that if the diffusion of oxygen in the metal phase were taken as the rate limiting step, the rate constant for the reaction would consist of several temperature dependent terms. These included the enthalpy term of reaction (6.6), the heat of activation for viscous flow of iron, the heat of activation for diffusion of oxygen in iron (8 Kcal/mole) and the heat of solution of oxygen in carbon-saturated iron. The resultant activation energy for diffusion control was calculated to be approximately 110 Kcal, well in agreement with those observed experimentally by Grimble and far greater than the 10 Kcal/gm. mole which Grimble said would indicate oxygen diffusion control.

Thus by a dubious process of elimination, Grimble concluded that the diffusion of oxygen across the boundary layer on the slag side was the rate controlling step in the diffusion controlled system.

6.5.3 Proposed Reaction Mechanism for Present Study

On the basis of the foregoing it was felt that the limiting step in this reaction system was reduced to a choice between a chemical control step or a diffusive one. It was further felt the most logical diffusive step was the diffusion of oxygen in the metal phase. However, because of the independence of the silicon transfer rate on stirring either or both

phases, and because of the seemingly negligible effect of introducing CO bubbles into the metal phase (from Fulton and Chipman data) this transport mechanism was considered to be less plausible than a chemical control step.

The rate controlling step was chosen to involve a chemical reaction, and the most logical one was the decomposition of silica at the slag/metal interface to form silicon and oxygen dissolved in the metal. The predominence of a direct chemical reaction over that of an electrochemical reaction as postulated by Wagner[83], was assumed for simplicity. The reaction mechanism is written:

$$SiO_2 \underset{k_2}{\overset{k_1}{\rightleftarrows}} \underline{Si} + 2\,\underline{O}_{S/M} \qquad (6.10)$$

$$\underline{O}_{S/M} = \underline{O}_{G/M} \qquad (6.11)$$

$$\underline{O}_{G/M} + \underline{C} = CO_{gas} \qquad (6.12)$$

k_1 ≡ forward reaction rate constant(moles of silicon/cm^2/sec)

k_2 ≡ reverse reaction rate constant(moles of silicon/cm^2/sec)

$\underline{O}_{S/M}$ ≡ oxygen concentration at slag/metal interface

$\underline{O}_{G/M}$ ≡ oxygen concentration at gas/metal interface

Reaction (6.10) is the rate controlling step, (6.11) is assumed rapid and (6.12) is taken to be at equilibrium. Assuming the order of reaction with respect to various chemical species is equal to the corresponding molecularity, the number of moles of silicon transferred per unit time is given by:

$$\dot{n}_{Si} = k_1 A\, a_{SiO_2} - k_2 A\, a_O^{\,2}\, a_{Si} \qquad (6.13)$$

where $\dot{n}_{Si} \equiv \frac{dn_{Si}}{dt} \equiv$ moles of silicon transferred per unit time

$a_{SiO_2} \equiv$ activity of silica in the slag at the slag/metal interface

$a_{Si} \equiv$ activity of silicon in the metal at the slag/metal interface

$a_O \equiv$ activity of dissolved oxygen in the metal phase at the slag/metal interface

$A \equiv$ slag/metal interfacial area, cm^2.

Since (6.11) is considered to be much quicker than (6.10), the oxygen activity at the slag/metal interface which is required for the solution of (6.13) is equal to the value at the gas/metal interface derived from reaction (6.12):

$$K_2 = \frac{P_{CO}}{a_O' \, a_C'}$$

where $K_2 \equiv$ equilibrium constant for reaction (6.12)

$a_i' \equiv$ activity of species i at the gas/metal interface

and

$$K_1 = \frac{k_1}{k_2}$$

$K_1 \equiv$ equilibrium constant for reaction (6.10)

Substituting k_2 in terms of k_1 and K_1 and replacing a_O by a_O' in (6.12), the following relationship is derived:

$$\dot{n}_{Si} = k_1 A \left[a_{SiO_2} - \frac{1}{K_1 K_2^2} \left[\frac{P_{CO}}{a_C'}\right]^2 a_{Si}\right] \qquad (6.14)$$

In the present system $a_{SiO_2} = a'_C = 1$. Grimble has shown that for reaction (2.61), even in neutral reaction atmospheres, the carbon monoxide partial pressure at the gas/metal interface is essentially one atmosphere, therefore (6.14) can be written:

$$\dot{n}_{Si} = k_1 A \left[1 - \frac{1}{K_1 K_2^2} a_{Si}\right] \qquad (6.15)$$

The values of the equilibrium constants K_1 and K_2 are obtained from the data of Chipman[122], and Rist and Chipman[131] and Richardson and Jeffes[113], respectively for 1400°C. The numerical value of $1/K_1 K_2^2$ was found to be approximately 14, and since in the present system, the activities of silicon are low ($<10^{-3}$), equation (6.15) may be simplified as follows, without introducing significant errors:

$$\dot{n}_{Si} = k_1 A \qquad (6.16)$$

Thus when the interfacial chemical reaction control mechanism is considered, the rate of silicon transfer to the metal phase per unit cross-sectional area is expected to be constant at a given temperature, providing the silicon activity remains sufficiently low (this criterion is met in the present experimental method where the silicon activity is near zero when the reaction commences and never exceeds 10^{-3} during the course of study). The linear relationship of silicon content and time of reaction, obtained in the present investigation, indicates that the reverse reaction is unimportant.

6.6 Interpretation of the Kinetic Results

In equation (6.16), the rate of the reaction is expressed in terms of the number of moles of silicon transferred across the slag/metal interface per unit time. The actual observed quantity is the concentration of silicon in wt.% as a function of time. For a direct comparison of theory and experiment to extract the values of the forward rate constant for reaction (6.10), a transformation of equation (6.16) into the proper form is desired. This has been accomplished in the following manner:

The rate of silicon transfer per unit volume, V, of metal phase is:

$$\frac{\dot{n}_{Si}}{V} = k_1 \frac{A}{V} \qquad (6.17)$$

Integrating (6.17) with V taken as constant gives:

$$\frac{n_{Si}}{V} = k_1 \frac{A}{V} t \qquad (6.18)$$

Converting moles/unit volume to wt.%:

$$\frac{n_{Si}}{V} = \frac{C_{Si}\ \rho}{100\ M_{Si}} \qquad (6.19)$$

ρ ≡ density of the metal phase (gm/cm^3)[109]

C_{Si} ≡ wt.% silicon in the metal phase

M_{Si} ≡ atomic weight of silicon (28.09)

Substituting for n_{Si} from equation (6.19) into equation (6.18) gives:

$$C_{Si} = \frac{2809\ k_1 A}{V\rho}\ t \qquad (6.20)$$

$$C_{Si} = k\ t \qquad (6.21)$$

The value of k may be obtained from the slope of the concentration - time plots and k_1, the forward reaction rate constant for reaction (6.10) can be calculated from the following relationship:

$$k_1 = \frac{kV\rho}{2809\ A} \qquad (6.22)$$

The rate expressions, equations (6.13 - 6.22) are proposed to be applicable for both the cases of sleeved and unsleeved graphite crucibles. Strictly speaking, it is not true for the unsleeved case since the electrochemical mechanism, which is not included in the formulation, is operating parallel to the simple slag-metal reaction. The purpose of this kinetic study is to determine the relative importance of these two simultaneous mechanisms. The apparent value of k_1 evaluated from the results obtained with unsleeved graphite crucible should be, in principle, higher than the true value. The difference of these rate constants will be used as the indication of the relative contributions of the individual mechanisms to the overall rate of reaction.

The forward reaction rate constants calculated from equation (6.22) utilizing the slopes of the kinetic curves are listed in Tables XI, XII and XIII for the unsleeved system, the unsleeved system utilizing the CO measuring furnace, and the sleeved system, respectively. The forward reaction rate constants for experiments 18, 19 and 20 of the sleeved system calculated from the 'equivalent slopes' discussed in the preceding chapter are listed in Table XIV.

From these results it is obvious that k_1 strongly depends on temperature, hence the exponential term dominates and the Arrhenius relationship may be used:

$$k_1 = A\, e^{-Q/RT} \qquad (6.23)$$

where the pre-exponential term A is taken as constant.

From equation (6.23):

$$\ln k_1 = -Q/RT + A' \qquad (6.24)$$

Q ≡ activation energy for the reaction

R ≡ gas constant

The values of $\ln k_1$ for all the kinetic experiments are shown as a function of 1/T in Figure 54. The type of furnace used was observed to have no noticeable effect on the reaction rate. The k_1 values for experiments 25 and 22 (done in the carbon resistance furnace) of the unsleeved and sleeved cases, respectively, did not vary appreciably from the corresponding experiments done in the molybdenum resistance furnace (within the experimental accuracy of the technique). Experiment 20 of the unsleeved system was not stirred over a period of sixty-nine hours and the k_1 value did not vary significantly from that expected, indicating that stirring of the metal phase has no effect on the kinetics. Experiments 13, 14 and 21 of the sleeved system were carried out using zirconium oxide sleeves (ZrO_2) extended to the bottom of the graphite crucible, and no effect on the expected values of k_1 was observed. In experiments 21 of the unsleeved sytem and 25 of the sleeved system the slag was not maintained at silica saturation, but the decrease in silica activity over

the experimental period was so small that the kinetics were unaffected. No effect of crucible geometry was observed on the value of k_1, as seen from experiments 25 and 26 of the unsleeved system when the bath height was 1/2 the normal value, and in the sleeved system where the slag/metal interfacial area in experiments 13, 14 and 21 was 1/3 greater than normal. The mode of sampling was also shown to have no influence on the value of k_1 since experiments 1, 25 and 26 of the unsleeved system and experiment 22 of the sleeved system were taken with graphite spoons with no appreciable difference in k_1. Also, experiment 16 of the unsleeved system was sampled by both graphite spoon and suction up a silica capillary, and the analyzed silicon contents were the same within the precision of the analytical technique. The analysis of various slags at random illustrates that the slag phases were essentially at silica saturation during the experimental periods.

The large k_1 values for sleeved experiments 18, 19 and 20 were expected since an additional reduction interface was introduced - the metal/silica sleeve interface. The observed values of k_1 are approximately twice the values for the case where the silica sleeves terminated at the slag/metal interface. In an attempt to calculate the excess silicon transferred, Sharma's data[94] was used since it dealt with the reduction of solid silica by carbon saturated iron. Unfortunately, the silicon transfer rate at the metal/silica sleeve interface done using Sharma's rate constant was found to be larger than the observed rate (due to both the metal/silica sleeve and slag / metal interfaces), by a factor of 10. This anomaly was attributed to the great variation in experimental conditions - in Sharma's work the melt was inductively stirred in a high frequency furnace

which could result in erosion of the silica along with the chemical reaction. The eroded silica could then react with carbon in the bulk metal, accounting for a large silicon transfer rate. No further attempt was made to analyze these results as it was considered sufficient to note that the additional reaction interface resulted in a double fold increase in the silicon transfer rate.

It was also seen that the reaction rates for experiments 18, 19 and 20 determined by the CO evolution rate agreed with those determined by the rate of silicon pick-up in the melt. The method, however,is not as accurate as the silicon analyses method because of the difficulty in analyzing such small CO quantities in the gas, but it does present an alternative, if for any reason the melt cannot be analyzed or disturbed.

The effect of crucible and metal geometry, and mode of sampling have been eliminated as possible rate varying steps. The results have thus been reduced to determining the effect of the electrochemical local cell reaction on the kinetics of the slag-metal reaction. This effect is discussed in the following section.

6.7 The Contribution of Electrochemistry to the Overall Kinetics

It was mentioned in the preceding section that the value of the apparent reaction rate constant for the unsleeved system should give an indication of the effect of the second interface (the slag/graphite interface where the local cell effect can occur) on the overall kinetics. If the local cell mechanism is operating, the amount of silicon transferred will increase accordingly, resulting in an increase in the apparent reaction rate constant.

The variation of k_1 for the unsleeved system from k_1 for the sleeved system is examined using the Arrhenius plot of Figure 54. In all, four separate sets of data are analysed:

1) Unsleeved experiments by the silicon analysis method.
2) Unsleeved experiments by the carbon monoxide measuring method.
3) Sleeved experiments by the silicon analysis method (omitting experiments 18, 19 and 20)
4) Sleeved experiments 18, 19 and 20.

The individual sets of data indicate a linear relationship of $\ln k_1$ with the inverse of the temperature, and the best straight lines were calculated for each set - the results are shown in Figure 55. The equations of the lines were calculated to a 95% confidence level by the least squares method presented in Appendix A. The activation energies for the individual data were calculated from the slopes and are listed in Table XXIV.

The three fully sleeved experiments yielded an activation energy of 112.6 ± 7.2 kcal/g.mole which was somewhat higher than those determined for the other data. There will be little comment on this result, except that far fewer experiments were done, which could account for this larger value. Also, the activation energy reflects a reaction occurring at two sites which are not necessarily equivalent. One site is a silica saturated slag in which the silica network has been modified by the presence of CaO and MgO, and the other is an unaltered solid silica network. Perhaps the silicon transferred at the metal/silica sleeve interface could be determined as that in excess of the silicon transferred at the slag/metal

interface which is known from the sleeved experiments which extended only to the slag/metal interface. In this manner the rate of reduction of the solid silica by carbon saturated iron will be determined, and hence the activation energy could be determined. However, it was felt that the data of these three experiments were insufficient to make conclusions concerning the solid silica reaction.

The sleeved experiments (less 18, 19 and 20) yielded an activation energy of 93.9 ± 13.4 kcal/g.mole. The unsleeved experiments yielded an activation energy of 99.7 ± 10.5 kcal/g.mole, and the unsleeved experiments by the CO measuring method yielded an activation energy of 98.8 ± 4.8 kcal/g.mole. Combining the data of these three systems yielded a composite activation energy of 97.1 ± 9.6 kcal/g..mole.

Two points thus remain to be resolved before the electrochemical contribution can be commented upon. First, it must be shown whether the three activation energies can be represented by a composite or pooled value which would indicate the same reduction mechanism in the three cases studied. Secondly, it must be determined whether there is any significant variation in the ordinate ($\ln k_1$) between the three lines; any displacement of the unsleeved line above the sleeved line would be indicative of an electrochemical contribution.

The three systems were analyzed by a pooling technique which is discussed in Appendix A. It was shown that the degree of deviation removed by using a pooled slope for the three sets of data instead of three individual slopes, was significant, and hence the data are best described as having one slope, or more precisely, one activation energy. The activation energy derived from the pooled slope is 97.5 $\pm$ 8.3 kcal/g.mole. It was also shown that within the experimental error limits of the present

study that there was no significant displacement in the ln k_1 direction between the three lines, hence the data are best described as one straight line as seen in Figure 54.

The results of the present investigation thus show that although the electrochemical local cell effect does exist when bare graphite crucibles are used (seen by the Faradayan Yield experiments), the contribution to the overall kinetics is insignificant within the experimental error of the method. This observation is in contradiction to the work of Grimble and Ward[4] who determined that at 1450°C the electrochemical contribution was of the same order of magnitude as the contribution from the slag/metal interfacial reaction. It is worthwhile to note that Grimble and Ward carried out only two experiments at one temperature. Figure 54 shows their results calculated on the same basis as the present investigation, and it is seen that the ln k_1 value for their sleeved experiment lies well in the range of the present data, but the ln k_1 value for their unsleeved experiment is higher than the corresponding results obtained in this investigation.

6.8 The Effect of Silicon on the Solubility of Carbon in Liquid Iron

The results of Chapter 5 show that as the silicon content of the metal phase increased, the carbon content decreased in a linear fashion, at least at low values of silicon. The decrease in carbon solubility from the silicon free system is best shown as a function of the silicon content, irrespective of the temperature, by:

$$\Delta C_C = - 0.37 C_{Si} \pm 0.56 C_{Si} \qquad (6.25)$$

Unfortunately, there is a large error due to the inaccuracies of the carbon determinations. In most cases, the small variation in the decrease in carbon solubility due to the silicon is of the same order of the degree of accuracy of the analytical technique (0.05%C) and a relatively large error is introduced. However, the average result is in agreement with that of Chipman et al.[102] who found the solubility decrease to be essentially independent of temperature and best represented by:

$$\Delta C_C = - 0.3 C_{Si} \qquad (6.26)$$

6.9 Error Analysis

6.9.1 Faradayan Yield Experiments

The errors inherent in the Faradayan yield experiments are largely due to the very low silicon transfer to the copper. The low silicon values in the copper necessitated the use of spectrographic techniques which were reproducible within $\pm$ 0.005 wt.% Si. The predicted silicon content was calculated from the measurement of the current passed, integrated over the time of reaction. The accuracy of these measurements were probably of the same order as the analytical technqiues, due to minute fluctuations in the current which was not measured continuously, but rather continually.

6.9.2 Kinetic Experiments

The calculation of the forward reaction rate constant involves several variables which are subject to error. The forward reaction rate constant is given by,

$$k_1 = \frac{kV\rho}{2809A}$$

which is written,

$$k_1 = \frac{kh\rho}{2809} \qquad (6.27)$$

where h is the height of the metal bath and is assumed constant.

The effect of the individual errors in the slope, the height and the density of the melt is determined by consecutively holding two variables constant and noting the effect of the error of one on the value of k_1, that is:

$$\left(\frac{dk_1}{dk} \right)_{h,\rho} = \frac{h\rho}{2809} \qquad (6.28)$$

$$\left(\frac{dk_1}{d\rho} \right)_{k,h} = \frac{kh}{2809} \qquad (6.29)$$

$$\left(\frac{dk_1}{dh} \right)_{k,\rho} = \frac{k\rho}{2809} \qquad (6.30)$$

Thus to determine the maximum possible error in k_1 due to errors in k, h and ρ, the numerical values of the individual errors are added:

$$\Delta k_1 = \frac{1}{2809} [\, h\rho\Delta k + kh\Delta\rho + k\rho\Delta h \,] \qquad (6.31)$$

$\Delta k_1 \equiv$ total error in k_1 due to errors in k, h and ρ

$\Delta k \equiv$ error in the slope

$\Delta\rho \equiv$ error in density

$\Delta h \equiv$ error in height

The error in the slope is determined from the least square line and is listed in Tables IX, X and XI. The average error is $\pm$ 18%, and the error in the density is estimated at $\pm$ 2%. The error in the height

measurement is estimated at $\pm$ 5%, due to curvature of the slag/metal interface, the dissolution of graphite from the crucible walls to maintain saturation, and the effect of removing metal by sampling.

As an example, the error in k_1 for unsleeved run number 9 which had a 18.3% error in the slope (which was close to the average error for all the runs) was calculated, where $k = 5.13 \times 10^{-4} \pm 0.94 \times 10^{-4}$ wt.% Si/min., $\rho = 6.84 \pm 0.14$ gm/cm^3 and $h = 3.06 \pm 0.15$, using expression (6.31):

$$\Delta k_1 = 0.97 \times 10^{-5}$$

Thus, the k_1 value is $3.83 \times 10^{-5} \pm .97 \times 10^{-5}$ or the error is 25%.

CHAPTER 7

DISCUSSION OF ELECTROMOTIVE FORCE EXPERIMENTS

7.1 Introduction

In this chapter, the results of the electromotive force measurements for similar slag-metal systems used in the kinetic study will be discussed. For all the experiments the molten electrolyte was silica saturated slag with the balance consisting of calcium oxide and magnesium oxide. The slag remained at silica saturation because it was in contact with a solid silica sleeve. The results of the Faradayan Yield experiments illustrated the existence of an electrochemical local cell mechanism which led to the design of several electrochemical cells to study the thermodynamics of the following three systems:

1) The oxidation of silicon by carbon monoxide gas to form silica and graphite.
2) The reduction of silica by graphite to form silicon dissolved in iron-silicon melts.
3) The reduction of silica by graphite to form silicon dissolved in iron-carbon-silicon melts.

The standard free energy change for (1) was evaluated from the experimental emf measurements, and the results were compared to those obtained from the literature and discussed. The emf measurements from (2) and (3) were used to calculate the activity of silicon in Fe-Si and Fe-C-Si melts, and in combination with chemical analyses and other

information from the literature, the activity coefficient of silicon in iron-silicon and iron-carbon-silicon alloys was calculated.

7.2 The Electrochemical Cell Reactions

As mentioned earlier, the electrochemical experiments were based on the occurrence of the local cell reaction as:

$2\ O^{2-} + 2\ C = 2\ CO + 4\ e$ slag/graphite electrode interface (anode)

$Si^{4+} + 4\ e = Si$ slag/metal interface (cathode)

The overall reaction is:

$$SiO_2 + 2\ C = Si + 2\ CO$$

The direction of the reaction was predicted from the available data on the thermodynamics of the system, which showed that the reaction would proceed as written if a silicon sink existed such that $a_{Si} < 1$. If no silicon sink existed, the silicon produced would be in a pure state and the reaction would only occur when the temperature exceeded a value near 1600°C. Thus, when Fe-C-Si and Fe-Si melts are used as silicon sinks, providing the silicon activity is low enough and the temperature is not excessively low, the reaction will go spontaneously as written. When pure silicon is used as the metal phase, at temperatures less than 1600°C, the reaction is reversed and silicon is then oxidized by CO.

7.3 Silicon as the Metal Phase

When silicon is used as the metal phase and graphite as the top electrode, (separated by the slag electrolyte) a chemical cell is formed such that an overall chemical reaction would take place if the metal

phase and graphite electrode were electrically connected. The electromotive cell is represented by the sequence:

$$Si/(SiO_2\text{-}CaO\text{-}MgO)_{liquid}, SiO_{2_{solid}}/C_{graphite}, CO \quad (7.1)$$

The cell sequence is written so the electron flow is from left to right, and the overall reaction is the oxidation of silicon by CO gas:

$$Si + 2\ CO = SiO_2 + 2\ C \quad (7.2)$$

The anodic reaction is:

$$Si = Si^{4+} + 4\ e \quad (7.3)$$

The cathodic reaction is

$$2\ CO + 4\ e = 2\ O^{2-} + 2\ C \quad (7.4)$$

The free energy change for reaction (7.2) is expressed by:

$$\Delta G = \mu_{SiO_2} + 2\ \mu_C - \mu_{Si} - 2\ \mu_{CO} \quad (7.5)$$

$\mu_i \equiv$ chemical potential of species i

In the present experimental set-up, both products and reactants were in their standard states (SiO_2 saturated slag, pure graphite electrode, pure silicon metal, CO gas at 1 atmosphere).

Therefore:

$$\Delta G^o = \mu^o_{SiO_2} + 2\ \mu^o_C - \mu^o_{Si} - 2\mu^o_{CO} \quad (7.6)$$

or,

$$\Delta G^o = -\ n\ F\ \varepsilon^o$$

Thus the measured potential was the standard emf for reaction (7.2) and was used to calculate the standard free energy change for the reaction. The results are shown as a function of temperature in Table XVIII and Figure 42. In this system, the top graphite electrode was positive as expected. There was no observed effect of the CO flow rate down the top electrode on the measured emf, even when the flow rate was zero. This led to the suspicion that carbon monoxide gas was being supplied by another source.

Initially it was thought that this source might possibly be a side reaction at the graphite/slag interface producing silicon monoxide and carbon monoxide gas, according to:

$$SiO_{2_{slag}} + C_{graphite\ electrode} = CO_{gas} + SiO_{gas} \qquad (7.7)$$

The standard free energy change for reaction (7.7) was calculated (see Appendix B) to be + 24,800 cal/gm.mole, at 1450°C.

Considering the sign and magnitude of this free energy change, it is unlikely that CO will nucleate at the slag/graphite electrode interface at 1 atm pressure hence this side reaction would not supply a source of CO. Another possible side reaction to produce CO at 1 atmosphere pressure was considered:

$$SiO_2 + 3\ C = SiC + 2\ CO \qquad (7.8)$$

The standard free energy change for reaction (7.8) was calculated to be + 7,400 cal/g.mole at 1450°C (see Appendix B). Again it is unlikely that reaction (7.8) would result in the nucleation of CO gas at 1 atm

pressure, because it is thermodynamically impossible. The graphite electrode/slag interface was microscopically examined for a possible third phase which might have been identified as SiC, but no such phase was observed. The presence of CO cannot, therefore, be ascribed to reaction (7.7) or reaction (7.8), but it is considered that the CO partial pressure at the cathode would remain at essentially 1 atmosphere for a considerable length of time after the CO flow rate was stopped, due to the adherence of CO bubbles to the electrode.

After these experiments were carried out, a white, spongy material was found precipitated on the upper graphite electrode and the lower graphite conductor, in the cooler regions of the furnace. The material was analyzed and identified as pure silica. A similar observation was made by Grimble[95], Turkdogan[92] and Birks[110]. This deposition of silica was attributed to the formation of silicon monoxide by the reaction:

$$SiO_2 + CO_g = SiO_g + CO_{2_g} \qquad (7.9)$$

The carbon monoxide which was blown down the graphite electrode reacted with the silica in the slag to form silicon monoxide and CO_2 gas. The problem of nucleating the SiO and CO_2 was eliminated because of the presence of the CO gas phase. The standard free energy change for reaction (7.9) was calculated to be 52,700 cal/g.mole (Appendix B). The silicon monoxide is very unstable and would be reoxidized in the cooler parts of the furnace to form a spongy silica deposit.

Grimble[95] qualitatively confirmed the nature of reaction (7.9) by pre-weighing a high silica slag into a platinum crucible and observing

essentially no weight loss over a 12 hour period at 1550°C. He concluded, therefore, that the SiO_2 deposit was the result of the oxidation of the SiO formed by reaction (7.9).

The standard free energy change calculated from the cell emf was a linear function of the temperature as seen from Figure 42. The best straight line representing the results was determined by the least square method described in Appendix A, and is given as:

$$\Delta G^o = - 153{,}600 + 82.5\ T \qquad (7.10)$$

where

$$\Delta H^o = - 153{,}600 \pm 700 \text{ cal/g.mole}$$

$$\Delta S^o = - 82.5 \pm 4.3 \text{ cal/g.mole } °K$$

The temperature range was extended to just below the melting point of silicon (1413°C), but the expected change in the slope of the line, associated with the entropy of fusion of silicon, was indeterminable from the results. The slope would be expected to decrease as the temperature descended through the melting point of silicon.

7.3.1 Comparison of the Experimentally Determined ΔG^o to Values from the Literature

The experimentally determined standard free energy change for the oxidation of silicon by carbon monoxide was compared to results from the literature.

Ramstad and Richardson[111] studied the equilibrium reactions:

$$SiO_2 + H_2 = H_2O + SiO \qquad (7.11)$$

$$SiO_2 + Si = 2\ SiO \qquad (7.12)$$

Using the literature data for $2\ H_2O = 2\ H_2 + O_2$, they calculated the free energy of formation of silica (β tridymite) to be:

$$\Delta G^O = -\ 222{,}800 + 47.6\ T \qquad (7.13)$$

Combining this value with the free energy of formation of carbon monoxide derived from the National Bureau of Standards' selected values[112], which is

$$\Delta G^O = -\ 56{,}700 - 40.4\ T \qquad (7.14)$$

the standard free energy change of reaction (7.2) is calculated to be:

$$\Delta G^O = -\ 166{,}600 + 88.0\ T \qquad (7.15)$$

Richardson and Jeffes[113] calculated the free energy of formation of silica from literature data of heats of formation at 20°C, entropies at 25°C and the specific heat of silicon, oxygen and silica such that

$$\Delta G^O = -\ 217{,}520 + 48.8\ T \qquad (7.16)$$

Combining this result with the free energy of formation of CO (7.14) yields the free energy change for reaction (7.2) as:

$$\Delta G^O = -\ 161{,}400 + 89.2\ T \qquad (7.17)$$

Rein and Chipman[112] calculated the free energy of formation of silica from the literature values for heat and entropies of formation of silica, giving,

$$\Delta G^O = -\ 226{,}500 + 47.5\ T \qquad (7.18)$$

Combining this with the free energy change for the formation of CO (7.14) gives the free energy change for reaction (7.2) as:

$$\Delta G^O = -\ 170{,}300 + 87.9\ T \qquad (7.19)$$

Schwertdfeger and Engel[68] measured the free energy of formation of silica by an electrochemical technique using chemical cells represented by the sequence:

$$Si/(CaO - SiO_2)_{liquid}, SiO_{2_{solid}}/Pt, O_2 \qquad (7.20)$$

They determined the free energy of formation of silica to be:

$$\Delta G = - 221,000 + 46.2\ T \qquad (7.21)$$

Combining their results with the free energy of formation of CO gives the standard free energy change for reaction (7.2) as:

$$\Delta G = - 165,800 + 86.6\ T \qquad (7.22)$$

It is thus seen that the present experimentally determined value (7.10) for the standard free energy change for reaction (7.2) is numerically less than the average derived from various literature values (7.15, 7.17, 7.19 ,7.22). The enthalpy change for the reaction is lower by 12,400 cal/g.mole than the average from the literature, and the entropy change is lower by 5.4 cal/g.mole °K, representing deviations of 8 and 6%, respectively,

At 1450°C: $\Delta G^o_{literature} = -14,500$ cal/gm.mole

$\Delta G^o_{present\ work} = - 11,500$ cal/gm.mole

The literature values predict that reaction (7.2) will go spontaneously up to a temperature of 1615°C, and the present experimental results predict a temperature up to 1588°C.

7.3.2 The Discrepancy of the Present Results with the Literature Values

The discrepancy between the literature results and the present results, while not excessive, is attributed to the widely varying means of determination of the standard free energy change. The values obtained from the literature were calculated using the results of at least two separate determinations, that for the formation of SiO_2 and CO.

The standard free energy change for the formation of SiO_2 has been the subject of some doubt in the past[114] (Chipman's note) but is now firmly established as being very near that given earlier by Rein and Chipman[112]. The present experimental system has the advantage over the others, in that the standard free energy change for reaction (7.2) is determined directly from a single experiment and no other experimental data from this or other investigations are employed in the final calculations. The experimental method, however, being a high temperature electrochemical cell technique, has all the inherent errors associated with the method. The reversibility of the reaction has been illustrated by the temperature dependence of the measured emf, the null effect of the electrode position in slag, and the electrode polarity. The effect of side reactions is indeterminate, including side reactions at the graphite electrode/slag interface and at the silicon/graphite crucible interface. Reaction (7.7) would occur at the graphite electrode/slag interface if there were any appreciable solubility of either SiO or CO in the slag. Grimble[95] has given evidence of CO solubility in this slag by a kinetic experiment starting with a high silicon Fe-C-Si alloy such that the oxidation of Si by CO would occur. When the reaction gas

contained no CO, the rate of Si depletion was negligible, but when a CO atmosphere was introduced, there was a noticeable decrease in silicon concentration with time. This indicated a transport of CO through the slag phase and hence a solubility of CO in the slag. A second possible side reaction at the slag/graphite interface is reaction (7.8), but this does not appear to be significant since no SiC was observed.

Side reactions at the silicon/graphite interface could be both the dissolution of carbon in silicon or a reaction between silicon and carbon to form silicon carbide:

$$C_{graphite} = C_{silicon}$$

$$Si_{liquid} + C = SiC_{solid} \qquad (7.23)$$

At 1450°C:

$$\Delta G^{o}_{SiC} = -12{,}100^{(112)}$$

The formation of silicon carbide is favored thermodynamically, and it does form, as seen from a microprobe trace across a silicon/graphite interface. It should be noted that SiC was observed only after a long contact time at high temperature. The growth of the SiC layer is expected to be slow, since the initial product layer would prevent any further contact of silicon and graphite and the reaction would be hindered. The amount of carbon in the silicon phase was analyzed as approximately 0.02%. Both the effect of the SiC formation and the dissolution of graphite in the silicon on the reversible emf are indeterminable, as are the electrode/slag side reactions. Thermodynamically speaking, the occurrence

of any reactions other than that being studied electrochemically constitutes an irreversible system. There appeared to be no thermal or induced emf's, since the emf dropped to zero as the graphite electrode was inserted into the silicon phase. It is unknown whether a thermal emf is produced when the graphite electrode is raised into the slag phase where the possibility exists that the two electrode surfaces are at different temperatures.

7.4 Iron - Silicon as the Metal Phase

As mentioned earlier, reaction (2.61) occurs below 1600°C (approximately) only if the activity of silicon in the metal phase is sufficiently low. With an Fe-Si alloy as the metal phase, this condition was satisfied most of the time. The iron-silicon system was examined in two ways, one using an electrochemical concentration cell and the other using an electrochemical chemical cell. The concentration cell was achieved by using a pure silicon electrode as the top electrode, and the iron-silicon alloy (separated from the graphite crucible by a layer of liquid silver) as the bottom electrode. The concentration cell is then represented by the sequence:

$$Si_{solid}/(SiO_2\text{-}CaO\text{-}MgO)_{liquid},\ SiO_{2_{solid}}/Fe\text{-}Si_{liquid} \qquad (7.24)$$

The reaction at the silicon electrode is the anodic dissolution of silicon:

$$Si = Si^{4+}_{slag} + 4\ e$$

The reaction at the Fe-Si electrode is the cathodic deposition of silicon:

$$Si^{4+}_{slag} + 4\ e = Si_{alloy}$$

The overall reaction is:

$$Si_{pure} = Si_{alloy} \qquad (7.25)$$

The system constitutes a concentration cell, resulting in a net transfer of silicon from one state to another. Thus,

$$\Delta G = RT \ln a_{Si}$$

and

$$a_{Si} = \exp\left(- \frac{nF\epsilon}{RT} \right) \qquad (7.26)$$

The silicon activities in the Fe-Si alloy were determined from the experimental emf, ϵ, and are shown in Table XX. In this experimental set-up the emf is always positive (top electrode negative) and approaches zero as the activity of silicon approaches unity.

The chemical cell was created using a graphite electrode as the top electrode, and a Fe-Si alloy as the bottom electrode. If the activity of the silicon in the Fe-Si alloy was kept low enough the reaction proceeded according to (2.61) but if it was large enough the reverse reaction occurred. In the former case, the top electrode would be the anode and would have a negative charge and in the latter case the top electrode would be the cathode having a positive charge. The chemical cell is represented by the sequence (for the low silicon case):

$$C,CO/(SiO_2\text{-}CaO\text{-}MgO)_{liquid},\ SiO_{2_{solid}}/Fe\text{-}Si_{liquid} \qquad (7.27)$$

The free energy change of the reaction is written in terms of the activities

of the reactants and products:

$$\Delta G = \Delta G^{\circ} + RT \ln \frac{a_{Si}\, p_{CO}^{2}}{a_{SiO_2}\, a_C^{2}}$$

Since $a_{SiO_2} = a_C = 1$ and $p_{CO} = 1$ atm and $nF\varepsilon = \Delta G$:

$$\varepsilon - \varepsilon^{\circ} = - \frac{RT}{nF} \ln a_{Si}$$

$$a_{Si} = \exp \left[- \frac{nF}{RT} (\varepsilon - \varepsilon^{\circ}) \right] \qquad (7.28)$$

The activities of silicon in the Fe-Si binary alloy were calculated from the emf data and are listed in Table XXII.

The standard electromotive force, ε°, was calculated from the standard free energy change of the reaction, as compiled by Rein and Chipman:

$T > 1413°C \quad \Delta G^{\circ} = + 170{,}300 - 87.9\ T$

$T < 1413°C \quad \Delta G^{\circ} = + 158{,}600 - 80.9\ T$

All the calculations were based on the assumption that the partial pressure of CO was 1 atmosphere, but in none of the experiments was CO supplied at the top graphite electrode. It is expected that CO would be present from the reaction of oxygen (introduced when sampling or adding to the melt) with graphite and also from the side reactions discussed earlier. These side reactions were shown to be unable to produce CO at 1 atm pressure, but CO could dissolve in the slag and the reaction would proceed. The results appear to be unaffected to any great extent by not supplying CO, but the variation of the experimental γ_{Si} from that calculated

from distribution experiments could be rationalized from the viewpoint of a lowered p_{CO}. From Figure 56, at $N_{Si} = 0.1$: ln γ_{Si}=-3.15 (experimental) and ln γ_{Si}=-2.85 (distribution experiments) Thus, γ_{Si}=0.00071 (experimental) and γ_{Si}=0.00141 (dist. exp). Thus, a_{Si}=0.000071 (exp.)and a_{Si}=0.000141 (dist. exp.)

The calculations were done assuming p_{CO} = 1 atm. However, if p_{CO} does not equal 1 atm, the experimentally determined activity is actually:

$$a_{Si_{exp.}} = a_{Si}\ p_{CO}^{2}$$

which follows from the stoichiometry of the reaction. Therefore,

$$p_{CO}^{2} = \frac{0.000071}{0.000141} = 0.5 \qquad \text{or,}$$

$$p_{CO} = 0.71 \text{ atm.}$$

The deviation of the present experimental results can thus be rationalized by a difference in the partial pressure of CO, but it will be shown later that this deviation is within the experimental error of the method.

7.5 Iron-Carbon-Silicon as the Metal Phase

7.5.1 Graphite as the Top Electrode

The chemical cell reaction is the same in this instance as when an Fe-Si binary is utilized as the metal phase. The only difference is that the silicon activity is determined in the Fe-Si-C ternary. When a graphite top electrode is used, the cell sequence is represented by:

$$C,CO/(CaO\text{-}MgO\text{-}SiO_2)_{liquid},SiO_{2_{solid}}/Fe\text{-}C\text{-}Si_{liquid} \qquad (7.29)$$

As before, :

$$a_{Si} = \exp\left[-\frac{nF}{RT}(\varepsilon - \varepsilon^{\circ})\right]$$

The activity of silicon in the ternary system was determined as a function of silicon content and temperature. The results are shown in Table XXIII. In the case of the ternary system, the slag-metal reaction is proceeding continuously, providing a constant supply of carbon monoxide to the top graphite electrode, so it would be expected that a CO flow down the electrode would have no effect on the measured emf. This was observed for experiments where CO gas was blown down the electrode at different rates.

The existence of the slag-metal reaction in this system adds suspicion to the assumption of thermodynamic reversibility of the cell reaction. The reversibility is implied qualitatively, however, by observations such as the sign of the emf, the null effect of electrode position on emf, the correct dependence of emf on the silicon content and to a smaller degree, the temperature dependence of the emf. The ternary system presented the greatest difficulty in obtaining a reproducible emf. In many cases, the emf fluctuated wildly and no measurements were obtainable . The causes of these fluctuations were thought to be the effect of CO bubbles leaving the graphite electrode, the total effect of side reactions and the slag-metal reaction, and the presence of hydroxyl ions in the slag.

7.5.2 Presence of Hydroxyl Ions in the Slag

Walsh et al.[115] measured the solubility of hydrogen in basic

open hearth slags to be 92 ppm at 1550°C and 1 atm pressure of water vapor. Several authors[116,117] suggested that hydrogen went into solution in slags or molten silicates in the form of the hydroxyl ion:

$$\{H_2O\} + O^{2-}_{slag} = 2\ (OH^-) \qquad (7.30)$$

If the hydroxyl ion were present in the slag, it could conceivably interfere with the anode reaction by participating in the anodic reaction in some way, such as:

$$2\ (OH^-) = H_2O + \frac{1}{2}\ O_2 + 2\ e \qquad (7.31)$$

An attempt was made to remove the offending ions before the experiment was started, by applying a D.C. and/or A.C. current across the slag. This resulted in temporary relief in some cases and no relief in others. Perhaps it would have been more effective if the electrolysis of the slag were continued for a longer period of time, but there would be the risk of severely polarizing the cell which could take days to recover, as was observed by Gluck[118] in his system.

7.5.3 Silicon Carbide as the Top Electrode

The ternary system was also studied using a silicon carbide electrode as the top electrode, creating another chemical cell represented by the sequence:

$$SiC,CO/(SiO_2\text{-}CaO\text{-}MgO)_{liquid},SiO_{2_{solid}}/Fe\text{-}Si\text{-}C_{liquid} \qquad (7.32)$$

The anodic reaction is postulated to be:

$$2\ O^{2-}_{slag} + \frac{2}{3}\ SiC = \frac{2}{3}\ SiO_2 + \frac{2}{3}\ CO + 4\ e \qquad (7.33)$$

The corresponding cathodic reaction would be:

$$Si^{4+} + 4\ e = Si$$

The overall reaction is:

$$\frac{1}{3}\ (SiO_2)_{slag} + \frac{2}{3}\ SiC_{electrode} = Si_{Fe,C,Si} + \frac{2}{3}\ CO_{gas} \qquad (7.34)$$

For which, ΔG°_{1450} = + 14,400 cal/g.mole (Appendix B).

If the activity of silicon in the ternary were low enough, it was expected that the reaction (7.34) would go as written, such that the silicon carbide electrode was negatively charged and the emf was positive. The results obtained by using an SiC electrode were too scattered to be of any value, and even when the electrode was shorted to the Fe-C-Si phase the emf fluctuated widely. The system exhibited no sign of reversibility, as the polarity of the SiC electrode changed from experiment to experiment. A possible offending side reaction which could occur at the electrode/slag interface is:

$$SiC + 2\ CO = SiO_2 + 3\ C \qquad (7.35)$$

After several attempts to measure reversible emf's using silicon carbide electrodes, all of which were unsuccessful, this series of electrochemical cell experiments was abandoned.

7.6 Activity Coefficient of Silicon in the Iron-Silicon Binary

The results discussed in section 7.3 were utilized to evaluate the activity coefficient of silicon in iron:

$$a_{Si} = \gamma_{Si} N_{Si} \qquad (7.36)$$

$$\gamma_{Si} = a_{Si}/N_{Si} \qquad (7.37)$$

γ_{Si} ≡ activity coefficient of silicon in iron-silicon alloys

a_{Si} ≡ experimentally determined activity of silicon in iron-silicon alloys

N_{Si} ≡ silicon content of iron in atomic fraction

The log γ_{Si} values are shown in Table XXII. The various log γ_{Si} values, evaluated at different temperatures, were converted to their respective values at 1420°C by the relationship:

$$\frac{d \ln \gamma_{Si}}{d\ 1/T} = \bar{L}_{Si}/R \qquad (7.38)$$

$\bar{L}_{Si}$ ≡ partial molal enthalpy of solution of silicon in iron Korber and Oelsen[119]

R ≡ gas constant

This was done so that the present results are more easily comparable to those from the literature. The results are plotted as log γ_{Si} vs. N_{Si} in Figure 56.

Smith and Taylor[120] determined the activity of silicon in iron from distribution experiments, with silicon distributing between iron and silver. From a knowledge of the activity of silicon in silver, determined from the silicon silver phase diagram of Hager[121], the activity of silicon in iron was determined. Their results are shown in Figure 56, along with other results from the literature corrected to 1420°C. The

results of Chipman et al.[122] and Chipman and Baschwitz[123], who used similar distribution experiments, are also presented. The three independent determinations done on similar distribution experiments are in good agreement, which might be expected since they would have common sources of error.

Schwerdtfeger and Engel[68] determined the activity of silicon in Fe-Si binaries from an electrochemical cell represented by the sequence:

$$Fe\text{-}Si/(CaO\text{-}SiO_2)_{liquid},\ SiO_{2_{solid}}/Pt,O_2 \qquad (7.39)$$

Their experimentally determined activity coefficients were larger than those determined from the distribution experiments by a small amount.

Sanbongi and Ohtani[76] also measured silicon activities by an electrochemical technique , using concentration cells represented by the sequence:

$$Si_{liquid}/(CaO\text{-}Al_2O_3\text{-}SiO_2)_{liquid},SiO_{2_{solid}}/Fe\text{-}Si_{liquid}$$

Their experimental set-up was different from the present work, permitting the silicon electrode to be operated in the molten state, with electrode connections to both sides of the concentration cell being made by graphite conductors. These results exhibited a relatively large scatter and the log γ_{Si} values were considerably higher than those for the previously discussed investigations.

Turkdogan et al.[124] measured silicon activities in Fe-Si binaries by two techniques. First, they measured equilibrium silicon contents in iron melts using silicon nitride crucibles (Si_3N_4) under 1 atmosphere of

nitrogen. The reaction studied was:

$$Si_3N_4 = 3\ Si_{Fe} + 2\ N_2 \qquad (7.40$$

Thus,

$$\Delta G^{o}_{7.40} = -\ RT\ \ln\ a^{3}_{Si}$$

The activity of silicon in iron was evaluated from the standard free energy change for reaction (7.40)[125], and the activity coefficient was calculated from the activity and the equilibrium silicon content. Secondly, the authors equilibrated Fe-Si binary melts with a silver melt as discussed previously. The results, while not presented here, are in reasonable agreement with the previously discussed distribution experiments.

The results of the present investigation using graphite as the top electrode (forming a chemical cell) yielded values of log γ_{Si} which were slightly less than those determined by the distribution technique. The present experimental value of log γ_{Si} determined using a concentration cell were considerably higher, falling into the range of values determined by Sanbongi and Ohtani[76], also using concentration cell measurements.

The maximum error of the emf measurements was estimated from the experimental scatter due to emf fluctuation to be 20%. If this error in the emf value is used in the calculations, the activity coefficient for an alloy containing 0.3 mole fraction silicon is log $\gamma_{Si} = -\ 1.90 \pm 0.23$. The experimental curve derived from the aforementioned distribution data lies very near the upper error limit of the present investigation. The results represented by these distribution data appear to be a good average of all the experimental data shown, with the exception perhaps of the data

from the concentration cell measurements of Sanbongi and Ohtani, and the present investigation.

All the data in Figure 56 was used to calculate the best straight line (Appendix A) which represented the variation of log γ_{Si} with N_{Si}. At 1420°C, this relationship is given by the line:

$$\log \gamma_{Si} = aN_{Si} + b \qquad (7.41)$$

where $a = + 5.21 \pm 0.58$

$b = - 3.04 \pm 0.83$

The scatter of the results of Sanbongi and Ohtani seemed the greatest of all the investigations, and could possibly be related to the method of emf measurement. In their system, graphite conductors were used to measure the emf between a silicon and a Fe-Si melt. The effect of inserting graphite into an Fe-Si melt in which the graphite would dissolve could be serious enough to cause considerable scatter in the data.

The best straight line for all the data, excluding the data of Sanbongi and Ohtani, and the concentration cell measurements of the present investigation, is again represented by equation (7.41) where:

$$a = + 5.67 \pm 0.41$$

$$b = - 3.38 \pm 0.49$$

This best straight line is illustrated in Figure 56, where it is seen that the distribution experiments seem to be a good representation of the true variation of log γ_{Si} with N_{Si}. When $N_{Si} = 0$, log $\gamma^{\circ}_{Si} = - 3.38 \pm$

0.49 which compares quite well to Matoba's[126] value of - 3.25 and Smith and Taylor's[120] value of - 3.44.

If the agreement of the present concentration cell measurements with those of Sanbongi and Ohtani are not fortuitous, the combined results would indicate that a side reaction at the pure silicon electrode/slag interface could be occurring, which is disrupting the true reversible emf to some extent.

7.7 Activity Coefficient of Silicon in the Iron-Carbon Silicon Ternary

From the activity of silicon in the Fe-C-Si ternary, and the silicon concentration, the activity coefficient for silicon in the ternary alloy has been calculated:

$$\gamma'_{Si} = a_{Si}/N_{Si} \qquad (7.42)$$

γ'_{Si} ≡ activity coefficient of silicon in the Fe-C-Si ternary

γ'_{Si} is a function both of its own concentration, and the carbon concentration, and is approximated by the product[127]:

$$\gamma'_{Si} = \gamma_{Si} \cdot \gamma^{C}_{Si} \qquad (7.43)$$

γ_{Si} ≡ activity coefficient of Si in the Fe-Si binary

γ^{C}_{Si} ≡ effect of carbon on the activity coefficient of silicon in the Fe-C-Si ternary

γ_{Si} is taken from the activity coefficient determined for the Fe-Si binary, using the data of Smith and Taylor[120] which appears to be a good average representation of the literature values. Equation (7.43) is written more conveniently as:

$$\log \gamma'_{Si} = \log \gamma_{Si} + \log \gamma^{C}_{Si} \qquad (7.44)$$

The $\log \gamma'_{Si}$ is determined from the emf data, $\log \gamma_{Si}$ is taken from the distribution experiments data discussed previously, so that

$$\log \gamma^{C}_{Si} = \log \gamma'_{Si} - \log \gamma_{Si} \qquad (7.45)$$

The results are listed in Table XXII and are shown in Figure 57 along with data from several other investigations from the literature.

Smith and Taylor[120] measured the activity of silicon in the Fe-C-Si ternay by determining the distribution of silicon between an Fe-C-Si alloy and an Ag-Si alloy. They also did equilibrium experiments with iron in graphite crucibles containing silica liners being brought into equilibrium with different partial pressures of carbon monxode. For the reaction:

$$SiO_2 + 2\ C = Si_{Fe} + 2\ CO \qquad (7.46)$$

the standard free energy change is given by:

$$\Delta G^\circ = -\ RT \ln a_{Si}\ p_{CO}^{2}$$

thus,

$$-\ RT \ln K = -\ (RT \ln a_{Si} + RT \ln p_{CO}^{2}) \qquad (7.47)$$

$$\log a_{Si} = \log K - 2 \log p_{CO}$$

K ≡ equilibrium constant for reaction (7.46)

p_{CO} ≡ experimental partial pressure of CO

From a knowledge of K and the experimental p_{CO}, the activity and activity coefficient were calculated. They noted that the scatter of log γ_{Si}^{C} values was considerably larger than the scatter of log γ_{Si} for the Fe-Si binaries. The magnitude of the scatter for both the distribution experiments and the equilibrium experiments was similar, being approximately $\pm$ 0.3 at high N_C.

Chipman et al.[122] utilized similar experiments, measuring the distribution of silicon between silver and iron, which are immiscible. They used silicon contents from N_{Si} = .15 to .55, and carbon contents up to N_C = 0.09. The experimental scatter of log γ_{Si}^{C} up to N_C = 0.09 is approximately $\pm$ 0.15. Chipman and Baschwitz[123] also used distribution experiments to measure log γ_{Si}^{C} for N_{Si} from 0.05 to 0.27 and for carbon contents up to N_C = 0.16. The experimental scatter in log γ_{Si}^{C} is approximately $\pm$ 0.3.

Schroeder and Chipman[128] modified the distribution experiments using Fe, Ag melts, such that they measured the silicon distribution between Fe-C-Si ternaries and Fe-Si binaries, connected by a silver bath which acted as the transport medium for silicon. It was hoped that in this way, uncertainties which arose from determining small silicon concentrations in silver solutions would be eliminated. The experiments were performed at 1420°C, and an attempt to operate at 1550°C was unsuccessful because at this high temperature the increased solubility of iron in the molten silver resulted into a transfer of iron between the ternary and binary alloys.

Turkdogan et al.[124] measured the activity of silicon in iron by similar equilibrium experiments used by Smith and Taylor[120]. These

authors equilibrated an Fe-C-Si alloy in a graphite crucible with a slag of known silica activity, under 1 atmosphere of CO, so that:

$$\Delta G^\circ = - RT \ln a_{Si}/a_{SiO_2} \qquad (7.48)$$

$$\log a_{Si} = \log K + \log a_{SiO_2} \qquad (7.49)$$

While the majority of the literature results depict the curve of $\log \gamma_{Si}^{C}$ vs N_C as either slightly concave upwards, or linear, the results of Turkdogan et al.[124] are depicted as being represented by a curve which is concave downward. These results appear to be high in the intermediate N_C range (0.04 to 0.12) and perhaps are due to non-attainment of equilibrium. Their results are also strongly dependent on silica activities which were determined from the work of Kay and Taylor[129]. The temperature of the experiment was shown to have no detectable effect on γ_{Si}^{C}.

Ohtani[77] measured the activity of silicon in Fe-C-Si ternary alloys by constructing electrochemical concentration cells, similar to those he used to evaluate silicon activities in the Fe-Si binary. The concentration cell is represented by the sequence:

$$Si_{liquid}/(CaO\text{-}Al_2O_3\text{-}MgO\text{-}SiO_2)_{liquid}\ \ MgO_{solid}/Fe\text{-}Si\text{-}C_{liquid}$$

The electrical connections to the silicon and alloy sides were made with molybdenum and graphite conductors, respectively, resulting in a thermal emf of the order 20 mV. Their results based on the $\log \gamma_{Si}$ results determined by Sanbongi and Ohtani[76] in a similar manner, are in good agreement with the previously discussed distribution and equilibrium

experiments. The scatter of the log γ_{Si}^{C} represent an experimental error of approximately $\pm$ 0.2. These authors noted that the experimental emf was unaffected by temperature.

The experimental scatter of the present investigation, which was done at carbon saturation and low silicon concentrations, is somewhat higher than the others, being approximately $\pm$ 0.51 at high N_C (0.190). The error appears to be reduced considerably as higher silicon and hence lower carbon alloys are used. The results of all the investigations discussed appear to be in good agreement, although the scatter in log γ_{Si}^{C} in most cases seems to be considerably higher than in similarly performed binary investigations. The relationship between log γ_{Si}^{C} and N_C appears to be best represented by a straight line in the low N_C region, with a slight curvature resulting at higher N_C, which is concave upward. The straight line is represented by:

$$\log \gamma_{Si}^{C} = + 5.2\ N_C$$

No attempt has been made to determine the temperature effect on the present experimental log γ_{Si} results, since the temperature correction would be far less than the experimental error.

7.8 Difficulties in Electromotive Force Measurements

The reproducibility of the experimental emf was very good when the metal phase was pure silicon, became worse when the metal phase was the Fe-Si binary and became considerably worse when the metal phase was the Fe-C-Si ternary. In general, for all three systems the emf became less stable at higher temperatures. In all the systems there were emf fluctuations,

but the fluctuations became more severe in the binary and ternary systems.

Initially it was felt that emf fluctuations were due to the discharge of hydroxyl ions in the slag at the graphite electrode, but the application of a D.C. or A.C. voltage across the cell seemed to offer only temporary improvement.

Electrochemical studies such as the present one, which are done at high temperatures, suffer from several obvious disadvantages:

1) The complete elimination of thermo-emf's is difficult.
2) The emf of the system may be reduced because of leakage due to the electric conductance of the components of the system at high temperatures.
3) The cell reaction may be uncertain, which makes n uncertain.
4) The effect of side reactions which become predominant at high temperature is indeterminate.
5) Some melts which contain oxides of Cr, Mn, Fe, etc., and carbides could have a component of electronic conduction present.

In the present system, a small temperature gradient did exist (because of the temperature profile of the furnace, Figure 18) and it is conceivable that the two electrode surfaces were not at the same temperature, and that in most cases this temperature difference was not constant. The condition would give rise to non-reproducible thermo emf. In the system where a silicon electrode was used as the top electode, for the Fe-Si binary, the measured emf's gave log γ_{Si} values somewhat larger than those determined from cells using graphite electrodes. The possibility exists that a C/Si thermo emf is present.

It was mentioned in Chapter 2 that conduction in an ionic melt

can occur by three means; cations, anions and electrons, where the transport number of the system is written:

$$t = t_c + t_a + t_e$$

The question arises whether slags of the type used are partial electronic conductors at these temperatures, in which case, the electronic component would need to be known before the measured emf could be used.

Malkin [5] showed that in the ternary systems $Na_2O \cdot CaO \cdot 4\ SiO_2$, Na_2O-$K_2O \cdot 4\ SiO_2$, $K_2O \cdot CaO \cdot 4\ SiO_2$ and $CaO \cdot MgO \cdot 3.25\ SiO_2$, the cation transport number was unity. It has been shown[130] that the current in silicate melts of this type is carried entirely by the cations ie. $\Sigma t_+ = 1$, or the electronic component of conduction is zero. In the present system, the slags became dark after each experiment, indicating either a solubility of carbon in the slag, or the presence of carbon as a precipitate. The carbon content of the slag was determined to be as high as 0.22 wt.%. The effect of this carbon on leakage through the melt is indeterminate.

The possibility of side reactions occurring in the system are plentiful and are discussed thoroughly in preceding sections.

CHAPTER 8

SUMMARY

This research project was initiated to study the local cell mechanism which was postulated by Wagner[83] to occur when slag-metal reactions were carried out in graphite crucibles. In particular, the local cell mechanism involved in the reduction of silica saturated slags by carbon saturated iron was investigated, with three purposes in mind. First, Faradayan cell experiments were performed which conclusively illustrated the existence of the local cell mechanism in this system. Second, a series of kinetic experiments on sleeved and unsleeved crucibles was used to show that the contribution of the local cell mechanism to the overall silica reduction rate is negligible in comparison to the reduction rate at the slag/metal interface. This observation has both academic and industrial significance. Prior to this investigation, the suggestion that the local cell mechanism could have a large influence on the transfer rate of silicon placed a considerable amount of uncertainty on previous kinetic studies in which only the slag/metal interface was considered as a reaction interface. Now it may be safely assumed that, for the reduction of silica at least, using graphite crucibles the second interface (slag/graphite) has no noticeable effect on the kinetics of the reaction.

A major problem in blast furnace technology has been and is the control of the hot metal chemistry. Modern technology has resulted in

the use of graphite lined hearths, so the present system is analogous to the slag/metal system in a blast furnace hearth. The implication of Wagner's local cell concept is that a graphite lined hearth would result in a correspondingly greater amount of silicon transferred to the hot metal. This condition is generally undesirable since the silicon will be oxidized in the steel-making furnace and costly lime additions would be necessary to maintain the required basicity level. The results of this investigation indicate that a graphite lined hearth would not be responsible for any increase in silicon pick-up in the hot metal.

Third, the existence of the local cell electrochemical reaction allowed the use of the reversible electromotive force technique to study the thermodynamics of several slag-metal systems. The oxidation of silicon by carbon monoxide was studied, and the standard free energy change for the reaction was determined to be:

$$\Delta G^\circ = - 153{,}600 + 82.5\ T$$

The use of this technique enabled the standard free energy change to be determined directly from the experimental results without necessitating the use of results of other investigations.

The activity of silicon in iron-silicon alloys was determined by this method and the results are in agreement with those from the literature. The majority of the previous work on this system had been done by a silicon distribution technique in which silicon was equilibrated between an iron phase and a silica phase. While the results were in agreement with one another, a different technique was necessary to confirm the accuracy of the method. This confirmation was provided by the present investigation. The present

results were then combined with other investigations to determine the relationship between the silicon activity coefficient and silicon concentration at 1420°C. The results are represented by the equation:

$$\log \gamma_{Si} = 5.67\ N_{Si} - 3.38$$

The technique was also used to determine the activity of silicon in iron-carbon-silicon alloys, from which the effect of carbon on the activity coefficient of silicon was calculated. The results of this investigation were not unique in the degree of reproducibility, for all the previous authors experienced similar uncertainties in this ternary system. The effect of carbon on the activity coefficient of silicon is best described by all the results as:

$$\log \gamma_{Si}^{C} = 5.2\ N_C$$

This expression is valid up to $N_C = 0.10$, but beyond this value some departure from linearity is noticed.

APPENDIX A

The best straight lines were determined by the least squares method of Spiegel[132]. For a system of data points designated (x_i, y_i) with y the imprecisely measured variable, the best straight line is calculated:

$$\tilde{y} = a + bx$$

$\tilde{y}$ ≡ estimated value of y for an observed value of X

a ≡ estimated value of y at X = 0

b ≡ slope of the line, or the regression coefficient

Using a least squares analysis, a and b are calculated:

$$b = \frac{(N\Sigma xy) - \Sigma x \Sigma y}{N\Sigma x^2 - (\Sigma x)^2}$$

N ≡ number of data points

$$a = \frac{\Sigma y \Sigma x^2 - \Sigma x \Sigma xy}{N\Sigma x^2 - (\Sigma x)^2}$$

The standard error of estimate for the 95% confidence interval is calculated from:

$$2\, S_{yx} = 2\ \mathrm{SQRT}\ ((\Sigma y^2 - a\Sigma y - b\Sigma xy)/N)$$

The 95% confidence limit for the regression coefficient is determined by:

$$b = b \pm \frac{t_{0.975}}{\sqrt{N-2}} \frac{S_{yx}}{Sx}$$

where $t \equiv$ student's t distribution

$$S_x \equiv \sqrt{\frac{\Sigma(x-\bar{x})^2}{N}}$$

In the calculations involving the kinetic experiments, it was necessary to know whether there were any significant difference in the various reaction rate constants for sleeved or unsleeved reactions. It was also imperative to determine if there were any significant differences in the activation energies determined from the slopes of the straight line plots. The method used is from Volk[133] for the comparison of several slopes. In this method it is necessary to determine the sums of squares of deviations from the best straight line through all the points, the best straight line through each set of points with a pooled estimate of the slope, and the best straight line through the individual sets, each with its own slope. If there is no significant decrease in the sum of squares deviation from the individual slopes, compared to the deviation when a pooled slope is utilized using an F test then a single pooled slope is sufficient to describe the data. The necessary data are shown in Tables XXV and XXVI

The ratio of the "between slopes mean square" and the "error mean squares" is tested against F at 2 and 43 degrees of freedom by converting to a normal distribution test using the method of Wallis and Roberts[134].

$$G = \sqrt[3]{F} \qquad a = \frac{2}{9(k-1)} \qquad b = \frac{2}{9(\Sigma n-k)}$$

$k \equiv$ number of sets of data

$\Sigma n \equiv$ total number of points

$$K = \frac{(1-b)\,G + \bar{a} - 1}{\sqrt{bG^2 + \bar{a}}}$$

$K \equiv$ standard normal variable

In the kinetic experiments it was found that $K = 0.818$, thus the probability is 0.21, or there is 80% probability of the 3 slopes having one pooled value. Also, the small value determined for the difference between means slope and pooled slope indicates no significant difference in the y values for the 3 lines.

TABLE XXV

ANALYSIS OF VARIANCE FOR KINETIC EXPERIMENTS

	$\Sigma' x^2$	$\Sigma' y^2$	$\Sigma' xy$	$\Sigma' C^2$	$\Sigma' \hat{y}^2$	slope b
Total	0.0000000097	22.953445	- 0.000431731	19.21567	3.737775	
Means	0.0000000002	0.383060	- 0.00000230	.02645	0.356610	
Difference	0.0000000095	22.510385	- 0.000429431	19.411953	3.158432	- 48,800
Set 1 (sleeved)	0.0000000026	6.325905	- 0.000124166	5.866844	0.459061	- 47,250
Set 2 (unsleeved)	0.0000000005	1.000258	- 0.000019625	0.975363	0.024895	- 49,700
Set 3 (unsleeved)	0.0000000057	15.244221	- 0.00285645	14.339379	0.904842	- 50,200
Sum	0.0000000088	22.570384	- 0.000429436	21.181586	1.388798	

TABLE XXVI

ANALYSIS OF VARIANCE FOR KINETIC EXPERIMENTS

Source of Variance	Sum of Squares	Degrees of Freedom	Mean Square
Means Correlation	0.356610	1	0.127171
Difference between Means Slope and Pooled Slope	0.222133	1	0.222133
Between Slope	1.769634	2	3.1316045
Error	1.388798	43	1,928760
Total	3.737175	47	

$$\Sigma' x^2 = \Sigma x^2 - \frac{(\Sigma x)^2}{N}$$

$$\Sigma' y^2 = \Sigma y^2 - \frac{(\Sigma g)^2}{N}$$

$$\Sigma' xy = \Sigma xy - \frac{\Sigma x \Sigma y}{N}$$

$$\Sigma' C^2 = \frac{(\Sigma' xy)^2}{\Sigma' x^2}$$

$$\Sigma' y^2 = \Sigma' y^2 - \Sigma' C^2$$

APPENDIX B

STANDARD FREE ENERGY CHANGE CALCULATIONS

1. Calculation of ΔG^o for the reaction:

$$SiO_{2_{slag}} + C_{graphite\ electrode} = CO_{gas} + SiO_{gas} \qquad (B.1)$$

The reaction can be written as consisting of three reactions:

$$Si + SiO_2 = 2\ SiO \qquad (B.2)$$

$$SiO_2 = Si + O_2 \qquad (B.3)$$

$$2\ C + O_2 = 2\ CO \qquad (B.4)$$

$$\Delta G^o_{B.1} = \frac{1}{2}\left[\ \Delta G^o_{B.2} + \Delta G^o_{B.3} + \Delta G^o_{B.4}\ \right]$$

$$\Delta G^o_{B.1} = \frac{1}{2}[(151{,}300-70.07T)^{(111)} + (226{,}500-47.5T)^{(123)} + (-53{,}400-41.9T)^{(113)}]$$

$$\Delta G^\circ_{B.1}{}_{1450°C} = +\ 24{,}800\ cal/$$

2. Calculation of ΔG^o for the Reaction:

$$SiO_{2_{slag}} + 3\ C_{graphite\ electrode} = SiC + 2\ CO \qquad (B.5)$$

Reaction (B.5) can be considered to consist of several reactions:

$$SiO_2 + 2\ C = Si + 2\ CO \qquad (B.6)$$

$$Si + C = SiC \qquad (B.7)$$

$$\Delta G^{o}_{B.5} = \Delta G^{o}_{B.6} + \Delta G^{o}_{B.7}$$

$$\Delta G^{o}_{B.5} = (170{,}000 - 87.9\ T) + (-\ 27{,}400 + 8.88\ T)^{(112)}$$

$$\Delta G^{o}_{B.5_{1450°C}} = +\ 7{,}400\ \text{cal}$$

3. Calculation of ΔG^{o} for the Reaction:

$$SiO_{2_{slag}} + CO_{gas} = SiO_{gas} + CO_{2_{gas}} \qquad (B.8)$$

Reaction (B.8) can be considered to consist of several reactions:

$$SiO_2 + H_2 = SiO + H_2O \qquad (B.9)$$

$$H_2O = H_2 + \tfrac{1}{2}\ O_2 \qquad (B.10)$$

$$CO + \tfrac{1}{2}\ O_2 = CO_2 \qquad (B.11)$$

$$\Delta G^{o}_{B.8} = \Delta G^{o}_{B.9} + \Delta G^{o}_{B.10} + \Delta G^{o}_{B.11}$$

$$\Delta G^{o}_{B.8} = (127{,}100\text{-}45.07T)^{(111)} + (+59{,}000\text{-}13.88T)^{(113)} + (-67{,}800\text{+}20.75T)^{(113)}$$

$$\Delta G^{o}_{B.8_{1450°C}} = +\ 52{,}700\ \text{cal}$$

4. Calculation of ΔG^{o} for the Reaction:

$$\tfrac{1}{3}\ SiO_{2_{slag}} + \tfrac{2}{3}\ SiC_{electrode} = Si_{Fe\text{-}C\text{-}Si} + \tfrac{2}{3}\ CO_{gas} \qquad (B.12)$$

Reaction (B.12) can be considered as consisting of several reactions:

$$\frac{1}{3}\,SiO_2 = \frac{1}{3}\,Si + \frac{1}{3}\,O_2 \qquad (B.13)$$

$$\frac{2}{3}\,SiC = \frac{2}{3}\,Si + \frac{2}{3}\,C \qquad (B.14)$$

$$\frac{2}{3}\,C + \frac{1}{3}\,O_2 = \frac{2}{3}\,CO \qquad (B.15)$$

$$\Delta G^{o}_{B.12} = \Delta G^{o}_{B.13} + \Delta G^{o}_{B.14} + \Delta G^{o}_{B.15}$$

$$= \frac{1}{3}\,(226{,}500-47.5T)^{(112)} + \frac{2}{3}\,(27{,}400-8.88T)^{(112)} + \frac{1}{3}\,(-53{,}400-41.9T)^{(113)}$$

$$\Delta G^{o}_{B.12} = +\ 14{,}400\ \text{cal.}$$

BIBLIOGRAPHY

1. Wagner, C., Phys. Chem. Steelmaking, Proc. (Dedham Mass. 1956, Pub. 1958) 237.
2. King, T. B. and Ramachandran, S., Ibid 125.
3. Baak, T. and King, T. B., unpublished work.!?
4. Grimble, M., Ward, R. G., and Williams, D. J., Jour. Iron and Steel Inst. 203, 264 (1965).
5. Malkin, V. I., Hutnické Listy, 12, 985 (1957).
6. Milazzo, G., Electrochemistry (Elsevier, Amsterdam, London and New York, 1963) 133.
7. Quagliano, J. V., Chemistry (Prentice-Hall, N. J., 1963).
8. Delimarskii, V. K., Akranian Khim. Zhur., 16, 414 (1950)
9. Hamer, W. J., Malmberg, M. S., and Rubin, B., Journ. Electrochem. Soc. 103, No. 1, 8 (1956).
10. Darken, L. S., and Gurry, R. W., Physical Chemistry of Metals (McGraw-Hill, New York, Toronto and London, 1953) 423.
11. Glasstone, S., The Elements of Physical Chemistry, (D. Van Nostrand, Toronto, 1946) 467.
12. Milazzo, G., Electrochemistry (Elsevier, Amsterdam, London and New York, 1963) 203.
13. Rey, M., Disc. Farad. Soc. 4, 257 (1948).
14. Whiteley, J. H. Proc. Cleveland Instn. Engrs. 59, 36 (1922-23).
15. Colclough, T. P., Jour. Iron and Steel Inst. 107, 267 (1923)
16. Schenck, H., BISRA translation, London (1945).

17. Back , R., Stahl and Eisen, 1, 351 (1931).

18. United States Steel, The Making, Shaping and Treating of Steel (Pittsburgh, 7th Ed. 1957), 253.

19. Philbrook, W. O. and Washburn, F. M., Basic Open Hearth Steelmaking (AIME, New York 1951) 190.

20. Darken, L. S. and Larsen, B. M., Trans. AIME 150, 87 (1942).

21. Winkler, T. B., and Chipman, J., Trans AIME, 167, 111 (1946).

22. Aiken, R. H., U. S. Patent 816142 (March 27, 1906).

23. Doelter, C., Monatsch., 28, 1313 (1907).

24. Farup, F., Fleischer, W. and Holtan, E., Chem. und Industrie., 12, 11 (1924).

25. Sauerwald, F. and Neuendorff, G., Ztsch. Elektrochem. 31, 643 (1928).

26. Wejnarth, A., Trans. Amer. Electrochem. Soc. 65, 177 (1934).

27. Martin, A. E. and Derge, G., Trans AIME 154, 104 (1943).

28. Rasch, C. and Hinrichsen, F., Electrochem., 14, 41 (1908).

29. Bockris, J. O'M., Kitchener, J. A., Ignatowicz, S. and Tomlinson, J. W., Farad. Soc. Discussions 4, 265 (1948).

30. Bockris, J. O'M., Kitchener, J. A. and Davies, A. E., Trans. Farad. Soc. 48, 536 (1952).

31. Bockris, J. O'M., Kitchener, J. A. and Ignatowciz, S. and Tomlinson, J. W., Trans. Farad. Soc. 48, 95 (1952).

32. Hofmann, U. H. and Morincek, B., Arch. fur das Eisen., 11/12, 523 (1954).

33. Herasymenko, P. and Speight, G. E., J. Iron and Steel Inst. 166, 169 (1950).

34. Simnad, M. T., Derge, G. and George, I., Trans AIME 200, 1386 (1954).

35. Glasstone, S., The Elements of Phsyical Chemistry (D. Van Nostrand, (Toronto, 1946) 406.

36. Ward, R. G., An Introduction to the Physical Chemistry of Iron and Steel Making (Arnold, London 1962) 44.

37. Herasymenko, P., Trans. Farad. Soc., 34.2, 1245 (1938).

38. Temkin, M., Acta Physicohcemica URSS 20, 411 (1945).

39. Herasymenko, q. and Speight, G. E., J. Iron and Steel Inst. 166, 289 (1950).

40. Flood, H. and Grjotheim, K., J. Iron and Steel Inst. 171, 64 (1952).

41. Flood, H., Forland, T. and Grjotheim, K., Z. Anorg. Chemie, 276, 289 (1954).

42. Pauling, L., The Nature of the Chemical Bond (Cornell University Press, Ithaca, 1960).

43. Bloom, H. and Heymann, T., Proc. Roy. Soc. A, 188, 392 (1946).

44. Endell, K. and Hellburgge, J., J. Glastech. Berg. 18, 33 (1940).

45. Gaskell, D. R., Ph.D. Thesis, McMaster University (1967).

46. King, T. B., The Physical Chemistry of Melts, (Inst. of Mining and Metallurgy, London 1953). 35.

47. Gaskell, D. R., University of Pennsylvania, private communication.

48. Kingery, W. D., Property Measurements at High Temperature (Wiley, N. Y. 1959).

49. Chang, L. C. and Derge, G., Trans. AIME 172, 90 (1946).

50. Fischer, W. A. Phys. Chem. Steelmaking Proc. (Dedham Mass. 1956), pub. 1958, p. 79.

51. Duckworth, H. E., Electricity and Magnetism (Toronto, Macmillan, 1960).

52. Kubashewski, O. and Hopkins, B. E., Oxidation of Metals and Alloys (Academic Press, N. Y. 1953).

53. Frenkel, J., Z. Phys. 35, 652 (1926).

54. Schottky, W., Z. Phys. Chem., 29, 335 (1935).

55. Wagner, C., Z. Phys. Chem., B22, 181 (1933).

56. Wagner, C., Naturwissenschaften, 31, 265 (1943).

57. Steele, B. C. H., and Alcock, C. B., Trans. AIME 233, 1359 (1965).

58. Lasker, M. F. and Rapp, R. A., Z. Phys. Chem., 49, 198 (1966).

59. Kiukolla, K. and Wagner, C., J. Electrochem. Soc. 104, no. 5, 308 (1957).

60. Roeder, G., Master's Thesis, McMaster University, 1964.

61. Rapp, R. A. and Maak, F., Acta Met. 10, 63 (1962).

62. Taylor, R. W. and Muan, A., Trans AIME 224, 500 (1962).

63. Aukrast, E. and Muan, A., Acta Met. 10, 555 (1962).

64. Schwerdtfeger, K. and Muan, A., Acta Met. 12, 905 (1964).

65. Schwerdtfeger, K. and Muan, A., Acta Met. 13, 509 (1965).

66. Sakagami, E. and Matsushita, M., Rep. Inc. Inst. Sci., Tokyo U., 7, 181 (1958).

67. Esin, O. A., Lepinskikh, B. M. And Musikhan, V. E., Application of Vacuum in Metallurgy, (Academy of Sciences, Moscow, 1960).

68. Schwerdtfeger, V. K., and Engell, H-J., Arch. fur das Eisen, 35, no. 5, 1, (1964).

69. Schwerdtfeger, V. K. and Engell, H-J., Trans AIME 233, 1327 (1965).

70. Schwerdtfeger, K., Trans AIME 236, 32 (1966).

71. Feldman, V. U., Arch. Fur das Eisen 34, no. 2, 1 (1963).

72. Sanbongi, K. and Omori, Y., Sci. Rep. Res. Inst. Tohoku U., Ser. A, 13, 175 (1961).

73. Sanbongi, K. and Ohtani, M., Sci. Rep. Res. Inst. Tohoku U., Ser. A, 5, 263 (1953).

74. Chipman, J. and Marshall, S., Trans. Am. Soc. Metals 30, 695 (1942).

75. Sanbongi, K. and Ohtani, M., Sci. Rep. Res. Inst. Tohoku U. Ser. A, 7, 204 (1955).

76. Sanbongi, K. and Ohtani, M., Sci. Rep. Res. Inst. Tohoku U. Ser. A, 5, 350 (1953).

77. Ohtani, M., Sci. Rep. Res. Inst. Tohoku U., Ser. A, 7, 487 (1955).

78. Ohtani, M., Sci. Rep. Res. Inst. Tohoku U., Ser. A, 9, 426 (1957).

79. Schenck, H. and Neumann, F., Arch. furdas Eisen., 29, 263 (1958).

80. Aurini, T. D., Master's Thesis, McMaster University, 1964.

81. Gomersall, D., Inland Steel Corporation, private communication.

82. Sproull, R. L., Modern Physics (John Wiley and Sons, N. Y., London, 1956) 315.

83. Wagner, C., The Physical Chemistry of Steelmaking (Wiley 1958) 237.

84. Eyring, H., The Physical Chemistry of Process Metallurgy, (Interscience, Vol. 7, 1961), 65.

85. Ramachandran, S., King, T. B. and Grant, N. J., Trans AIME 206, 1549 (1956).

86. Ramachandran, S. and King, T. B., The Physical Chemistry of Steel Making, Wiley, 1958) 125.

87. Ward, R. G. and Salmon, K. A., J. Iron and Steel Inst. 196, 393 (1960).

88. Ward, R. G. and Salmon, K. A., J. Iron and Steel Inst. 201, 222 (1963).

89. Fulton, J. C. and Chipman, J., Trans AIME 215, 888 (1959).

90. Ward, R. G., An Introduction to the Physical Chemistry of Iron and Steel Making (Arnold, London, 1962) 173.

91. Schuhmann, R., Trans. AIME 218, 1130 (1960).

92. Turkdogan, E. T., Grieveson, P. and Beisler, J. F., Trans AIME 227, 1265 (1963).

93. Rawling, J. R. and Elliot, J. F., Trans AIME 233, 1539 (1965).

94. Sharma, S. Master's Thesis, McMaster University (1965).

95. Grimble, M. Ph.D. Thesis, University of Sheffield (1962).

96. Wojcek, W. M., Ph.D. Thesis, University of Pittsburgh (1966).

97. Kershaw, P. Ph.D. Thesis, McMaster University (1968).

98. Levin, E. M., Robbins, C. R. and McMurdie, H. F., Phase Diagrams for Ceramists (The American Ceramic Society, 1964).

99. Kelly, J., Spectrographic Laboratory, Steel Company of Canada, Limited, Hamilton, Ontario.

100. Baker, L. A. Ph.D. Thesis, University of New South Wales (1965).

101. Hanson, M., Constitution of Binary Alloys (McGraw-Hill, N. Y. 1958).

102. Chipman, J., Alfred, R. A., Gott, L. W., Small, R., Wilson, D. M., Thomson, C. N., Guernsey, D. L. and Fulton, J. C., Trans. Am. Soc. Metals 44, 1215 (1952).

103. Bodsworth, C., Physical Chemistry of Iron and Steel Manufacture (Longmans, London, 1963).

104. King, T. B., Massachusetts Institute of Technology, private communication.

105. Kozakevitch, P., Liquids: Structure, Properties, Solid Interactions (Elsevier, edited by T. J. Hughes, 1965) 243.

106. Rawling, J. R., Ph.D. Thesis, Massachusetts Institute of Technology, 1962.

107. Novokhatskiy, I. A. and Ershov, G. S., Russion Metallurgy (Metally) 4, 11 (1966).

108. Darken, L. S. and Gurry, R. W., Physical Chemistry of Metals (McGraw-Hill, New York, Toronto, London, 1953).

109. Lucas, L. D., Compt. rend. 248, 2336 (1959).

110. Birks, Ph.D. Thesis, University of Sheffield, 1960.

111. Ramstad, H. F. and Richardson, F. D., Trans AIME 221, 1021 (1961).

112. Rein, R. H. and Chipman, J., J. Phys. Chem. 67, 839 (1963).

113. Richardson, F. D. and Jeffes, J. H. E., J. Iron and Steel Inst., 160, 261 (1948).

114. Chipman, J., J. Amer. Chem. Soc. 83, 1762 (1961).

115. Walsh, J. H., Chipman, J., King, T. B. and Grant, N. J., Trans AIME 206, 1568 (1956).

116. Tomlinson, J. W., J. Soc. Glass Tech. 40, 25 (1956).

117. Russel, L. E., J. Soc. Glass Tech. 41, 304 (1957).

118. Gluck, J. V., Ph.D. Thesis, University of Michigan, 1965.

119. Korber, F. and Oelsen, W., Mitt. Kaiser Wilhelm Inst. Eisenforsch, 18, 109 (1936).

120. Smith, G. and Taylor, J., J. Iron and Steel Inst. 202, 577 (1964).

121. Hager, J., Trans AIME 227, 1000 (1963).

122. Chipman, J., Fulton, J. C., Gokcen, N., and Caskey, G. R., Acta Met. 2, 439 (1954).

123. Chipman, J., Baschwitz, R., Trans AIME 227, 473 (1963).

124. Turkdogan, E. T., Grieveson, P. and Beisler, J. F., Trans AIME 227 1258 (1963).

125. Pehlke, R. D. and Elliot, J. F., Trans. Met. Soc. AIME 215, 781 (1959).

126. Matoba, S., Gunji, K. and Kuwana, T., Trans. Nat. Res. Inst. Metals Tokyo 3, 1 (1961).

127. Wagner, C., The Thermodyanics of Alloys (Addison-Wesley Press, Cambridge 1952).

128. Schroeder, D. and Chipman, J., Trans. AIME 230, 1492 (1964).

129. Kay, D. A. R. and Taylor, J., Trans. Faraday Soc. 56, 1372 (1960).

130. Bockris, J. O'M., White, J. L. and Mackenzie, J. D., Physicochemical Measurements at High Temperatures (Butterworths, London, 1959) 262.

131. Rist, A. and Chipman, J. Phys. Chem. Steelmaking, Proc. (Dedham, Massachusetts 1956, Pub. 1958) 3.

132. Spiegel, M. R., Theory and Problems of Statistics (Schaum, New York 1961).

133. Volk, N., Applied Statistics for Engineers (McGraw-Hill, N. Y. 1958).

134. Wallis, W. A. and Roberts, H. V., Statistics (Free Press, Illinois, 1956).

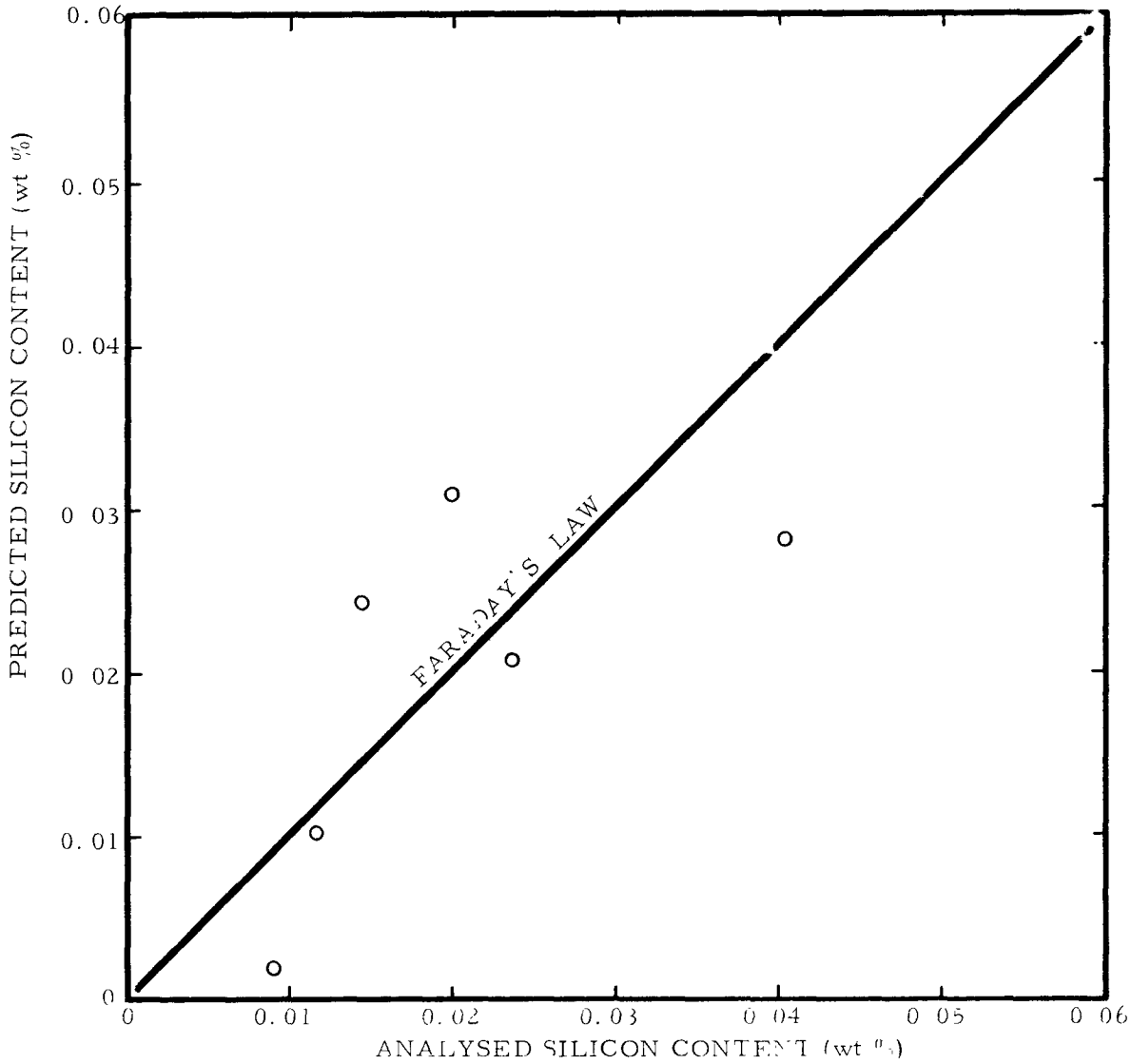

FIGURE 22 - FARADAYEN YIELD EXPERIMENT RESULTS
(Large SiO_2 Crucible)

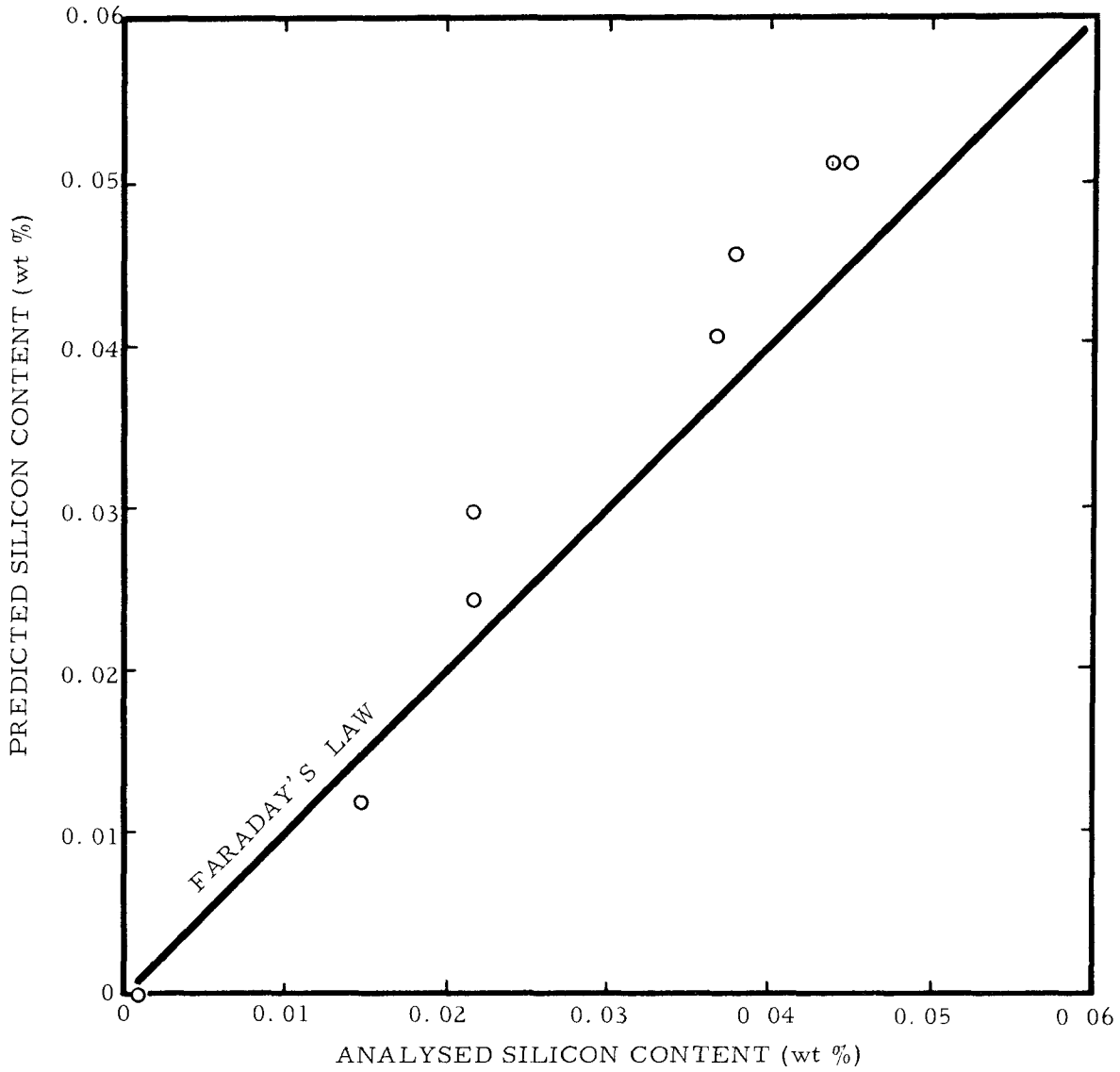

FIGURE 23 - FARADAYEN YIELD EXPERIMENT RESULTS
(Small SiO_2 Crucible)

FIGURES 24 to 31 - SILICON CONCENTRATION-TIME CURVES
(Unsleeved Crucibles)

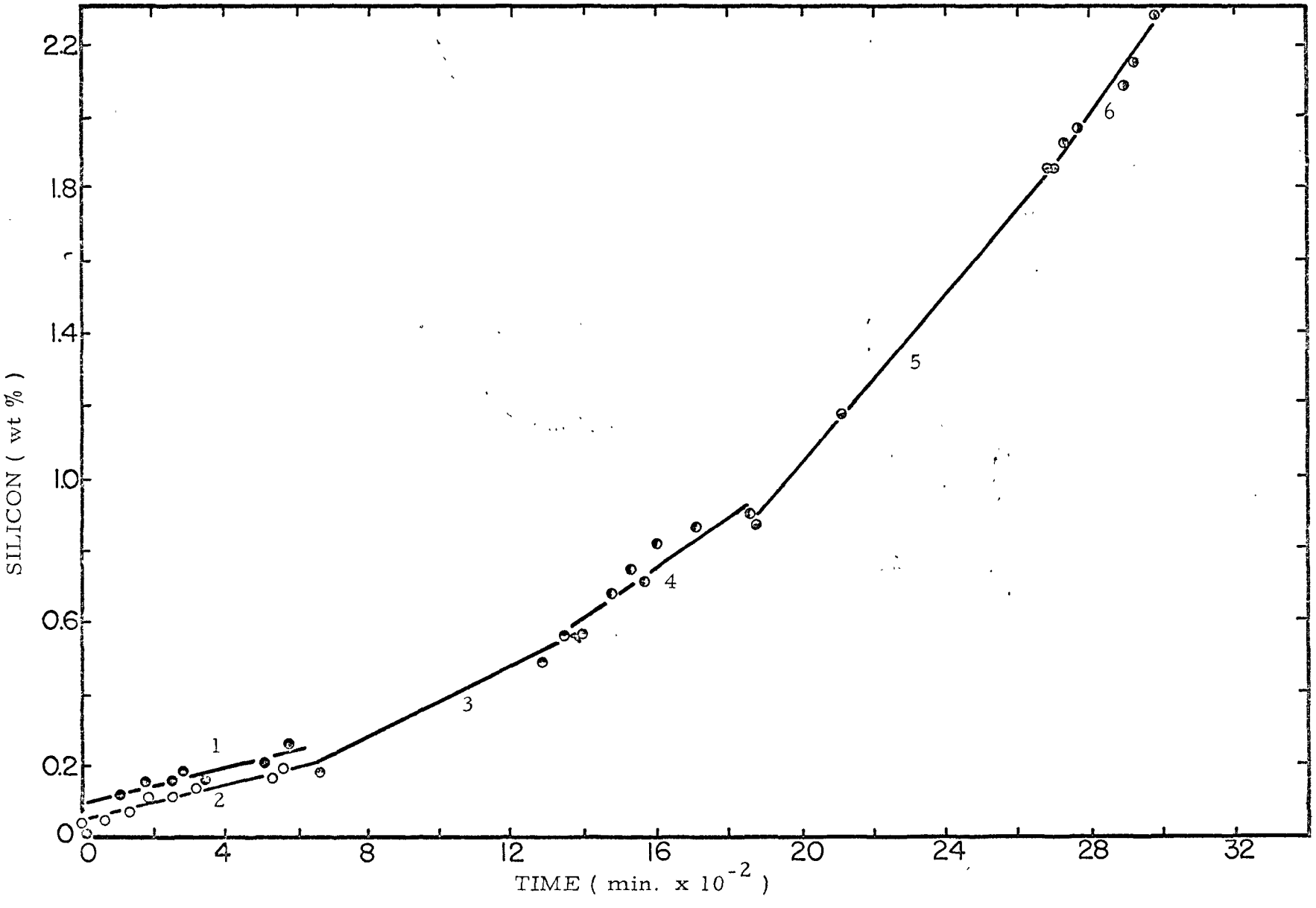
SILICON (wt %)
2.2
1.8
1.4
1.0
0.6
0.2
0
0
4
8
12
16
20
24
28
32
TIME (min. x 10^-2)
1
2
3
4
5
6

Figure 24

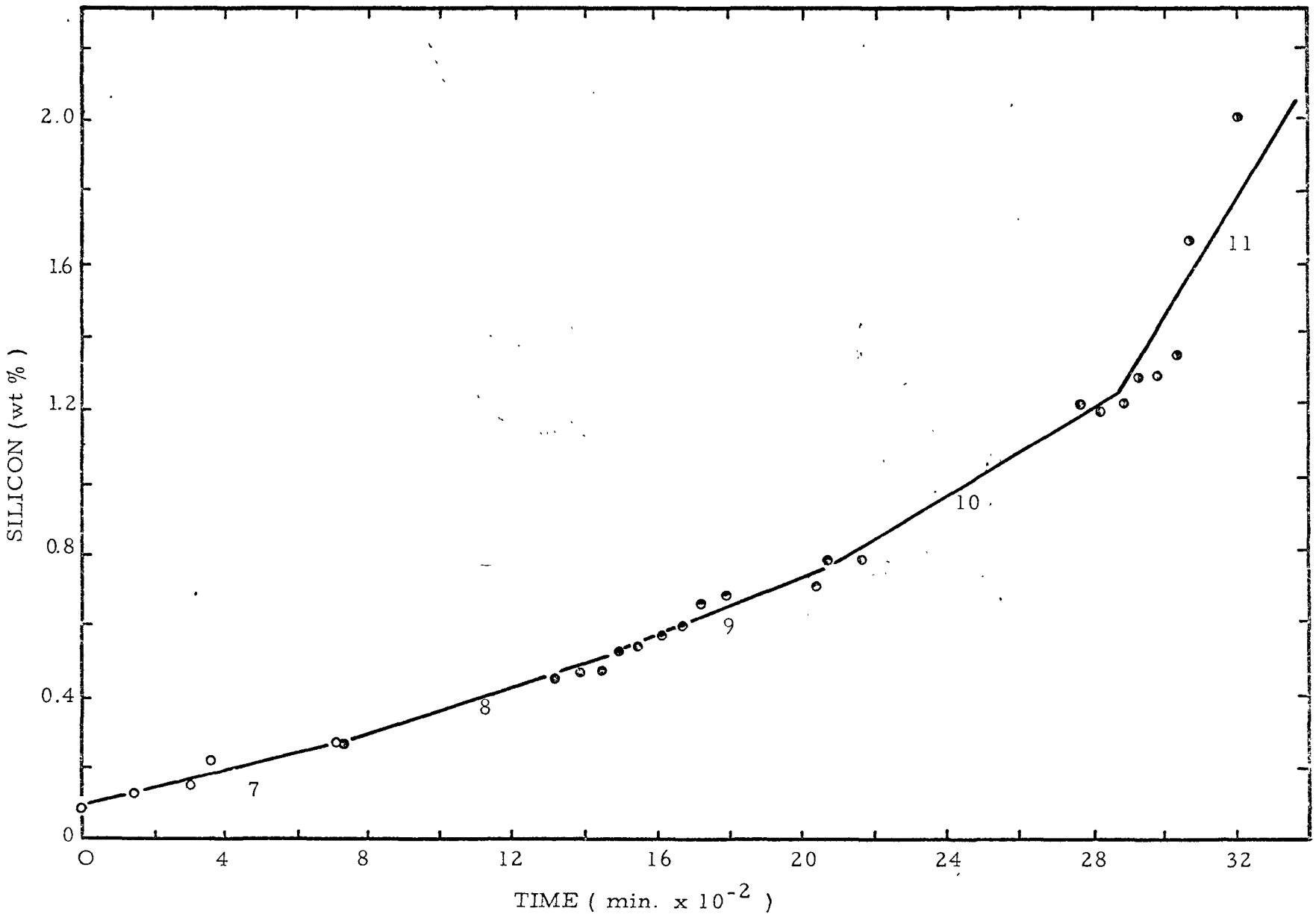
SILICON (wt %)
2.0
1.6
1.2
0.8
0.4
0
0
4
8
12
16
20
24
28
32
TIME (min. x 10^{-2})
7
8
9
10
11

Figure 25

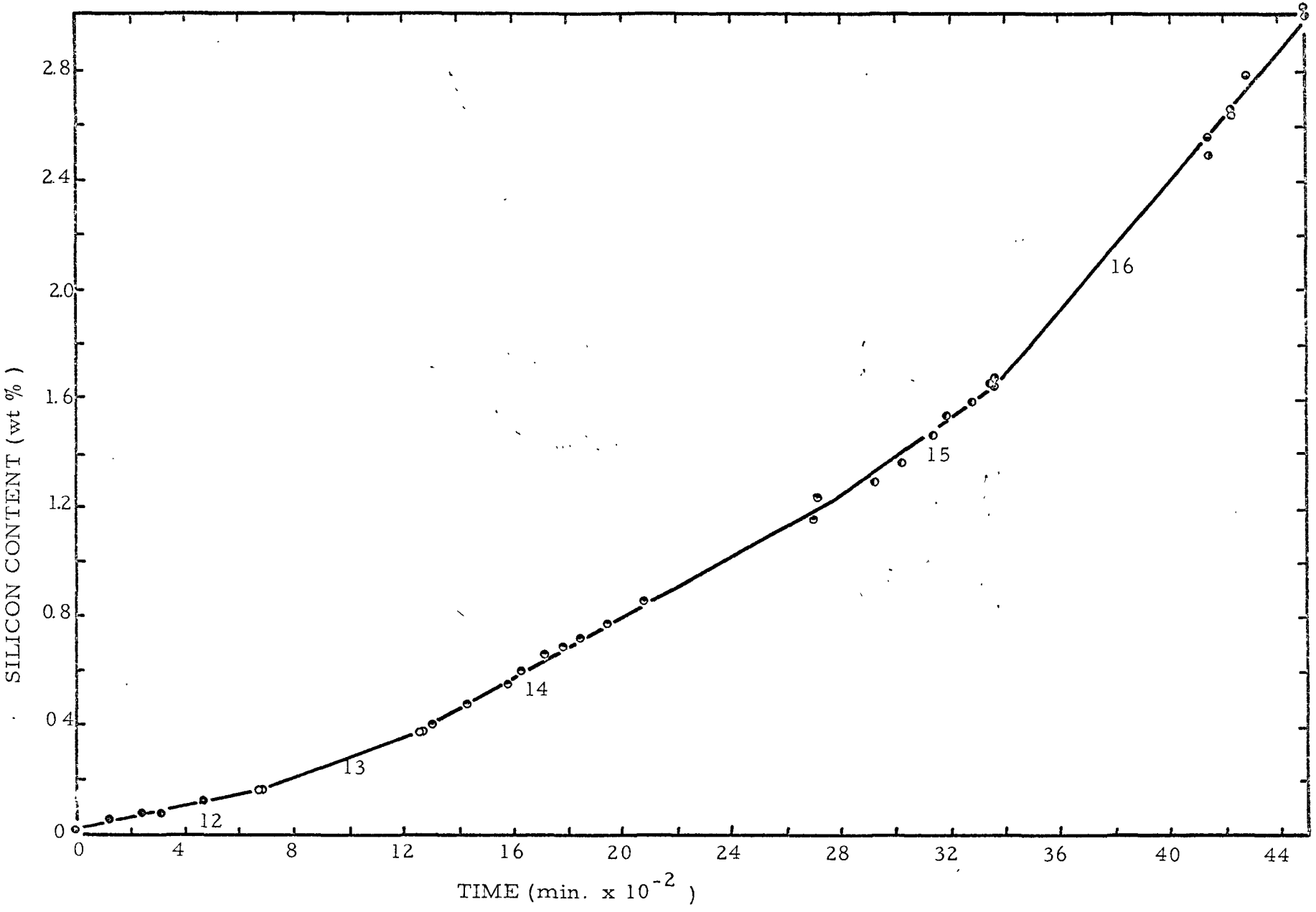
SILICON CONTENT (wt %)
2.8
2.4
2.0
1.6
1.2
0.8
0.4
0
0
4
8
12
16
20
24
28
32
36
40
44
TIME (min. x 10^{-2})
12
13
14
15
16

Figure 26

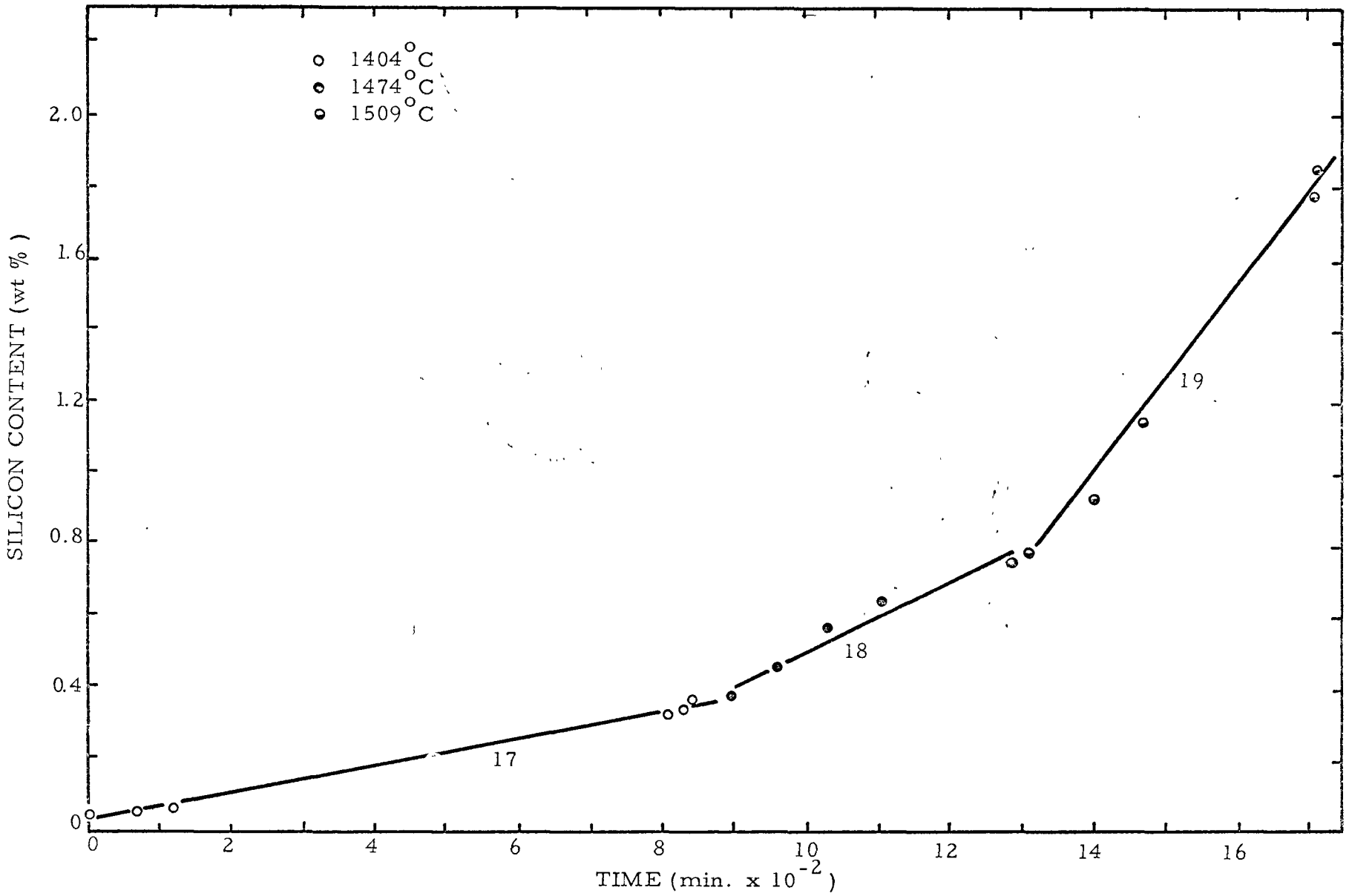
1404°C
1474°C
1509°C
SILICON CONTENT (wt %)
2.0
1.6
1.2
0.8
0.4
0
0
2
4
6
8
10
12
14
16
TIME (min. x 10^-2)
17
18
19

Figure 27

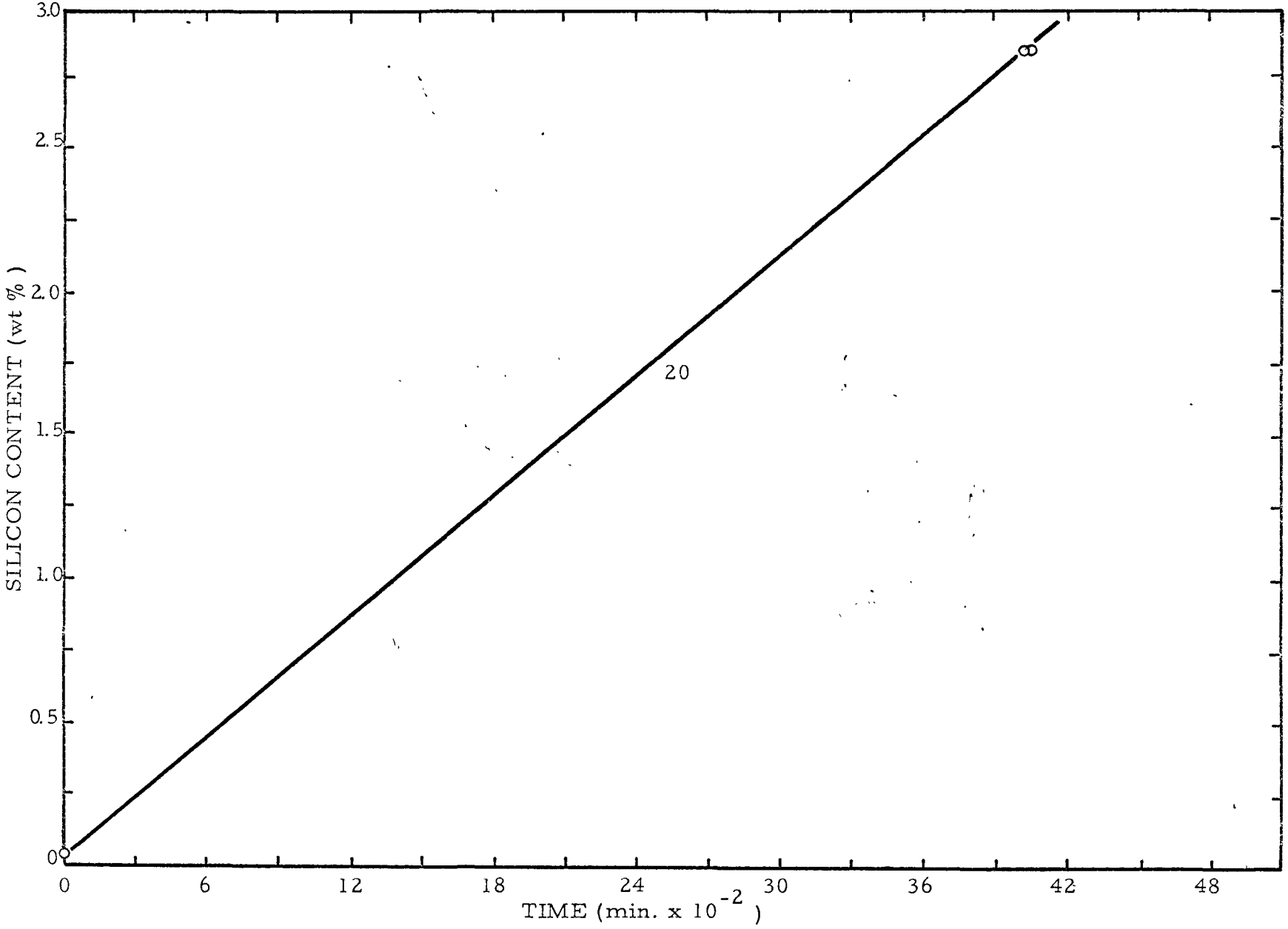
3.0
2.5
2.0
1.5
1.0
0.5
0
SILICON CONTENT (wt %)
20
∞
0
6
12
18
24
30
36
42
48
TIME (min. x 10^-2)

Figure 28

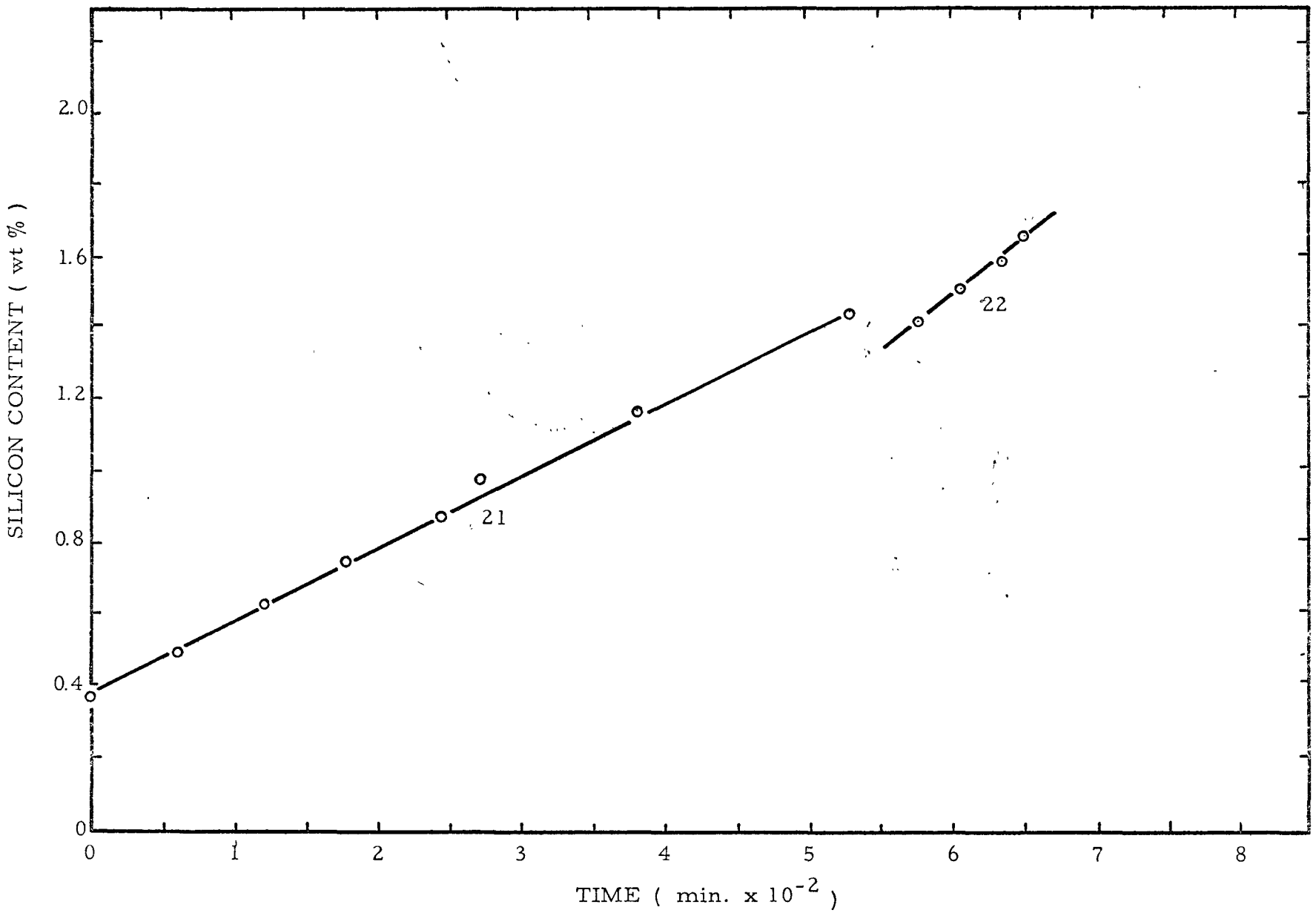
SILICON CONTENT (wt %)
2.0
1.6
1.2
0.8
0.4
0
0
1
2
3
4
5
6
7
8
TIME (min. x 10^{-2})
21
22

Figure 29

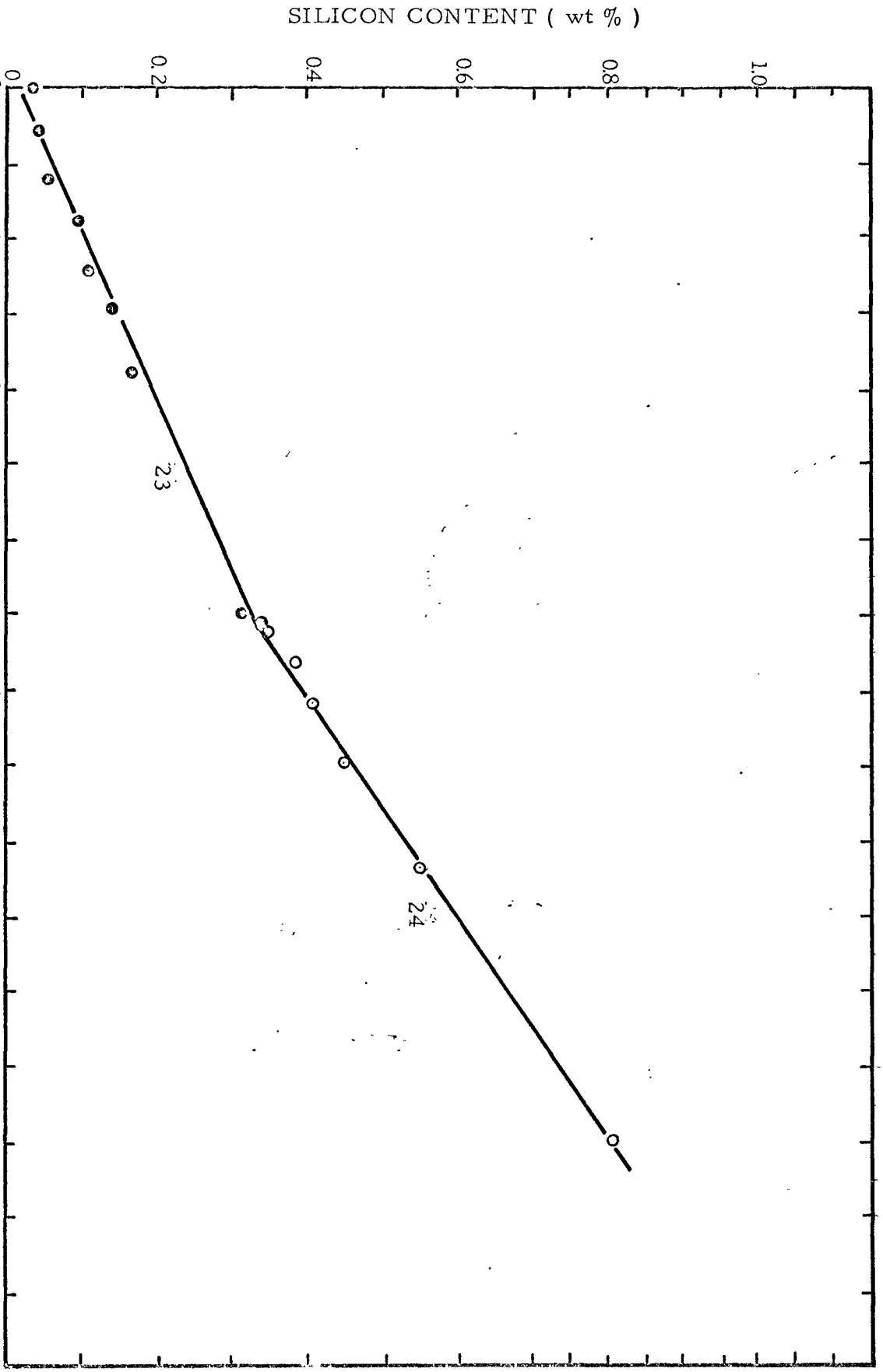
SILICON CONTENT (wt %)
0.2
0.4
0.6
0.8
1.0
0
4
8
12
16
20
24
28
32
TIME (min. x 10^{-2})
23
24

Figure 30

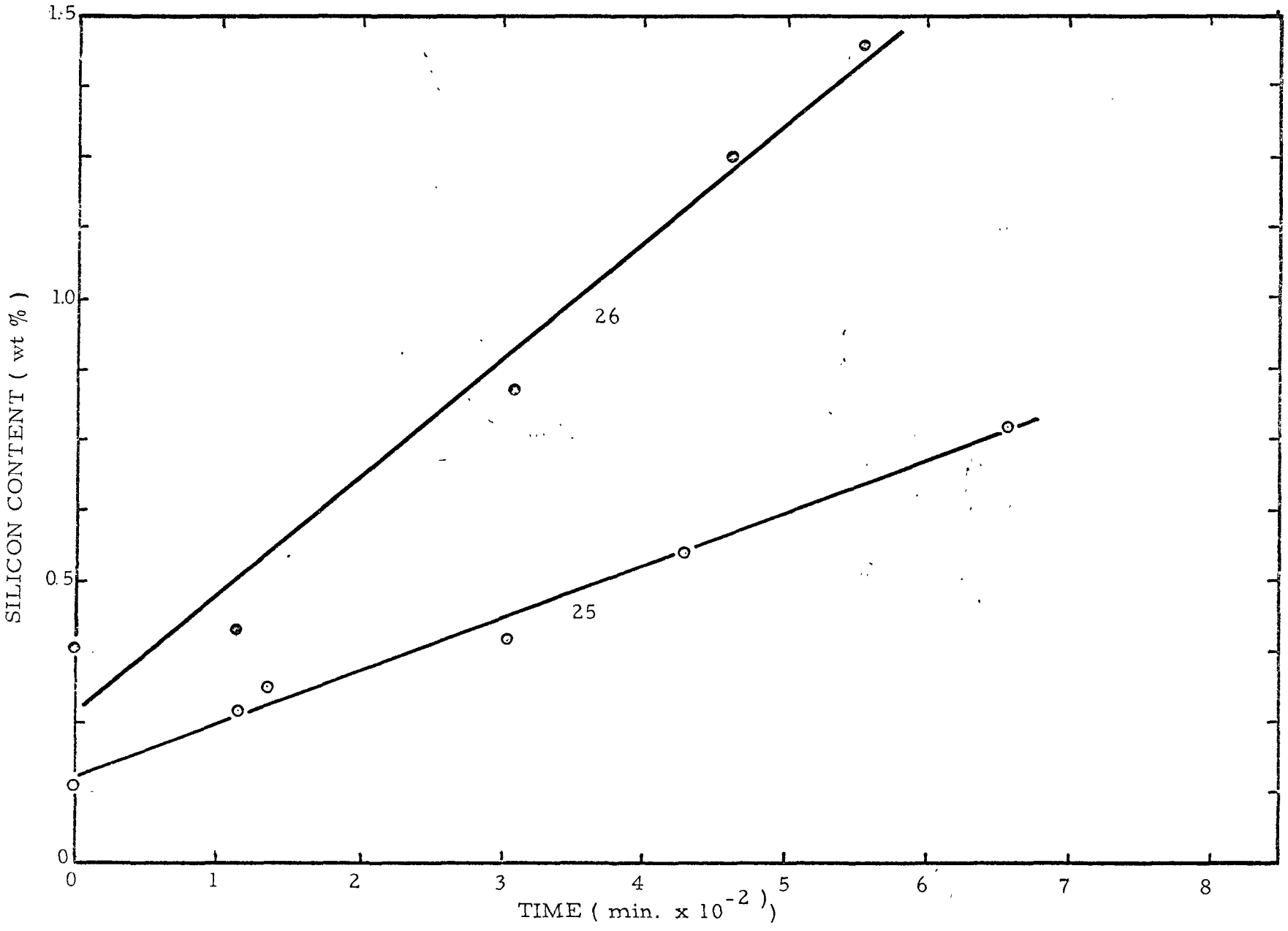

Figure 31

FIGURES 32 and 33 - PELLET DISTANCE AS A FUNCTION OF TIME
(Carbon Monoxide Furnace)

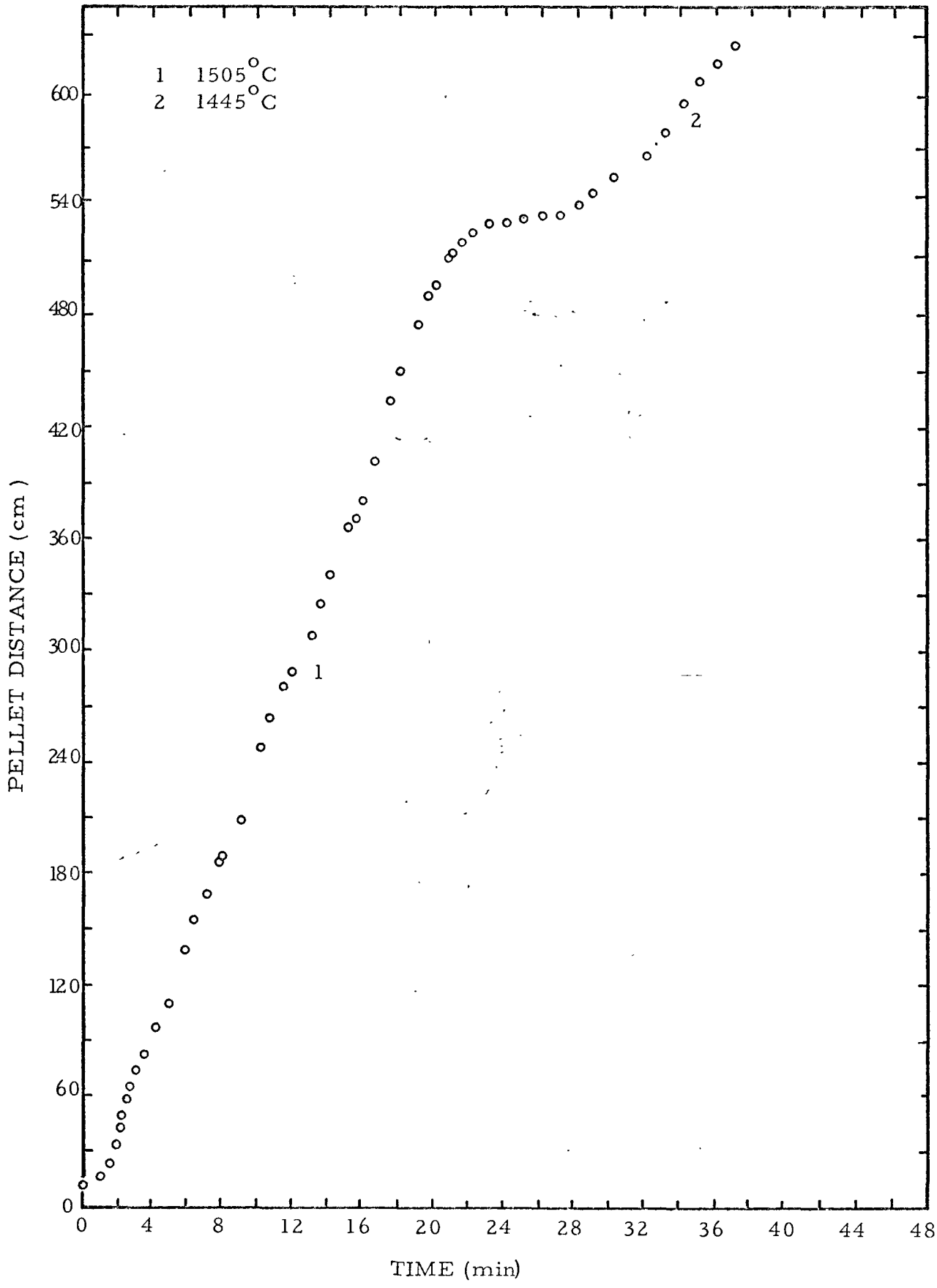
1 1505°C
2 1445°C
PELLET DISTANCE (cm)
TIME (min)
0
60
120
180
240
300
360
420
480
540
600
0
4
8
12
16
20
24
28
32
36
40
44
48
1
2

Figure 32

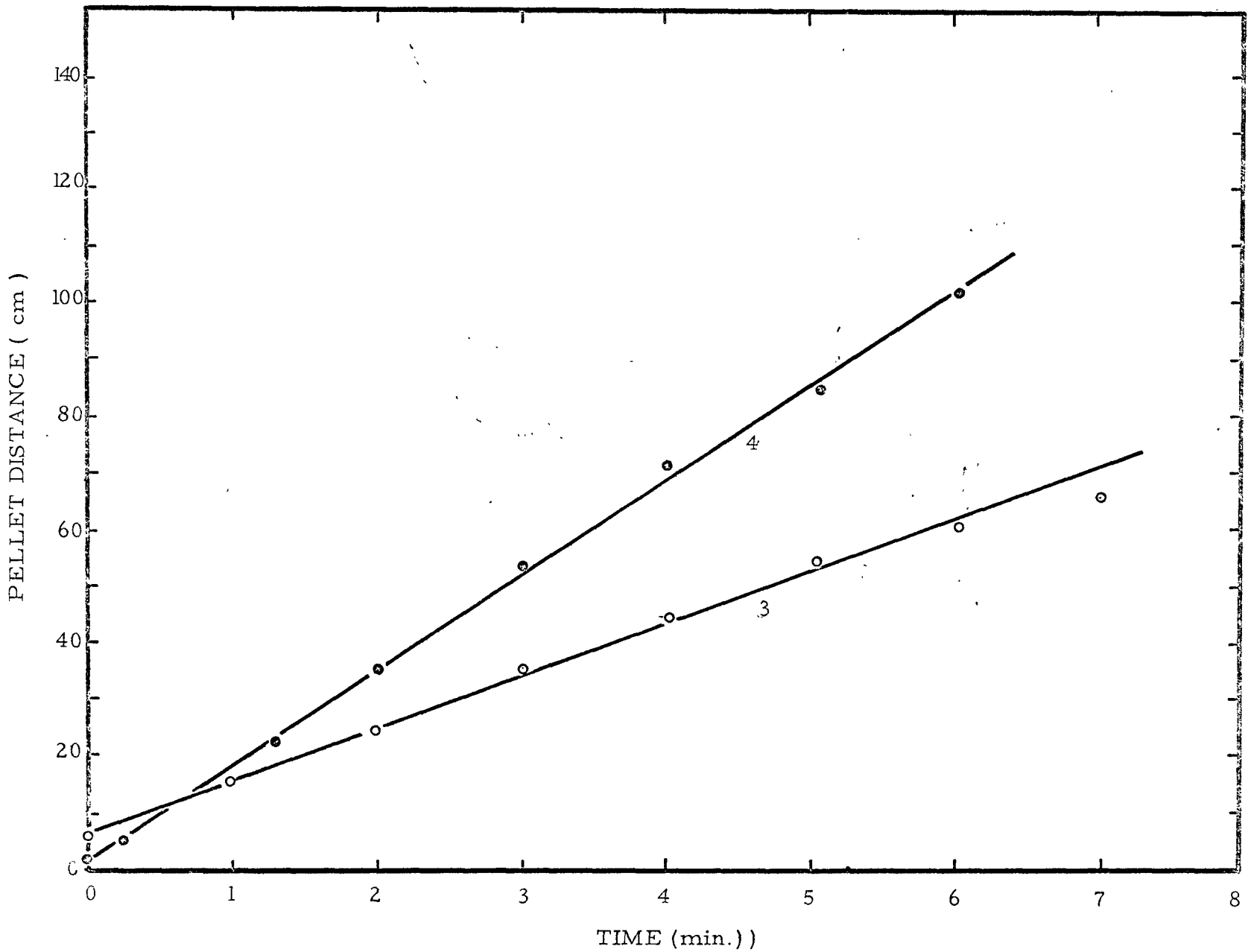
PELLET DISTANCE (cm)
140
120
100
80
60
40
20
0
0
1
2
3
4
5
6
7
8
TIME (min.))
4
3

Figure 33

FIGURES 34 to 41 - SILICON CONCENTRATION-TIME CURVES
(Sleeved Crucibles)

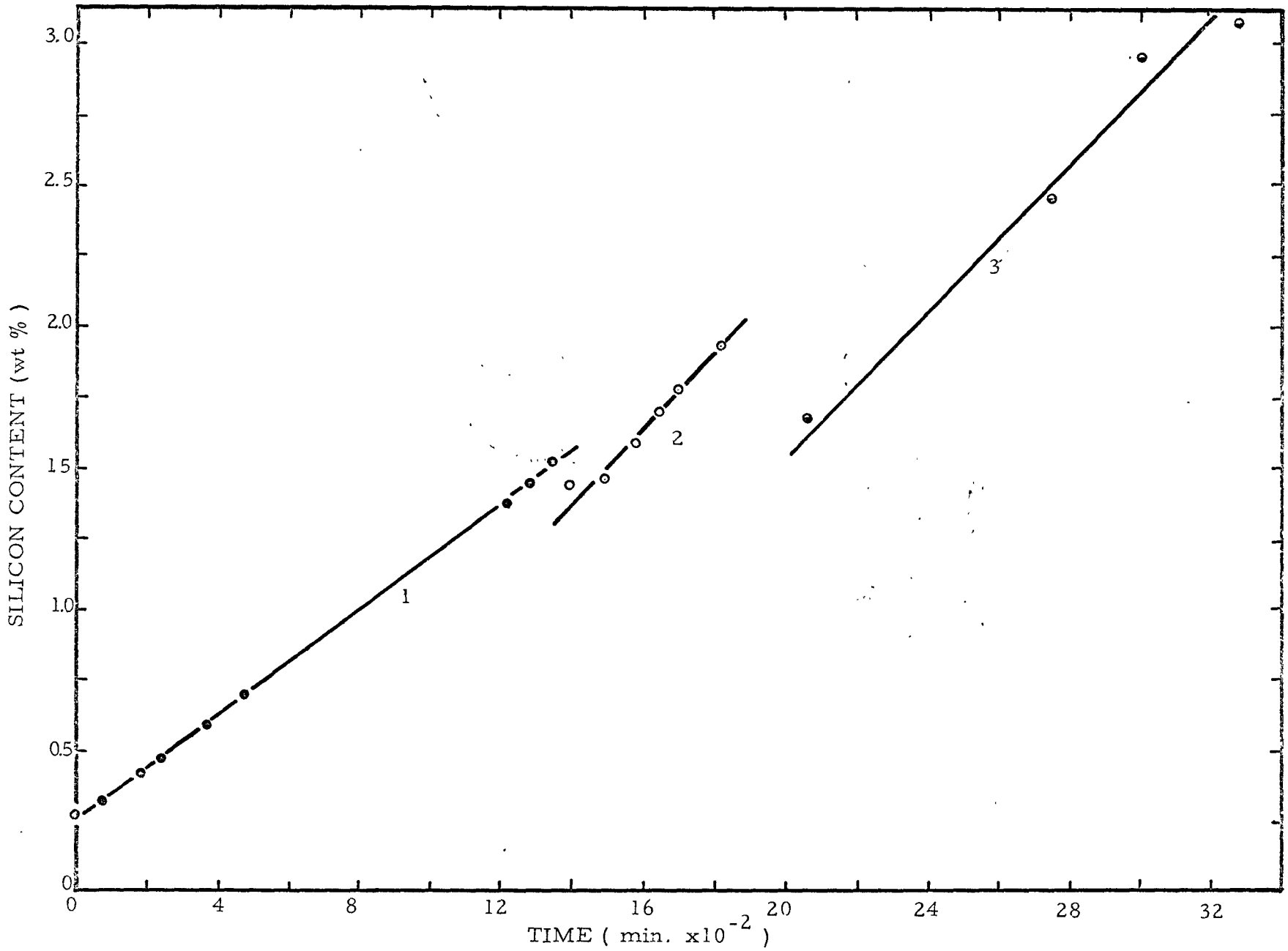
SILICON CONTENT (wt %)
3.0
2.5
2.0
1.5
1.0
0.5
0
0
4
8
12
16
20
24
28
32
TIME (min. x10^{-2})
1
2
3

Figure 34

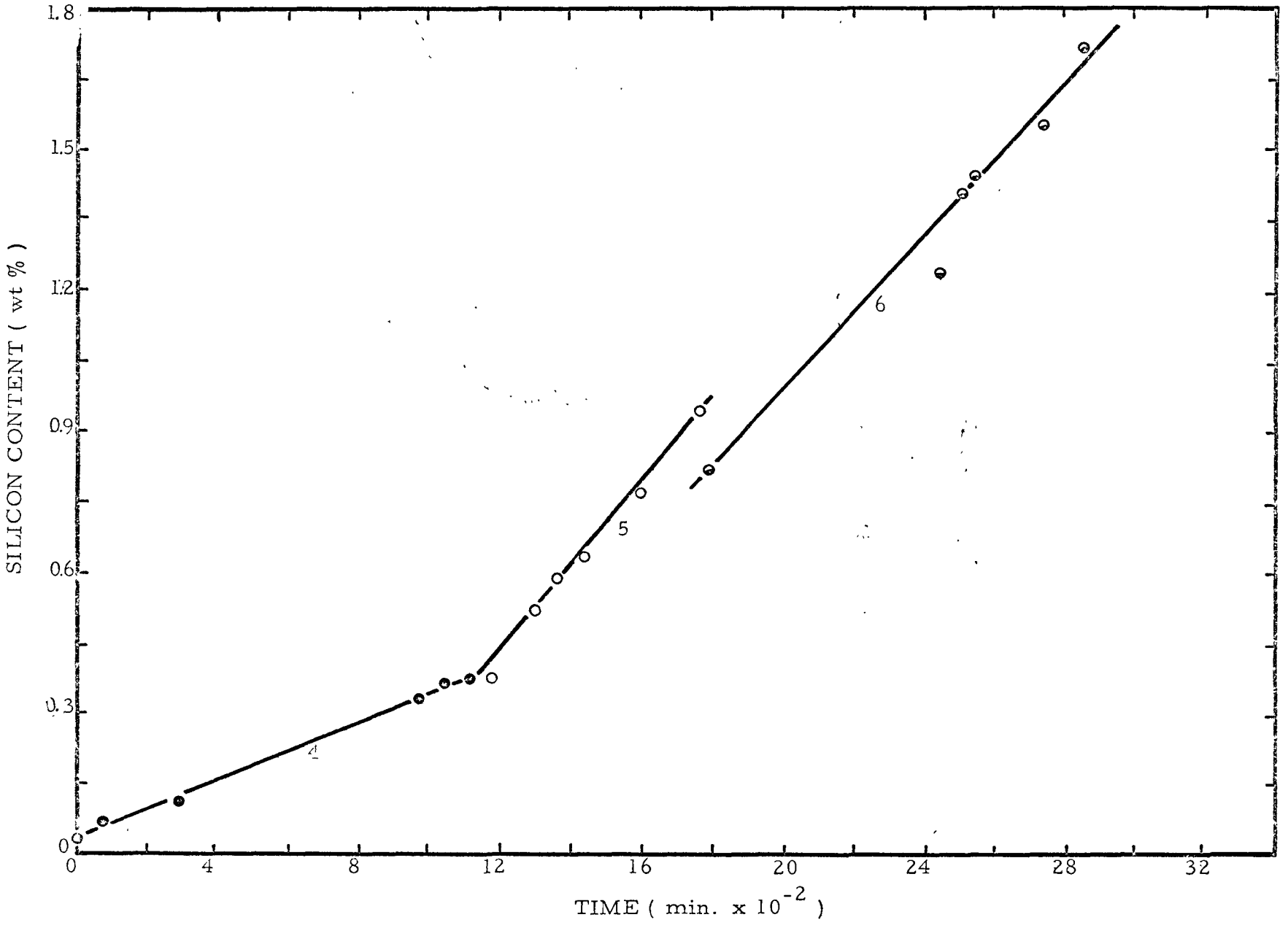
1.8
1.5
1.2
0.9
0.6
0.3
0
SILICON CONTENT (wt %)
0
4
8
12
16
20
24
28
32
TIME (min. x 10^-2)
5
6

Figure 35

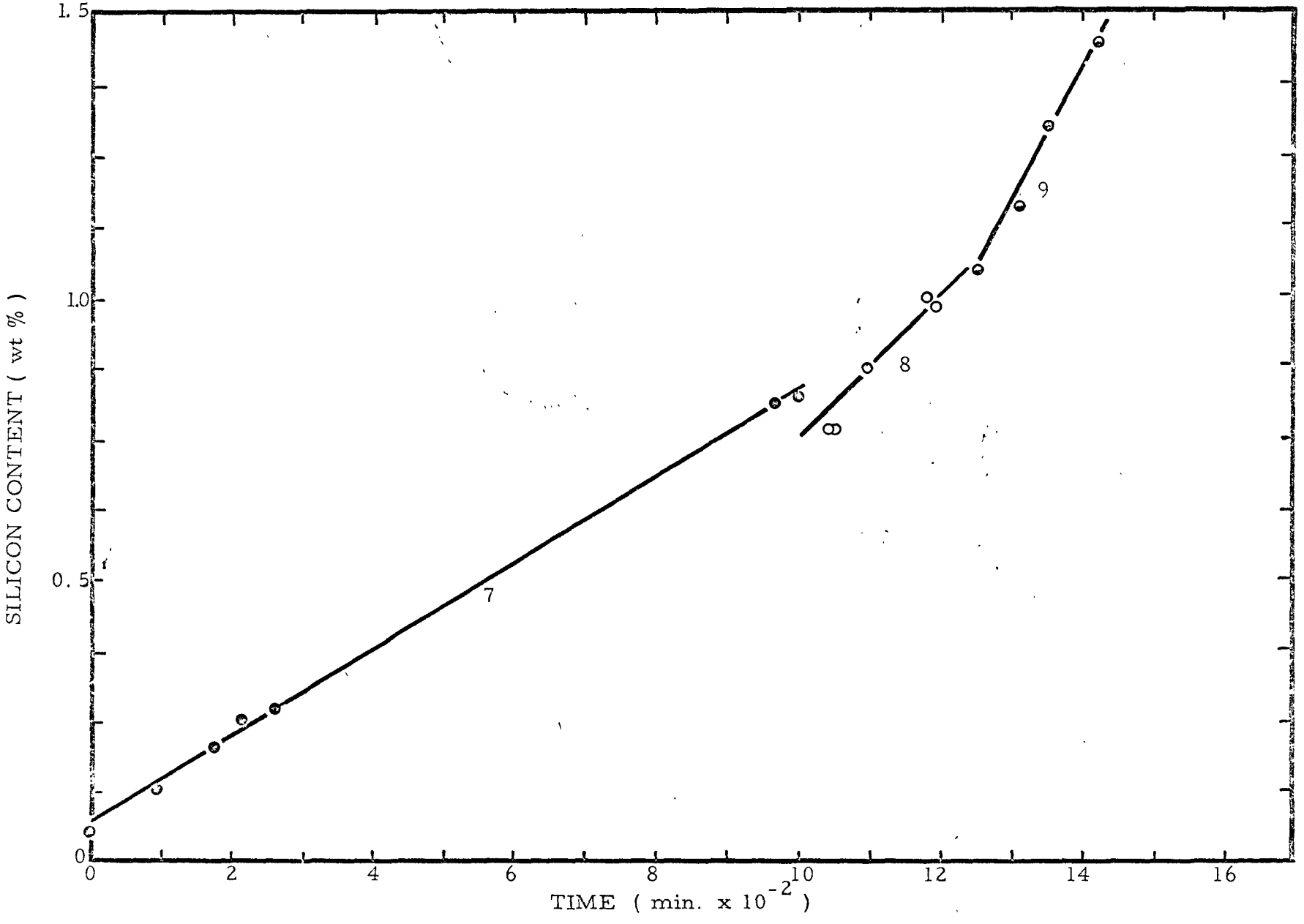
1.5
1.0
0.5
0
SILICON CONTENT (wt %)
0
2
4
6
8
10
12
14
16
TIME (min. x 10^-2)
7
8
9

Figure 36

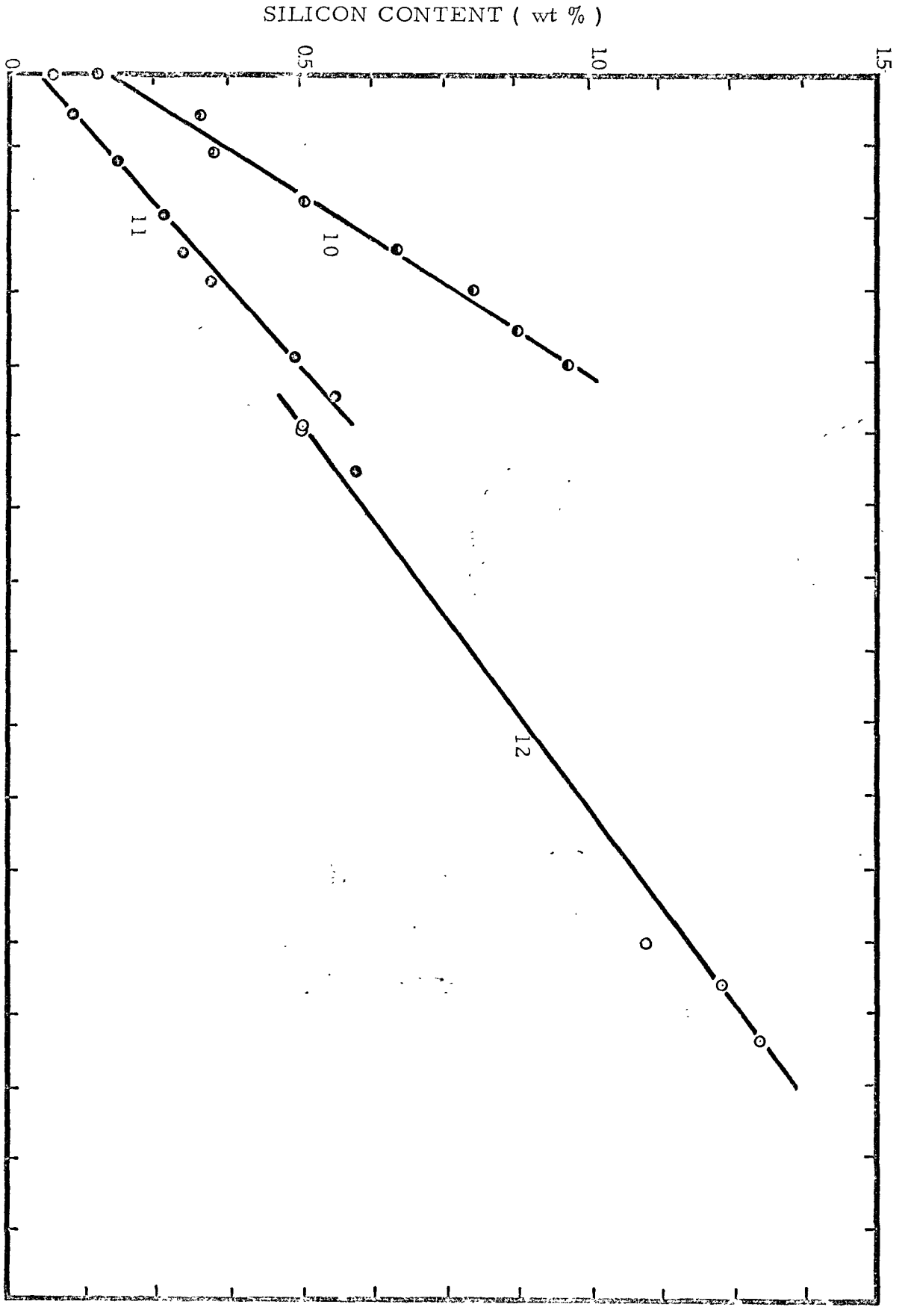
SILICON CONTENT (wt %)
0
0.5
1.0
1.5
0
2
4
6
8
10
12
14
16
TIME (min. x 10^{-2})
10
11
12

Figure 37

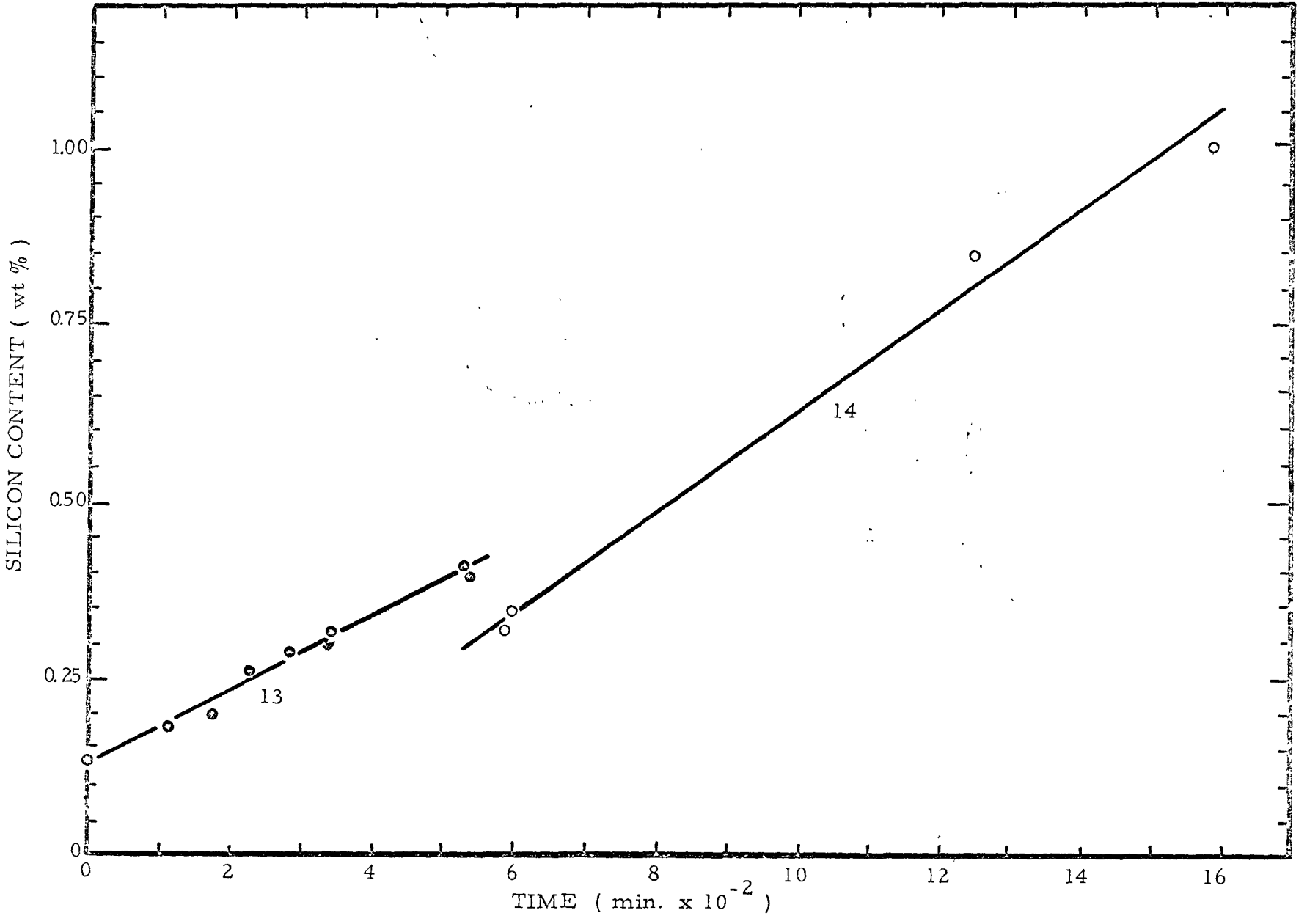
SILICON CONTENT (wt %)
1.00
0.75
0.50
0.25
0
13
14
0
2
4
6
8
10
12
14
16
TIME (min. x 10^-2)

Figure 38

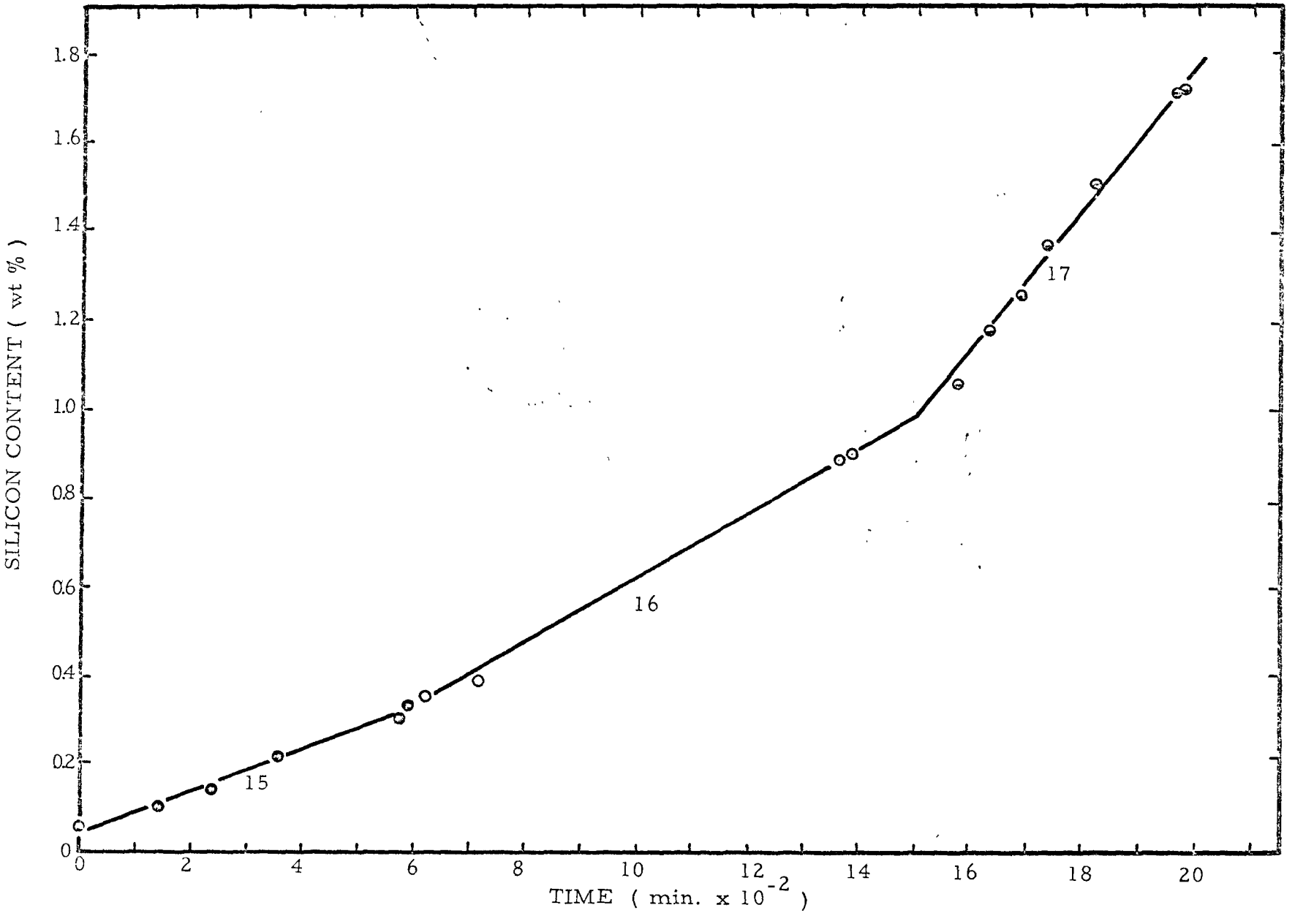
SILICON CONTENT (wt %)
1.8
1.6
1.4
1.2
1.0
0.8
0.6
0.4
0.2
0
0
2
4
6
8
10
12
14
16
18
20
TIME (min. x 10^-2)
15
16
17

Figure 39

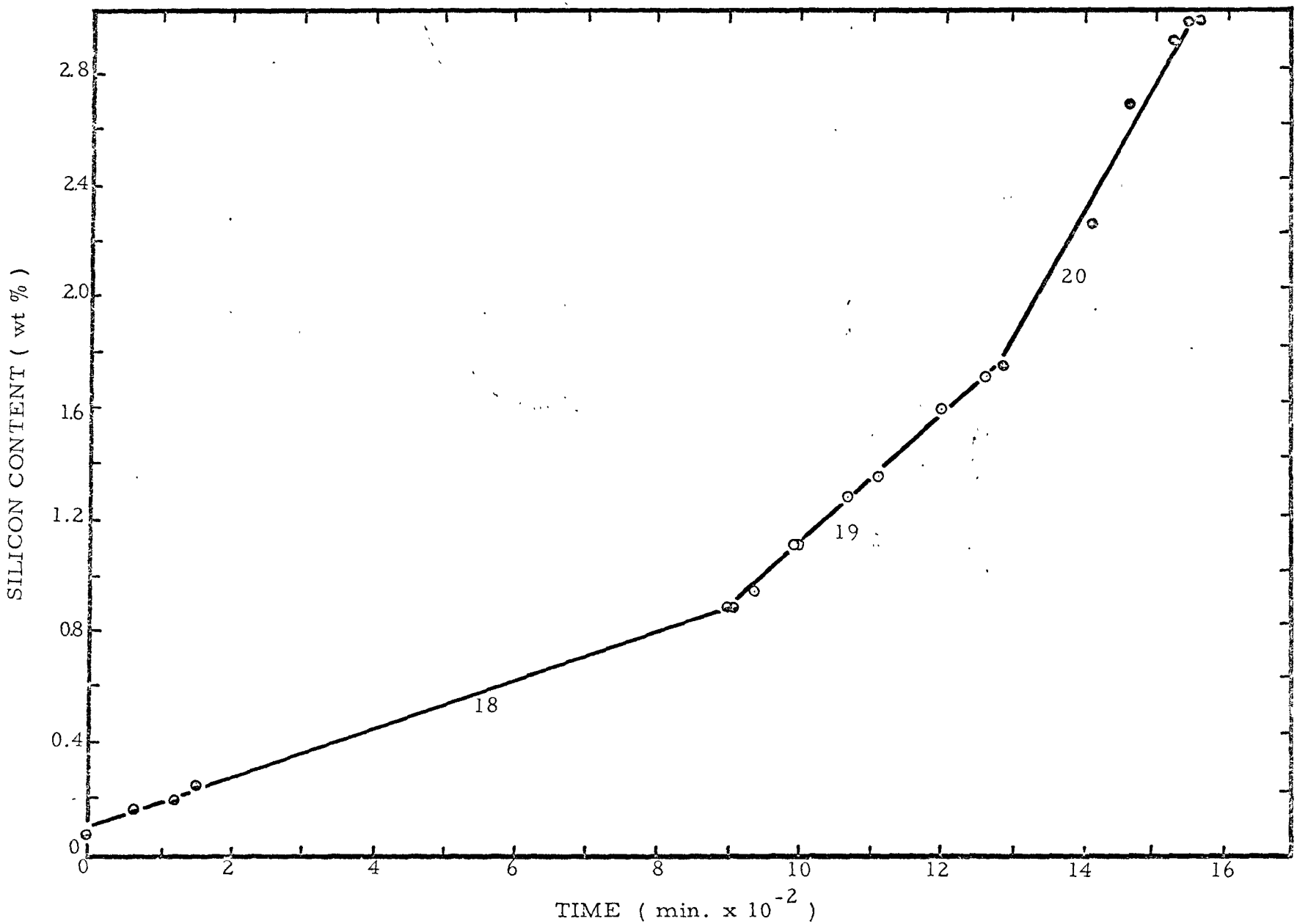
SILICON CONTENT (wt %)
2.8
2.4
2.0
1.6
1.2
0.8
0.4
0
0
2
4
6
8
10
12
14
16
18
19
20
TIME (min. x 10^-2)

Figure 40

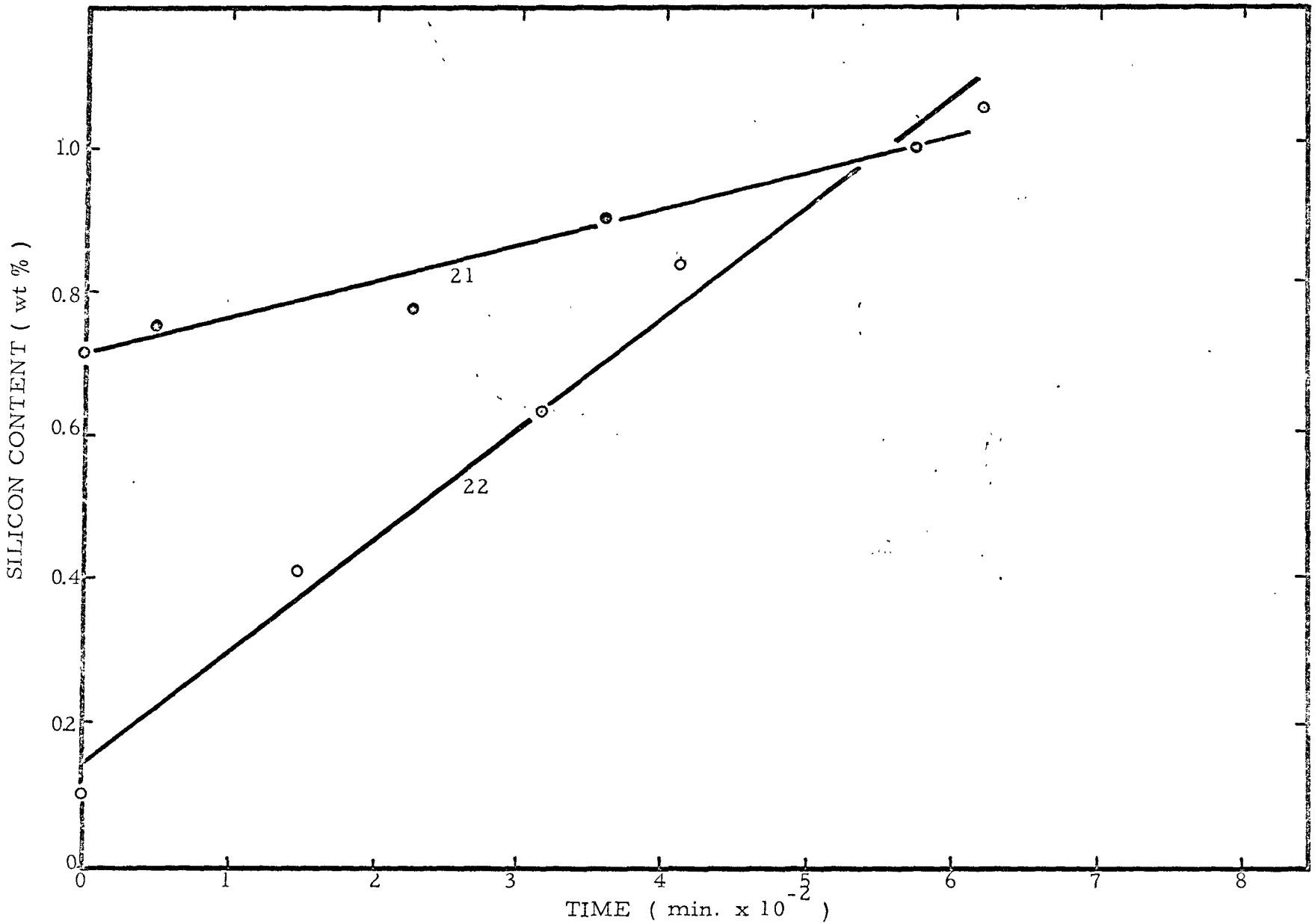
SILICON CONTENT (wt %)
1.0
0.8
0.6
0.4
0.2
0
21
22
0
1
2
3
4
5
6
7
8
TIME (min. x 10^-2)

Figure 41

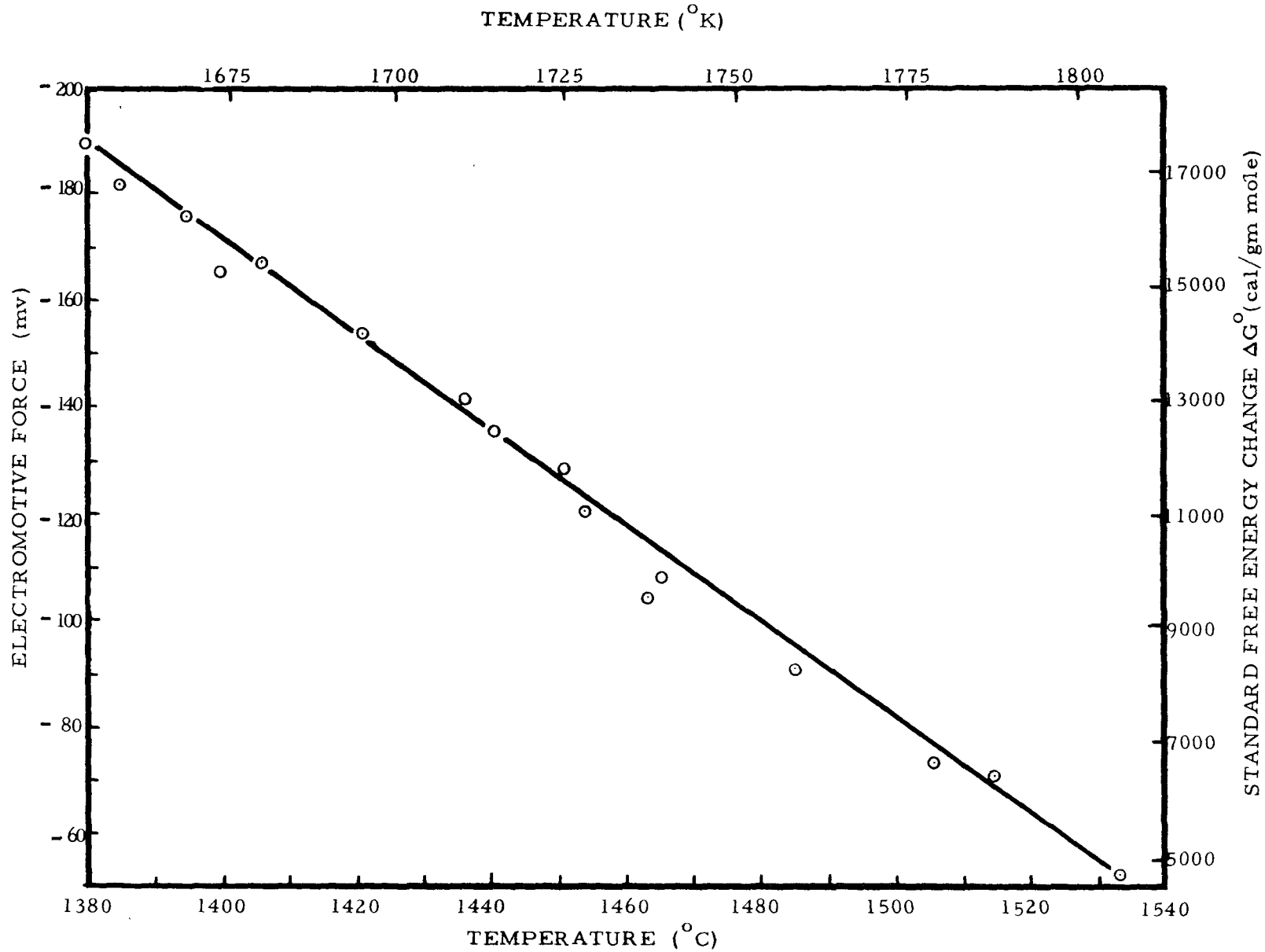

FIGURE 42 - ELECTROMOTIVE FORCE AND ΔG° AS A FUNCTION OF TEMPERATURE

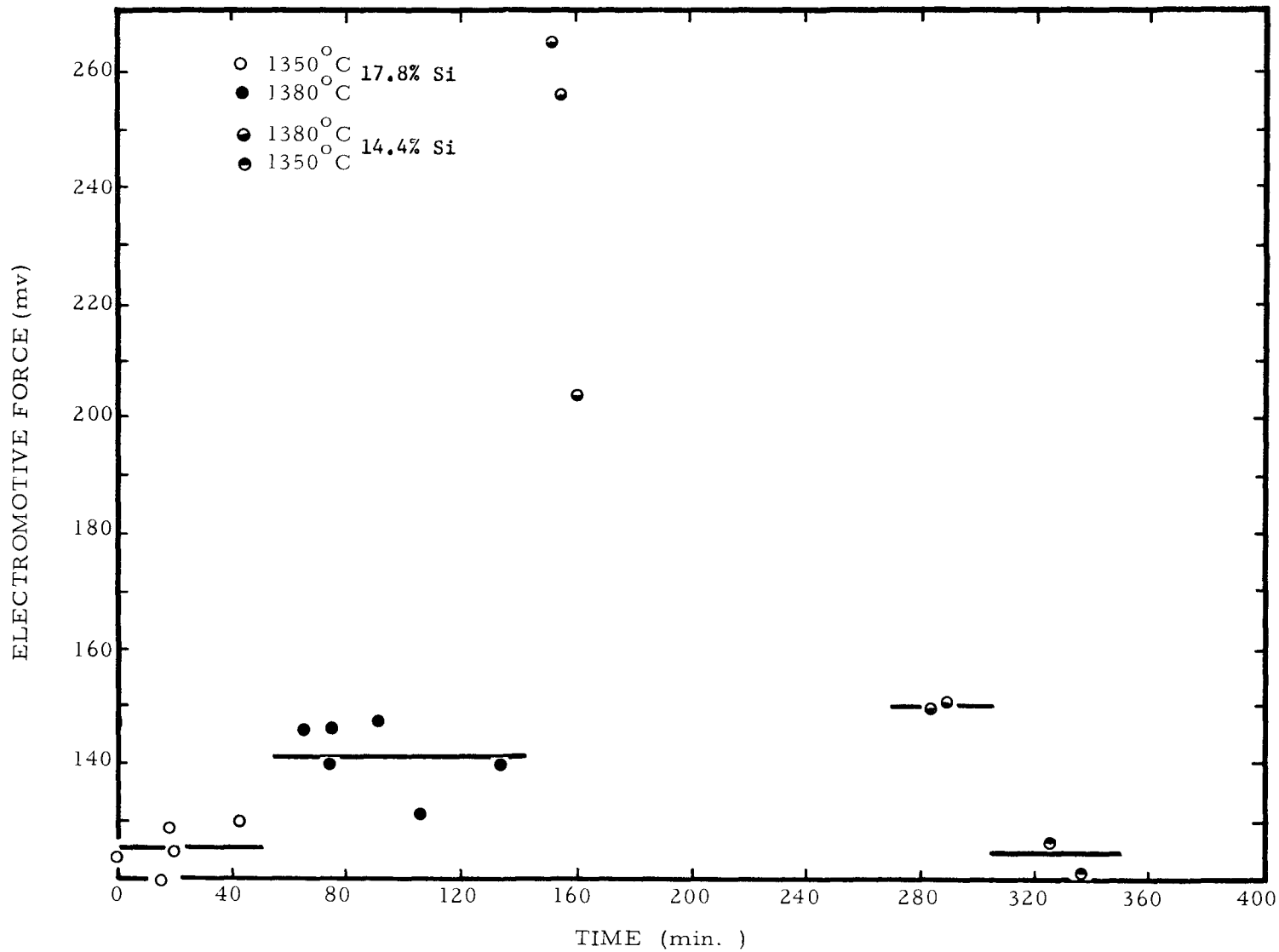

FIGURE 43 - ELECTROMOTIVE FORCE AS A FUNCTION OF TIME
(Fe-Si as the Metal Phase with an Si Top Electrode)

FIGURES 44 to 46 - ELECTROMOTIVE FORCE AS A FUNCTION OF TIME

(Fe-Si as the Metal Phase with a Graphite Top Electrode)

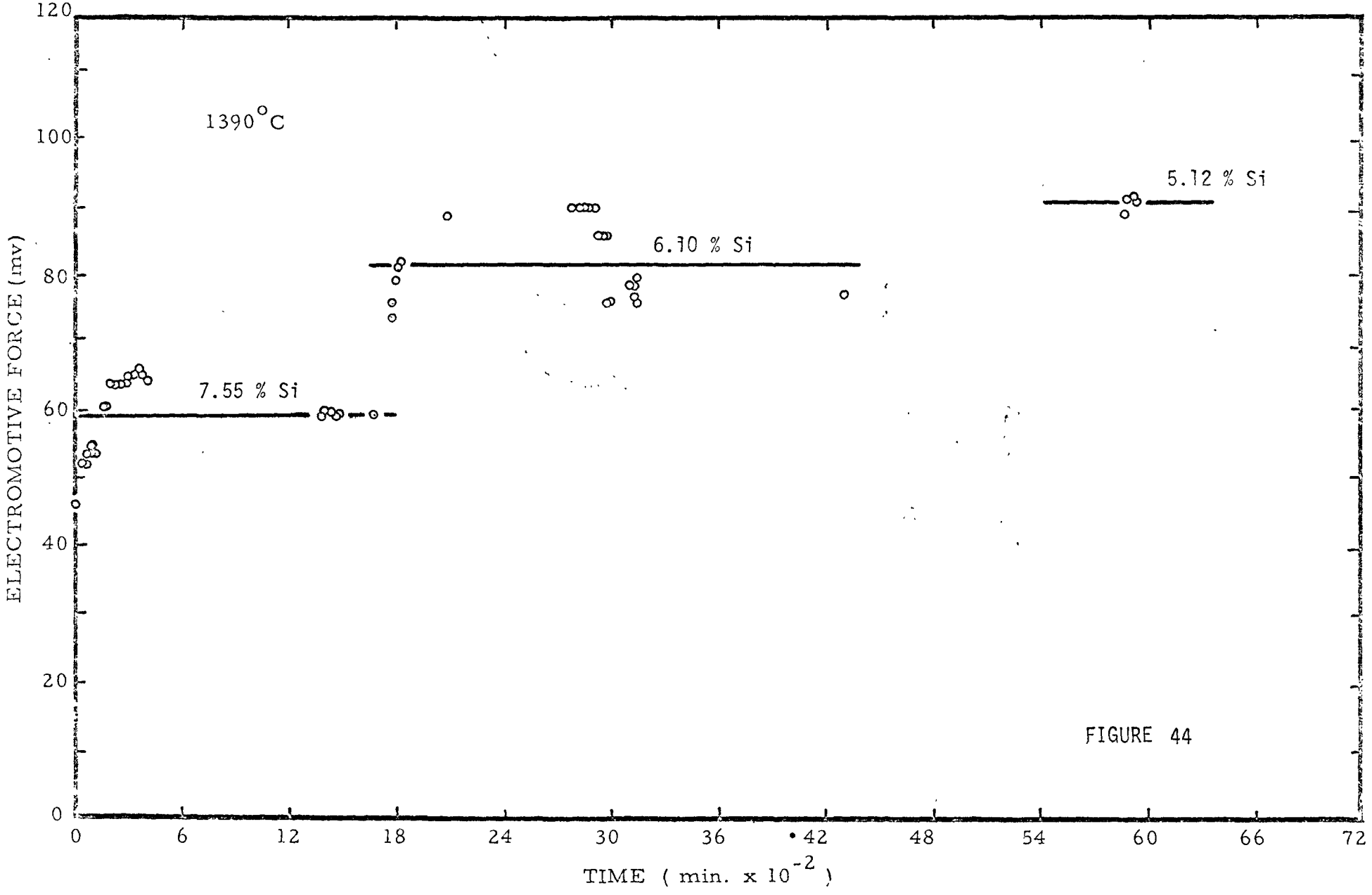
120
100
80
60
40
20
0
1390°C
7.55 % Si
6.10 % Si
5.12 % Si
ELECTROMOTIVE FORCE (mv)
0
6
12
18
24
30
36
42
48
54
60
66
72
TIME (min. x 10^-2)

FIGURE 44

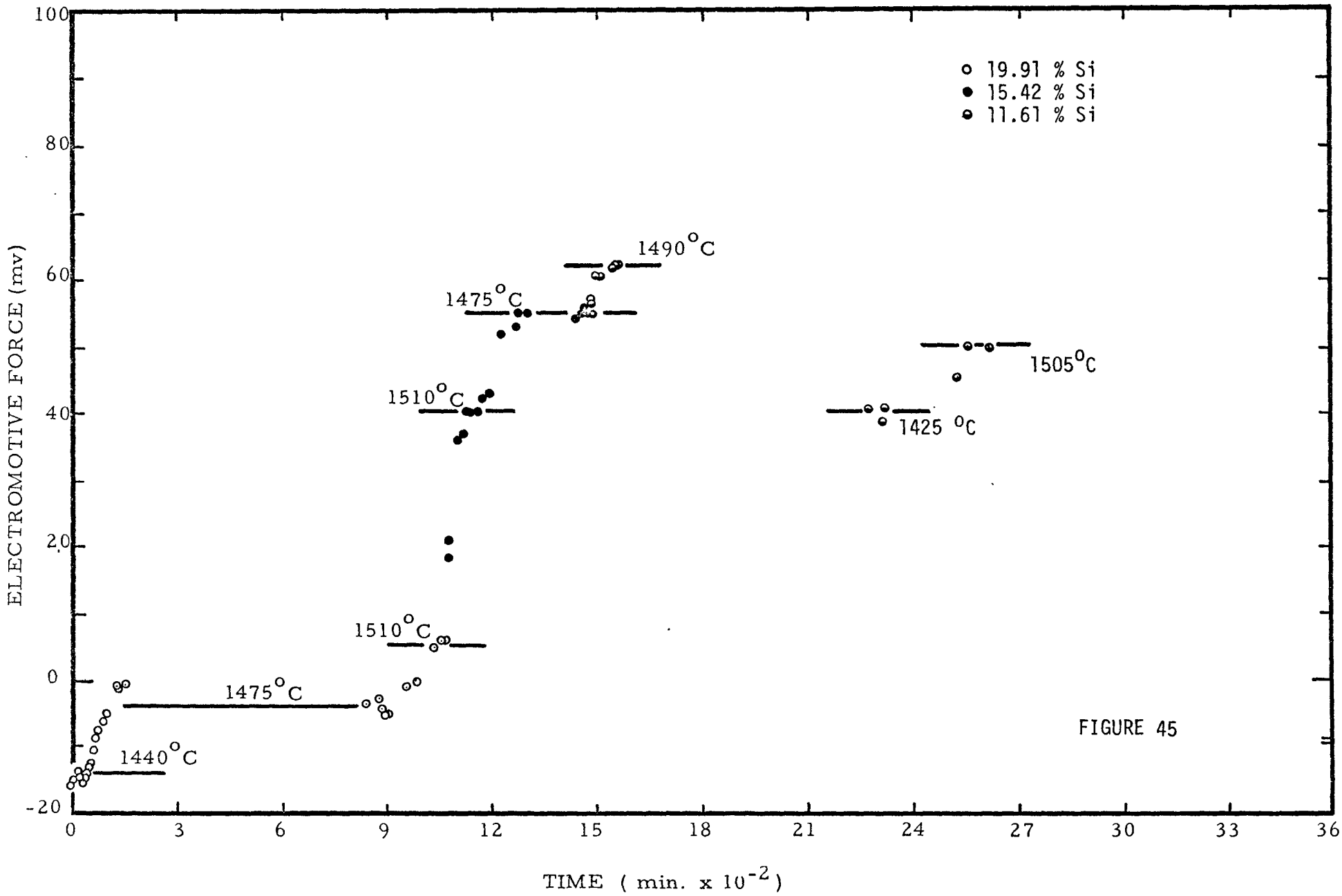
100
80
60
40
20
0
-20
0
3
6
9
12
15
18
21
24
27
30
33
36
ELECTROMOTIVE FORCE (mv)
TIME (min. x 10^{-2})
19.91 % Si
15.42 % Si
11.61 % Si
1490°C
1475°C
1505°C
1510°C
1425 °C
1510°C
1475°C
1440°C

FIGURE 45

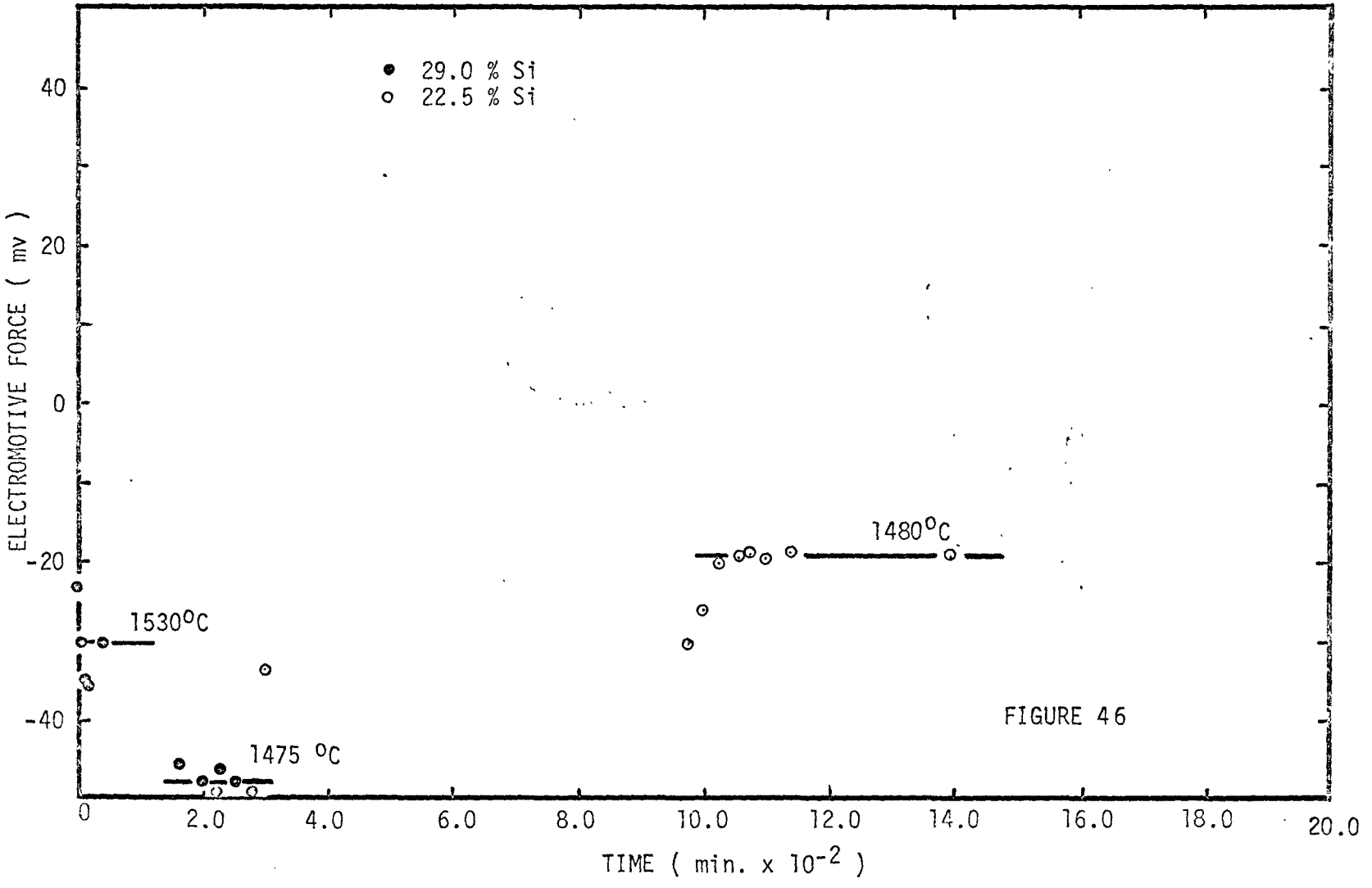
● 29.0 % Si
○ 22.5 % Si
1530°C
1480°C
1475 °C
ELECTROMOTIVE FORCE (mv)
TIME (min. x 10⁻²)
40
20
0
-20
-40
0
2.0
4.0
6.0
8.0
10.0
12.0
14.0
16.0
18.0
20.0

FIGURE 46

FIGURES 47 to 53 - ELECTROMOTIVE FORCE AS A FUNCTION OF TIME.
(Fe-C-Si as the Metal Phase with a Graphite Top Electrode)

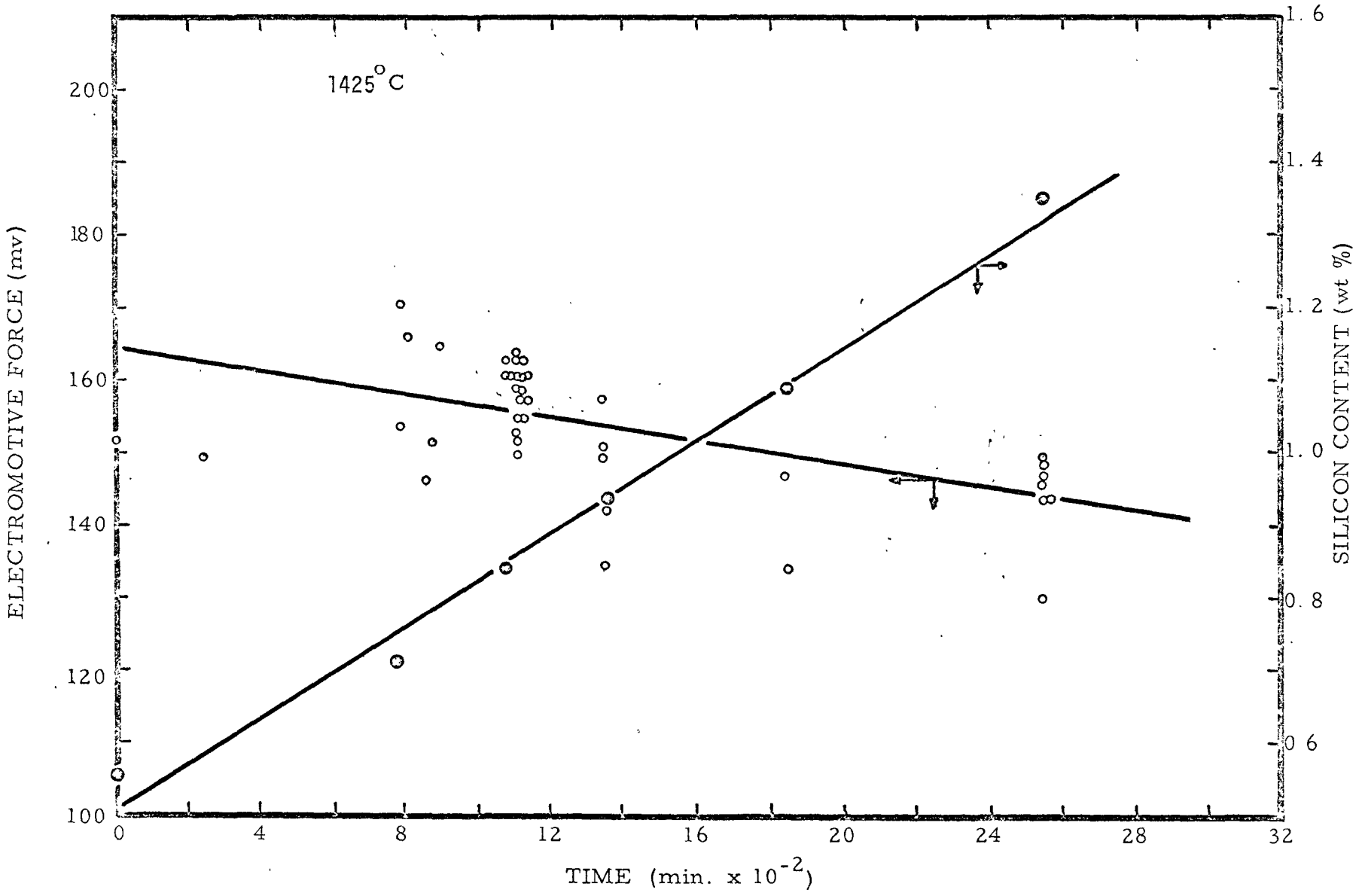
1425°C
ELECTROMOTIVE FORCE (mv)
SILICON CONTENT (wt %)
TIME (min. x 10^{-2})
200
180
160
140
120
100
1.6
1.4
1.2
1.0
0.8
0.6
0
4
8
12
16
20
24
28
32

FIGURE 47

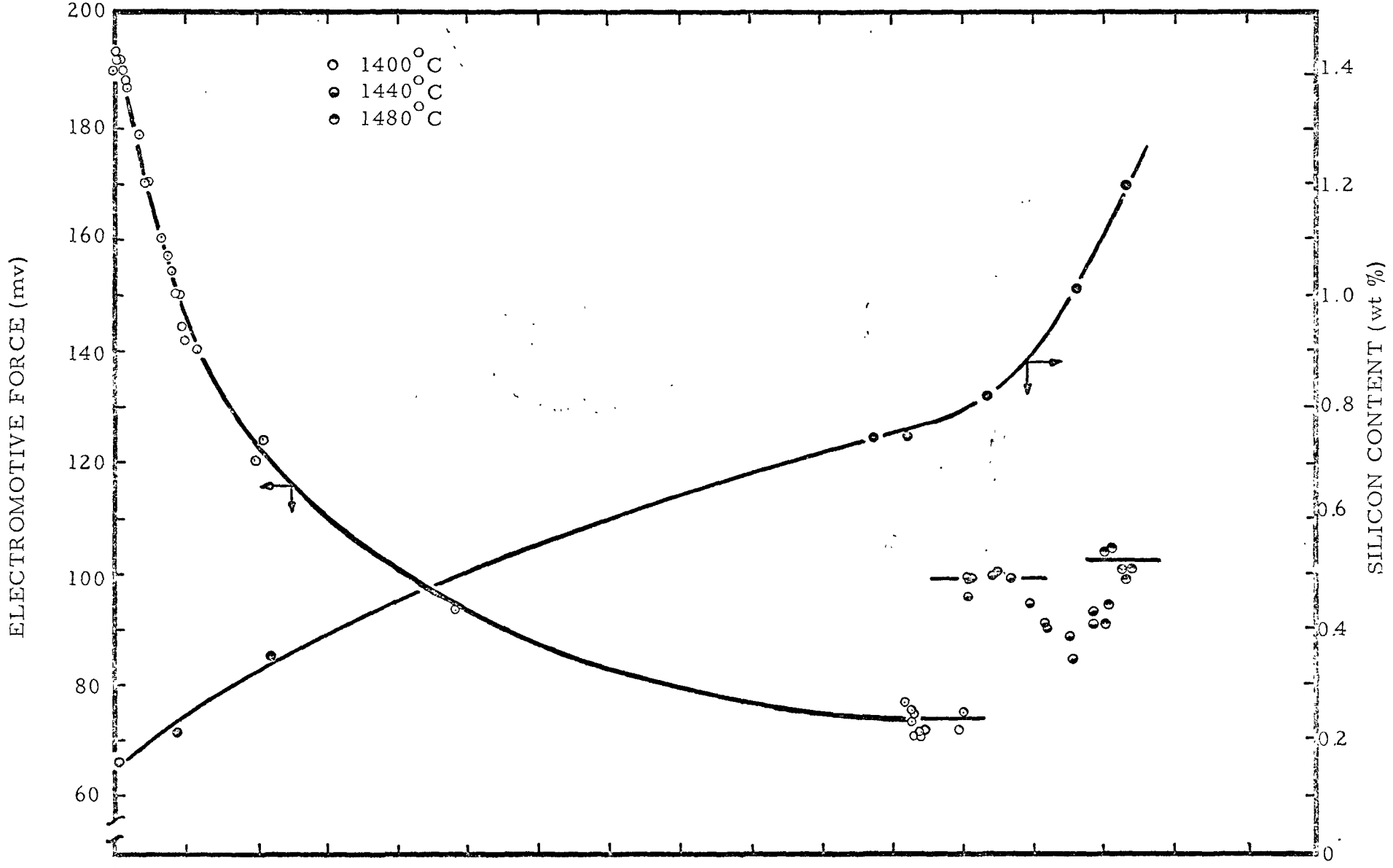
1400°C
1440°C
1480°C
ELECTROMOTIVE FORCE (mv)
SILICON CONTENT (wt %)
TIME (min. x 10⁻²)
200
180
160
140
120
100
80
60
1.4
1.2
1.0
0.8
0.6
0.4
0.2
0
0
2
4
6
8
10
12
14
16

FIGURE 48

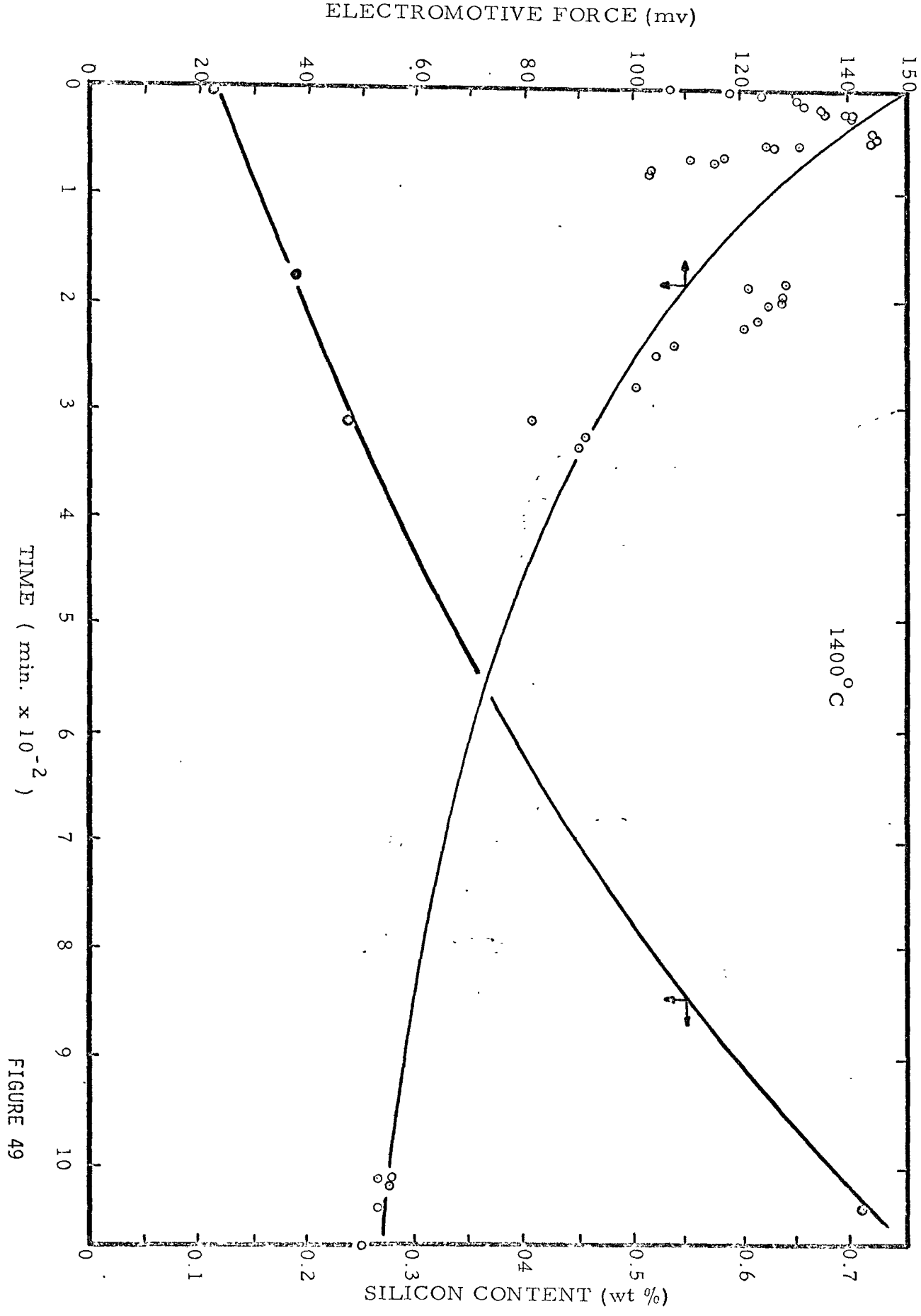
ELECTROMOTIVE FORCE (mv)
0
20
40
60
80
100
120
140
150
1400°C
TIME (min. x 10^{-2})
0
1
2
3
4
5
6
7
8
9
10
SILICON CONTENT (wt %)
0
0.1
0.2
0.3
0.4
0.5
0.6
0.7

FIGURE 49

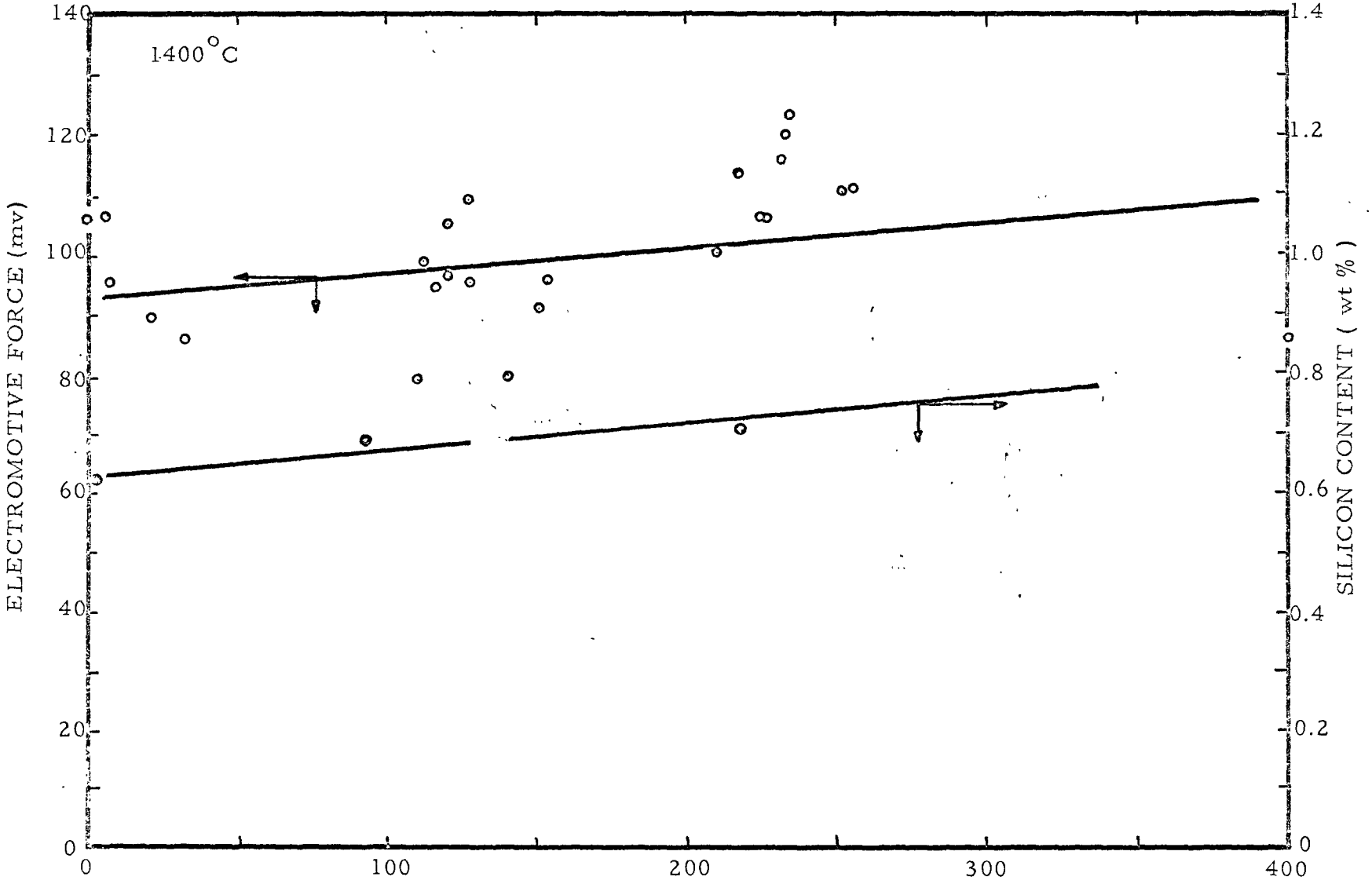
1400°C
ELECTROMOTIVE FORCE (mv)
SILICON CONTENT (wt %)
TIME (min.)
0
20
40
60
80
100
120
140
0
0.2
0.4
0.6
0.8
1.0
1.2
1.4
0
100
200
300
400

FIGURE 50

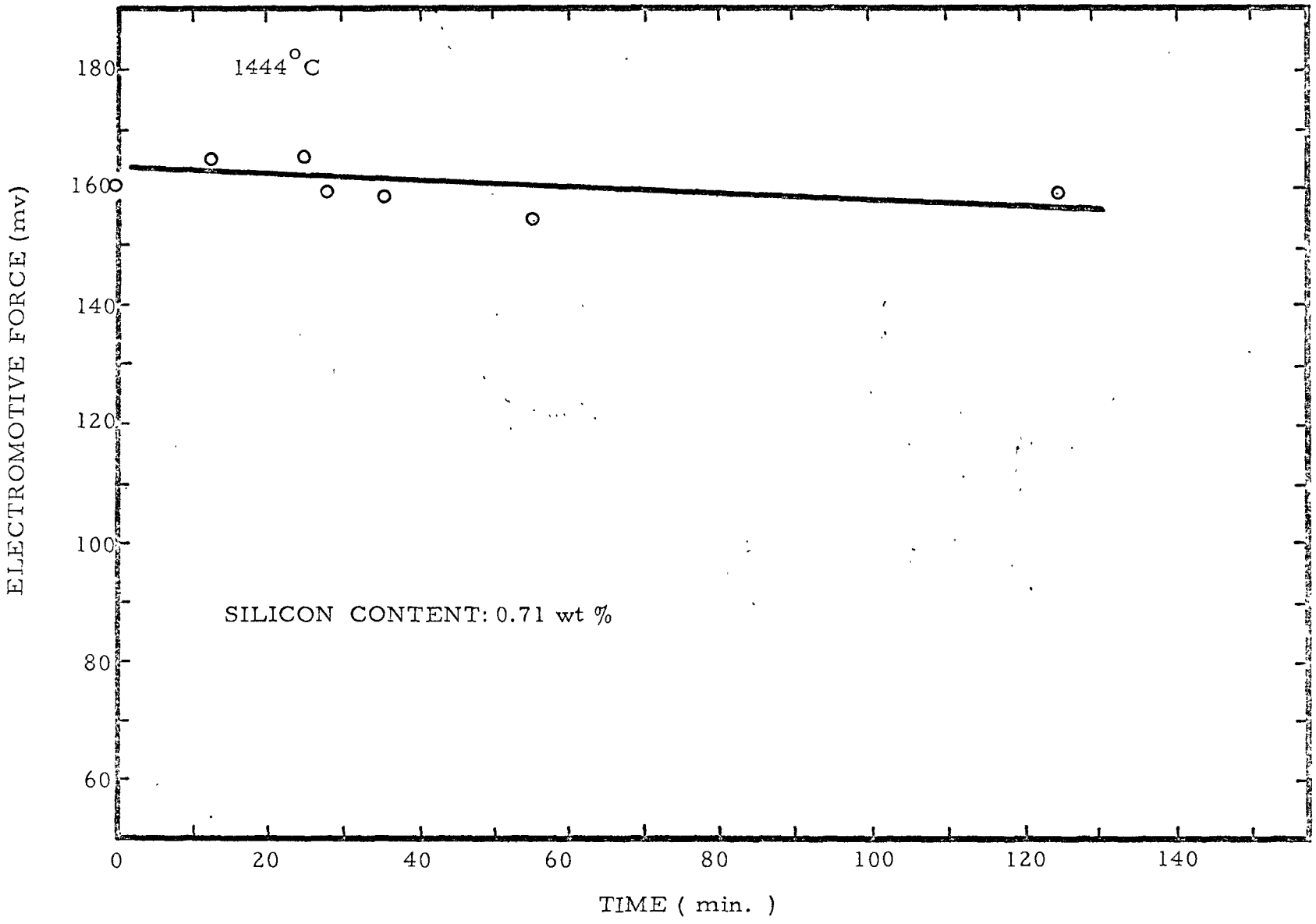
1444°C
SILICON CONTENT: 0.71 wt %
ELECTROMOTIVE FORCE (mv)
180
160
140
120
100
80
60
0
20
40
60
80
100
120
140
TIME (min.)

FIGURE 51

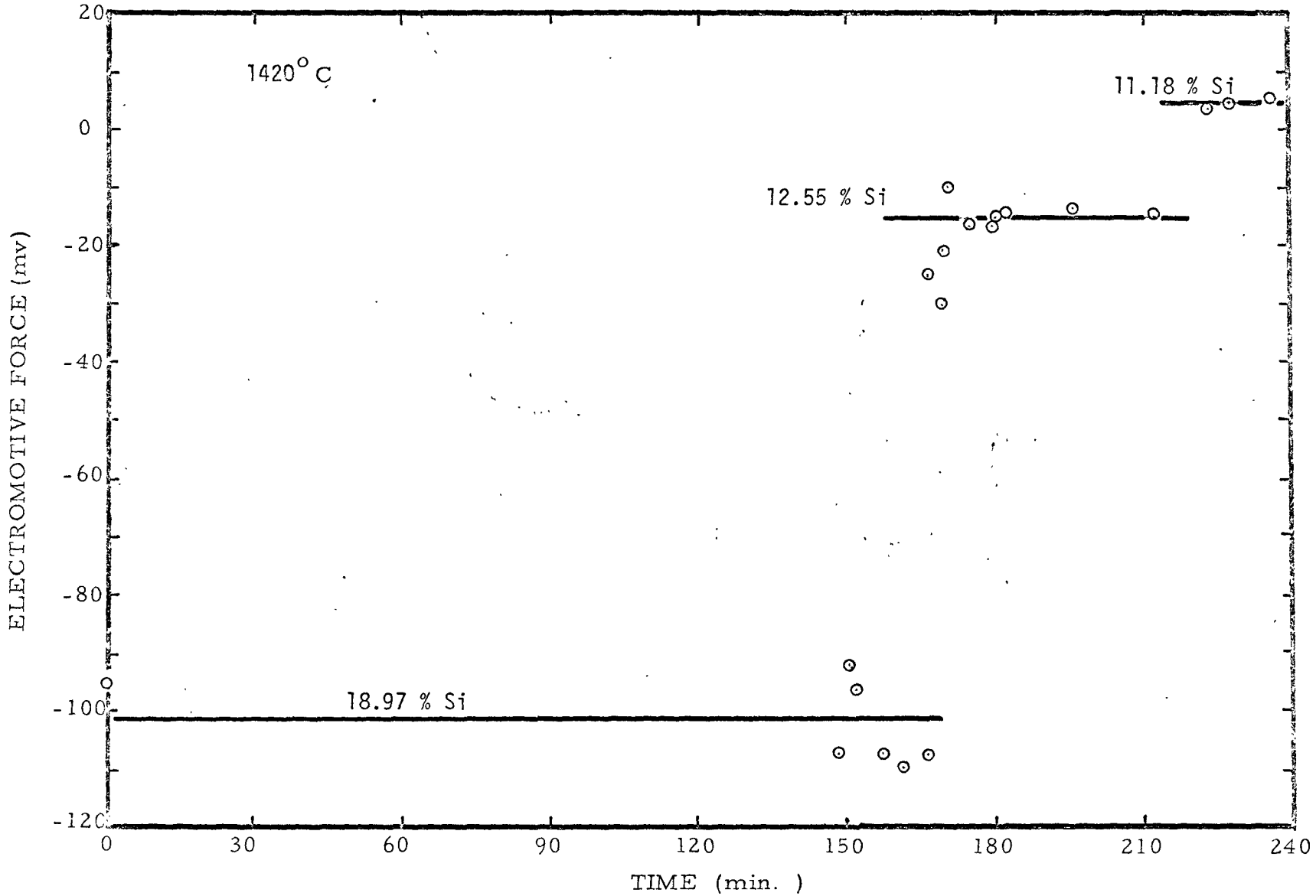
1420° C
11.18 % Si
12.55 % Si
18.97 % Si
ELECTROMOTIVE FORCE (mv)
TIME (min.)
20
0
-20
-40
-60
-80
-100
-120
0
30
60
90
120
150
180
210
240

FIGURE 52

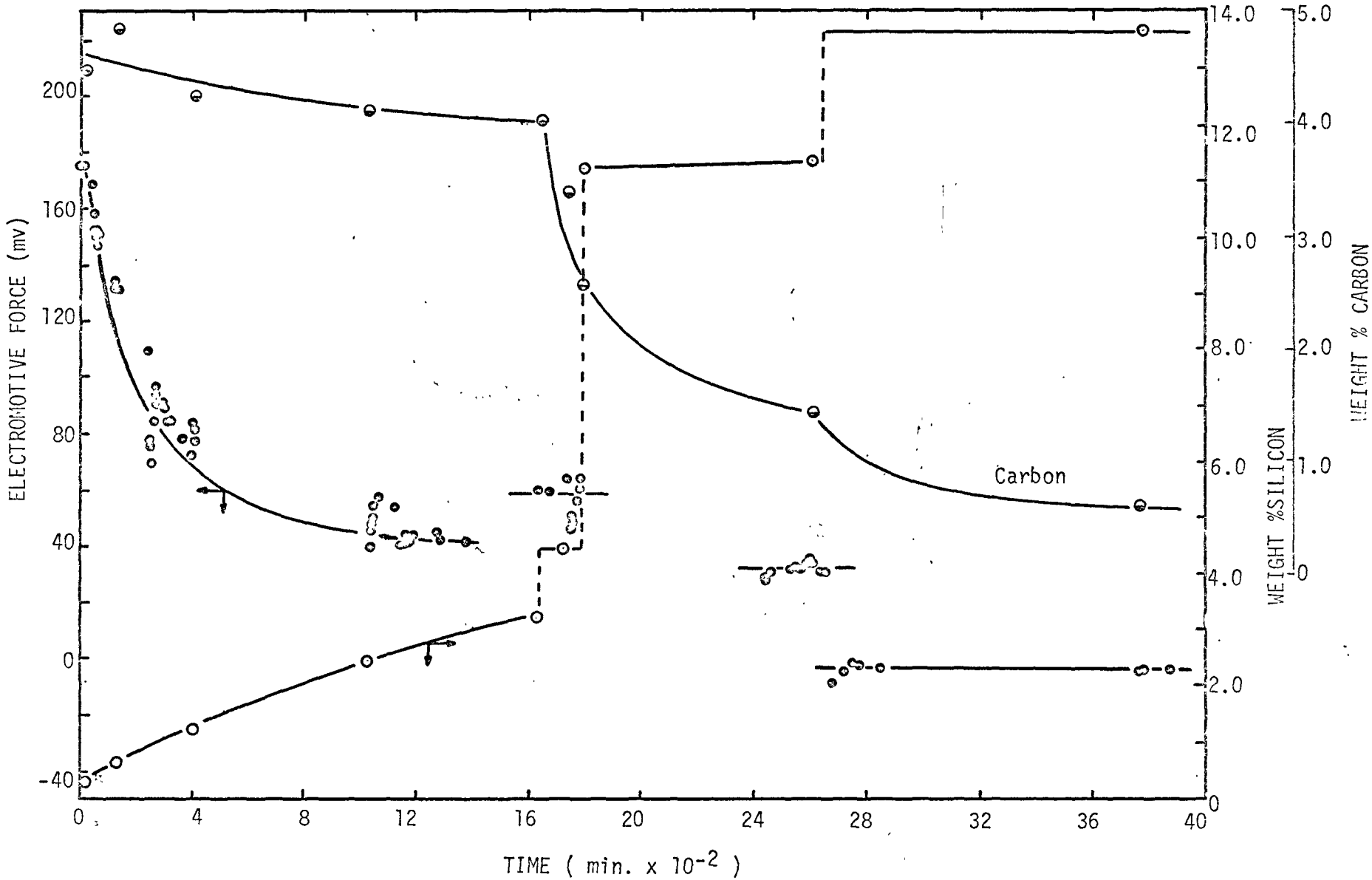
ELECTROMOTIVE FORCE (mv)
200
160
120
80
40
0
-40
0
4
8
12
16
20
24
28
32
36
40
TIME (min. x 10-2)
14.0
12.0
10.0
8.0
6.0
4.0
2.0
0
WEIGHT %SILICON
5.0
4.0
3.0
2.0
1.0
0
WEIGHT % CARBON
Carbon

FIGURE 53

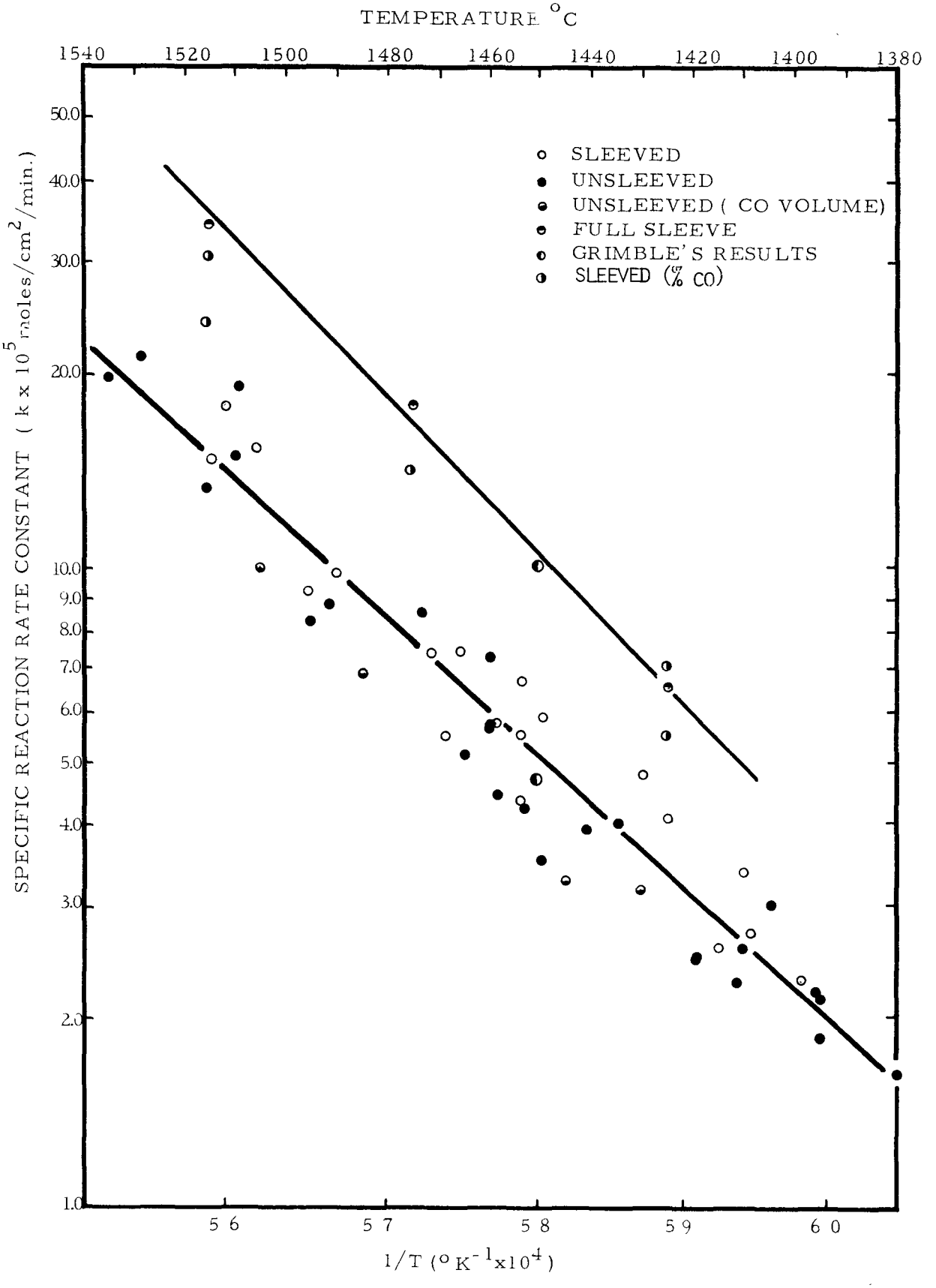

FIGURE 54 - SPECIFIC REACTION RATE CONSTANT AS A FUNCTION OF TEMPERATURE (Pooled Slope)

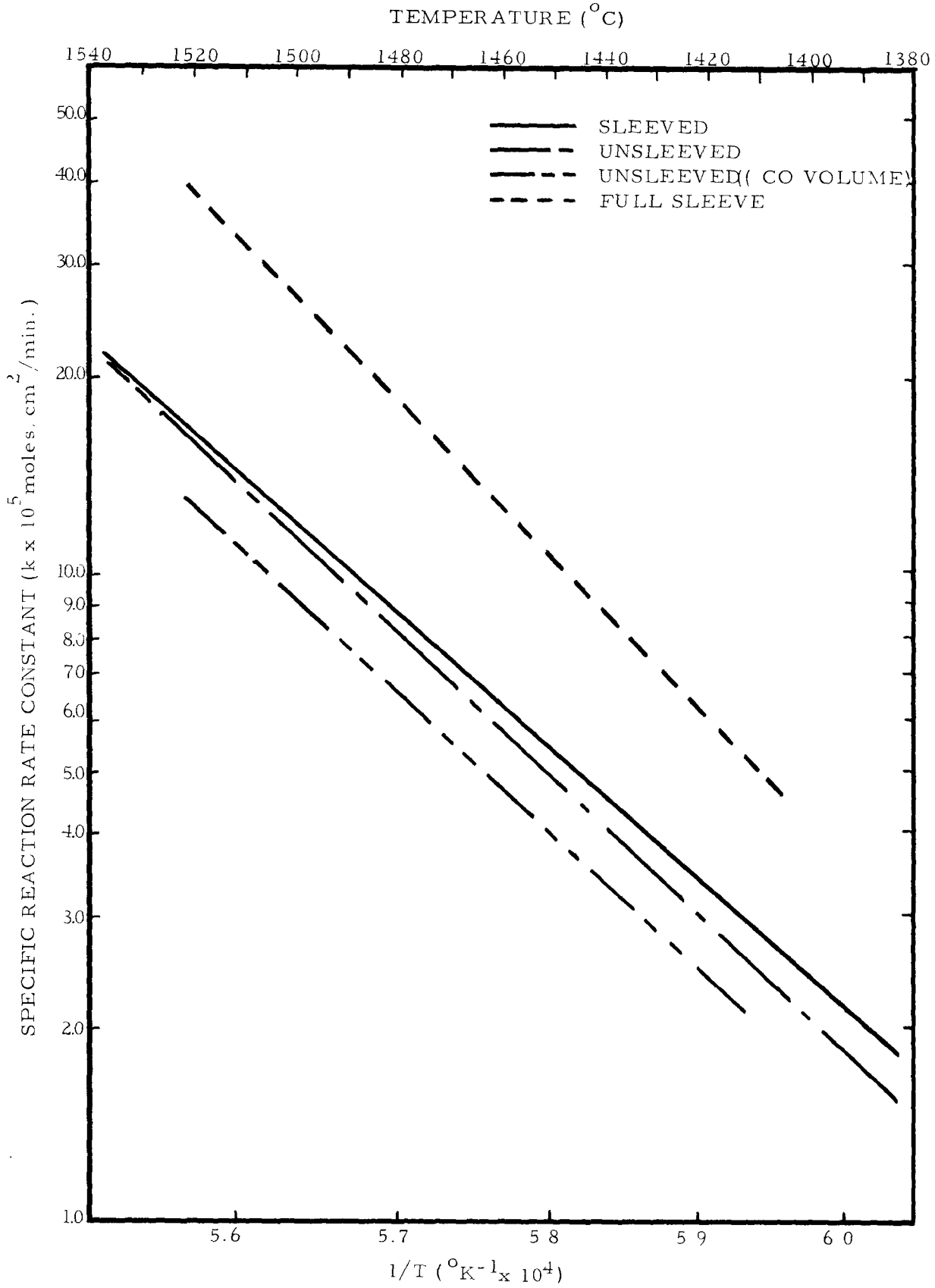

FIGURE 55 - SPECIFIC REACTION RATE CONSTANT AS A FUNCTION OF TEMPERATURE (Individual Slopes)

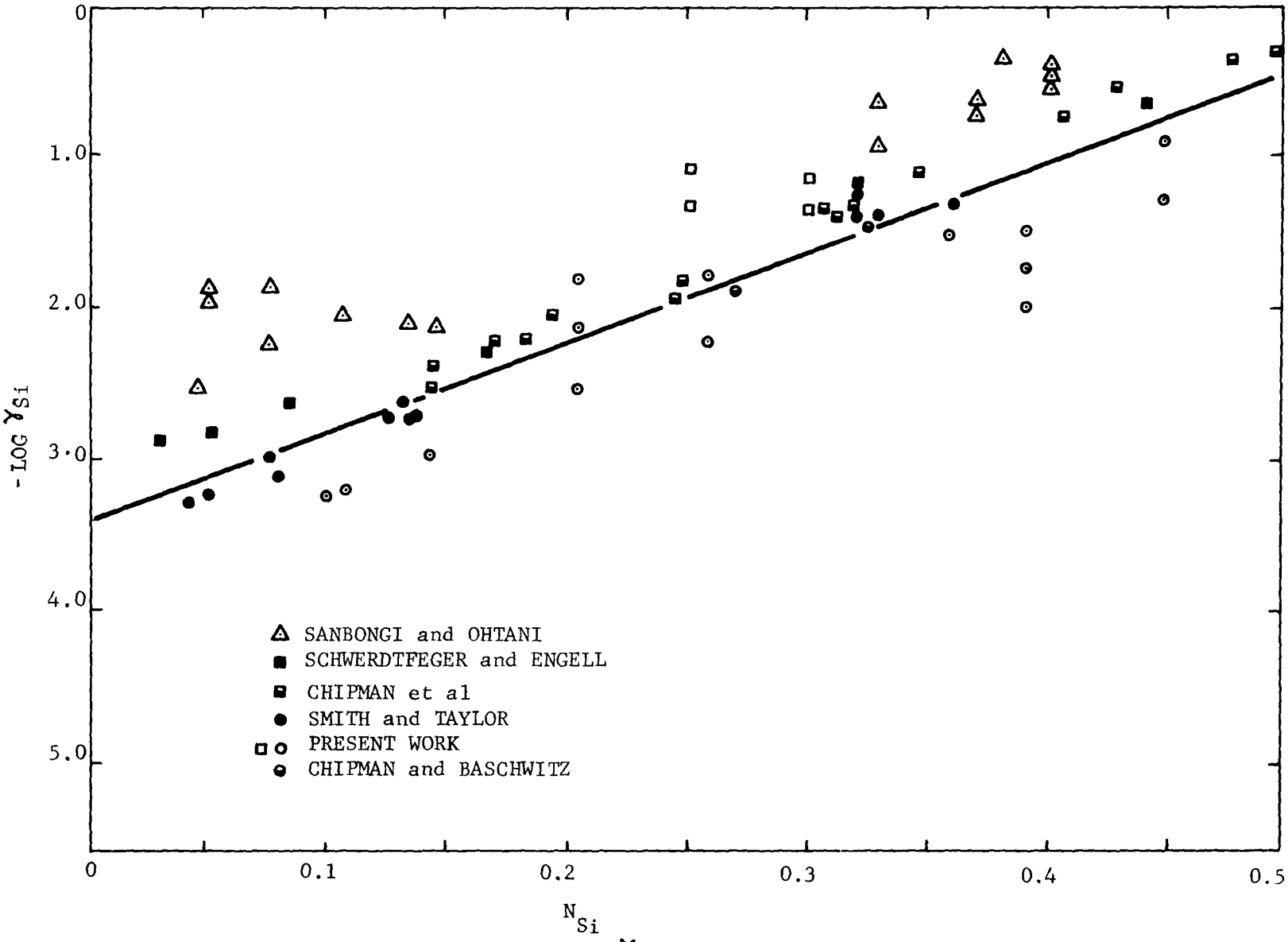

FIGURE 56- LOG γ_{Si} AS A FUNCTION N_{Si}

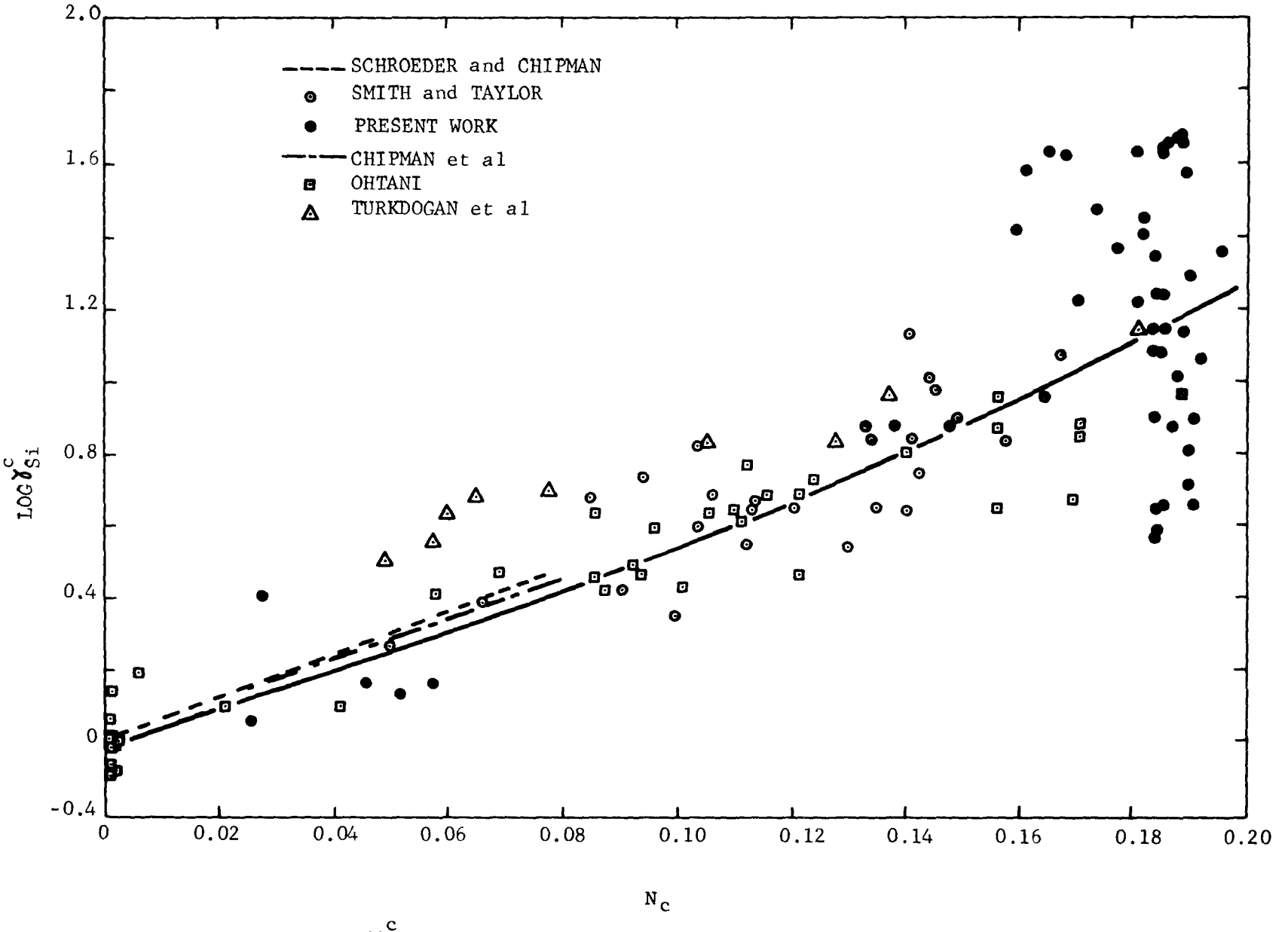

FIGURE 57- LOG γ^c_{Si} AS A FUNCTION OF N_c